DEPARTMENT OF THE INTERIOR

U.S. GEOLOGICAL SURVEY

Aspects of the Petrology, Mineralogy, and Geochemistry of the Granitic Rocks Associated with Questa Caldera, Northern New Mexico

By

Brigitte Dillet

and

Gerald K. Czamanske

Open-file Report 87-258

[1]U.S. Geological Survey, 345 Middlefield Rd., Menlo Park, California.

Aspects of the Petrology, Mineralogy, and Geochemistry of the Granitic Rocks Associated with Questa Caldera, Northern New Mexico

By

Brigitte Dillet and Gerald K. Czamanske, U.S. Geological Survey

This report consists largely of the Ph.D. thesis prepared by Brigitte Dillet and defended at the University of Clermont-Ferrand, France, in February, 1987. From December, 1983 through December, 1985 Ms. Dillet was supported by a grant from the French Government to carry out this thesis study at the offices of the U.S. Geological Survey in Menlo Park, California, under the guidance of Gerald Czamanske. Expenses for field work and part of 1986 were contributed by the U.S. Geological Survey as part of a comprehensive study of the volcanic and plutonic rocks associated with Questa caldera

Appendices B through L have been added to the thesis to provide accurate sample locations, supplemental major- and minor-element data, and electron microprobe analyses obtained by G.K.C. for allanite, apatite, chevkinite, feldspars, and sphene in the Questa granitoids.

NOTES:

1. Because early pagination is used in the thesis, pages 8, 9, [illegible], [illegible], 179, and 185 do not exist.

2. Because of unavoidable systems changes, pages 221 through 225 cannot be reproduced and are difficult to read. Users may obtain unreduced copies of these pages by directly contacting Gerald Czamanske.

Table of Contents

INDEX

LIST OF PLATES

LIST OF TABLES

LIST OF FIGURES

INTRODUCTION

REGIONAL GEOLOGY

Questa caldera is located in northern New Mexico (U.S.A.) in the southern part of the Sangre de Cristo Range of the Rocky Mountains, along the east margin of the Rio Grande Rift zone (fig. 1).

Late Cretaceous to early Eocene time is marked, in the southern Rocky Mountains, by the Laramide orogeny which rejuvenated Paleozoic uplifts (Tweto, 1975). Starting near the end of the Cretaceous, the orogeny was also accompanied by magmatic activity, which had been essentially absent since Precambrian time. Magmatic activity continued through middle Cenozoic time with similar characteristics.

Both early and middle Cenozoic volcanism are characterized by continental lavas and breccias of intermediate composition (andesite to rhyodacite) erupted from many scattered volcanoes, through and onto orogenic and postorogenic terranes (Lipman and others, 1972; Steven, 1975). Locally large volumes of more silicic ash-flow tuff were subsequently erupted and caused formation of calderas, especially in the San Juan Mountains (central southern Colorado, fig.1). These lavas and ash-flow tuffs are interpreted as eruptive products from underlying batholithic magma chambers (Lipman and others, 1972). In the southern Rocky Mountains these inferred batholiths are characterized by low gravimetric anomalies and exposed epizonal plutons.

Andesitic volcanism is known to be related to plate convergence and subduction, at island or continental-margin active arcs. Increase of alkali contents in igneous rocks across such arcs is characteristic (Rittman, 1953). Study of Cenozoic volcanism through all western United States (Lipman and others, 1972) shows alkali enrichment (especially in K) eastward from the continental margin and suggests that the middle Cenozoic andesitic rocks were related to a subduction system. Correlation of K_2O content (at 60 wt% SiO_2) with depth to the Benioff seismic zone beneath volcanoes of the western United States (Lipman and others, 1972) according to the method of Hatherton and Dickinson (1969) suggests the presence of two subparallel gently-dipping (20°) subduction zones underneath the western United States during early and middle Cenozoic time; the western zone was emerging at the continental margin and the eastern zone was beneath the continental plate.

As middle Tertiary volcanic activity ended, much of the southern Rocky Mountains had been mantled by a volcanic plateau. Late Oligocene to early Miocene time was characterized by a dramatic change in volcanic associations in the southern Rocky Mountains (and in much of the western United States). Volcanism becomes "fundamentally basaltic" (Christiansen and Lipman, 1972) and is accompanied by regional normal faulting and crustal extension. The volcanic associations consist mainly of basaltic lava flows and silicic rocks of lesser volume, including (1) basaltic fields, (2) differentiated basaltic and alkalic fields, and (3) bimodal basalt-rhyolite fields (Christiansen and Lipman, 1972). Such fields are typical of areas characterized by tectonic extension. This change in the tectonic regime of the western United States during late Cenozoic time is interpreted as corresponding to the intersection of the East Pacific Rise with a mid-Tertiary continental margin trench, around

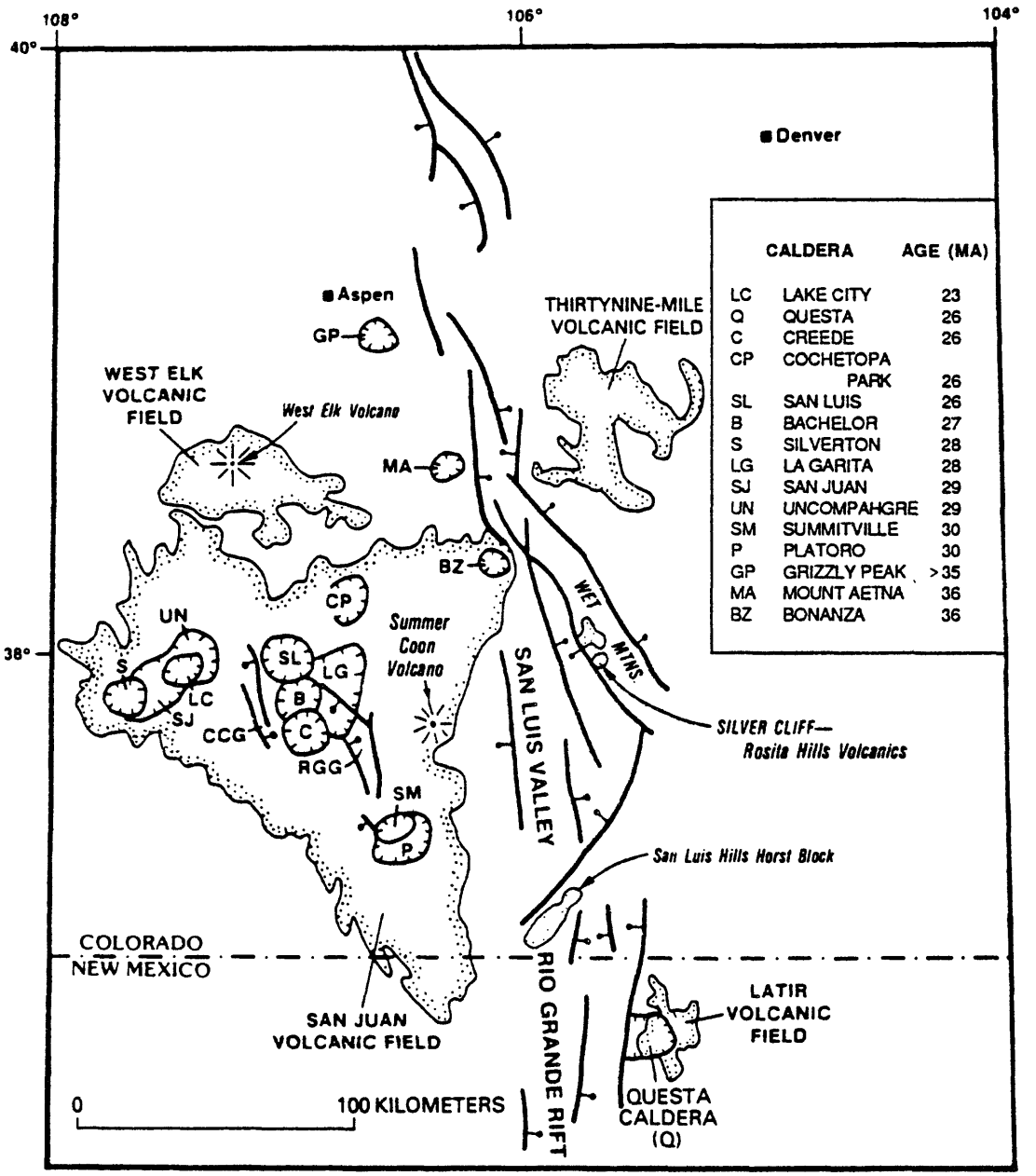

Fig. 1. Index map showing relation of Questa caldera to the Rio Grande Rift and other Oligocene and early Miocene volcanic centers of southern Colorado and northern New Mexico. Modified from Varga and Smith (1984).

30 Ma (Atwater, 1970; Christiansen and Lipman, 1972). The collision resulted in direct contact between the American and western Pacific plates along a right-lateral fault system (the San Andreas fault system).

The extensional regime was characterized by the formation of numerous basins and ranges over the same areas affected by deformation during the Laramide orogeny (Christiansen and Lipman, 1972). In the southern Rocky Mountains, the Rio Grande Rift zone is the dominant feature related to late Cenozoic extension. It extends for more than 800 km, from central Colorado to Mexico, and is 15 to 60 km wide. It consists of en-echelon grabens, bounded on one side, or both, by fault-block mountains (Lipman and Menhert, 1975).

QUESTA MAGMATIC SYSTEM

Questa caldera is part of the Latir volcanic field, one of the largest middle Tertiary volcanic systems in northern New Mexico (Lipman, 1983). The Latir volcanic field is located southeast of the southern Rocky Mountains Tertiary volcanic field defined by Steven (1975); it has been disrupted by late cenozoic extensional faulting, and truncated along its west side by the Rio Grande Rift zone. The Latir field encompasses the time of change from a compressional to an extensional tectonic regime; volcanic activity started in Oligocene time and the volcanic rocks most often directly overly Precambrian metamorphic and plutonic rocks. Before eruption of the Amalia Tuff which caused the formation of Questa caldera, dominantly intermediate composition -- but varying from basaltic to rhyolitic -- lavas and tuffs were erupted from central volcanoes clustered near the area of subsequent caldera collapse (Lipman, 1983). Precaldera volcanism occurred during a relatively short period of time, from 28.5 to 26.5 Ma (Lipman and others, 1986). Four different precaldera volcanic units are recognized by Lipman (1983). Near the base of the section are discontinuous rhyolitic tuff and lava flows of Tetilla Peak. A second unit consists of dominantly intermediate-composition lavas and associated volcaniclastic rocks, which range in composition from olivine basalt to rhyodacite. The third unit, the Latir Peak quartz latite, is found mainly as thick flows and domes in the northeast part of Questa caldera. The last precaldera formation was the comendite of Ortiz Peak, which marks the petrologic evolution of the Questa magmatic system just prior to caldera formation.

Eruption of the Amalia Tuff, 26.5 Ma (Lipman and others, 1986), resulted in formation of Questa caldera. Remnants of the Amalia Tuff have been found as far as 25 km to the northeast of the caldera in the Underwood Lakes area and 45 km to the southwest near the village of Peteca in the Tusas Mountains; its volume has been estimated to more than 200 km^3. It consists of high-silica alkali rhyolite, and is weakly compositionally zoned from alkalic fayalite rhyolite at the bottom to peralkaline rhyolite at the top. This zonation probably reflects a zonation in the magma chamber itself at the time of eruption (Hildreth, 1981). The peralkalinity of the Amalia Tuff makes it unique in the southern Rocky Mountains. Mildly peralkaline rhyolitic lava flows, associated with eruption of the Amalia Tuff and petrologically similar to it, are locally preserved north and south of the caldera.

Rocks of the Latir volcanic field were subsequently overlain by formations of the Santa Fe group. These formations consist mainly of

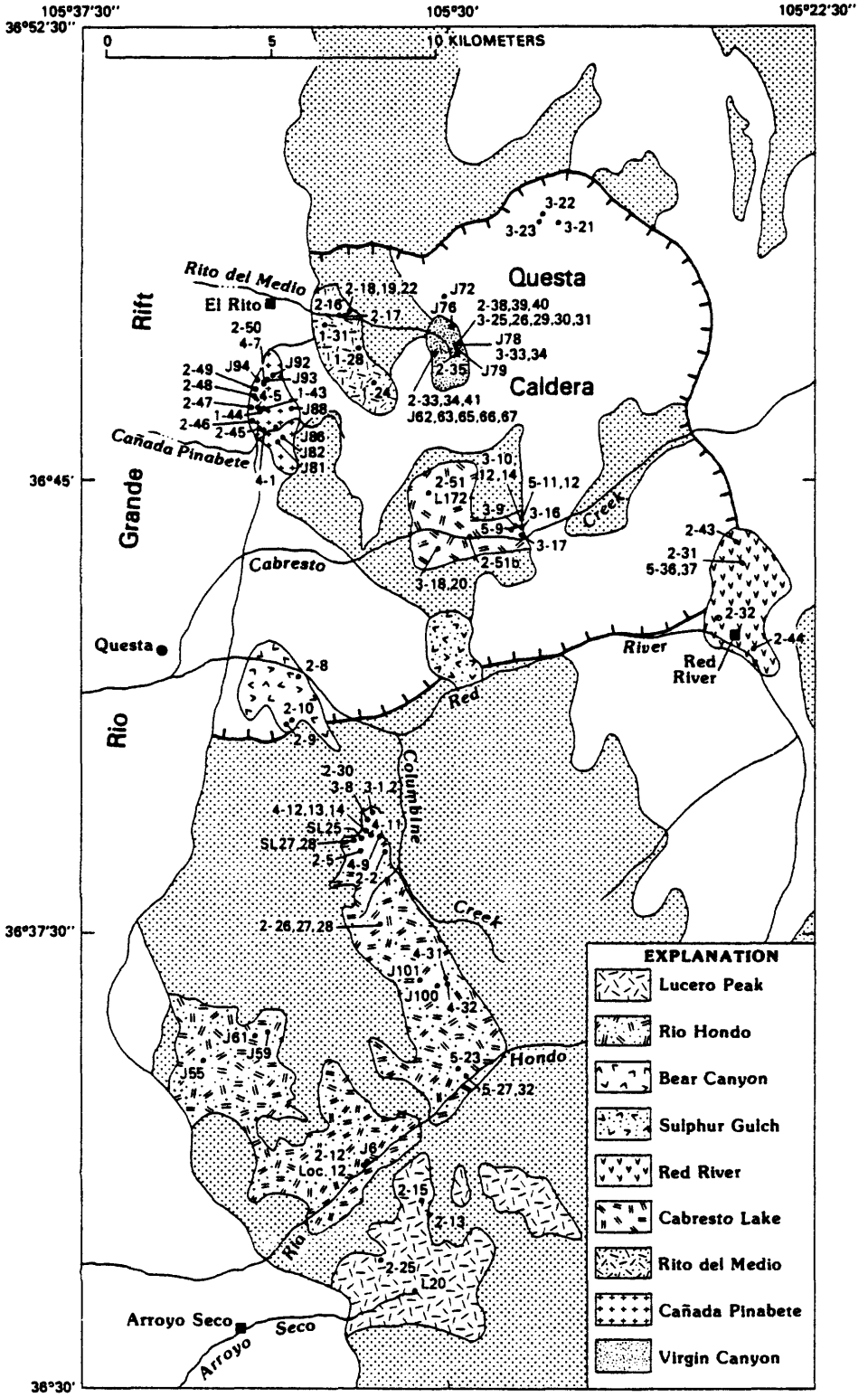

Fig. 2. Generalized geologic map of the Questa area showing distribution of post-caldera plutons and sample locations. Geology from Reed and others (1983) and Lipman and Reed (1986). Sample numbers shortened for clarity, i.e. 2-10 and J78 represent, respectively, 82QC10 and Q83J78. Stippled area underlain by Precambrian rocks; unpattered area by pre-caldera volcanic rocks, Amalia Tuff, and rift sediments.

sedimentary rocks, formed largely of Precambrian detritus, overlain by unconsolidated Pleistocene fan deposits. Volcaniclastic components of the sedimentary sequence include much detritus of the Latir volcanic field. Interlayered with these sedimentary formations are basalt flows, which range in composition from basanite to silicic alkalic basalt.

Subsequent to the formation of Questa caldera, nine intrusive bodies of granitic composition were emplaced within a period of about 4 million years (26 to 22 Ma), within and outside the caldera, over an area of 20 by 35 km (fig. 2). Concurrent with this volcanic and plutonic activity, was the opening of the Rio Grande Rift, which started 26-28 Ma. Extensional faulting associated with the rift has controlled the structure of Questa caldera and associated volcanic and plutonic rocks. Post-Miocene tilting to the northeast has exposed deeper rocks to the south (Rio Hondo mesozonal pluton) and shallower rocks to the north (volcanic rocks of the Latir volcanic field and epizonal intracaldera plutons).

The granitic rocks associated with Questa caldera are thought to represent high-level components of a large composite batholith, interpreted as the source for the Amalia Tuff and cogenetic volcanic rocks (Lipman, 1983). This is supported by regional gravity data (Cordell, 1978).

Concurrent studies have been done on this well-exposed complex which exhibits relations between volcanic and plutonic cogenetic rocks. Areal geology has been mapped by Reed, Lipman, and Robertson (1983). The chronology of the nine bodies is somewhat difficult to determine, because they were emplaced within a short period of time (about 4 m.y.) and the later intrusions may well have reset the ages of the earlier ones. Five plutons were emplaced at about 25-26 Ma, just after eruption of the Amalia Tuff. After a hiatus of 2-3 m.y., the four other plutons were emplaced at 21-23 Ma (Lipman and others, 1986). Among the older plutons, four are located inside the caldera and are high-level subvolcanic intrusions interpreted as related to the resurgence of the caldera; the larger and more mafic Rio Hondo pluton was emplaced south of the caldera.

Paleomagnetic data have helped to establish the chronology of the older intrusions. The first two bodies intruded after eruption of the Amalia Tuff were the Virgin Canyon and Canada Pinabete plutons, located in the northern part of the caldera. Both plutons underwent the major tilting related to the Rio Grande Rift which affected the precaldera volcanics and the Amalia Tuff (Hagstrum and others, 1982; Hagstrum and Lipman, 1986). Both plutons consist mainly of fine-to-medium-grained metaluminous biotite granite, but are bordered on their northern contacts by a 20-100 m thick "screen" of peralkaline granite containing sodic pyroxene and alkali amphibole. The Virgin Canyon pluton has been dated at about 26 Ma (Lipman and others, 1986); because of similarity of structure and petrographic units, the Canada Pinabete pluton is also interpreted to have been emplaced at about 26 Ma.

The Rito del Medio pluton was emplaced next, and lies spatially between the Virgin Canyon and Canada Pinabete plutons; it has been dated at 25-26 Ma (Lipman and others, 1986). Paleomagnetic data show that this body is less tilted than the Virgin Canyon and Canada Pinabete plutons, and therefore indicate that it is slightly younger. The Rito del Medio pluton consists

essentially of quartz-alkali feldspar granite, with minor biotite and muscovite. Its most distinctive feature is the presence of miarolitic cavities (up to 6 cm across) filled with quartz, alkali feldspar, muscovite, and accessory fluorite and hematite.

The Cabresto Lake pluton is also related to resurgence of the caldera. However it differs from the more silicic northern intracaldera plutons of Virgin Canyon, Canada Pinabete, and Rito del Medio, in having characteristics that are transitional between them and the more mafic Rio Hondo pluton to the south. The main unit of the pluton is an amphibole-biotite granite, characterized by the presence of small dark enclaves. The Cabresto Lake pluton has yielded discordant K-Ar and fission track ages of between 24.6 and 21.5 Ma, which are interpreted as recording a time of emplacement at about 25-26 Ma, with resetting at 22-23 Ma associated with emplacement of intrusions along the southern caldera margin (Lipman and others, 1986).

The Rio Hondo pluton, emplaced south of Questa caldera, displays features of a deeper intrusion and grades from biotite-amphibole granodiorite in lower and more southerly parts of the pluton, to biotite-bearing silicic granite near the roof of the pluton and, in greater volume, to the north in the canyon of Columbine Creek. The granodiorite contains large alkali feldspar megacrysts and, in certain areas, numerous dark microgranular enclaves. The pluton is cut by a northeast-trending dike swarm of rhyolitic to basaltic composition, with rhyolitic to quartz latite compositions being most common. The Rio Hondo pluton has also yielded discordant ages between 26 and 19 Ma (Lipman and others, 1986). Rb/Sr mineral isochrons (C. M. Johnson, written communication, 1983) give an age of 25.7 $\pm$ 2 Ma. These data are interpreted as indicating primary cooling of the pluton at 25-26 Ma, and resetting associated with emplacement of the younger intrusions at 21-23 Ma.

Among the four younger intrusions, three are located along the south caldera margin: the Bear Canyon and Sulphur Gulch plutons and the Red River intrusive complex. They are thought to be parts of a ring intrusion, and postdate caldera collapse (Lipman, 1983; Lipman and others, 1986). These plutons were probably emplaced at about 22-23 Ma (Lipman and others, 1986) and are thought to have caused partial resetting of K-Ar ages for the Cabresto Lake and Rio Hondo plutons. Study of these caldera ring intrusions is somewhat difficult because of alteration and poor exposure. They are pyritized and the Sulphur Gulch pluton hosts a major molybdenum deposit.

The Lucero Peak pluton is the youngest intrusion of the Questa magmatic system (21-22 Ma; Lipman and others, 1986). It crops out just to the southeast of the Rio Hondo pluton but lacks the cross-cutting dikes typical of the Rio Hondo pluton; this indicates younger emplacement for the Lucero Peak pluton, in agreement with geochronologic data. The Lucero Peak pluton consists of medium-grained biotite granite, which is locally altered and contains pyrite and molybdenite.

THIS STUDY

The present study is concerned with the petrology and mineralogy of the granitic plutons, based on petrographic study and extensive electron microprobe analyses of mineral phases, principally opaque oxide and mafic

silicate minerals. Rock chemistry is also briefly presented. Further interpretation of whole-rock chemical and isotopic variations in both plutonic and cogenetic volcanic rocks can be found in Johnson (1986).

The granitic rocks of the Questa area crop out as nine discrete plutons, emplaced in an area of only 20 X 35 km, over an interval of about 4 m.y. (Lipman and others, 1986). Viewed as samples of a magma chamber of batholithic dimensions (Lipman, 1983 and 1984), it was anticipated that there might be similarities and unifying trends in the mineralogical characteristics of the plutons. On the other hand, considering numerous distinct differences in the character of the plutons in outcrop and the shallow levels of magma emplacement, it was expected that there would be distinctions of mineral assemblage and mineral chemistry among, and even within, plutons.

Based on numerous previous studies of granitic rocks, it was decided that study of the mafic silicate phases could be expected to give significant insight into the similarities and distinctions among the plutons. Moreover, even though Fe,Ti-oxide minerals are typically reequilibrated in granitic rocks, preliminary microscopic studies indicated that, in association with sphene, the relations among the opaque oxide minerals were sufficiently varied and complex to make their study significant.

The representative samples for which data are reported here were chosen from a much larger sample collection. Whole-rock chemistry was obtained for more than 140 plutonic rock samples and more than 200 samples were studied in thin section.

page 10 follows

CHAPTER I

Petrography

and

Chemistry

PART I: PETROGRAPHY

1. VIRGIN CANYON

The Virgin Canyon pluton is the easternmost body among the three northern intracaldera plutons and outcrops over an area of about 0.3 km^2, in Virgin Canyon. Most of the outcrop is on the northeast side of the canyon (west flank of Venado Peak), but outcrop is also found across the canyon on a spur that extends northwest from Cabresto Peak. Among the four intracaldera plutons, the Virgin Canyon pluton is the structurally highest intrusion. It intrudes Precambrian rocks and Tertiary volcanic rocks of the caldera floor. Emplacement of the intracaldera plutons is interpreted to be related to the postcollapse resurgence of the caldera, subsequent to the eruption of the Amalia Tuff (Lipman, 1983). K-Ar sanidine and fission-track zircon ages are concordant at about 26 Ma for this pluton (Lipman and others, 1986) and paleomagnetic data show that it has been tilted to the northeast (Hagstrum and Lipman, 1986).

Three units constitute the Virgin Canyon pluton. Cropping out in the north part of the intrusion on Venado Peak is peralkaline granite which contains sodic pyroxene and alkali amphibole. Against Tertiary andesite, this granite has a porphyritic texture, with a fine-grained groundmass; it grades to a more equigranular rock to the south, away from the contact. A second unit, early metaluminous biotite-bearing granite, crops out south and west of the peralkaline unit. The contact between these two units is abrupt, occuring beneath a meter width of talus, and is presumed to be intrusive. The texture of the early metaluminous granite changes from porphyritic near the peralkaline unit, to equigranular towards the core of the pluton. This granite has crystallized later (if only by a few thousand years) than the peralkaline granite. The third unit, a later metaluminous biotite-bearing granite, intrudes the early metaluminous granite. As evidenced by interfingering relations, this later granite was intruded while the early granite was only partly crystallized. Apparently, small adjustments during the emplacement and crystallization process have led to a sequence of auto-intrusive events.

A 5-m-wide rhyolite dike cuts the peralkaline unit of the pluton on the southwest flank of Venado Peak.

Petrography

The peralkaline granite is characterized by its texture and mineralogy. It grades from very fine-grained porphyritic at the rim of the pluton (Plate I.1, a), to almost seriate near the contact with the early metaluminous granite (Plate I.1, b). Study of samples 83QC30, 83QC29, and 82QC38 representing a section on the flank of Venado Peak that extends from the contact with Tertiary andesites to the contact with the early metaluminous granite, shows that the proportion of phenocrysts and the grain size of the groundmass increase away from the border of the intrusion (Table I.1.1).

The most abundant phases are alkali feldspar and quartz (Table I.1.1); each forms phenocrysts and is a major constituent of the groundmass. As phenocrysts, both display dominantly euhedral shapes, with irregular border zones against the groundmass; these zones are especially well developed on alkali feldspar. Thus, the phenocrysts finished crystallizing while the groundmass was solidifying. Quartz phenocrysts are roughly equant, up to 12 mm across, but may contain embayments filled with groundmass minerals. Their extinction is often undulatory, especially at the margin of the unit. Alkali feldspar phenocrysts are elongated, and up to 20 mm long. They are micromesoperthitic, and boundaries between different crystals are often outlined by small albite grains; rarely they appear to be zoned. Plagioclase is rare and mostly occurs as a groundmass phase, although exceptional phenocrysts can be found. Its mode increases toward the margin of the unit.

Alkali amphibole and sodic pyroxene are the predominant mafic silicate phases. These primary minerals crystallized over a considerable span of time, as they can be found both as euhedral to subhedral phenocrysts or microphenocrysts, and as anhedral grains in the groundmass. Alkali amphibole phenocrysts are up to 4mm long, the sodic pyroxene phenocrysts up to 2.5 mm. The earlier phase is probably alkali amphibole which is often more euhedral than the sodic pyroxene and may be partly rimmed by it (Plate III.1, c). Alkali amphibole is commonly zoned, with altered brown richteritic cores surrounded by clear blue arfvedsonitic rims (Plate III.1, a). Tetrasilicic mica occurs as a reaction product within the richteritic amphibole cores. It may occur as single laths or as mats almost replacing the entire core (Plate III.1, b and c). Aggregates consisting mostly of tetrasilicic mica can also be found, associated with biotite, opaque oxide minerals, and minor arfvedsonite and sodic pyroxene (Plate III.1, d). Modal alkali amphibole content increases from 1 percent at the border of the pluton (83QC30), to more than 2 percent towards the metaluminous unit (82QC38, Table I.1.1). Sodic pyroxene is almost always fresh, and decreases in amount toward the core of the intrusion where, near the contact with the metaluminous granite, it is a trace constituent (Table I.1.1). Biotite is a rare unstable mafic phase in the peralkaline facies, and appears either as phenocrysts or associated with the tetrasilicic mica aggregates.

Accessory phases are diverse, but always amount to less than 2 modal percent (Table I.1.1), opaque oxide minerals being dominant. They include the typical accessory minerals of granitic rocks, apatite, zircon, and sphene. Fluorite is often present. The peralkaline facies is also characterized by the rare-earth-bearing phase chevkinite-perrierite. Magnetite and ilmenite are found in the groundmass, as well as forming small phenocrysts (up to 1.5 mm across). Notable is the occurrence of sphene; near the margin of the unit (83QC30 and 83QC29) sphene crystallized early and later reacted to ilmenite; near the contact with the early metaluminous granite (82QC38) it crystallized late and formed irregular rims around earlier ilmenite crystals.

Plotted in the QAP diagram (fig. I.1), this unit falls in the alkali-feldspar granite field (Streckeisen, 1976). Alkali feldspar being mesoperthitic and the essential feldspar present, it is a hypersolvus granite as defined by Bonin (1972, 1977).

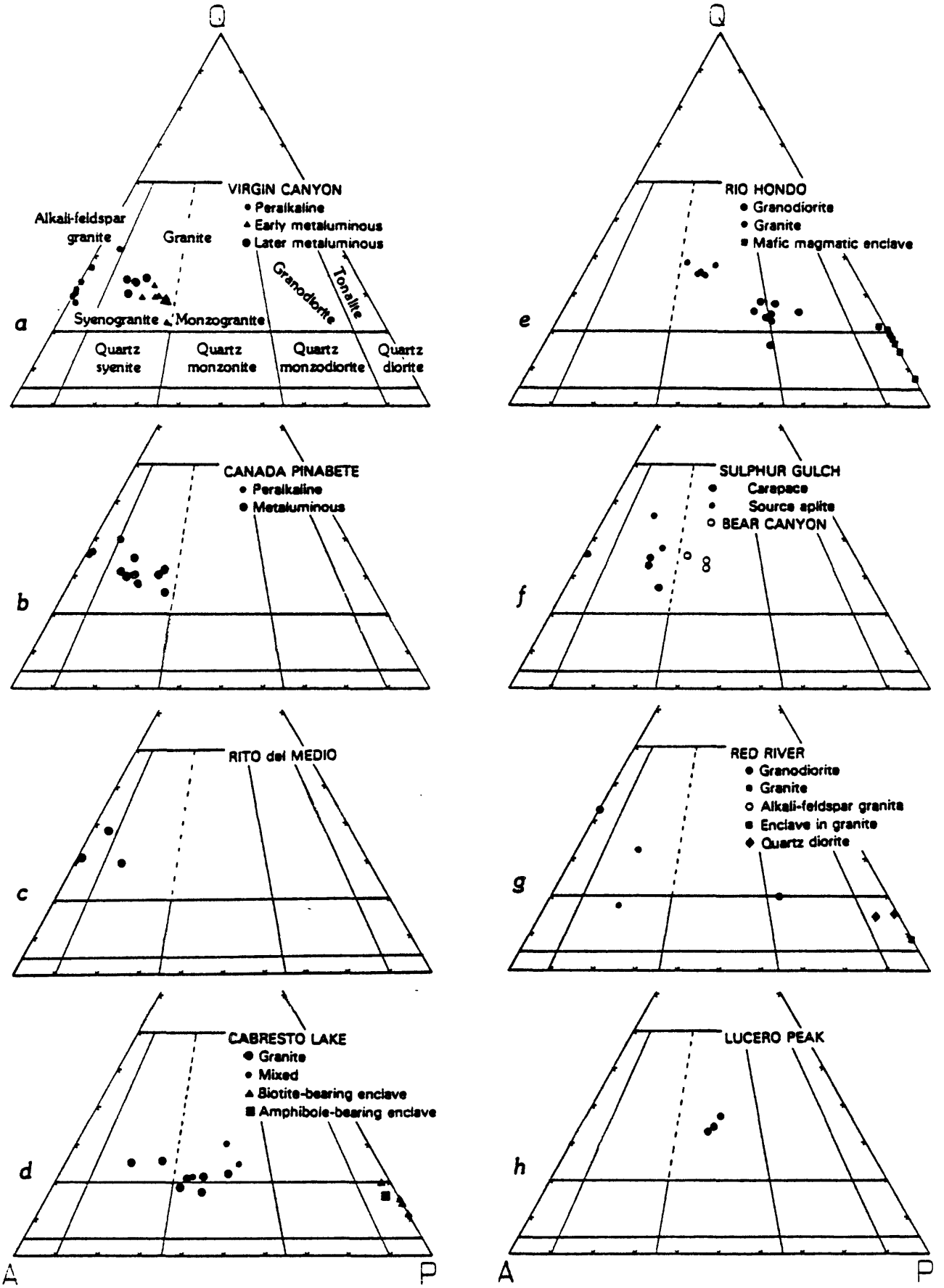

Fig. I.1. QAP diagrams (Streckeisen, 1976) for the individual Questa plutons.

Table I.1: Modal analyses of samples from the VIRGIN CANYON pluton (counted in thin section, unless otherwise noted).

Table I.1.1: Peralkaline granite.

Sample number	82QC34	82QC38	83QC29	83QC30	Q83J62	Q83J63	Q83J67
Quartz	29.6	28.2	35.0	40.1	31.9	29.5	26.8
Alkali feldspar	64.3	67.7	59.1	51.0	64.3	66.4	68.4
Plagioclase	0.1	0.0	0.65	4.7	0.1	0.0	1.5
Acmite	1.9	0.3	1.7	0.9	1.4	0.0	0.7
Arfvedsonite	1.2	2.2	1.9	1.5	1.1	2.3	1.2
Opaque minerals	1.1	1.1	0.9	1.2	0.95	1.1	0.9
Accessories	0.6*	0.5	0.75#	0.6	0.25	0.7	0.5@
Phenocrysts	51.8	-	47.0	39.8	51.8	-	57.2
Groundmass	48.2	-	53.0	60.2	48.2	-	42.8
Size&	0.05-0.15	0.2-1.8	0.05-0.1	$\leq$0.05	0.05-0.15	0.1-2.2	0.05-0.15

* Accessory minerals + 0.4 vol% tetrasilicic mica.
\# Accessory minerals + 0.2 vol% biotite + 0.3 vol% tetrasilicic mica.
@ Accessory minerals + 0.3 vol% tetrasilicic mica.
& range or size of groundmass.

Table I.1.2: Early metaluminous granite.

Sample number	82QC33*	82QC39	82QC40	82QC41	83QC25	83QC34	Q83J65	Q83J66
Quartz	28.3	27.5	28.2	25.7	28.2	31.1	26.9	20.8
Alkali feldspar	52.7	46.3	48.1	45.2	49.4	48.1	47.9	48.6
Plagioclase	16.2	21.5	19.7	21.7	19.3	17.4	21.7	24.5
Biotite	1.3	2.4	1.8	3.6	1.5	1.9	2.0	3.2
Opaque minerals	1.1	1.5	1.4	2.0	1.2	0.75	1.1	1.5
Accessories	0.4	0.8	0.8	1.8	0.4	0.75	0.4	1.4

* Quartz, alkali feldspar, and plagioclase counted on stained slabs.

Table I.1.3: Later metaluminous granite.

Sample number	82QC35	83QC33	Q83J78	Q83J79
Quartz	33.1	32.9	32.4	29.0
Alkali feldspar	49.2	54.1	52.5	55.2
Plagioclase	14.9	10.2	13.0	12.3
Biotite	1.2	1.2	1.0	1.4
Opaque minerals	0.8	1.2	0.6	1.7
Accessories	0.8	0.4	0.5	0.4

The texture of the early metaluminous granite grades from porphyritic at the contact with the peralkaline unit (Plate I.1, c), to more equigranular away from the contact (Plate I.1, d), showing that the porphyritic texture is due to chilling against the peralkaline granite. At the contact with the later metaluminous granite, there is a margin, a few centimeters thick, of a finer grained facies composed essentially of quartz and alkali feldspar and in which thin plates of biotite form polygonal arrangements (Plate III.2, b).

The largest and most abundant phases are alkali feldspar, plagioclase, and quartz (Table I.1.2), which form phenocrysts in the porphyritic facies. Euhedral to subhedral plagioclase is often zoned; the rims are often clear, but the cores are altered. Alkali feldspar started crystallizing at the same time as the other felsic minerals, but was probably the last phase to end its crystallization, because it is often quite anhedral. It is perthitic, although less so than in the peralkaline granite. Alkali feldspar may mantle plagioclase.

Biotite, the only mafic mineral present, forms 1.3 to 3.4 volume percent of the rock. In the porphyritic facies it forms small phenocrysts. It is typically brown or greenish-brown, often with a distinct darker core surrounded by a lighter rim (Plate III.2, a). The accessory minerals are more abundant than in the peralkaline granite (1.8 to 3.8 volume percent). Magnetite and ilmenite are most abundant; sphene appears as small euhedral crystals and is nowhere reacted to ilmenite; apatite, zircon, and fluorite are common; chevkinite is rare.

This unit falls in the granite field and syenogranite subfield of the Streckeisen diagram (fig. I.1; Streckeisen, 1976). This granite is subsolvus in the sense of Bonin (1972, 1977), because it contains plagioclase as well as alkali feldspar.

The texture of the later metaluminous granite is medium-grained equigranular, with small vugs a few millimeters across filled with quartz, alkali feldspar, opaque oxide minerals, muscovite, fluorite, and clay minerals; locally the texture is micropegmatitic. The contact with the early metaluminous unit is characterized by a margin, a few centimeters thick, of finer grained granite containing almost no mafic minerals. This fine-grained margin is thinner than that which characterizes the early metaluminous granite in its contact with this unit.

The mineralogy is the same as that in the early metaluminous granite, but the proportions of phases are rather different (Table I.1.3). This unit contains less plagioclase (10 to 15 volume percent) and more quartz and alkali feldspar. The biotite content is about 1 percent and accessory minerals form 1 to 2 volume percent of the rock. As in the early metaluminous granite, biotite is distinctly zoned. Clay minerals are notable and form pale yellow aggregates sparsely distributed in the rock (<0.5 percent), filling some of the cavitites. Accessory minerals are opaque oxide minerals (0.6 to 1.7 vol%), sphene (sometimes reacted to ilmenite), apatite, zircon, fluorite, allanite, and chevkinite.

This unit is also a syenogranite (fig. I.1; Streckeisen, 1976), and plots between the peralkaline and early metaluminous granites. It is a subsolvus granite in the sense of Bonin (1972, 1977).

Table I.2: Modal analyses of samples from the CANADA PINABETE pluton (counted in thin section, unless otherwise noted).

Table I.2.1: Peralkaline granite.

Sample number	82QC49	Q83J94	84QC7
Quartz	38.4	35.0	34.5
Alkali feldspar	52.3	60.1	60.0
Plagioclase	6.0	1.2	0.9
Arfvedsonite	2.6	2.0	3.8
Opaque minerals	0.4	0.85	0.5
Accessories	0.3*	0.85#	0.3*
Phenocrysts	41.2	45.0	45.3
Groundmass	58.8	55.0	54.7

* Accessory minerals + sodic pyroxene.
\# Accessory minerals + tetrasilicic mica.

Table I.2.2: Metaluminous granite.

Sample number	82QC47	82QC48*	Q83J81*	Q83J82	Q83J87*	Q83J88*	Q83J93*	84QC2
Quartz	29.3	29.7	30.4	26.8	29.8	34.0	25.2	30.9
Alkali feldspar	54.9	47.3	56.9	53.7	54.5	52.1	49.6	47.1
Plagioclase	12.7	19.4	10.4	15.6	13.8	11.8	23.1	19.9
Biotite	1.6	3.0#	1.3	2.0	0.7	1.8	)	0.9
Opaque minerals	0.7	0.3	0.65	1.3	1.1	0.2	2.1	0.7
Accessories	0.8	0.3	0.35	0.6	0.1	0.1	)	0.5

* Quartz, alkali feldspar, and plagioclase counted on stained slabs.
\# Biotite + amphibole.

Table I.3: Modal analyses of samples from the RITO del MEDIO pluton (counted in thin section, unless otherwise noted).

Sample number	81S24	82QC17*	82QC18*	82QC22
Quartz	28.8	37.8	37.7	30.2
Alkali feldspar	57.5	57.2	56.8	65.6
Plagioclase	11.1	3.6	3.5	0.8
Biotite	1.6	)	)	1.4
Opaque minerals	0.75	1.4#	2.0#	1.5
Accessories	0.25	)	)	0.5

* Modal analyses on stained slabs.
\# Biotite + muscovite + opaque minerals + accessories, as indicated by use of)'s.

2. CANADA PINABETE

The Canada Pinabete pluton is exposed along the western front of the Sangre de Cristo mountains. It crops out 1.5 km north and south of the Canada Pinabete, over an area of about 3 km^2. The pluton intrudes Precambrian schists and quartzites and Tertiary volcanoclastic sedimentary rocks of the caldera floor and is interpreted to be related to postcollapse resurgence of the caldera (Lipman, 1983; Lipman and others, 1986). This pluton has not been dated, but from petrographic and structural similarities with the Virgin Canyon pluton, its age is inferred to be about 26 Ma. The Canada Pinabete pluton probably represents the same intrusive sequence as the Virgin Canyon pluton, the main argument being that the Canada Pinabete pluton has been tilted to the northeast like the Virgin Canyon pluton (Hagstrum and Lipman, 1986), while the other intracaldera plutons have not been.

Because of the relatively low elevation (2400 to 2900 m), bushy vegetation covers most of the pluton and contacts are not seen. The main facies of the intrusion is a very fine-grained, light-coloured biotite granite, which becomes coarser and richer in biotite to the north. At the north end of the pluton, one finds scattered outcrops of peralkaline granite porphyry containing alkali amphibole and rare sodic pyroxene; this unit is indistinguishable from the peralkaline granite of Virgin Canyon. Although no contact can be seen between the biotite granite and this peralkaline unit, it can be inferred from a sharp break in topography.

Petrography

The texture of the peralkaline granite is porphyritic with a very fine-grained groundmass (Plate I.1, e).

Quartz and alkali feldspar phenocrysts are euhedral, with irregular rims against the groundmass. The alkali feldspar is micromesoperthitic and albite grains are common between grains. Arfvedsonitic amphibole forms subhedral, fresh phenocrysts, ingrequently containing tetrasilicic mica. Rarely, the association tetrasilicic mica + biotite + arfvedsonite + quartz can be found. The groundmass contains the same phases, as well as sodic pyroxene, opaque oxides and other accessory minerals. Plagioclase is rare and exists essentially as a groundmass phase. Sodic pyroxene is rare and can be considered an accessory mineral, along with sphene, apatite, zircon, and fluorite. Sphene has reacted to opaque oxide minerals, which can also form small phenocrysts.

This granite is identical to the peralkaline granite of Virgin Canyon, except for the amount of sodic pyroxene. Based on the QAP diagram (Streckeisen, 1976), it is an alkali-feldspar granite (Table I.2.1, fig. I.1); it is a hypersolvus granite as defined by Bonin (1972, 1977).

The texture of the predominant biotite granite is mostly fine-grained equigranular, often granophyric (Plate I.1, f), and the rock resembles the later metaluminous granite of Virgin Canyon. Miarolitic cavities (Plate I.1, f) filled with quartz, alkali feldspar, opaque oxides, muscovite, and clay

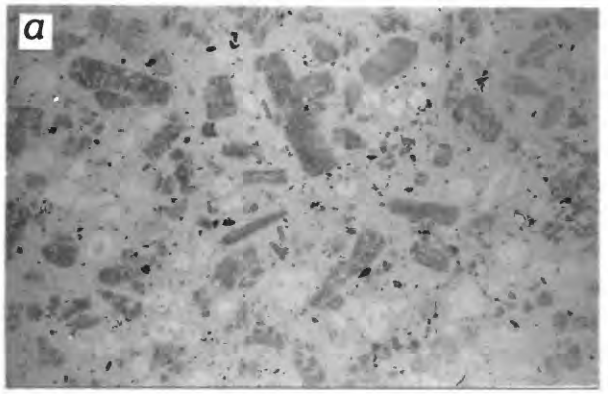
a

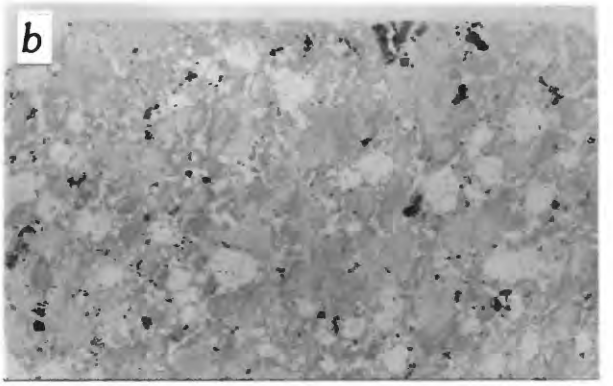
b

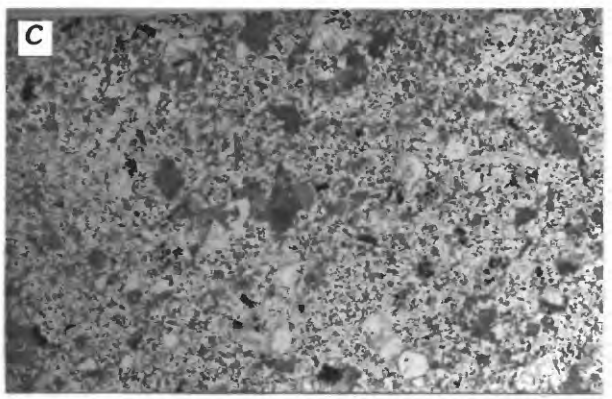
c

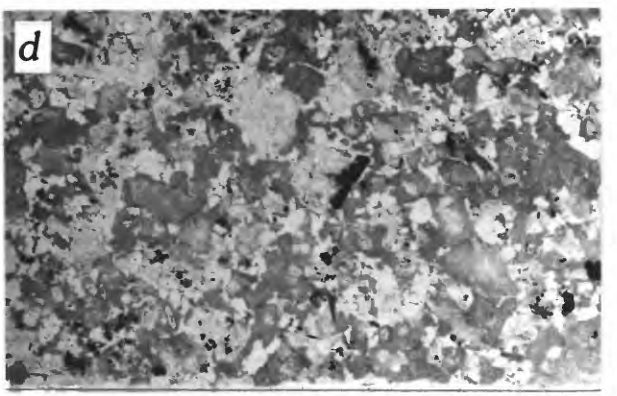
d

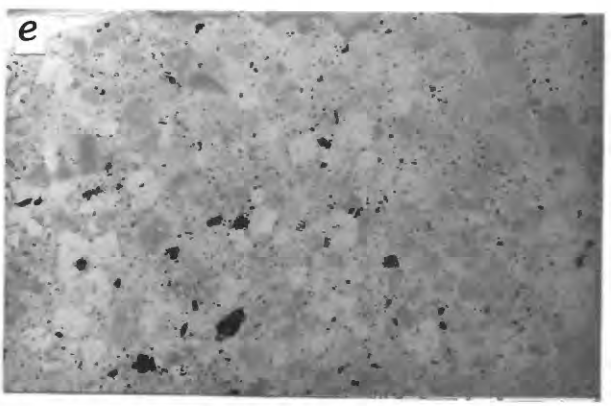
e

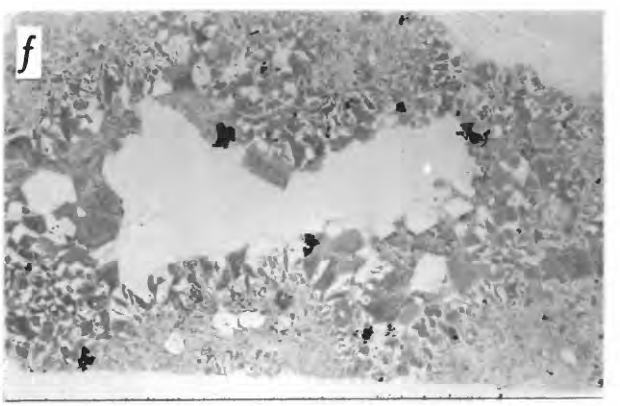
f

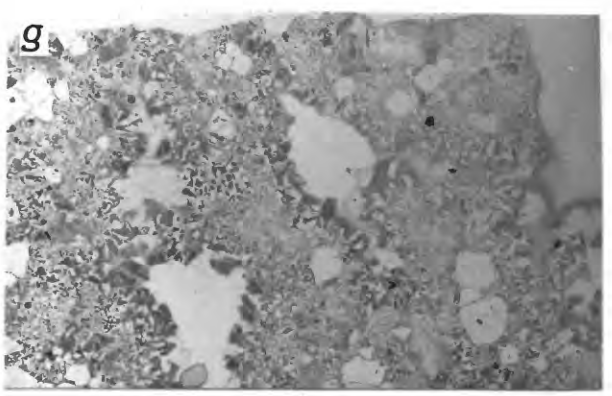
g

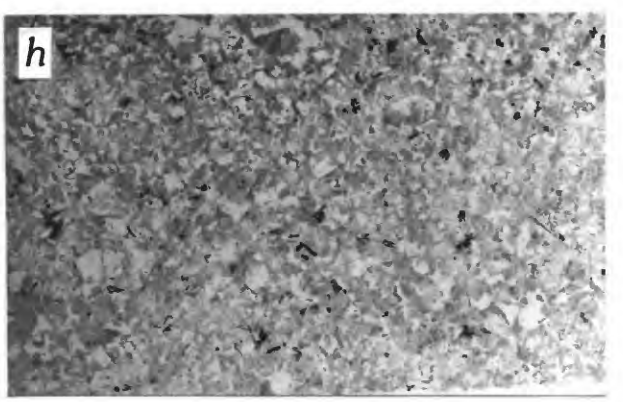
h

minerals, are characteristic of some localities. Northwards, the granite becomes medium-grained, and does not contain cavities; some of the coarser grained samples in this area resemble the porphyritic facies of the early metaluminous granite in Virgin Canyon.

The main phases are alkali feldspar, quartz, and plagioclase (Table I.2.2). The alkali feldspar is microperthitic, altered, and may surround plagioclase, which is sometimes zoned. Biotite, the typical mafic mineral, often displays dark irregular cores and lighter rims. Coarse muscovite grains are common in the cavities, and finer grained muscovite can be found in the rock itself (sometimes as radiating aggregates). In the coarser facies to the north, amphibole locally occurs with biotite. The abundance of the accessory minerals is similar to that in the peralkaline granite; apatite, sphene, zircon, fluorite, chevkinite, and opaque oxides are common, while allanite, chevkinite, euxinite, and monazite are rarer phases. Davidite is well represented in one sample.

This rock falls in the syenogranite subfield of the granite field of the QAP diagram (fig. I.1; Streckeisen, 1976); it is a subsolvus granite as defined by Bonin (1972, 1977).

PLATE I.1: Textures of granitic rocks from the Virgin Canyon, Canada Pinabete, and Rito del Medio plutons. Thin sections 20 X 40 mm.

(a) Peralkaline granite of Virgin Canyon. Porphyritic facies from near contact with wall rock andesite; sample 82L62A.

(b) Peralkaline granite of Virgin Canyon. Seriate facies from near contact with early metaluminous granite; sample 82QC38.

(c) Early metaluminous granite of Virgin Canyon. Porphyritic facies from near contact with peralkaline granite; sample Q83J65.

(d) Early metaluminous granite of Virgin Canyon. Typical more equigranular facies; sample Q83J66.

(e) Peralkaline granite of Canada Pinabete. Porphyritic texture with large dark aggregates of alkali amphibole; sample 84QC7.

(f) Metaluminous granite of Canada Pinabete. Granophyric facies with large miarolitic cavity from close to border of pluton; black grains on sides of cavity are hematite intergrown with ilmenorutile; sample 82QC45.

(g) Granite of Rito del Medio. Granophyric texture with miarolitic cavities; sample 81S28.

(h) Granite of Rito del Medio. Fine-grained texture typical of the contaminated border facies; sample 82QC22.

3. RITO del MEDIO

The Rito del Medio pluton, one of the three northern intracaldera plutons, is emplaced spatially west of the Virgin Canyon pluton and north of the Canada Pinabete pluton. It is exposed at the range front, both north and south of the Rito del Medio, over an area of about 3 km^2. The pluton intrudes Precambrian schists and quartzites of the caldera floor; it is interpreted as being emplaced during the resurgence of the caldera (Lipman, 1983). K-Ar dating gives an age of 25-26 Ma (Lipman and others, 1986). Paleomagnetic data indicate that it is not tilted like the Virgin Canyon and Canada Pinabete bodies, showing that its emplacement probably followed the structural disruption related to the Rio Grande Rift (Hagstrum and others, 1982; Hagstrum and Lipman, 1986).

The granite of Rito del Medio is quite homogeneous. Only close to the sharp roof contact with Precambrian rocks does it show variation in texture. There, within a zone several meters wide, it may become irregularly richer in quartz or biotite, and may be characterized by the presence of pegmatite and aplitic dikes. Textures reminiscent of unidirectional solidification textures (Shannon and others, 1982) are locally present.

Petrography

The texture of the Rito del Medio granite is medium- to coarse-grained equigranular, commonly granophyric (Plate I.1, g). Characteristic miarolitic cavities, up to 6 cm, but typically less than 1 cm across, are filled with quartz, alkali feldspar, and muscovite; fluorite and opaque oxides are common but less abundant.

Quartz and feldspars form at least 96.5 volume percent of the rock (Table I.3). Quartz is an earlier phase than alkali feldspar, which is microperthitic and often altered; plagioclase is not abundant. The predominant mafic phases are biotite and muscovite. Biotite is often in small irregularly zoned crystals, muscovite is common in the cavities, but also occurs as radiating aggregates or as inclusions in alkali feldspar. The most abundant accessory minerals are opaque oxides; others are sphene (often reacted to ilmenite), zircon, apatite, and fluorite; rare chevkinite, monazite, and thorite occur in vugs.

Samples with a granophyric texture contain more biotite, while those with an equigranular texture contain more muscovite. Near the margin of the pluton, samples richer in biotite contain no muscovite, and biotite occurs as thin elongate plates (Plate I.1, h). Such samples are also characterized by abundant euhedral sphene crystals.

This rock is an alkali-feldspar granite (fig. I.1), as defined by Streckeisen (1976); it is a hypersolvus granite in the sense of Bonin (1972, 1977).

4. CABRESTO LAKE

This pluton is located essentially north of Cabresto Creek, in the Cabresto Lake area, spatially between the three northern intracaldera plutons and the intrusions along the south caldera ring fracture. It is exposed over an area of about 1.75 km^2. The Cabresto Lake pluton is one of the four intracaldera intrusions emplaced during the resurgence of the caldera (Lipman, 1983). It mainly intrudes Precambrian schists and quartzites of the caldera floor (Reed and others, 1983). This intrusion has yielded discordant F-T and K-Ar ages of between 24.6 and 21.45 Ma. These data are interpreted as recording initial emplacement and cooling (at about 25-26 Ma), then reheating and partial resetting (at about 22-23 Ma) related to the emplacement of intrusions along the southern caldera margin (Lipman and others, 1986). Paleomagnetic data show that the pluton is not tilted (Hagstrum and Lipman, 1986), indicating that this intrusion is younger than the Virgin Canyon and Canada Pinabete plutons.

The Cabresto Lake pluton consists mainly of coarse-grained amphibole-biotite granite, with a porphyritic tendancy (Plate I.2, a). On the edges of the intrusion (especially the Weary Willy mine, west of Italian Canyon), the rock is finer grained and porphyritic (Plate I.2, b). This facies is a border phase (an apophysis?) of the intrusion. Many very fine-grained, angular-shaped xenoliths indicate the proximity of the country rocks. In the same area, west of Italian Canyon, the granite is heterogeneous, probably due to uncomplete mixing between the granitic magma itself and a more mafic magma (Plate I.2, c). In this "mixed unit", the texture remains fine-grained porphyritic; rapakivi feldspars and quartz xenocrysts surrounded by mafic silicates are typical. However, all intermediates are found in the mixed unit between light-colored and darker colored monzogranite. Another feature of the Cabresto Lake pluton is the presence of numerous, varied enclaves, which will be described in the discussion of petrography.

A few late aplite dikes cut the intrusion, especially around Cabresto Lake.

Petrography

The texture of the granitic unit is coarse-grained, with a porphyritic tendency (Plate I.2, a); crystal sizes vary from 1 to 10 mm. The dominant minerals are alkali feldspar, plagioclase, and quartz (Table I.4.1); mafic minerals constitute 6 to 8 volume percent in the typical facies, 2 to 3 percent in the border facies.

Alkali feldspars are microperthitic and altered; they can be mantled by plagioclase (rapakivi texture). Alkali feldspar crystallized quite early as large subhedral crystals, but ended crystallization last as small grains. Quartz finished crystallizing before alkali feldspar. Plagioclase is euhedral to subhedral, often zoned, mostly longer than 5 mm, and often has altered cores.

Table I.4: Modal analyses of samples from the CABRESTO LAKE pluton.

Table I.4.1: Granite.

	typical facies			border facies		
Sample number	CL	82QC51	82QC51b	83QC10	83QC16	83QC17	83QC18
Quartz	19.7	20.2	20.7	17.5	25.1	16.8	24.2
Alkali feldspar	45.2	41.0	34.4	47.9	50.3	44.9	57.4
Plagioclase	29.3	32.3	37.0	28.8	22.0	35.0	14.9
Mafic minerals	5.8	6.5	7.9	5.8	2.6	3.3	3.5
Amphibole	0.7	0.6	0.7	0.0	0.0	0.0	0.0
Biotite	3.2	4.8	4.7	3.4	1.5	2.5	1.7
Opaque minerals	1.3	0.7	1.5	1.6	0.9	0.5	1.5
Accessories	0.6	0.4	1.0	0.8	0.2	0.3	0.3

Felsic minerals counted on stained slab, mafic minerals counted in thin section.

Table I.4.2: Mixed facies.

	lighter		darker
Sample number	85QC11	83QC14	85QC12
Quartz	19.9	26.6	21.5
Alkali feldspar	43.5	29.7	29.3
Plagioclase	29.9	31.4	36.0
Amphibole	0.2	6.8	7.5
Biotite	3.6	2.9	4.0
Opaque minerals	2.0	1.4	1.1
Accessories	0.9	1.2	0.6
Total mafic minerals	6.7	12.3	13.2

Modal analyses in thin section.

Table I.4.3: Enclaves.

		bbe			abe
Sample number	82QC51b	83QC14	83QC16	83QC17	83QC12
Quartz	11.5	14.5	8.0	12.2	11.5
Alkali feldspar	0.0	1.5	0.0	0.0	2.4
Plagioclase	71.0	57.1	64.0	68.0	57.6
Amphibolee	0.0	3.2	0.0	0.0	19.9
Biotite	12.6	18.2	20.4	14.1	2.0
Opaque minerals	2.4	2.7	6.9	2.9	6.3
Accessories	2.5	2.8	0.7	2.8	0.3
Total mafic minerals	17.5	26.9	28.0	19.8	28.5

Modal analyses in thin section.

Biotite and amphibole are the mafic mineral phases. Amphibole is always euhedral and contains many inclusions (sphene, biotite, apatite, and opaque oxides). It may be altered to chlorite along cleavages. Amphibole content is always less than 0.5 volume percent and grains may be up to 8 mm long. Biotite is sometimes zoned, with a darker core; it is mostly euhedral to subhedral, but may be anhedral. It usually contains many inclusions, especially apatite, but also zircon, sphene, and opaque oxides, and is often partly altered to chlorite. Accessory minerals average 2 volume percent, opaque oxides about 1 volume percent. Among the other accessory phases, sphene is the most conspicuous; it forms large euhedral crystals to 0.3 X 1.8 mm and commonly 1.0 mm long. Large grains of apatite, zircon, and allanite are also present.

The border facies has a more porphyritic texture (Plate I.2, b) with a groundmass grain size less than 0.1 mm, and phenocrysts up to 8 mm long. Except for the lack of amphibole, the border facies contains the same minerals as the typical facies, but in different proportions (Table I.4.1) because it is more felsic.

The typical facies falls on the limit between the quartz-monzonite field and the monzogranite subfield of the QAP diagram (fig. I.1; Streckeisen,1976), and might best be termed an amphibole-biotite monzogranite. The most felsic samples of the border facies are syenogranite. The typical facies is a subsolvus granite as defined by Bonin (1972, 1977).

The texture of the mixed unit is fine-grained porphyritic (Plate I.2, c), with quartz xenocrysts surrounded by mafic silicates, and rapakivi feldspars. In the lighter facies, felsic minerals form more than 90 volume percent of the rock (Table I.4.2). Perthitic rapakivi feldspar and plagioclase are the main phenocrysts. Biotite and rare amphibole may also be found as phenocrysts. Plagioclase is zoned, cores often being full of inclusions and altered, rims being limpid. The groundmass consists of the same minerals, as well as quartz and accessory minerals. Among the latter, opaque oxides are the most abundant, while sphene and apatite are less abundant.

In the darker facies, felsic minerals form less than 90 volume percent of the rock (Table I.4.2). In contrast to the lighter facies, plagioclase is more abundant than alkali feldspar and is the main phenocrystic phase. It can be surrounded by alkali feldspar and is typically zoned, with an altered core full of inclusions. Alkali feldspar is less perthitic than in the lighter facies. Alkali feldspar and quartz are mainly constituents of the groundmass. Amphibole and biotite form more than 10 volume percent of the rock, amphibole being more abundant than biotite, in contrast to the lighter facies. Both mafic minerals form small phenocrysts, but are mainly found in the groundmass. Accessory minerals are the same as in the lighter facies, but are less abundant.

This mixed facies falls in the monzogranite subfield (fig. I.1) of the Streckeisen diagram (1976). The lighter facies is quite similar to the granitic facies, but the darker facies is more mafic and contains less alkali feldspar.

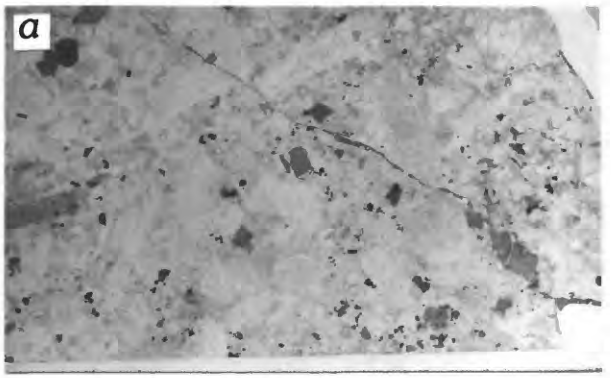
a

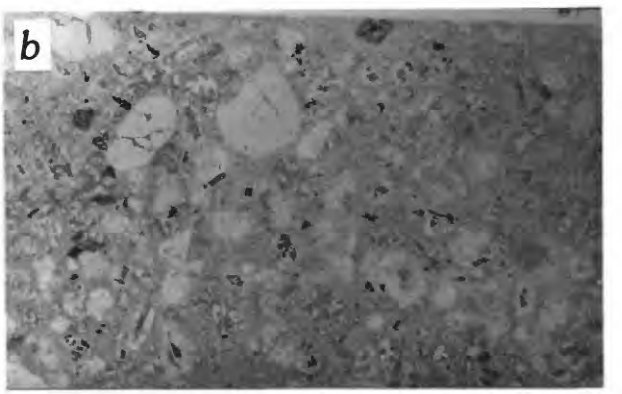
b

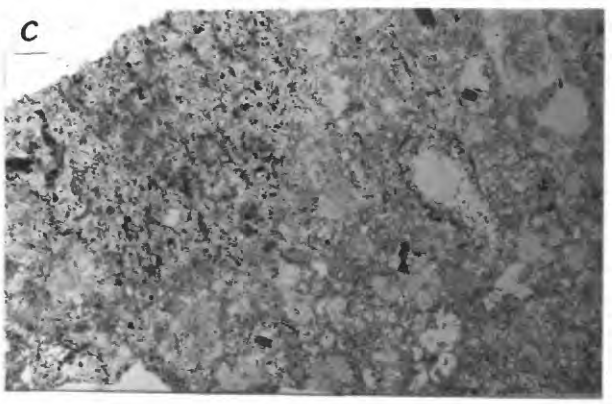
c

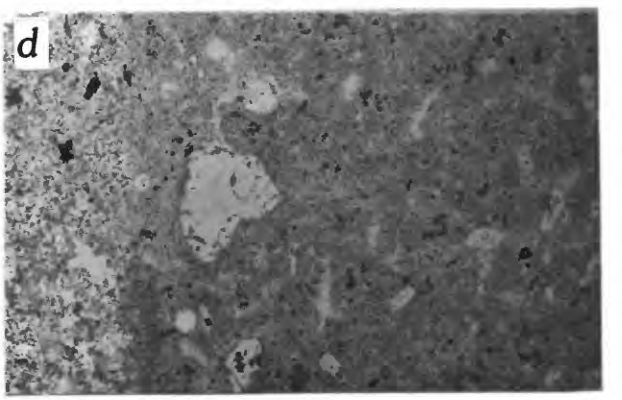
d

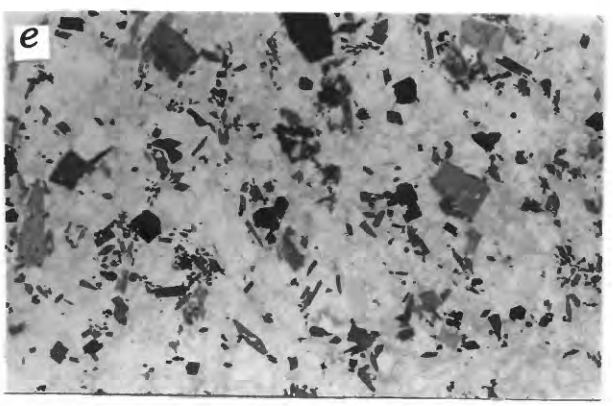
e

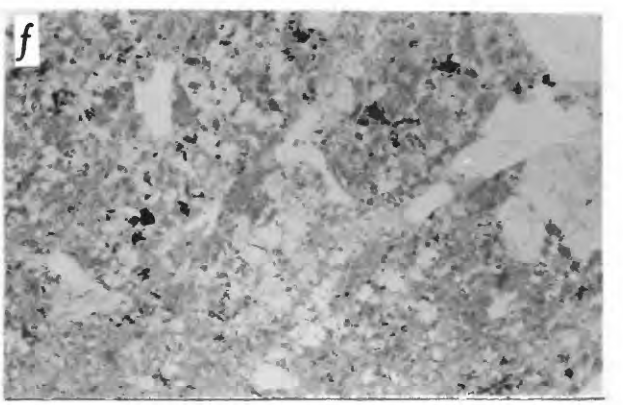
f

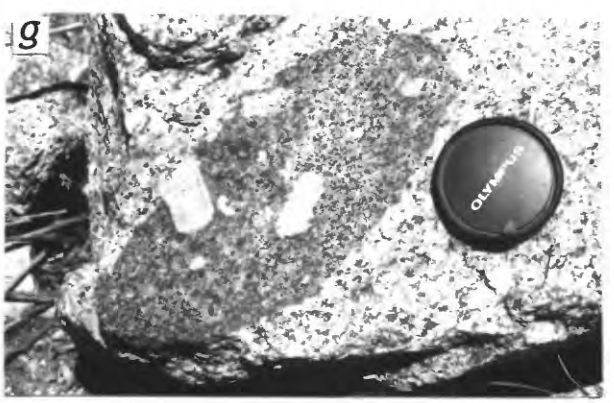
g
OLYMPUS

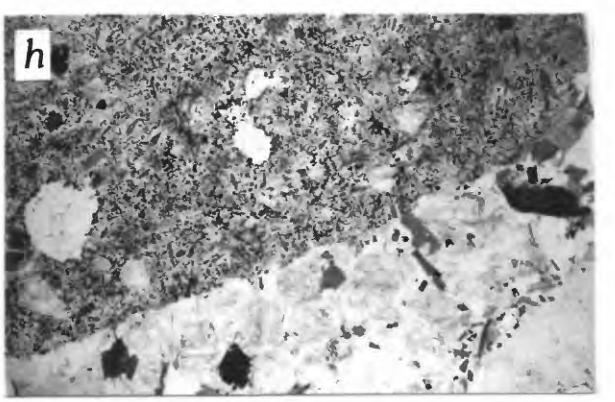
h

PLATE I.2: Textures of granitic rocks from the Cabresto Lake and Rio Hondo plutons. Thin sections 20 X 40 mm.

(a) Granite of Cabresto Lake. Typical facies with porphyritic texture characterized by large euhedral biotite and amphibole; sample 82QC51b.

(b) Granite of Cabresto Lake. Border facies with porphyritic texture characterized by large feldspar and quartz grains and lozenge-shaped aggregates of biotite and quartz; sample 83QC18.

(c) Mixed unit of Cabresto Lake. Fine-grained porphyritic texture with quartz xenocryst (center left) surrounded by fine-grained mafic silicates; note biotite-bearing enclave (lower right); sample 83QC14A.

(d) Amphibole-bearing enclave (right) in the granite of Cabresto Lake (left); note large resorbed quartz xenocryst; sample 83QC12.

(e) Granodiorite of Rio Hondo. Coarse-grained porphyritic texture with euhedral biotite and amphibole phenocrysts; sample 82QC26.

(f) Granite of Rio Hondo. Brecciated facies near contact with Precambrian roof; note post-consolidation hairline fractures; sample 82QC30.

(g and h) Mafic magmatic enclave in the granodiorite of Rio Hondo. Note sharp rounded contact of enclave with host granodiorite, and occurrence of alkali-feldspar megacryst across contact; sample 82QC12.1.

The Cabresto Lake pluton is characterized by the presence of two types of enclaves; both types are found in the granitic unit as well as in the mixed unit. One type contains biotite as the predominant mafic silicate and is termed biotite-bearing enclave or "bbe". The other contains amphibole and is therefore called amphibole-bearing enclave or "abe".

Biotite-bearing enclaves are usually rounded and small (a few centimeters across, rarely up to 10 cm across; Plate I.2, c). They are common and may constitute 0.3 volume percent of the rock. Their texture is equigranular, medium- to fine-grained. The main mineral phases are plagioclase and biotite (Table I.4.3), biotite usually being less well formed than plagioclase. Both are altered: plagioclase to sericite and biotite to chlorite. Quartz averages 10 volume percent. Opaque oxide minerals, sphene, and apatite are the typical accessory phases. Sphene appears mostly as late anhedral interstitial grains. Apatite forms large grains as well as acicular crystals. Acicular apatite grains are commonly included in plagioclase. In a QAP diagram (Streckeisen, 1976), this type of enclave is a quartz diorite (fig. I.1), and can be termed a biotite quartz diorite.

Amphibole-bearing enclaves (Table I.4.3) are less common; they are larger (more than 10 cm across) and have crenulated margins; their texture is microgranular porphyritic (Plate I.2, d). Some large quartz crystals are

probably xenocrysts and some coarse-grained fragments with sharp outlines, enclosed in these enclaves, probably represent pieces of the host granitoid. The groundmass consists mainly of plagioclase, amphibole, opaque oxides, and acicular apatite; scarcer biotite and quartz also occur. Plagioclase is the most common phenocryst; it is always zoned, often rounded, and encloses acicular apatite. Other phenocrysts are amphibole, rare biotite, quartz, and opaque oxides. Alkali feldspar is rare. The main accessory minerals are opaque oxides and apatite (as large crystals and acicular crystals); sphene is scarce. Based on the QAP diagram, this type of enclave may be called a biotite-amphibole quartz diorite (fig. I.1; Streckeisen, 1976).

Based on the presence of acicular apatite (Wyllie and others, 1962) in both types of enclave, they are interpreted as microgranular enclaves (Didier, 1959), microgranitoid enclaves (Vernon, 1983), or mafic magmatic-enclaves (Bernard Barbarin, personal communication). They are interpreted to record a mixing event between a mafic magma and a more felsic magma.

5. RIO HONDO

The Rio Hondo pluton is located south of Questa caldera. It is the largest intrusion in the Questa area and crops out west of Columbine Creek, and mostly north of the Rio Hondo, over an area of about 8 x 9 km. The Rio Hondo pluton mainly intrudes metamorphosed plutonic rocks of Precambrian age (Reed and others, 1983). On the northeast side of the pluton, the contact is linear and steep, and seems to be localized by a major regional northwest-trending fault. Otherwise, most visible contacts dip gently and appear to reflect the roof of the intrusion (Lipman, 1983). Large areas of the pluton are cut by hundreds of northwest-trending rhyolitic to quartz latitic dikes, interpreted to represent intrusions of liquid interior portions of the batholith into its consolidated margins (Lipman, 1983). From isotopic data, primary cooling of this pluton is estimated at about 26-25 Ma (Lipman and others, 1986).

The Rio Hondo pluton consists mainly of coarse-grained granodiorite (Plate I.2, e) which grades into silicic granite in the roof zone and toward the north along the west side of Columbine Creek. A significant feature of the main granodiorite facies is the presence of mafic-magmatic enclaves of varying size and character (Plate I.2, g and h). As easily seen in road cuts east of Italianos Canyon, these enclaves are most abundant where the granodiorite contains more abundant alkali-feldspar phenocrysts (to 5 cm across); such areas can also be characterized by biotite-rich schlieren (Plate I.3, a and b). The 3540-meter peak just northwest of Gavilan Canyon is a revealing locality. There, porphyritic granodiorite, similar to that exposed at the 2700-meter level in Hondo Canyon, persists to within a few tens of meters of the summit. The summit itself, however, is composed of finer grained, more silicic granitic rock, believed to have formed a zone just beneath the Precambrian roof. Finer grained silicic granite has also been noted in exposures on the west side of Columbine Creek, between 2640 and 2940 meters elevation, on the southeast corner of the nose that lies opposite the confluences of Deer Creek and Placer Fork. There, one finds a gradual decrease in grain size within rocks of similar mode (Table I.5.2), toward the

contact with the Precambrian roof. At the contact, a classic coarse unidirectional solidification texture (Shannon and others, 1982) or "stock scheider" is developed; inward pointed quartz crystals to 10 cm across are common and apparently coherent, skeletal crystals to 40 cm across can be seen. Bladed alkali feldspar crystals, several centimeters across, are common. On the northeast side of the nose, directly west of the confluence of Deer Creek, are spectacular cliffs which form the extreme north end of the Rio Hondo pluton. These cliffs are composed of a highly silicic rock (78.5 wt% SiO_2) which appears to have been hydraulically fractured to form an auto-breccia (Plate I.2, f). Tiny late quartz crystals line open gashes less than 1 mm wide, but up to several centimeters long.

Many dikes cut the Rio Hondo pluton; most are of rhyolitic composition. They may be up to 10 m wide, with sharp chilled margins several centimeters or tens of centimeters thick. There are fewer quartz latite dikes, which have less sharp contacts than the rhyolite dikes, and still fewer dikes of basaltic composition. It is possible to find, in some talus in the Gavilan Canyon area, blocks with complicated relations between quartz latite and granodiorite. Contacts may be rather irregular and are sometimes characterized by a mixed zone between granodiorite and quartz latite. These quartz latite dikes were probably intruded while the pluton was still partly molten.

Petrography

The texture of the granodiorite is porphyritic with a medium-grained groundmass (1 to 5 mm; Plate I.2, e), but in the southwest part of the pluton it is more equigranular. Mafic and accessory minerals form 10 to 20 volume percent of the rock (Table I.5.1).

Plagioclase is euhedral to subhedral, zoned, and commonly altered. Alkali feldspar is perthitic and also altered; it is an early phase as phenocrysts and can be mantled by plagioclase (rapakivi texture). It was the last mineral to crystallize in the groundmass. Quartz is often interstitial, but ended its crystallization before alkali feldspar. Amphibole and biotite may constitute up to 17 volume percent of the rock, but typically compose 10 percent. Amphibole and biotite are both euhedral and contain inclusions such as opaque oxides, apatite, zircon, and sphene; inclusions are more abundant in biotite, and amphibole can contain biotite as inclusion. Biotite can be altered to chlorite. The most abundant accessory minerals are opaque oxides (predominantly magnetite) and sphene. Sphene forms euhedral crystals to 4 mm long, sometimes containing opaque oxide minerals as inclusions. Apatite is common and can be up to 0.7 mm long. Allanite and zircon, often included in biotite, are present.

This facies mainly falls in the granodiorite field of the QAP diagram (fig. I.1; Streckeisen, 1976); it is an amphibole-biotite granodiorite.

Table I.5: Modal analyses of samples from the RIO HONDO pluton.

Table I.5.1: Granodiorite.

Sample number	82QC12	82QC26	82QC28	Q83J55	Q83J58	Q83J59	Q83J61	84QC32
Quartz	24.2	13.0	25.2	20.8	21.4	20.6	22.4	22.5
Alkali feldspar	20.4	24.0	23.7	23.4	23.0	23.1	25.6	16.7
Plagioclase	43.5	43.2	41.0	43.6	44.0	44.6	40.0	50.2
Mafic minerals	11.9	19.8	10.1	12.2	11.6	11.7	12.0	10.6
Amphibole	-	10.3	-	5.6	-	4.5	3.0	4.5
Biotite	-	6.8	-	4.8	-	4.7	7.2	4.5
Opaque minerals	-	1.7	-	1.2	-	1.4	1.0	1.1
Accessories	-	1.0	-	0.6	-	1.1	0.8	0.5

Modal analyses on stained slabs; mafic minerals, when detailed, were counted in thin section.

Table I.5.2: Silicic granite.

Sample number	Q83SL27	84QC9	84QC11	84QC12	84QC13
Quartz	36.2	34.3	34.3	37.2	34.3
Alkali feldspar	31.3	35.3	35.7	37.6	36.3
Plagioclase	29.0	27.1	26.4	22.2	26.4
Mafic minerals	3.5	3.3	3.6	3.0	3.0
Biotite	1.7	2.4	2.5	1.5	1.7
Opaque minerals	0.9	0.6	0.5	0.9	1.1
Accessories	0.9	0.3	0.6	0.6	0.2

Felsic minerals counted on stained slabs, mafic minerals counted in thin section.

Table I.5.3: Enclaves.

Sample number	82QC12.1	82QC12.6	82QC28	84QC31	85QC27	85QC28	85QC29
Quartz	9.5	14.9	4.7	9.3	10.7	8.5	10.7
Alkali feldspar	0.0	1.1	0.0	0.0	0.0	0.0	0.0
Plagioclase	40.3	53.8	59.9	44.5	48.1	50.2	43.8
Hornblende	14.0	11.5	1.6	19.6	16.1	16.0	15.2
Biotite	30.3	15.5	30.0	20.9	18.4	19.4	24.8
Opaque minerals	2.2	1.8	2.0	2.4	2.9	1.7	1.6
Accessories	3.7	1.4	1.8	3.3	3.8	4.2	3.9
Total mafic minerals	50.2	30.2	35.4	46.2	41.2	41.3	45.5

Modal analyses in thin section.

The texture of the silicic granite is coarse-grained, slightly porphyritic, with mainly plagioclase phenocrysts and a few rapakivi feldspars. It becomes medium- and fine-grained porphyritic near the contact with Precambrian granite. The rock consists of quartz, alkali feldspar, and plagioclase; the mafic and accessory mineral content is always less than 4 volume percent (Table I.5.2).

Plagioclase is euhedral to subhedral, with sericitized cores, and is often zoned. Alkali feldspar is perthitic, sometimes mantled by plagioclase (rapakivi texture), and usually altered. Quartz and plagioclase crystallized about at the same time, and alkali feldspar is mostly a later phase. The only mafic mineral is biotite; it contains many inclusions (opaque oxides, apatite, and zircon) and is often chloritized. Other than opaque oxides, the most abundant accessory phase is sphene, which is present as euhedral crystals up to 1.4 mm long. Apatite and zircon are common; allanite is less abundant.

This facies falls in the monzogranite subfield of the QAP diagram (fig. I.1; Streckeisen, 1976); it is a biotite monzogranite.

The mafic-magmatic enclaves are varied in size, grain size, texture, and mafic silicate content. They always have a rounded shape, and lack chilled margins (Plate I.2, g and h). Their texture can be equigranular (microgranular to fine grained), or porphyritic, containing plagioclase phenocrysts (up to 15 mm long, typically 5 mm long), mafic mineral clots (a few mm across), and alkali feldspar phenocrysts similar to those in the granodiorite.

The enclaves are mainly composed of plagioclase and mafic silicates (Table I.5.3). Plagioclase is usually zoned and is altered in many samples. Biotite and amphibole, the only mafic silicates present, are found in all enclaves. Biotite is always more abundant than amphibole and both minerals can be found in quite different amounts in different enclaves. Both mafic minerals occur as small individual, subhedral crystals as well as clusters. Quartz occurs both as an interstitial phase (as a constituent of the enclave) and as large crystals with undulatory extinction, surrounded by fine-grained mafic silicates. These large crystals are interpreted as xenocrysts from the host granitoid (Cantagrel and others, 1984). Alkali feldspar, as a late interstitial phase, is rare; it is more common as randomly distributed phenocrysts. These phenocrysts may lie across the contact between enclave and granodiorite, and are xenocrysts as well. Accessory minerals form 3 to 6 percent of the enclaves (Table I.5.3); these are mainly opaque oxides (about 2 volume percent), sphene (1-3 volume percent), and apatite (1-3 volume percent). Opaque oxides are present as early euhedral crystals. Sphene can be euhedral, but is often corroded or anhedral. Apatite occurs as large prismatic crystals, as in the enclosing granitoid, and as long narrow needles which are often broken. These apatite needles are enclosed in other phases, mainly plagioclase (groundmass and phenocrysts) and biotite; they are less common in amphibole and sphene. They are also found in the margins of the quartz xenocrysts.

These enclaves are amphibole-biotite quartz diorites, sometimes quite tonalitic (fig. I.1; Streckeisen, 1976).

6. SOUTHERN CALDERA MARGIN INTRUSIONS

The southern caldera margin intrusions, including the Bear Canyon pluton, the Sulphur Gulch pluton, and the Red River intrusive complex, are characterized by notable alteration. These intrusions are of significant interest because the Sulphur Gulch pluton hosts a world-class molybdenum ore body. Significant Mo is also present in the Bear Canyon pluton. Drilling has shown the Bear Canyon and Sulphur Gulch plutons to be connected in the shallow subsurface. Poor outcrops and extensive alteration obscure relations in the Red River area and the highly variable intrusive units there have been grouped into an "intrusive complex" for lack of better understanding.

Because of limited time, concurrent mineralogical studies of the mine units by Steven A. Atkin of Molycorp, and the complexities of the Sulphur Gulch and Red River areas, the southern caldera margin intrusives have not been as thoroughly studied as other plutons of the Questa area.

The Bear Canyon pluton, the westernmost intrusion along the southern margin of the caldera is located mostly south of the Red River and crops out over an area of about 3.5 km^2. The Sulphur Gulch pluton crops out mostly north of the Red River, between the Bear Canyon pluton and the Red River intrusive complex; it underlies an area of about 3 km^2. The Red River intrusive complex is mainly located north and west of the town of Red River; it crops out over a large area of about 30 km^2.

These three intrusions follow the south margin of the caldera and post-date its formation. They intrude the Precambrian schists and granites of the caldera wall and the Tertiary volcanic rocks of the caldera floor and fill. They are hydrothermally altered and contain molybdenum mineralization (Lipman, 1983; Leonardson and others, 1983). Because of its location, and its contacts (steep to the northeast, gentle to the southwest) the Bear Canyon pluton is thought to be controlled by the same structures which controlled emplacement of the Rio Hondo pluton (Lipman, 1983). The Bear Canyon and the Sulphur Gulch plutons have yielded K-Ar biotite ages of about 23 Ma (Laughlin and others, 1969).

The Sulphur Gulch pluton, has been mined for molybdenum for many years. From underground cross-sections in the mine, Steven A. Atkin (personal communication) has been able to distinguish two major units: a carapace granite and a source aplite. As suggested by their names, the carapace is recognized as a slightly older unit, into which the source aplite was emplaced. The carapace rock is a heterogeneous porphyritic aplite, which may be in contact with Precambrian schists or Tertiary andesitic rocks. The source aplite is rarely in contact with Tertiary andesitic rocks and displays three facies: (1) a non-porphyritic equigranular aplite, (2) a coarse granite, and (3) a seriate granite. The source aplite is commonly cut by quartz veins which can form up to 90 percent of the rock. Because of extensive migration of fluids through the rock it is extremely difficult to obtain representative samples in which mafic silicates and opaque oxide minerals can be studied. Relatively less altered samples of underground exposures have been provided by Steve A. Atkin.

The Red River intrusive complex seems to consist of a different rock type at each good exposure (granodiorite to granite porphyry) and each rock type may represent a different phase of magmatic activity.

Petrography

1) Bear Canyon (Table I.6)

The texture of the Bear Canyon granite is fine-grained porphyritic to medium grained, less porphyritic. The rock is leucocratic and the essential minerals are alkali feldspar, quartz, and plagioclase (Plate I.3, c). Alkali feldspar is perthitic, euhedral to anhedral, often altered; exsolved albite can be found between alkali-feldspar grains. Plagioclase is zoned and cores are altered; it is never anhedral. Quartz has slightly undulatory extinction. In the finer grained facies, these minerals form phenocrysts with rims intricately intergrown with the groundmass, indicating that they ended their crystallization at the time the groundmass solidified. The only mafic mineral, biotite, is not abundant and is an earlier phase. It encloses accessory phases such as apatite and opaque oxides. The most abundant accessory minerals are opaque oxides; apatite, zircon, allanite, and sphene are minor phases; chevkinite and euxinite are rare.

The Bear Canyon granite is a biotite monzogranite (fig. I.1; Streckeisen, 1976).

2) Sulphur Gulch (Table I.7)

The carapace granite is porphyritic, with a fine-grained groundmass (0.05 to 0.2 mm); phenocrysts can be up to 8 mm long. The most abundant phenocrysts are large euhedral quartz grains, sometimes embayed by alkali feldspar. Plagioclase phenocrysts are euhedral and zoned; small plagioclase phenocrysts can be found enclosed in alkali feldspar. Perthitic alkali feldspar phenocrysts can be euhedral, but are more commonly anhedral; rims are often intergrown with the groundmass. In the freshest samples, biotite occurs as phenocrysts, partially reacted to chlorite and opaque oxide minerals; often mafic silicates are completely reacted to chlorite (after biotite) or to chlorite and calcite (after amphibole?). Accessory phases such as opaque oxide minerals (to 0.7 mm across), apatite, and large zircon grains (to 0.05 X 0.18 mm) are common. Early sphene may form large (to 2.1 mm long) euhedral crystals and allanite is common. The groundmass is essentially formed by alkali feldspar and quartz; rarely plagioclase occurs as a groundmass constituent as well.

The aplitic facies of the source aplite is fine grained (to 0.3 mm), equigranular, and mainly constituted of alkali feldspar and quartz. Biotite is rare and shows anhedral margins. Euhedral pyrite is quite common and there are no opaque oxides minerals.

Table I.6: Modal analyses of samples from the BEAR CANYON pluton.

Sample number	82QC8	82QC9	82QC10
Quartz	34.7	33.5	31.5
Alkali feldspar	39.9	36.3	36.1
Plagioclase	23.9	29.0	29.2
Mafic minerals	1.5	1.2	3.2
Biotite	0.8	0.6	1.9
Opaque minerals	0.7	0.6	1.3

Felsic minerals counted on stained slabs; mafic minerals counted in thin section.

Table I.7: Modal analyses of samples from the SULFUR GULCH pluton.

	Carapace			Source aplite		
Sample number	3417	3439	3440	aplite 1685	coarse 82QC55	seriate 3438
Quartz	33.7	32.0	26.2	35.5	36.6	45.5
Alkali feldspar	47.7	49.0	49.6	63.2	44.0	42.2
Plagioclase	15.7	16.1	21.4	0.7	17.1	11.2
Biotite*	0.5	1.9	1.6	0.3	0.8	0.6
Opaque minerals	1.6	1.0#	1.2	0.3	1.5	0.5

* Biotite and or chlorite.
# 0.6 vol% Opaque minerals + 0.4 vol% sphene.

Table I.8: Modal analyses of samples from the RED RIVER intrusive complex.

Sample number	82QC44*	82QC43	85QC36.2	82QC32c*	85QC36.1	82QC31	85QC37B
Quartz	16.5	17.0	29.1	41.9	6.0	12.4	13.4
Alkali feldspar	21.2	63.3	48.2	55.7	0.0	4.6	0.6
Plagioclase	44.7	16.5	13.1	0.1	64.3	67.4	72.8
Biotite	5.6	1.8	8.2	0.6	20.0	12.0	10.2
Amphibole	9.2						
Opaque minerals	2.5	1.4	1.0	1.7	7.4	3.6	3.0
Accessories	0.3#	-	0.4@	-	2.3&	-	-

* Felsic minerals counted on stained slabs.
# Sphene; @ Apatite + Sphene; & Apatite.

The coarse granite (0.3 to 0.6 mm) contains some larger crystals (to 5 mm). Slightly perthitic alkali feldspar, quartz, and plagioclase are essential phases; plagioclase is subhedral, while alkali feldspar and quartz are more anhedral. Biotite is the only mafic silicate and is often reacted to chlorite. Pyrite is a common accessory phase and there are no opaque oxide minerals.

The seriate granite has a distinct porphyritic texture, with a very fine-grained groundmass (less than 0.05 mm). Euhedral quartz grains (to 5 mm) with groundmass embayments constitute the majority of the phenocrysts. Perthitic alkali-feldspar phenocrysts (to 5 mm) are euhedral, but may have margins intergrown with groundmass minerals. Plagioclase phenocrysts (to 1.6 mm) are euhedral. There is sparse chlorite after biotite. Pyrite, anhedral magnetite, and a few zircons formerly enclosed in biotite are the only accessory phases.

Except for the aplitic facies of the source aplite which is an alkali-feldspar granite, the Sulphur Gulch pluton is formed of syenogranite (fig. I.1; Streckeisen, 1976). The main petrographic distinction between the carapace unit and the source aplite is in the accessory assemblage: it is more diverse in the carapace granite (euhedral sphene-apatite-zircon-opaque oxide minerals-allanite) than in the source aplite (pyrite-rare zircon).

3) Red River (Table I.8)

Four different rock types (possibly corresponding to three different magmatic phases) were studied from four localities of the Red River intrusive complex; their field relations are obscure. The most mafic sample (82QC44) is a granodiorite in the QAP diagram (fig. I.1; Streckeisen, 1976). Its texture is porphyritic, with a fine-grained groundmass (0.1 to 0.2 mm) and feldspar phenocrysts up to 5 mm long (Plate I.3, d). Plagioclase occurs as large, euhedral zoned phenocrysts and is free of inclusions. Alkali feldspar is found both as anhedral perthitic phenocrysts, commonly containing amphibole and/or opaque oxides as inclusions, and as a groundmass constituent. Quartz occurs mainly in the groundmass. Amphibole is present as large euhedral phenocrysts, which often enclose biotite, and as small euhedral crystals which probably crystallized just before the groundmass of quartz and alkali feldspar. Biotite occurs only as phenocrysts; partial alteration to chlorite is common. Common accessories are opaque oxides, sphene, and apatite. Opaque oxide grains are usually small for this relatively mafic unit (to 0.24 mm), euhedral, and enclosed in other phases such as alkali feldspar and amphibole. Euhedral sphene can be up to 1.5 mm long and may enclose opaque oxides.

A second rock type, a syenogranite (fig. I.1; Streckeisen, 1976), was found in two localities (samples 82QC43 and 85QC36). It is also porphyritic, with a fine-grained groundmass (usually less than 0.1 mm; Plate I.3, e). Phenocrysts are plagioclase, alkali feldspar, quartz, and biotite; the groundmass is predominantly quartz and alkali feldspar. Plagioclase phenocrysts (to 1 cm) are rather euhedral and zoned; quartz phenocrysts can be

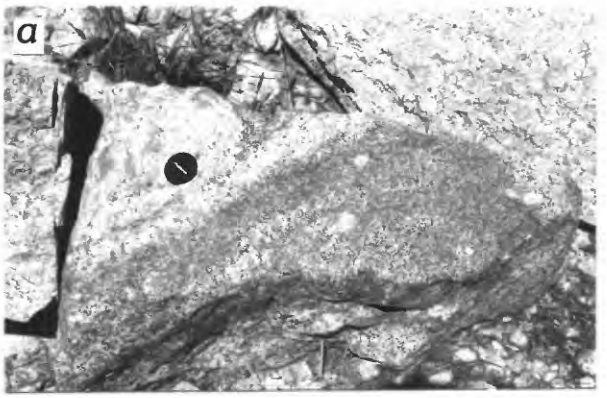
a

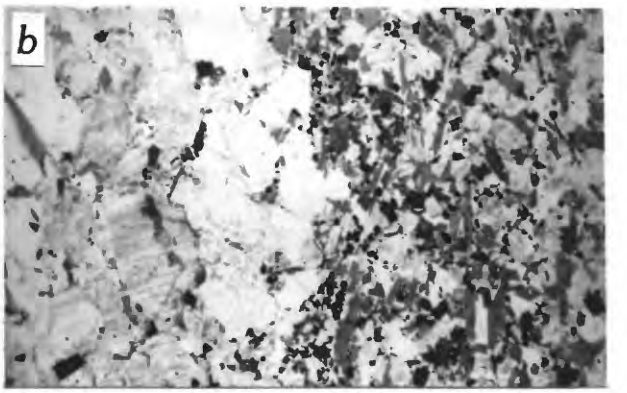
b

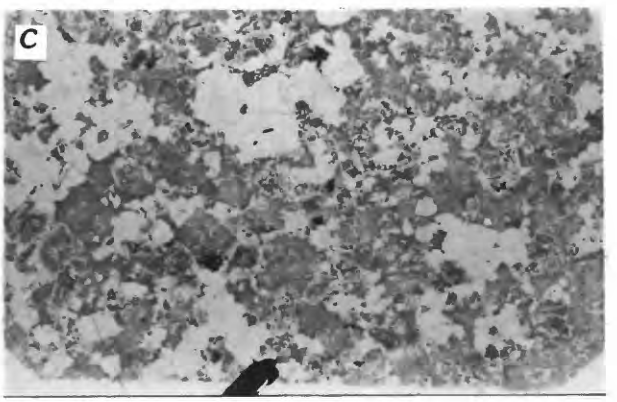
c

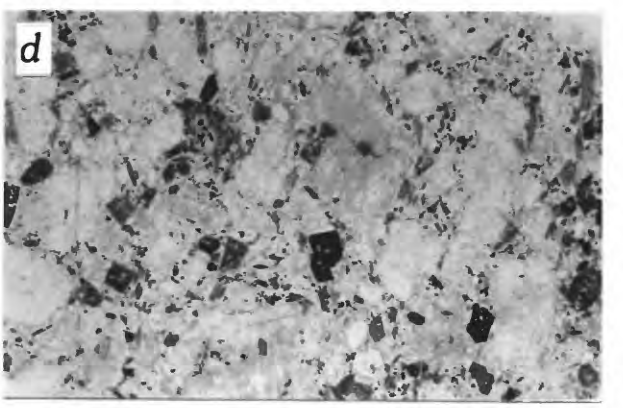
d

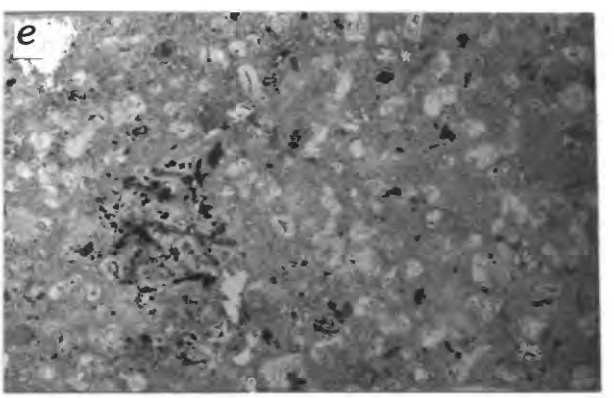
e

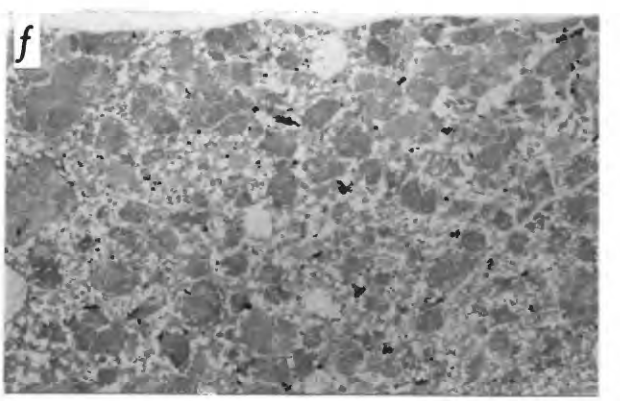
f

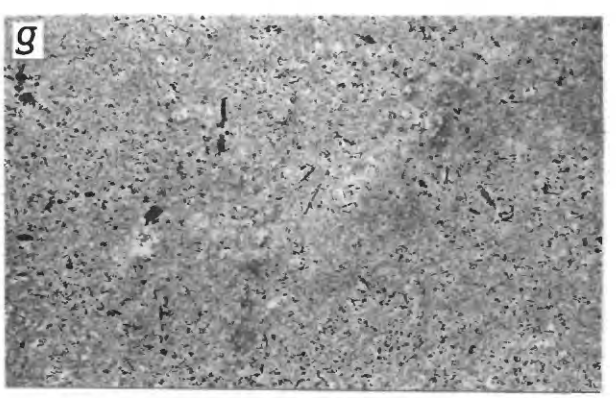
g

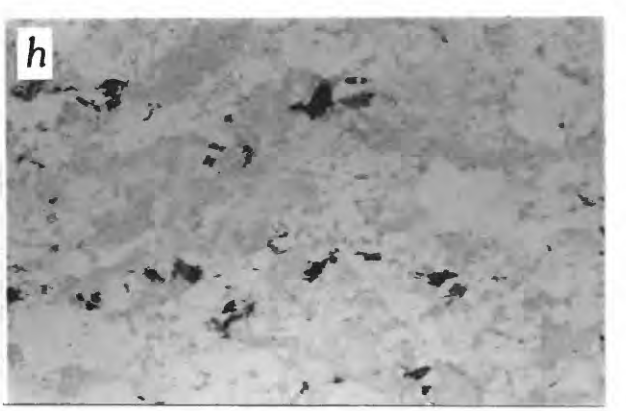
h

up to 0.8 cm across; alkali feldspar phenocrysts (to 2 mm) are rounded and perthitic. Biotite occurs as euhedral phenocrysts (to 1 mm) often containing apatite and/or zircon, or as finer grained aggregates of laths in different orientations, associated with quartz. Sphene, pyrite, and opaque oxides are the most abundant accessory minerals. Notable in this rock type are small rounded enclaves rich in plagioclase and biotite, which resemble the biotite-bearing enclaves found in the Cabresto Lake pluton (Plate I.3, e). They also contain quartz, pyrite, opaque oxides, and acicular, as well as blocky, apatite. Interstitial alkali feldspar may be present. Local pyrite concentrations in the host rock may be related to the presence of these enclaves.

The most silicic sample from the Red River complex (82QC32) is an alkali-feldspar granite (fig. I.1; Streckeisen, 1976). Its texture is porphyritic, with a fine-grained groundmass (to 0.4 mm; Plate I.3, f). Alkali feldspar phenocrysts (to 3 mm across) are predominant; quartz also occurs as phenocrysts (to 3 mm). Alkali feldspar and quartz constitute the groundmass, where quartz may be rather euhedral. Opaque oxides can be euhedral to rather anhedral; biotite is usually anhedral, apparently having crystallized after quartz. Monazite is rare.

A fourth rock type (82QC31 and 85QC37b) is found at the locality of sample 85QC36; its texture is equigranular, fine grained (0.1 to 0.2 mm; Plate I.3, g). This rock is essentially made up of subhedral plagioclase (to 0.2 mm) and biotite (to 0.1 mm). Quartz is common, opaque oxides and acicular apatite are typical, and alkali feldspar is rare and perthitic. Aggregates of calcite and opaque oxide minerals are the apparent replacements of primary amphibole. This rock, which resembles the small rounded enclaves described for the syenogranite, is a quartz diorite (fig. I.1; Streckeisen, 1976)

PLATE I.3: Textures of granitic rocks from the Rio Hondo, Bear Canyon, and Lucero Peak plutons and the Red River intrusive complex. Thin sections 20 X 40 mm.

(a and b) Schlieren in the granodiorite of Rio Hondo; note coarse-grained texture of schlieren; sample 82QC12.3.

(c) Granite of Bear Canyon; sample 82QC8.

(d) Granodiorite of Red River. Porphyritic texture with fine-grained groundmass; sample 82QC44.

(e) Granite of Red River. Porphyritic texture; note presence of small rounded enclave; sample 85QC36.2.

(f) Alkali-feldspar granite of Red River; sample 82QC32c.

(g) Quartz diorite of Red River; sample 82QC31.

(h) Granite of Lucero Peak. Coarse-grained equigranular texture; sample 82QC15.

Although not so well exposed, the locality represented by samples 82QC31 and 85QC36 is reminiscent of the locality in the Cabresto Lake pluton at the Weary Willie mine. Both localities are characterized by enclaves and examples of intimate "mixing" between a felsic matrix and a more mafic component. In both cases, the process has apparently led to precipitation of pyrite.

7. LUCERO PEAK

The Lucero Peak pluton is not completely mapped, because the southern part of it is on Indian sacred land. That part which is mapped is located between Hondo Canyon to the north and Arroyo Seco to the south. It covers an area of at least 20 km^2. The Lucero Peak pluton was emplaced farthest from the caldera, directly south of the Rio Hondo pluton, but everywhere separated from it by a septum of Precambrian rocks (Reed and others, 1983). K-Ar and fission-track ages are concordant at about 21 Ma (Lipman and others, 1986).

Intrusive relations of the Lucero Peak granite with the Precambrian country rocks are sharp and show moderate to steep dips outward; xenoliths of country rock are extremely rare. However, the contacts are nearly flat lying over the central part of the body. Under the flat lying roof the granite has a finer grained facies a few meters thick. The western slopes of Lucero Peak appear to be the exhumed roof of the pluton. Over the entire area, the granite is broken, and characterized by numerous silicified fractures, quartz veins, and aplite dikes. The dikes and quartz veins are often deformed by displacement or by chevron-type folding. This border zone is also characterized by small slickensides. These features show that there was motion after crystallization of the intrusion and suggest that the granite of Lucero Peak was forcefull intruded in the brittle zone, with movement during and after the final stages of the crystallization. In the 300-m-deep gorge east of Lucero Peak, the granite is unusually broken by many fractures, and large xenoliths of Precambrian roof rocks are found. Development of the zone of weakness that evolved into the gorge may have been related to extension associated with development of the Rio Grande Rift during consolidation of the Lucero Peak pluton.

Petrography

The texture of the Lucero Peak granite is coarse-grained equigranular (Plate I.3, h). The rock was deformed when it was largely crystalline, leading to undulatory extinction in quartz, kink-bands in biotite, and granulation along grain boundaries.

The dominant minerals are quartz, alkali-feldspar and plagioclase, in about equal proportions (Table I.9). Among them, zoned plagioclase is the earlier phase; alkali feldspar and quartz crystallized essentially at the same time and are each subhedral to anhedral; alkali feldspar is always microperthitic. Biotite is the only mafic mineral; having crystallized before the main phases, it is mostly euhedral. Biotite contains early accessory minerals such as apatite and opaque oxides. The most characteristic accessory minerals are apatite, allanite, and opaque oxides; sphene and zircon are more rare.

Table I.9: Modal analyses of samples from the LUCERO PEAK pluton.

Sample number	80L20	82QC15	82QC25
Quartz	33.6	31.7	36.2
Alkali feldspar	33.4	34.5	30.1
Plagioclase	31.3	29.9	30.7
Mafic min.	1.7	3.9	3.0
Biotite	1.2	2.6	2.2
Opaque minerals	0.3	0.9	0.8
Accessories	0.2	0.4	0.0

Felsic minerals counted on stained slabs; mafic minerals counted in thin section.

In the Streckeisen diagram (1976), the granite of Lucero Peak falls in the monzogranite subfield (fig. I.1); it is a biotite monzogranite.

8. DISCUSSION

Lameyre and Bowden (1982) have distinguished four major series of granitoids on the quartz—alkali-feldspar—plagioclase (QAP) diagram (fig. I.2). Three of these associations —the calc-alkaline, alkaline, and tholeiitic series— include trends from mafic to silicic compositions which relate to fractional crystallization. The fourth association—mobilizates associated with migmatites—is always characterized by quartz-rich compositions.

The calc-alkaline and alkaline associations are of particular interest among the granitic rocks associated with Questa caldera. The calc-alkaline series is subdivided into a low-K or calc-alkaline trondjhemitic series, a medium-K or calc-alkaline granodioritic series, and a high-K or calc-alkaline monzonitic series. To the alkaline series also belong metaluminous rocks which plot in the syenogranite and granosyenite fields of the QAP diagram.

Calc-alkaline series rock associations are related to compressive areas (orogen or subduction zones) such as the Sierra Nevada and the mountain chains of Peru and Chile. Alkaline series rock associations are related to extensive areas (oceanic or continental rifts) such as those in Niger, Nigeria, Corsica, the Oslo graben, and the Kerguelen islands.

Lameyre and Bowden (1982) relate the three major trends of the calc-alkaline associations to space and time within the orogen, with an evolution from early, internal, low-K magmatism, to a late, external, high-K magmatism. Notable about the Questa magmatic system is the absence of syenitic rocks commonly associated with alkaline magmatism.

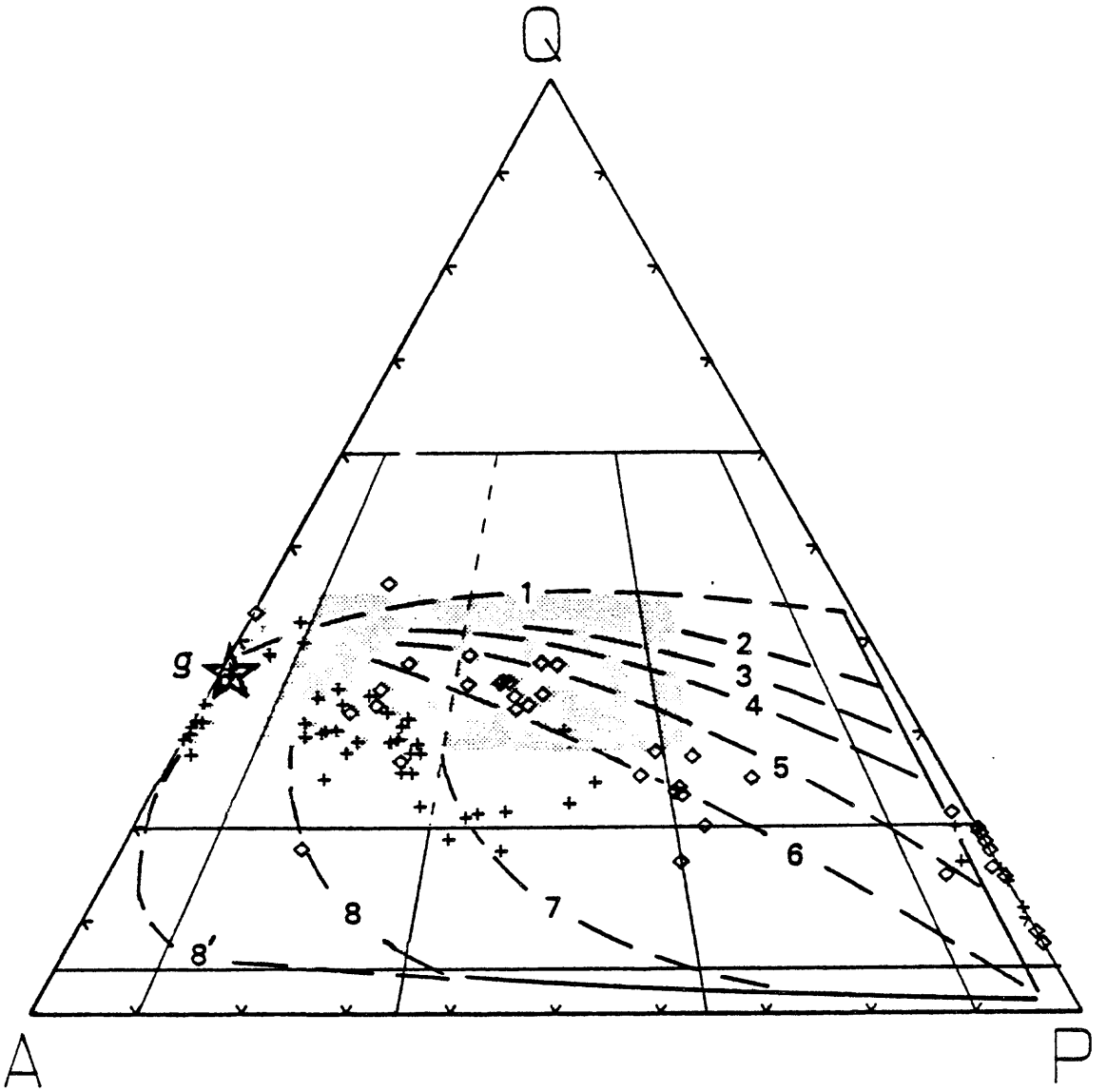

Fig. I.2. All Questa granitic rocks plotted in a QAP diagram showing the median trends in various plutonic suites (Lameyre and Bowden, 1982): 1, tholeiitic; 2 and 3, calc-alkaline trondhjemitic (low K); 4, 5, and 6, calc-alkaline granodioritic (medium K); 7, calc-alkaline monzonitic (high K); 8, aluminous trend in alkaline provinces; 8', alkaline silica oversaturated; g, granitic differentiates; shaded area, granitic rocks of crustal origin. Crosses: Virgin Canyon, Canada Pinabete, Rito del Medio, and Cabresto Lake plutons. Diamonds: Rio Hondo, Bear Canyon, Sulphur Gulch, and Lucero Peak plutons and Red River intrusive complex.

Plotting 88 modal analyses for the Questa granitic rocks in the QAP diagram shows interesting features (fig. I.2). All units of the Rio Hondo pluton and the granites of the Bear Canyon and Lucero Peak clearly cluster around the calc-alkaline granodioritic trend of Lameyre and Bowden. The mixed unit of the Cabresto Lake pluton and the granodiorite, quartz diorite, and enclaves in the granite of the Red River intrusive complex also plot on the same medium-K calc-alkaline trend. The granite of Cabresto Lake plots on the calc-alkaline monzonitic trend. The metaluminous granites of the Virgin Canyon and Canada Pinabete plutons fall between the calc-alkaline monzonitic trend and the trend defined by metaluminous rocks associated with alkaline-series rock associations; the granite of the Red River intrusive complex plots in that same area. The peralkaline granites of the Virgin Canyon and Canada Pinabete plutons fall at the end of the trend defined by alkaline-series rock associations. Typical Rito del Medio granite, the aplitic facies of the source aplite unit of Sulphur Gulch, and the alkali-feldspar granite of Red River all fall in the alkali feldspar-granite field of the QAP diagram, near the field of granitic differentiates of Lameyre and Bowden (fig. I.2).

Based on the Lameyre and Bowden interpretation, the Questa magmatic system records evolution from medium-K to high-K, calc-alkaline magmatism, related to compressional tectonics, followed by alkaline magmatism, related to extensional tectonics . This is in agreement with the geologic history of the area, in that the middle Tertiary marked the time of change from a compressional regime associated with calc-alkaline magmatism to an extensional regime associated with alkaline magmatism. However, geochronological studies based on K-Ar and fission track dates, as well as paleomagnetic measurements, show that the plutons associated with Questa caldera obey an inverse time relation; the northern, more alkaline, intracaldera plutons being slightly older than the southern more calc-alkaline intrusions.

K-Ar ages and paleomagnetic data relate to time of solidification and therefore give only the chronology of solidification of the plutons. The Rio Hondo pluton, which is petrographically similar to granitoids from the Sierra Nevada batholith and shows the most typical calc-alkaline features, is chemically similar to precaldera volcanic rocks of intermediate composition (Johnson, 1986). Lipman (1983) considers the Rio Hondo pluton to represent a deep part of the magma chamber related to the Latir volcanic field and the Questa magmatic system. Lower parts of the magma chamber may well have evolved at an early stage, before the change in tectonic settings, whereas the upper parts of the magma chamber appear to have evolved toward peralkaline compositions at the time of extension. The small peralkaline stocks of Virgin Canyon and Canada Pinabete probably cooled quickly after emplacement at a high level in the crust. It is not surprising that they might have solidified before the southern calc-alkaline intrusions, which represent more slowly cooled, deeper parts of the magma chamber. This is also supported by structural data which show that the base of the volcanic rocks of the Latir volcanic field is about two kilometers higher to the south than in the north. This structural feature may be related to differential post-Miocene uplift (Lipman, 1983) which could be due to the rise of these light magmas through the crust (Lipman, 1986, personal communication).

Notable about the calc-alkaline association of the Questa magmatic system is the compositional gap between the compositions of granodiorite and mafic-magmatic enclaves. This shows that crystal fractionation was not the only process involved in the evolution of the Questa magmatic system and that mixing probably occurred between more mafic and more silicic magmas. Such mixing is recorded by the presence of enclaves in the Cabresto Lake and Rio Hondo plutons and in the Red River intrusive complex.

Only one phase of magma mixing may have occurred during evolution of the Rio Hondo pluton, where only one type of mafic-magmatic enclave is found. Evolution was afterwards controlled by crystal fractionation, as shown by the trend from granodiorite to granite compositions that characterizes this pluton.

In the Cabresto Lake pluton, two phases of magma mixing may have occurred, as shown by the presence of two types of mafic-magmatic enclaves; an early mixing is recorded by small diffusely-bounded biotite-bearing enclaves and a later mixing by the larger and more irregular, sharply-bounded amphibole-bearing enclaves. Occurrence of a mixed unit also attests to magma mixing during evolution of the Cabresto Lake magma; the mixed unit is thought to be related to the same mixing event as the amphibole-bearing enclaves.

PART II: WHOLE-ROCK CHEMISTRY

More than 140 samples of Questa granitoids were analysed by X-ray fluorescence analysis in the USGS laboratories in Denver, Colorado. Trace-element data obtained by an energy dispersive (Kevex) procedure, rare-earth-element data obtained by isotope dilution, and O, Pb, Nd, and Sr isotopic data for many of these rocks are presented and discussed by Johnson (1986). Data for selected samples are presented in Table I.10. Also reported in Table I.10 are rock norms and agpaitic indices ($(Na_2O+K_2O)/Al_2O_3$, molar ratio). The following discussion is based on study of these selected samples; for further discussion see Johnson (1986).

$(Na_2O+K_2O)/Al_2O_3$ ranges from 0.96 to 1.03 in peralkaline rocks, and from 0.65 to 0.96 in all other rock types; values less than 1 are common in peralkaline rocks. Although an agpaitic index of 1 or more has long been considered an index of peralkalinity, Giret and others (1980) show that values as low as 0.9 can be appropriate for distinguishing peralkalinity. The present study, based on occurrence of sodic phases such as alkali amphibole and sodic pyroxene, shows that an agpaitic index of about 0.96 is the distinction of peralkalinity in the Questa granitic rocks.

Data in Table I.10 are presented in Harker variation diagrams (fig. I.3), which show a regular evolution from mafic compositions (granodiorite, mafic-magmatic enclaves, and quartz latite dikes in the Rio Hondo pluton; granodiorite and quartz diorite in the Red River intrusive complex) with high Al_2O_3, FeOt, MgO, CaO, and TiO_2 contents, toward more silicic compositions. Na_2O is rather constant through the whole range of SiO_2 content; K_2O increases slightly with SiO_2 content.

As seen in Table I.10 and figure I.3, aspects of the chemistry of the peralkaline rocks distinguish them from other rocks. Most notably, FeOt is relatively high and Al_2O_3 relatively low in the peralkaline units compared to the metaluminous units of the northern intracaldera plutons. The composition of the peralkaline granites of Virgin Canyon and Canada Pinabete is similar to that of the Amalia Tuff and cogenetic peralkaline rhyolite.

A plot of Na_2O+K_2O against SiO_2 (fig. I.4) shows that the granite of Cabresto Lake falls in an area distinct from the regular trend defined by units in the Rio Hondo pluton; it contains more Na_2O+K_2O and plots among data representing the northern intracaldera plutons. This is in agreement with modal analyses which show a greater proportion of alkali feldspar in the granite of Cabresto Lake, as compared to the granodiorite or granite of Rio Hondo (fig. I.1).

Plotting the data of Table I.10 in a ternary diagram for the system Quartz-Albite-Orthoclase-H_2O (fig. I.5) gives information related to conditions of crystallization in these different plutons. An important conclusion of the work of Tuttle and Bowen (1958) was that minimum melting compositions of crystallizing granitic melts, represented by the system Q-Ab-Or-H_2O, reflect pressure of crystallization. Subsequent studies, cited in the caption to figure I.5, have evaluated the effects of pressure, absence of an aqueous phase, and addition of anorthite to the system. The Questa granitic rocks which contain over 70 weight percent SiO_2 have an average An content of

Table I.10. Chemical analyses and rock norms for representative samples of the Questa granitic rocks.

			VIRGIN CANYON PLUTON									CANADA PINABETE PLUTON					
	Amalia Tuff	Peralkaline rhyolite	Peralkaline granite				Early metaluminous granite		Rhyolite dike	Later metaluminous granite		Peralkaline granite	Typical granite			Magnetite-free granite	
	Q82J41P	Q83J124	Q83J63	82QC38	83QC29	83QC30	82QC41	82QC39	83QC31	82QC33	82QC35	84QC7	Q83J93	Q83J82	84QC1	82QC48	Q83J88
SiO_2	77.4	77.3	75.3	75.2	76.3	77.0	69.6	72.7	73.2	72.9	74.8	76.8	73.1	73.8	77.6	73.9	76.8
Al_2O_3	12.0	11.6	12.5	12.3	12.1	11.9	14.0	13.4	13.8	13.5	12.7	11.7	13.5	13.8	12.1	13.6	12.6
Fe_2O_3	1.37	1.32	1.10	1.14	1.33	1.33	2.19	1.18	1.41	1.19	0.87	0.96	1.35	0.95	0.55	0.59	0.44
FeO	0.10	0.22	0.49	0.34	0.25	0.15	1.06	0.55	0.27	0.62	0.47	0.51	0.44	0.26	0.18	0.75	0.32
MgO	<0.10	<0.10	0.14	0.12	<0.10	<0.10	0.50	0.25	0.28	0.26	0.19	<0.10	0.27	0.24	<0.10	0.29	0.12
CaO	0.09	<0.02	0.28	0.14	0.03	<0.02	0.89	0.75	0.37	0.83	0.56	0.14	0.50	0.51	0.34	0.77	0.25
Na_2O	3.90	4.13	4.38	3.99	4.33	4.31	3.63	3.60	4.14	3.77	3.51	4.32	3.90	3.84	3.96	3.81	3.77
K_2O	5.04	4.78	4.73	4.79	4.63	4.47	5.12	4.90	5.15	4.95	4.89	4.60	4.86	5.33	4.61	5.08	4.69
TiO_2	0.10	0.15	0.20	0.19	0.17	0.13	0.57	0.28	0.27	0.28	0.24	0.16	0.25	0.23	0.09	0.27	0.13
P_2O_5	<0.05	<0.05	<0.05	<0.05	<0.05	<0.05	0.11	0.05	0.07	0.06	<0.05	<0.05	0.06	<0.05	<0.05	0.05	<0.05
MnO	<0.02	0.11	0.12	0.11	0.12	0.05	0.10	0.07	0.02	0.07	0.08	0.14	0.05	0.03	<0.02	0.05	0.04
CO_2	-	-	-	<0.01	-	-	0.01	<0.01	<0.01	<0.01	<0.01	-	-	-	-	-	-
LOI	0.58	0.58	0.67	0.29	0.49	0.55	0.81	0.51	0.80	0.35	0.27	0.51	0.93	0.64	0.54	0.55	0.49
Total	100.00*	100.36	99.96	98.67	99.90	100.06	99.59	99.25	99.89	98.79	98.64	99.99	99.21	99.68	100.13	99.71	99.70
Q	35.2	35.3	31.2	33.3	33.3	34.7	26.6	31.2	28.4	30.0	34.3	34.0	30.5	29.8	36.2	30.1	36.3
C	0.09	-	-	0.42	-	-	1.13	0.93	0.91	0.58	0.74	-	1.06	0.91	0.10	0.55	0.99
Or	29.8	28.3	28.0	28.3	27.4	26.4	30.3	29.0	30.4	29.3	28.9	27.2	28.7	31.5	27.2	30.0	27.7
Ab	33.0	33.1	37.1	33.8	36.5	36.3	30.7	30.5	35.0	31.9	29.7	34.6	33.0	32.5	33.5	32.5	31.9
An	0.12	-	0.48	0.37	-	-	3.70	3.39	1.38	3.73	2.45	-	2.09	2.20	1.36	3.49	0.91
Ac	-	1.67	-	-	0.16	0.13	-	-	-	-	-	1.75	-	-	-	-	-
Di	-	-	0.46	-	-	-	-	-	-	-	-	0.31	-	-	-	-	-
Hy	0.25	0.25	0.14	0.30	0.25	0.25	1.24	0.62	0.70	0.65	0.47	0.73	0.67	0.60	0.25	1.26	0.38
Mt	0.10	0.63	1.39	0.90	0.71	0.27	2.09	1.19	0.15	1.42	1.08	0.52	0.86	0.27	0.39	0.86	0.64
Hm	1.30	0.31	0.14	0.52	0.79	1.10	0.75	0.36	1.31	0.21	0.13	-	0.76	0.76	0.29	-	-
Il	0.19	0.29	0.38	0.36	0.32	0.25	1.08	0.53	0.51	0.53	0.46	0.30	0.48	0.44	0.17	0.51	0.25
Ap	0.12	0.12	0.12	0.12	0.18	0.12	0.26	0.12	0.16	0.14	0.12	0.12	0.14	0.12	0.12	0.12	0.12
(Na+K)/Al	0.99	1.03	0.99	0.96	1.00	1.00	0.82	0.84	0.90	0.86	0.87	1.03	0.87	0.88	0.95	0.87	0.90

*Calculated to 100 wt% anhydrous.

Table I.10.—continued.

	RITO del MEDIO PLUTON			CABRESTO LAKE PLUTON				RIO HONDO PLUTON							
	Granite			Granite											Qtz. latite
	Typical		Border	Typical	Border	Mixed	Enclave*	Granodiorite				Granite		Enclave	dike
	82QC18A	81S28	82QC22	82QC51	83QC18	83QC14	83QC12	82QC26	Q83J59	Q84J6	82QC2	84QC13	82QC30	Q84J61	Q83J100
SiO_2	77.1	77.5	75.3	70.5	72.4	68.6	61.9	61.8	66.3	68.8	71.2	76.9	78.5	58.5	65.4
Al_2O	12.5	12.3	12.7	14.6	14.3	14.8	15.9	15.6	15.0	14.5	14.4	12.4	10.8	16.3	15.3
Fe_2O_3	0.47	0.51	1.18	1.22	0.97	1.53	2.90	2.04	1.88	1.71	1.13	0.63	0.58	3.70	2.01
FeO	0.19	0.20	0.46	0.84	0.56	1.26	2.40	2.45	1.62	1.53	0.97	0.37	0.31	3.75	1.94
MgO	0.14	<0.10	0.21	0.60	0.42	1.35	2.21	2.14	1.74	1.37	0.85	0.27	0.18	3.25	1.96
CaO	0.12	0.28	0.25	1.47	0.71	2.19	3.75	3.97	2.99	2.76	1.87	0.73	0.46	4.32	3.26
Na_2O	4.03	3.92	3.42	4.15	4.21	4.40	4.79	3.84	4.17	4.21	4.03	3.67	2.84	4.78	4.32
K_2O	4.59	4.47	6.06	4.42	4.85	3.99	3.40	3.56	3.52	3.41	3.93	4.51	4.41	2.73	3.33
TiO_2	0.08	0.07	0.20	0.43	0.29	0.47	1.04	0.78	0.59	0.53	0.35	0.15	0.15	1.23	0.66
P_2O_5	<0.05	<0.05	<0.05	0.13	0.09	0.17	0.47	0.34	0.26	0.20	0.12	<0.05	<0.05	0.45	0.30
MnO	0.06	0.04	0.04	0.05	0.06	0.11	0.22	0.06	0.04	0.05	0.03	<0.02	0.02	0.13	0.05
CO_2	-	-	-	<0.01	-	-	-	0.38	-	-	-	-	<0.01	-	-
LOI	0.25	0.08	0.19	0.40	0.53	0.36	0.39	0.87	0.77	0.90	0.54	0.42	0.25	0.88	0.56
Total	99.58	99.54	100.06	98.82	99.39	99.23	99.37	97.45	98.88	99.97	99.42	100.12	98.56	100.02	99.09
Q	35.8	37.0	31.5	25.8	27.5	21.5	11.5	14.9	20.4	24.0	27.6	36.5	44.0	7.26	18.4
C	0.80	0.62	0.18	0.63	1.05	-	-	-	-	-	0.40	0.27	0.64	-	-
Or	27.1	26.4	35.8	26.1	28.7	23.6	20.1	21.0	20.8	20.2	23.2	26.7	26.1	16.1	19.7
Ab	34.1	33.2	28.9	35.1	35.6	37.2	40.5	32.5	35.3	35.6	34.1	31.1	24.0	40.4	36.6
An	0.27	1.06	0.91	6.44	2.94	8.85	11.8	14.8	11.8	10.6	8.49	3.30	1.96	15.0	12.5
Di	-	-	-	-	-	0.72	2.91	2.13	1.04	1.42	-	-	-	2.82	1.34
Hy	0.35	0.25	0.52	1.49	1.05	3.50	4.84	5.95	4.37	3.36	2.44	0.67	0.45	8.79	5.15
Mt	0.58	-	1.03	1.62	1.16	2.22	4.21	2.96	2.73	2.48	1.64	0.82	0.63	5.37	2.91
Hm	0.07	0.73	0.47	0.10	0.17	-	-	-	-	-	-	0.06	0.15	-	-
Il	0.15	0.09	0.38	0.82	0.55	0.89	1.98	1.48	1.12	1.01	0.67	0.29	0.29	2.34	1.25
Ap	0.12	0.12	0.12	0.30	0.21	0.39	1.09	0.79	0.60	0.46	0.28	0.12	0.12	1.04	0.70
(Na+K)/Al	0.93	0.92	0.96	0.80	0.85	0.78	0.73	0.65	0.71	0.73	0.76	0.88	0.88	0.66	0.70

*Amphibole bearing.

Table I.10—continued.

	BEAR CANYON PLUTON		SULPHUR GULCH PLUTON		RED RIVER INTRUSIVE COMPLEX				LUCERO PEAK PLUTON	
	Granite		Carapace	Source aplite	Grano-diorite	Granite	Alkali-feldspar granite	Quartz diorite	Granite	
	82QC10	82QC8	3440	1685	82QC44	82QC43	82QC32C	82QC31	82QC15	80L20
SiO_2	75.0	76.2	72.4	77.0	64.3	71.9	75.8	63.4	75.9	76.8
Al_2O_3	13.1	12.4	13.6	12.60	14.9	14.4	13.1	17.0	12.7	12.9
Fe_2O_3	0.68	0.36	1.95	0.65	2.02	0.98	0.51	2.17	0.55	0.61
FeO	0.43	0.28	0.90	0.40	2.21	0.47	0.30	2.12	0.42	0.28
MgO	0.19	0.15	0.52	0.20	2.28	0.42	0.17	1.58	0.23	0.20
CaO	0.71	0.41	1.17	0.55	3.65	0.67	0.22	2.49	0.79	0.50
Na_2O	3.68	3.35	4.39	2.90	3.80	4.47	4.21	4.99	3.57	3.70
K_2O	4.46	5.04	4.34	5.10	3.52	4.73	5.07	2.91	4.32	4.62
TiO_2	0.19	0.10	0.20	0.10	0.64	0.32	0.15	0.82	0.14	0.11
P_2O_5	<0.05	<0.05	0.09	0.07	0.31	0.10	<0.05	0.35	<0.05	<0.10
MnO	0.03	<0.02	0.06	0.03	0.05	0.04	0.02	0.15	0.04	0.04
CO_2	<0.01	<0.01	0.23	<0.01	0.24	-	-	-	<0.01	<0.01
LOI	0.56	0.95	0.90	0.84	0.84	0.64	0.28	1.13	0.24	0.12
Total	99.09	99.32	100.52	100.45	98.52	99.14	99.88	99.11	98.96	99.99
Q	34.9	36.4	27.4	39.3	18.4	26.0	31.3	16.1	36.6	36.5
C	1.05	0.81	-	1.48	-	0.95	0.41	1.95	0.84	1.14
Or	26.4	29.8	25.6	30.1	20.8	28.0	30.0	17.2	25.5	27.3
Ab	31.1	28.3	37.1	24.5	32.2	37.8	35.6	42.2	30.2	31.3
An	3.20	1.71	4.59	2.27	13.2	2.67	0.77	10.1	3.59	1.83
Di	-	-	0.49	-	2.30	-	-	-	-	-
Hy	0.47	0.46	1.07	0.59	6.01	1.05	0.42	4.96	0.73	0.49
Mt	0.93	0.52	2.52	0.94	2.93	0.72	0.60	3.15	0.80	0.71
Hm	0.04	-	0.21	-	-	0.49	0.10	-	-	0.12
Il	0.36	0.19	0.38	0.19	1.22	0.61	0.29	1.56	0.27	0.21
Ap	0.12	0.12	0.21	0.16	0.72	0.23	0.12	0.81	0.12	0.23
(Na+K)/Al	0.83	0.88	0.88	0.82	0.68	0.87	0.95	0.67	0.83	0.86

Fig. I.3. Variation of oxides (wt%) against SiO_2 (wt%) for the Questa granitic rocks (after Harker, 1909). Crosses, peralkaline granites of Virgin Canyon and Canada Pinabete, Amalia Tuff, and peralkaline rhyolite; diamonds, metaluminous granites of Virgin Canyon and Canada Pinabete and granite of Rito del Medio; triangles, units and rock types of the Cabresto Lake pluton; x's, units and rock types of the Rio Hondo pluton; inverted triangles, units and rock types of the late mineralized plutons.

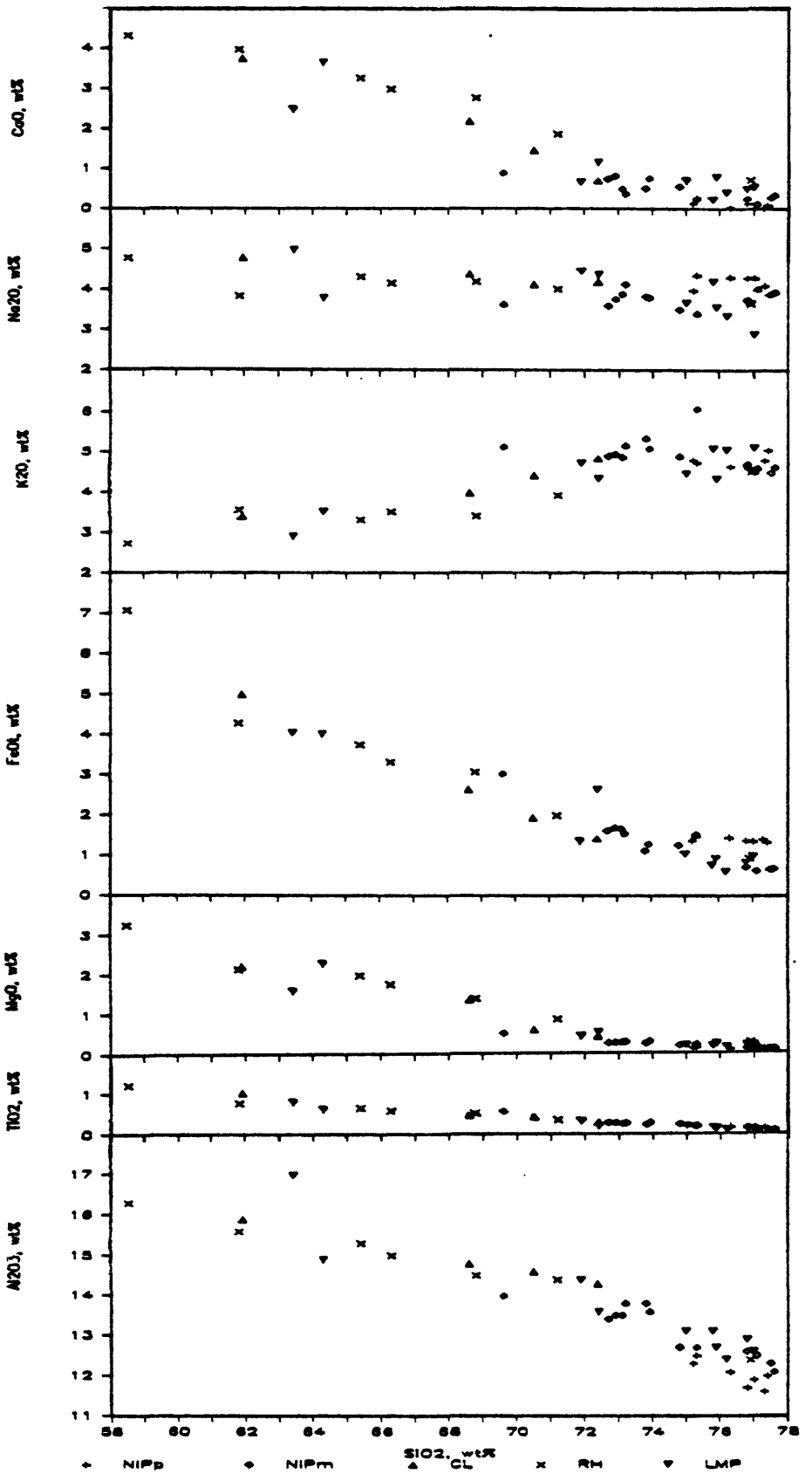
CaO, wt%
Na2O, wt%
K2O, wt%
FeOt, wt%
MgO, wt%
TiO2, wt%
Al2O3, wt%
SiO2, wt%
NIPp
NIPm
CL
RH
LMP

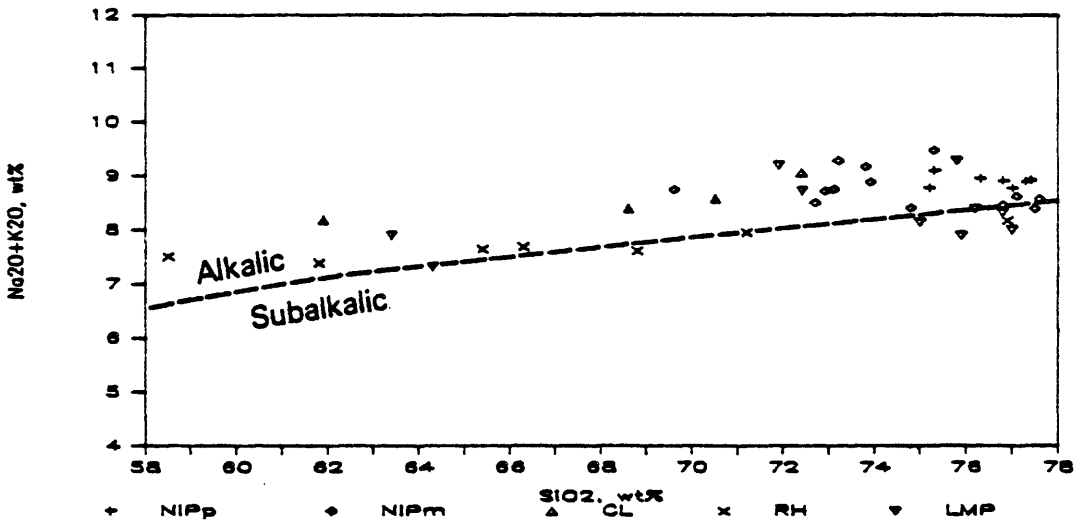

Fig. I.4. Na_2O+K_2O (wt%) against SiO_2 (wt%) for the Questa granitic rocks (after Miyashiro, 1978). Dashed line separates the alkalic field (above) from the subalkalic field (below). Same symbols as in fig. I.3.

about 3 mole percent. Figure I.5 shows that the trend of the data points corresponds well with the experimental studies and converges in a region expected for crystallization at pressures of about 1 kbar in water-saturated melts. It is of interest that the mafic-magmatic enclave (Q84J6I) and quartz latite dike (Q83J100) from the Rio Hondo pluton correspond well with the general trend. The three points which are conspicuously aberrant in figure I.5 can be readily explained. Sample 82QC22 is from the contaminated contact facies of the Rito del Medio pluton, whereas samples 82QC30 and 1685 are silicified samples of the granite of Rio Hondo and the source aplite of Sulphur Gulch, respectively.

Chemical data for the Questa granitic plutons show that there are two main rock series (fig. I.4), in agreement with data from modal analyses. Johnson (1986) demonstrates, based on Pb isotopic data, that the silicic resurgent intrusions were derived from different sources and/or parental magmas than are represented by the Rio Hondo pluton.

Because of continuation of chemical and mineralogical zonation, the peralkaline granites are interpreted as unerupted portions of the magma which produced the Amalia Tuff and associated peralkaline rhyolite. Complexities in this correlation, such as lack of Zr zonation in the peralkaline granites, are probably related to evolution of the magma between the time of caldera collapse and resurgence (Johnson, 1986).

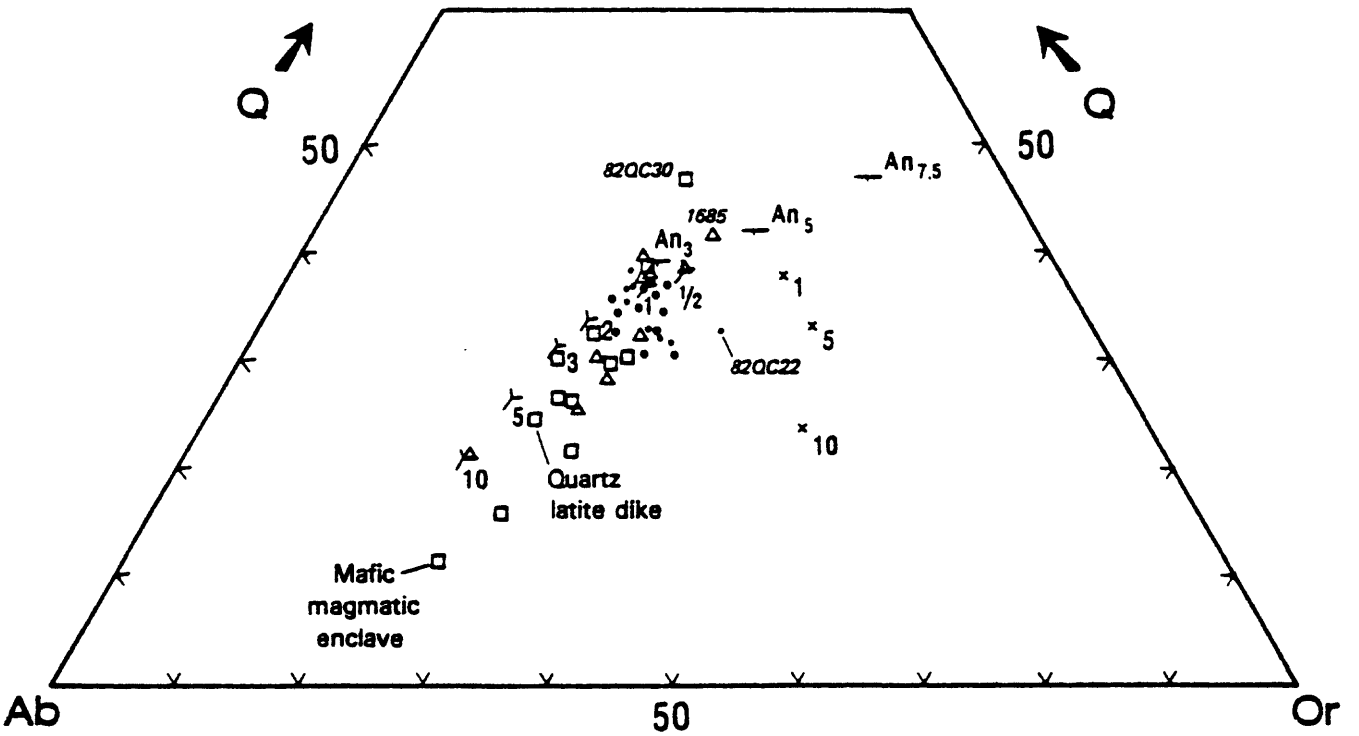

Fig. I.5. Representation of bulk compositions of Questa granitic rocks (Table I.10) in terms of normative Q+Ab+Or. Virgin Canyon pluton represented by small dots; Canada Pinabete and Rito del Medio plutons by large dots; Cabresto Lake and Rio Hondo plutons by squares; Bear Canyon, Sulphur Gulch, Red River, and Lucero Peak plutons by triangles. Minima at indicated pressures (in kilobars) as follows: Y are taken from Luth and others (1964) and relate to the "granite" system, SiO_2-$NaAlSi_3O_8$-$KAlSi_3O_8$-H_2O, where $P_{H2O} = P_{total}$; T are from James and Hamilton (1969) and relate to addition of 3, 5, and 7.5 wt% An to the "granite" system at $P_{H2O} = P_{total} = 1$ Kbar; x are from Luth (1969) and relate to the dry "granite"system where $P_{H2O} = 0$.

Although good trends appear in Harker diagrams (fig. I.3) Johnson (1986) indicates that the Questa granitic plutons are not related by simple crystal fractionation processes. For example, the northern intracaldera plutons cannot be derived by crystal fractionation from magmas represented by the granite of the Cabresto Lake or the granodiorite of Rio Hondo, or from intermediate-composition magma such as that represented by the precaldera quartz latite. Moreover, within the northern intracaldera plutons, the peralkaline granites cannot be simply related to the metaluminous granites by crystal fractionation. However, Johnson shows that crystal fractionation may have been an important process in the differentiation of individual plutons; the different facies of the Cabresto Lake and Rio Hondo plutons were probably derived by crystal fractionation, as already suspected from modal analyses.

Consideration of trace element data (from Jonhson, 1986) brings up an interesting feature of the Questa granitic rocks. The REE pattern is the same as that reported by Harris (1985) for the Jabel Sayid complex in the Arabian shield. Alkaline rocks (peralkaline and metaluminous granites from Virgin Canyon and Canada Pinabete) are HREE enriched with strong negative Eu anomalies, while calc-alkaline rocks are HREE depleted with no Eu anomalies (fig. I.6). The alkaline rocks are Sr depleted (to 23 ppm in peralkaline granite and to 225 ppm in metaluminous granite) and the calc-alkaline rocks display high Sr content (to 1000 ppm).

A plot of Nb + Y against Rb (after Pearce and others, 1984) allows the geochemical characteristics of the Questa granitic rocks to be related to tectonic environment (fig. I.7). The Nb- and Y-enriched peralkaline rocks plot in the WPG (within-plate granite) field while the Nb- and Y-depleted calc-alkaline rocks plot in the VAG (volcanic arc granite) field of Pearce. The metaluminous rocks from the Virgin Canyon and Canada Pinabete plutons mainly plot in the WPG field but some fall also in the VAG field. The Cabresto Lake units plot in the VAG field and overlap with data from the metaluminous granites. Data from the late mineralized plutons plot in the VAG field and, except for the Red River intrusive complex, are characterized by high Rb compared to all other Questa granitic rocks.

From Pb and Nd isotopic data, Johnson (1986) concludes that "...most of the Questa parental magmas have interacted with the crust prior to eruption or solidification." He considers the peralkaline rocks to have been derived from magmas which interacted most extensively with the crust; direct melting of a

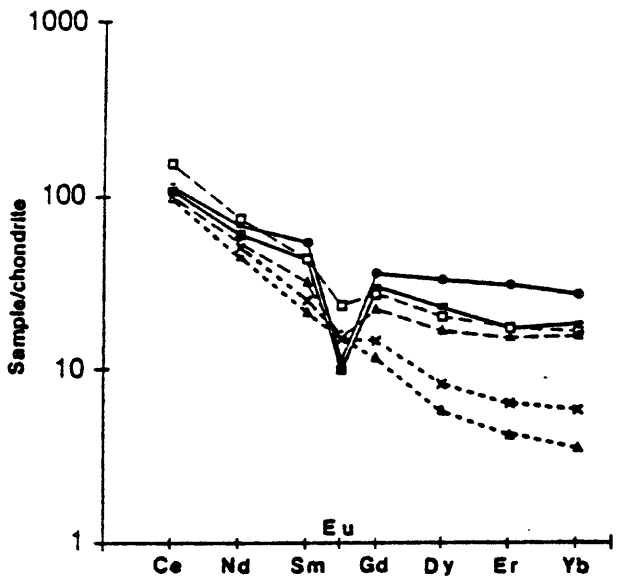

Fig. I.6. Chondrite-normalized REE patterns for selected samples of the Questa granitic system (data from Johnson, 1986). Dots, peralkaline granite of Virgin Canyon; black squares, peralkaline granite of Canada Pinabete; squares, early metaluminous granite of Virgin Canyon; black triangles, later metaluminous granite of Virgin Canyon; triangles, granodiorite of Rio Hondo; crosses, mafic-magmatic enclave in Rio Hondo granodiorite.

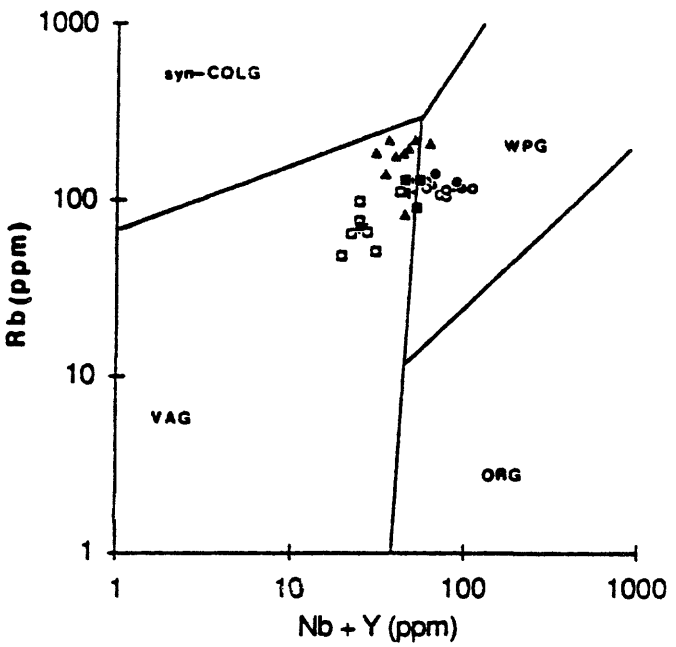

Fig. I.7. Nb + Y against Rb (ppm) for Questa granitic rocks (data from Johnson, 1986; field boundaries from Pearce and others, 1984). Dots, peralkaline granites of Virgin Canyon and Canada Pinabete; circles, metaluminous granites of Virgin Canyon and Canada Pinabete; black squares, Cabresto Lake; squares, Rio Hondo; triangles, late mineralized plutons.

Pb-enriched, previously hybridized, crust is even a possibility. He also suggests that the metaluminous granite in the northern intracaldera plutons may have originated in the crust, although this indication is not as clear as for the peralkaline rocks.

The Cabresto Lake and Rio Hondo plutons have the same Sr, Nd, and Pb isotope compositions as precaldera, intermediate-composition quartz latite. Furthermore, major-element and trace-element compositions of the mafic granitoid units in these plutons are indistinguishable from those of the precaldera intermediate-composition rocks. Johnson (1986) suggests that these two plutons represent the "...waning stages of the precaldera magmatism." and that they "...may have been ascending from the lower crust as peralkaline magmas were generated at higher levels in the crust." By the time of emplacement, these two plutons were largely crytalline and could not assimilate as much country rock as the magmas related to the northern intracaldera plutons.

Notable about the granite of Cabresto Lake is the fact that its character is intermediate between that of the granodiorite of Rio Hondo and the northern intracaldera metaluminous granites; this is evident in modal, major-element, and trace-element data. The Cabresto Lake granite is characterized by low Mg and Ca and high Na+K contents compared to the granodiorite of Rio Hondo. At a given Sr content, the Cabresto Lake pluton is Ba, Y, Zr, and Nb enriched, and Th depleted compared to the Rio Hondo pluton; concentrations of these elements are closer to those in the northern intracaldera plutons (Johnson,1986).

Of interest in the Cabresto Lake and Rio Hondo plutons is the presence of mafic-magmatic enclaves which record a mixing event. Good correlation between MgO and Ni in the mafic units of the Rio Hondo pluton suggests that these units are the product of mixing between intermediate-composition magmas and relatively primitive basaltic magmas (Johnson, 1986). Occurrence of distinct biotite-bearing and amphibole-bearing enclaves in the Cabresto Lake pluton may record two mixing events.

Sr and Pb isotopic data allowed Johnson (1986) to conclude that late-stage assimilation of upper crustal rocks occurred during differentiation of the late mineralized plutons, but do not indicate whether they are products of crystal fractionation of intermediate-composition magmas or direct melts of crustal rocks. Trace-element data for the Bear Canyon and Sulphur Gulch plutons (high Rb, Y, Nb, HREE, Pb, Th, and U) are incompatible with the former interpretation; thus, different source rocks of parental magmas are required to explain their origin.

Petrographic and chemical data indicate the occurrence of two rock series among the Questa granitic rocks. As shown by trace-element and isotope data, they are related to several different sources. Geochemical (fig. I.7) and tectonic characteristics relate the alkaline rocks at Questa to within-plate intracontinental magmatism, derived from upper mantle sources. Isotope data (Pb and Nd) indicate large interactions with the upper crust. From their chemistry and tectonic environment, the calc-alkaline rocks can be related to a volcanic arc, calc-alkaline, intracontinental environment. As indicated by isotope data, the Cabresto Lake and Rio Hondo plutons did not interact as much with the upper crust as the northern intracaldera plutons because they were emplaced as crystal-rich magmas. They are characterized by one or more mixing events with more mafic magmas at some time during their differentiation.

CHAPTER II

Opaque Oxide Minerals

PART I: TEXTURES

A number of textures are widespread among the opaque oxide minerals of the Questa granitic rocks and are summarized in Table II.1. Most of these textures are of an exsolution type, resulting either from unmixing or from oxidation or reduction "exsolution" of a dissolved constituent. Other textures are of a replacement type, caused by metasomatism or oxidation.

1. EXSOLUTION TEXTURES

a) Ilmenite-hematite exsolution intergrowths can be of two types: (1) ilmenite grains containing hematite exsolution bodies, and (2) hematite grains containing ilmenite lenses or blebs. These intergrowths are the only true exsolution textures found in the Questa granitic rocks.

It has been long recognized that hematite and ilmenite form a continuous solid-solution series at high temperature. Carmichael (1961) estimated that temperature to be above 950°C. Lindsley (1973) suggests from natural occurrences (e.g. Rumble, 1971; Kretchsmar and McNutt, 1971) and experimental data that the consolute temperature must be no higher than 800°C. In his theoretical model, Burton (1985) calculates a temperature of 714°C.

At lower temperatures, hematite and ilmenite are not miscible in all proportions and over an intermediate range of compositions a solvus is intercepted (fig. II.1) and exsolution takes place along the (0001) direction of the host crystal. From experiments on natural hemo-ilmenite crystals, Carmichael estimated that compositions in the range Ilm_6 to Ilm_{88} would exsolve an ilmenite- or hematite-rich solid solution. However, Kretchsmar and McNutt (1971), based on electron microprobe analyses of natural samples, moved that range to higher ilmenite compositions (Ilm_{28} to Ilm_{95}). Theoretical considerations strongly support this more asymmetric solvus (Burton, 1985).

Authors have commonly observed two sets (generations) of exsolutions in ilmenite-hematite crystals; an earlier set of larger, somewhat irregular lenses or blebs of hematite in ilmenite or ilmenite in hematite, which, in turn may contain a later set of thinner, more regular lenses or lamellae of the host (Plate II.1, d; Edwards, 1954; Carmichael,1961; Ramdohr,1969; Kretchsmar and McNutt, 1971). Burton (1985) presents a detailed explanation of the relation between these two exsolution processes. The larger bodies are referred to as discontinuous (Yund and McCallister, 1970; Kretchsmar and McNutt, 1971), "non-coherent" (Brett,1964), or asymmetrical exsolution (Burton, 1985); the smaller bodies, also considered to be later, are said to result from continuous, "coherent", or symmetrical exsolution. Kretchsmar and McNutt accepted Carmichael's consolute temperature of 950°C and found that the change from discontinuous to continuous exsolution occurs at about 800°C on both limbs of the solvus, at the approximate compositions Ilm_{85} and Ilm_{40}. It should be noted that these data are not in accord with Lindsley's estimate that the consolute temperature lies at less than 800°C (fig. II.1). Burton estimates the change between asymmetric and symmetric two-phase regions to occur between 550° and 500°C. According to Kretchsmar and McNutt's interpretation of their data, five different textures can result from slow cooling, depending on the initial composition in the system ilmenite-hematite (Table II.2).

Table II.1: Inventory of opaque oxide textures in the Questa granitic plutons.

PLUTON	Unit or facies	Textural feature (1)	(2)	(3)	(4)	(5),(6) (7)	(8)	(9)
VIRGIN CANYON	Peralkaline		XXX	X	XX	5		XXX
	Early metaluminous	X	XX				XX	XXX
	Later metaluminous	X	XX		X		XX	XXX
CANADA PINABETE	Peralkaline		XXX				X	XXX
	Metaluminous	X	XX				XX	XXX
RITO del MEDIO		XX	XXX		XX		XX	XX
CABRESTO LAKE	Granite	XX	XX			6	XX	XX
	Mixed	XX	XX			6	XX	XX
	Biotite-bearing enclaves	XX	XX				XX	X
	Amphibole-bearing enclaves	XX	XX			6	X	X
RIO HONDO	Granodiorite	XX	X			6,7	X	X
	Granite	XX	XX			6	XX	XX
	Enclaves	XX	X			6,7	X	X
BEAR CANYON		X	X				X	XX
SULPHUR GULCH, Carapace		X	X		X		XX	X
RED RIVER INTRUSIVE COMPLEX	Granodiorite	X	X			6,7	X	X
	Granite		X		X		X	X
	Alkali-feldspar granite							X
	Quartz diorite						X	
LUCERO PEAK		X	XX				X	X

Note. X = present; XX = common; XXX = abundant. Textural features: (1) ilmenite-hematite exsolution intergrowths;(2) ilmenite-magnetite intergrowths; (3) magnetite-ilmenite intergrowths; (4) ilmenite aggregates after sphene; (5) irregular sphene after ilmenite; (6) euhedral sphene after ilmenite and magnetite; (7) sphene coronas around magnetite; (8) oxidation of ilmenite to hematite plus rutile; (9) oxidation of magnetite to hematite.

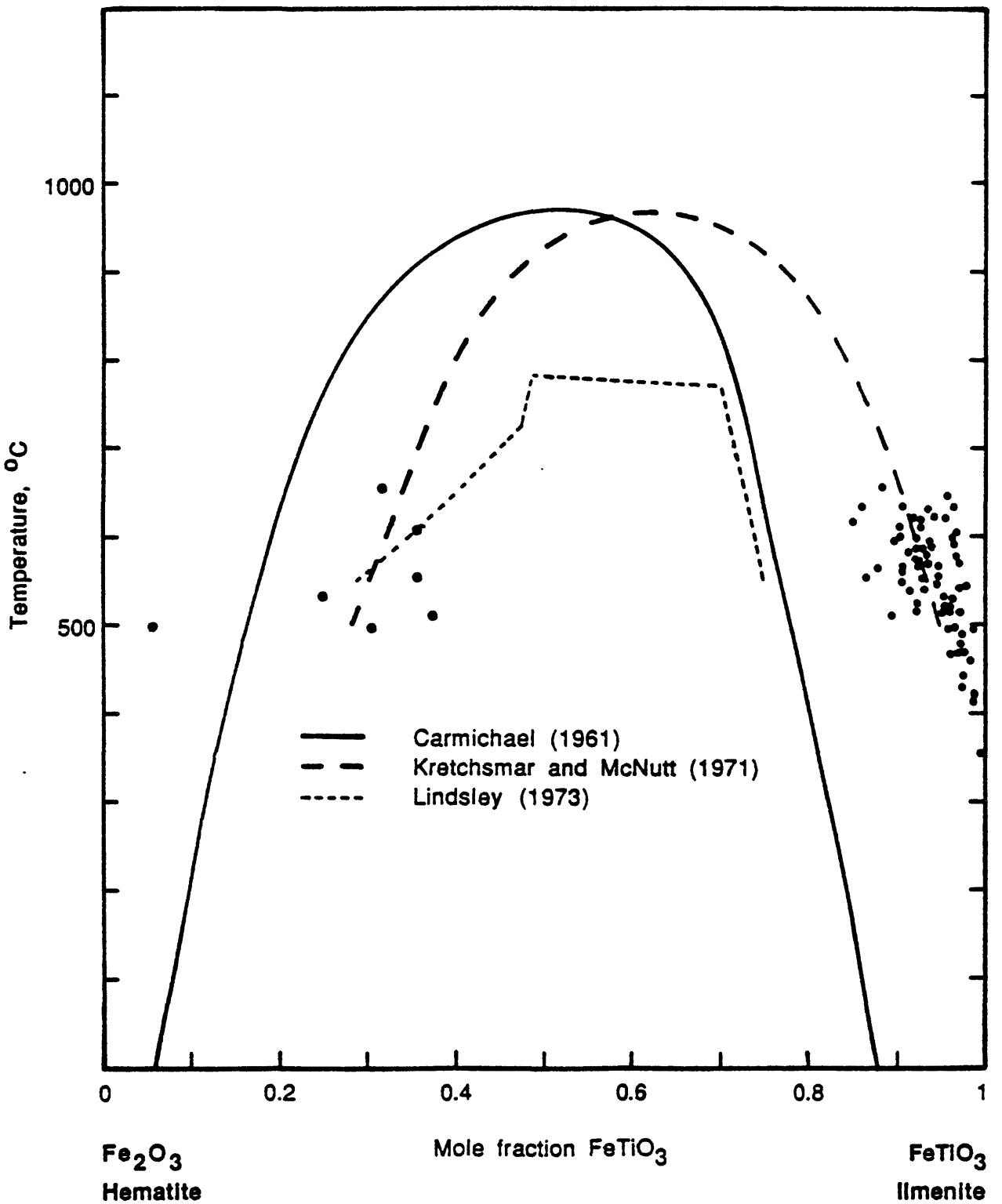

Fig. II.1. The system hematite-ilmenite, showing the miscibility gaps reported by Carmichael (1961; solid), Kretchsmar and McNutt (1971; long dashes), and Lindsley (1973; short dashes). Data for the Questa granitic rocks are represented by dots.

Table II.2: Types if ilmenite-hematite exsolution intergrowth.

Composition range	Process	Texture
Ilm_0-Ilm_{28}	No exsolution	Homogeneous hematite
Ilm_{28}-Ilm_{40}	Continuous exsolution of ilmenite from hematite	Small lenses or lamellae of ilmenite in hematite
Ilm_{40}-Ilm_{85}	Discontinuous exsolution down to 800°C, followed by continuous exsolution	Large discs or lenses and small lenses or lamellae of exsolved phase in host phase
Ilm_{85}-Ilm_{95}	Continuous exsolution of hematite in ilmenite	Small lenses or lamellae of hematite in ilmenite
Ilm_{95}-Ilm_{100}	No exsolution	Homogeneous ilmenite

Ilmenite-hematite exsolution intergrowths are common, but not everywhere present in the Questa granitic plutons. In the Virgin Canyon and Canada Pinabete plutons, they are rare and only present in the metaluminous granites. Ilmenite is the host and hematite exsolved as very small droplets or lamellae (<0.005 mm across).

In the Rito del Medio pluton these intergrowths are more common; one finds both hematite containing ilmenite exsolution lenses (Plate II.1, a and b) and ilmenite containing hematite exsolution lenses (Plate II.1, c). More rarely, some intergrowths could be the result of discontinuous exsolution, followed by continuous exsolution.

PLATE II.1: Photomicrographs of ilmenite-hematite exsolution intergrowths.

(a and b) Hematite (light gray) containing one set of ilmenite exsolution lamellae (dark gray). Exsolution-free overgrowth of hematite is oscillatory zoned with respect to TiO2 (7.2 to 2.6 wt%). Vug, Rito del Medio granite, sample 82QC17. Bars are 100 microns long.

(c) Ilmenite (light gray) containing one set of fine hematite exsolution lamellae (white). Rito del Medio granite, sample 81S28. Bar is 50 microns long.

(d) Complex oxide assemblage enclosed in translucent sphene. Ilmenite (gray) contains two sets of hematite exsolution bodies (light gray). Larger bodies of hematite contain fine exsolution lenses of ilmenite. Next to lower, large hematite exsolution body is an oxidation mat of hematite plus rutile. At edge of ilmenite are angular medium-gray magnetite grains. Mafic magmatic enclave in granodiorite of Rio Hondo, sample 82QC12. Bar is 50 microns long.

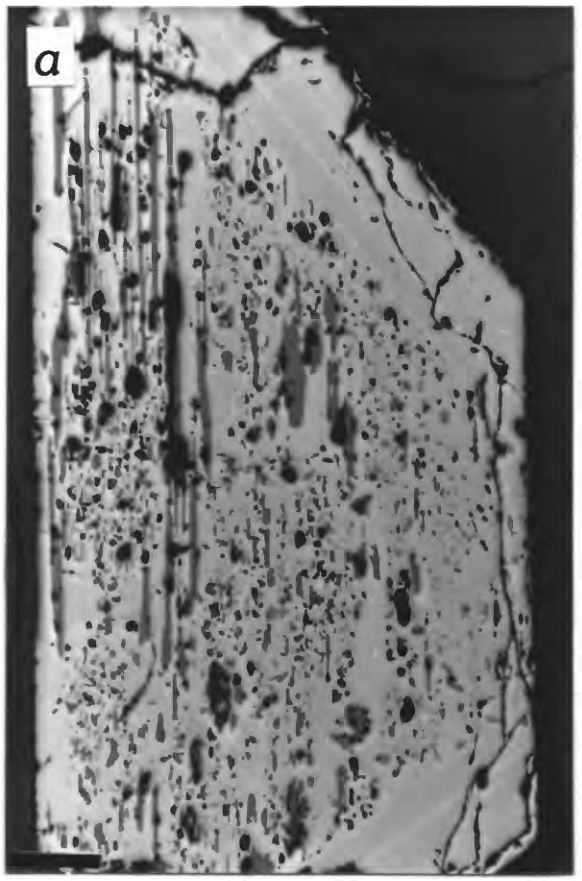
a

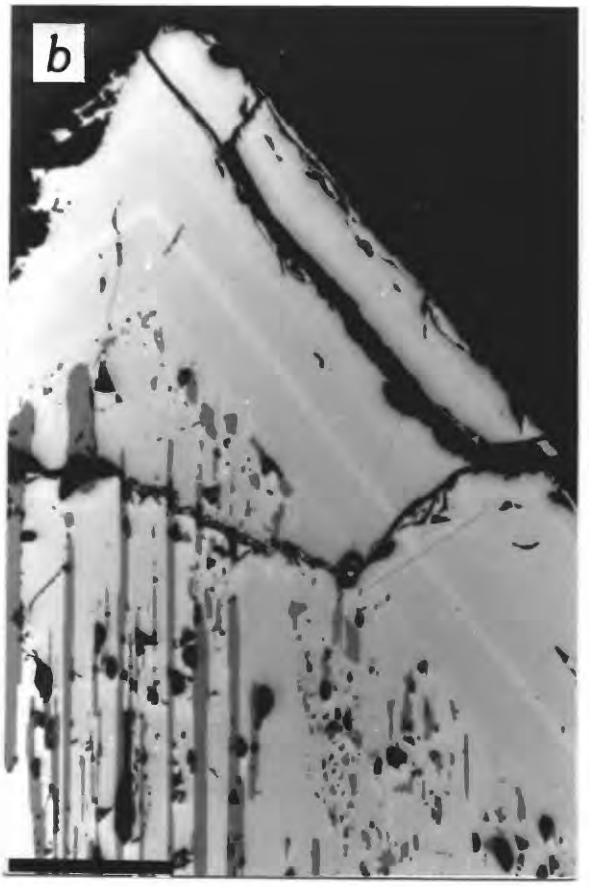
b

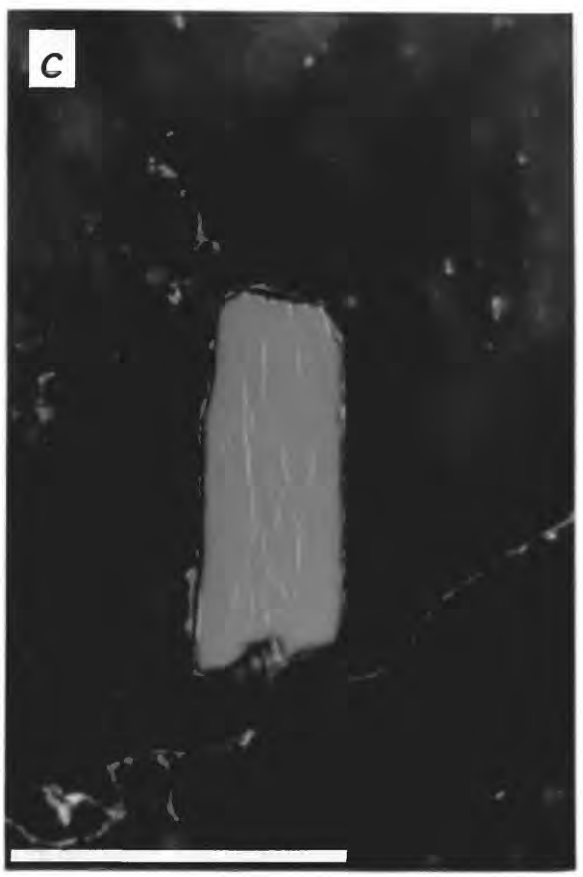
c


d

Only one type of exsolution lamellae is found in the Cabresto Lake pluton; hematite is always exsolved from ilmenite as thin long lenses or lamellae.

Ilmenite is quite rare in the Rio Hondo pluton and, in both the granodiorite and the granite, ilmenite-hematite intergrowths occur only in rounded grains enclosed in sphene (Plate II.1, d). Both continuous and discontinuous exsolution processes occurred, one set of exsolution lenses being predominant. When two sets of exsolution products are present, ilmenite is always in greater proportion than hematite.

Rare fine hematite exsolution lenses occur in ilmenite in the Bear Canyon pluton. In the carapace unit of the Sulphur Gulch pluton and in the granodiorite of the Red River intrusive complex, both primary isolated ilmenite and rounded ilmenite grains enclosed in sphene may contain one set of hematite exsolution products.

Hematite is commonly exsolved from ilmenite in the Lucero Peak pluton. The exsolution products occur as lenses which are so small as to be hardly seen under the microscope at 400X magnification.

b) Ilmenite-magnetite intergrowths compose textures in which magnetite is the host phase and magnetite-ilmenite intergrowths are those in which ilmenite is the host phase. These two textures are not true exsolution textures because they do not result from simple unmixing of a dissolved constituent.

(1) Ilmenite-magnetite intergrowths are common in igneous rocks and often have been described in mafic suites. They are also common in more silicic rocks and are well displayed in the Questa granitic rocks, especially within the intracaldera plutons.

Ilmenite-magnetite intergrowths were long interpreted as due to unmixing of a $FeTiO_3$ component dissolved in magnetite at high temperature. However, experiments have shown that it is impossible to homogenize such intergrowths by simple heating (Vincent and others, 1957; Basta, 1960). Furthermore, the solubility of ilmenite in magnetite at high temperature (above 1000°C) is too limited to explain the extensive ilmenite-magnetite intergrowths found in many natural samples. From heating experiments, Basta (1960, p. 1026) concluded:

> "...at the temperature of formation of igneous rocks, only very restricted solid solution is possible between magnetite (Fe_3O_4) and alpha-$FeTiO_3$ (ilmenite); possibly not more than 5 to 10% of alpha-$FeTiO_3$."

TiO_2 in titaniferous magnetite is therefore considered to be dissolved as ulvospinel (Fe_2TiO_4). Magnetite and ulvospinel are known to form a complete solid solution at temperatures above 600°C (Vincent and others, 1957) and a temperature of less than 455°C was suggested recently for the consolute temperature of the magnetite-ulvospinel solvus (Price, 1981). Moreover, by heating ilmenite-magnetite intergrowths in a reducing atmosphere, Wright (1959) obtained homogeneous magnetite-ulvospinel solid solutions. Thus, it is

now accepted that ilmenite-magnetite intergrowths are due to oxidation of the ulvospinel component from a magnetite-ulvospinel solid solution. Note that ilmenite intergrown along (111) planes of magnetite cannot be due to oxidation of earlier exsolved ulvospinel, because ulvospinel unmixes along the (100) planes of magnetite. From his experimental data, Lindsley (1962, p. 106) suggested that ilmenite-magnetite intergrowths originate by direct oxidation of magnetite-ulvospinel solid solutions to magnetite-rich spinel and ilmenite.

The term "exsolution" will be used as defined by Buddington and Lindsley (1964, p. 322) to refer to ilmenite-magnetite intergrowths resulting from oxidation of magnetite-ulvospinel solid solutions. The different textures which can result from such an oxidation were described by Buddington and Lindsley (1964, p. 323) as follows:

> "From the microtextures of natural oxide minerals we conclude that increasing degrees of oxidation and diffusion result in a systematic series of fabrics from (1) a single-phase homogeneous spinel; through (2) trellis intergrowths of thin ilmenite lamellae in all sets of (111) planes of the host; (3) sandwich intergrowths of thick ilmenite lamellae predominantly in one set of (111) planes; (4) granules of ilmenite within the magnetite; to (5) granules or occasional lamellae of ilmenite on external borders of the magnetite."

It is to be noted that in some cases it is difficult to decide whether ilmenite granules next to magnetite grains are due to type (5) "exsolution" from magnetite, or to primary crystallization of ilmenite. Some of these ilmenite granules could have a compound origin, and may consist of a primary core, surrounded by secondary ilmenite "exsolved" from magnetite (Kretchsmar and McNutt, 1971).

All five types of intergrowth can be observed in the granitic rocks associated with Questa caldera (Table II.3). Homogeneous magnetite is more common in plutons located outside the caldera, whereas "exsolution" textures are well displayed within the intracaldera plutons. Estimates of the abundance of the various types of intergrowths within each pluton are summarized in Table II.3.

The peralkaline granite of Virgin Canyon is characterized mainly by ilmenite granules within or along the borders of magnetite grains (Plate II.2, d); type (3) lamellae are usually rare, but locally more abundant. In both metaluminous granites, types (2) and (3) ilmenite lamellae are most abundant; granules are more rare and are developed mainly at the borders of magnetite grains. Locally, magnetite can be homogeneous, especially in samples containing little ilmenite.

Ilmenite-magnetite intergrowths in the peralkaline granite of Canada Pinabete are similar to those in the peralkaline granite of Virgin Canyon. In the metaluminous granite, magnetite can be locally homogeneous, but usually one or more "exsolution" textures occur. Short type (2) lamellae evenly distributed in all (111) planes of magnetite (Plate II.2, c) are as commonly seen as broader (up to 0.003 mm wide) type (3) lamellae. Types (4) and (5) ilmenite granules are common as well (Plate II.2, c).

Table II.3: Inventory if ilmenite-magnetite intergrowths in the Questa granitic plutons.

PLUTON	Unit or facies	Type (1)	Type (2)	Type (3)	Type (4)	Type (5)
VIRGIN CANYON	Peralkaline		X	X	XXX	XXX
	Early metaluminous	X	XX	XXX	X	X
	Later metaluminous		XX	XXX	X	X
CANADA PINABETE	Peralkaline				XXX	XXX
	Metaluminous	X	XX	XX	XX	XX
RITO del MEDIO			XX	XXX	X	X
CABRESTO LAKE	Granite	XX		XXX	XX	XX
	Mixed	X	X	XXX	XX	XX
	Biotite-bearing enclaves	XXX		XX		
	Amphibole-bearing enclaves	XX	X	XXX		
RIO HONDO	Granodiorite	XXX		X		
	Granite	XX		XX	X	X
	Enclaves	XXX		X	X	
BEAR CANYON		XXX				XX
SULPHUR GULCH	Carapace				X	X
	Source aplite	X				
RED RIVER INTRUSIVE COMPLEX	Granodiorite	XXX		X		
	Granite	XX				XX
	Alkali-feldspar granite	XX				
	Quartz diorite	XXX				
LUCERO PEAK		XXX		X		XX

Note. X = present; XX = common; XXX = abundant. Textural features: (1) single-phase homogeneous magnetite; (2) trellis intergrowths of thin ilmenite lamellae in all sets of (111) planes of the host; (3) sandwich intergrowths of thick ilmenite lamellae predominantly in one set of (111) planes; (4) granules of ilmenite within the magnetite; (5) granules or occasional lamellae of ilmenite on external borders of magnetite.

In the Rito del Medio granite, ilmenite "exsolution" is most common as types (2) and (3) lamellae (Plate II.2, a), granules being much less common. Type (2) lamellae are the best displayed; these short ilmenite lamellae usually contain small black grains which are presumed to be gahnite spinel based on electron microprobe traverses.

The Cabresto Lake granite and its mixed facies are mostly characterized by broad type (3) ilmenite lamellae and fewer ilmenite granules of types (4) and (5). Both types of enclave within the Cabresto Lake pluton contain broad (up to 0.01 mm across) type (3) ilmenite lamellae (Plate II.2, b); amphibole-bearing enclaves also contain a set of short lamellae hosting small spinel grains.

In the granodiorite of Rio Hondo, ilmenite "exsolution" from magnetite is rare and only seen as type (3) lamellae; magnetite is most often homogeneous (following reequilibration). Ilmenite-magnetite intergrowths are a little more common in the granite; type (3) lamellae are most abundant and granules rare. Also scarce in the mafic-magmatic enclaves, ilmenite "exsolution" textures are of types (3) and (4).

In the Bear Canyon pluton, ilmenite "exsolved" from magnetite as type (5) granules only. Ilmenite in the carapace unit of the Sulphur Gulch pluton is found as both types (4) and (5) granules.

Ilmenite "exsolved" from magnetite is rare and occurs as type (3) lamellae in the granodiorite of the Red River intrusive complex. Ilmenite in the Red River granite is found as type (5) "exsolution" granules.

In the Lucero Peak granite, the most common texture resembles type (5) exsolutions; it is not obvious, however, whether these ilmenite granules result from oxidation of magnetite or from primary crystallization. The granules associated with magnetite are quite large and could be the product of both processes. Type (3) lamellae are present in the Lucero Peak granite, but are rare.

(2) Magnetite lamellae in ilmenite have not often been described in the literature. They have been found in metamorphic rocks such as orthogneisses of the Adirondack area (Buddington and others, 1963) and paragneisses of the Franklin area (Baker, 1955; Buddington and Lindsley, 1964). They were also described in trachy basalts from Teneriffe (Haggerty and others, 1966).

In these intergrowths, magnetite occurs as lamellae parallel to the basal plane of the host. Buddington and Lindsley (1964) reproduced such textures in synthetic material by reducing Fe_2O_3-rich ilmenites in an fO_2-buffered atmosphere. Magnetite lamellae in ilmenite are interpreted as due to reduction "exsolution" of Fe_2O_3 dissolved in ilmenite (Buddington and others, 1963; Buddington and Lindsley, 1964). In studying the paragneisses of the Franklin area, Buddington and Lindsley (1964) concluded that this partial reduction probably occured subsequent to the oxidation processes leading to the formation of hematite after magnetite, and hematite plus rutile after ilmenite. Textures in the Questa granitic rocks indicate the opposite sequence of events; magnetite "exsolved" from ilmenite is commonly oxidized to hematite.

PLATE II.2: Photomicrographs of ilmenite-magnetite intergrowths.

(a) Magnetite containing types (2) and (3) ilmenite "exsolution" lamellae (darker gray). Finer, type (2) lamellae are punctuated by minute gahnitic spinel grains. Magnetite is slightly oxidized to hematite (white). Rito del Medio granite, sample 82QC16. Bar is 100 microns long.

(b) Magnetite (light gray) containing type (3) ilmenite "exsolution" lamellae. Amphibole-bearing enclave in granite of Cabresto Lake, sample 85QC9. Bar is 100 microns long.

(c) Magnetite containing types (2), (4), and (5) ilmenite "exsolution" products (darker gray) and partially oxidized to hematite (white). Metaluminous granite of Canada Pinabete, sample 82QC46.1. Bar is 100 microns long.

(d) Magnetite containing types (4) and (5) ilmenite "exsolution" products. Martitization (white) of magnetite is extensive. Peralkaline granite of Virgin Canyon, sample 83QC29. Bar is 100 microns long.

Among the Questa plutons, magnetite lamellae in ilmenite occur only locally in the peralkaline granite of Virgin Canyon; they characterize samples having a more seriate texture. Magnetite lamellae occur in ilmenite grains of irregular shape which may be bordered by an irregular and incomplete rim of sphene (Plate II.3, a and b). This association can be found enclosed or partially enclosed in alkali amphibole. The magnetite lamellae can be up to 0.005 mm wide when individual and up to 0.04 mm across when coalescent. The lamellae are partially oxidized to hematite along their (111) planes. Magnetite lamellae in ilmenite are found in samples in which ilmenite "exsolved" from magnetite by oxidation of its Fe_2TiO_4 component (Plate II.3, b).

2. REPLACEMENT TEXTURES

a) Textures involving small-scale metasomatism occur locally in the Questa granitic plutons. In these textures sphene is involved, either as a reactant (1) or a product (2) to (4).

(1) Granular aggregates of ilmenite grains in different crystallographic orientations often conform to an obvious lozenge shape and are considered to represent a replacement of sphene (Plate II.4, a). This texture is found in the Virgin Canyon and Rito del Medio plutons and in the Red River intrusive complex. In the Virgin Canyon pluton, ilmenite aggregates are typical of the marginal facies of the peralkaline granite near its contact with wall-rock andesite, and of the later metaluminous granite. A sphene grain with an ilmenite corona was found in the later metaluminous granite (Plate II.3, c) and a sphene relict was also found within an ilmenite aggregate in the peralkaline granite (Plate II.3, d). In the Rito del Medio granite, ilmenite

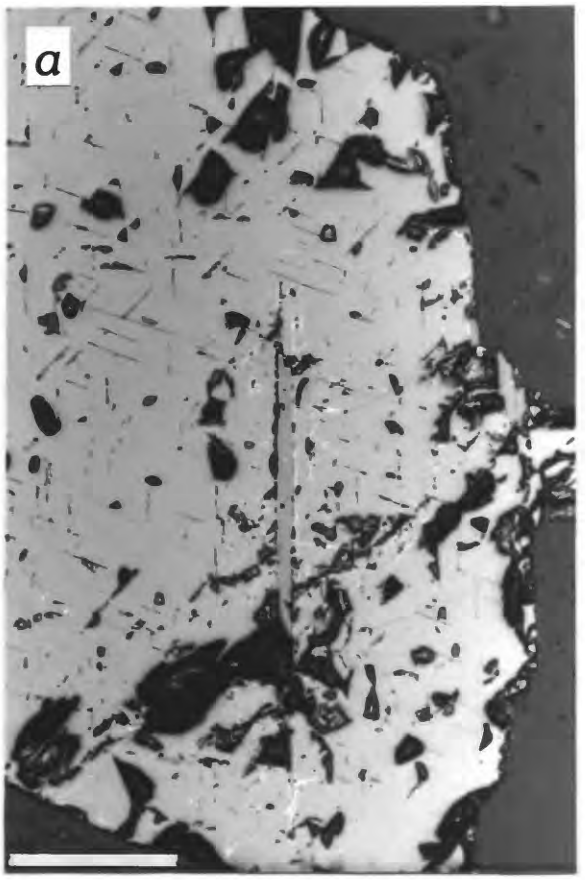
a

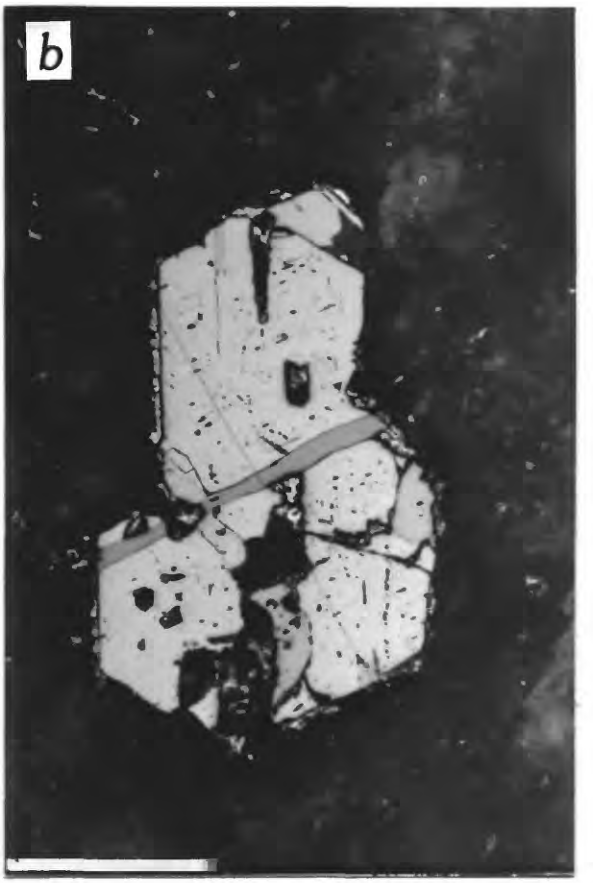
b

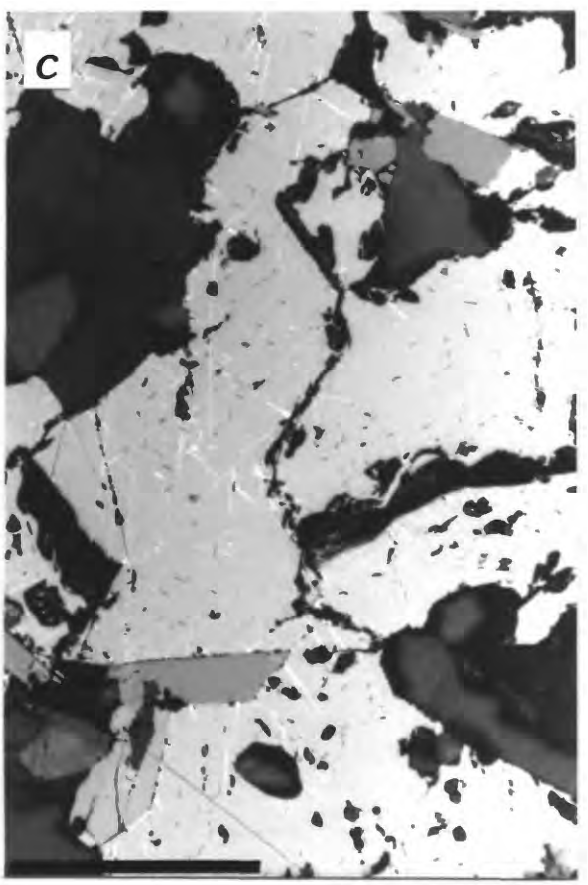
c

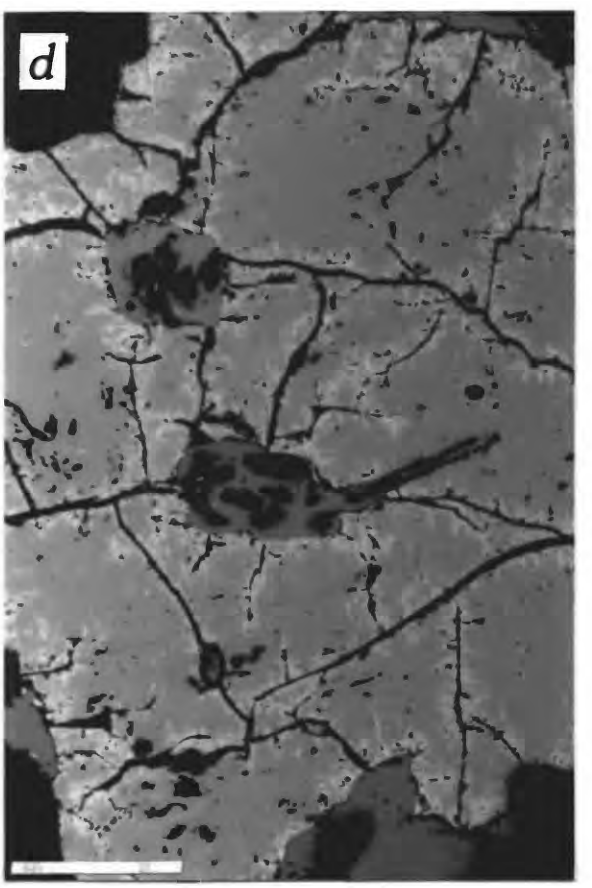
d

PLATE II.3: Photomicrographs of magnetite-ilmenite intergrowths.

(a) Ilmenite (medium gray) containing magnetite "exsolution" products (lighter gray) which are partly oxidized to hematite (white). Ilmenite host is surrounded in places (upper left and lower right) by a thin irregular rim of sphene (darker gray). Peralkaline granite of Virgin Canyon, sample Q83J63. Bar is 100 microns long.

(b) Lower grain is magnetite containing type (5) ilmenite "exsolution" products (darker gray) and showing oxidation to hematite (white). Two upper grains are ilmenite, one containing magnetite lamellae (lighter gray), partially oxidized to hematite (white); both ilmenite grains are surrounded by an irregular rim of sphene. Peralkaline granite of Virgin Canyon, sample 82QC38. Bar is 100 microns long.

Photomicrographs of ilmenite-magnetite-sphene intergrowths.

(c) Ilmenite (black), forms a corona around euhedral sphene. Transmitted light. Later metaluminous granite of Virgin Canyon, sample Q83J79. Bar is 100 microns long.

(d) Sphene core within an aggregate of ilmenite (black). Transmitted light. Peralkaline granite of Virgin Canyon, sample 83QC29. Bar is 100 microns long.

---

grains constituting the aggregates are usually coarser than in the Virgin Canyon pluton and may contain hematite exsolution bodies (Plate II.4, a). In the Red River intrusive complex such aggregates are found in the granitic unit. The shape of these aggregates and sphene relicts found in the Virgin Canyon pluton lead to the conclusion that the granular aggregates of ilmenite formed by replacement of early crystallized sphene.

(2) A texture in which sphene is a product occurs quite locally in the Virgin Canyon pluton and is characteristic of the more seriate samples of the peralkaline granite. In this association, rounded and irregular ilmenite grains are surrounded by irregular sphene rims. Ilmenite may or may not contain magnetite lamellae partially oxidized to hematite (Plate II.3, a and b).

(3) In a third association, sphene can be large and quite euhedral and contains irregular, rounded ilmenite grains as well as much less common magnetite with more euhedral shapes. It is significant that all ilmenite grains are not in the same optical orientation. The ilmenite grains are usually unmixed, displaying one or two sets of hematite exsolution products, and are often partially oxidized to hematite plus rutile. The magnetite grains can be partially oxidized to hematite. Ilmenite and magnetite grains are usually more abundant in the cores of sphene crystals (Plate II.1, d; Plate II.4, b and c), but may also occur towards the rim of sphene crystals, in a fairly well-defined, lozenge-shaped zone (Plate II.7, a). This texture is characteristic of the Cabresto Lake and Rio Hondo plutons, where it is found in all rock types except the biotite-bearing enclaves of the Cabresto Lake pluton; it is also characteristic of the granodiorite of the Red River intrusive complex.

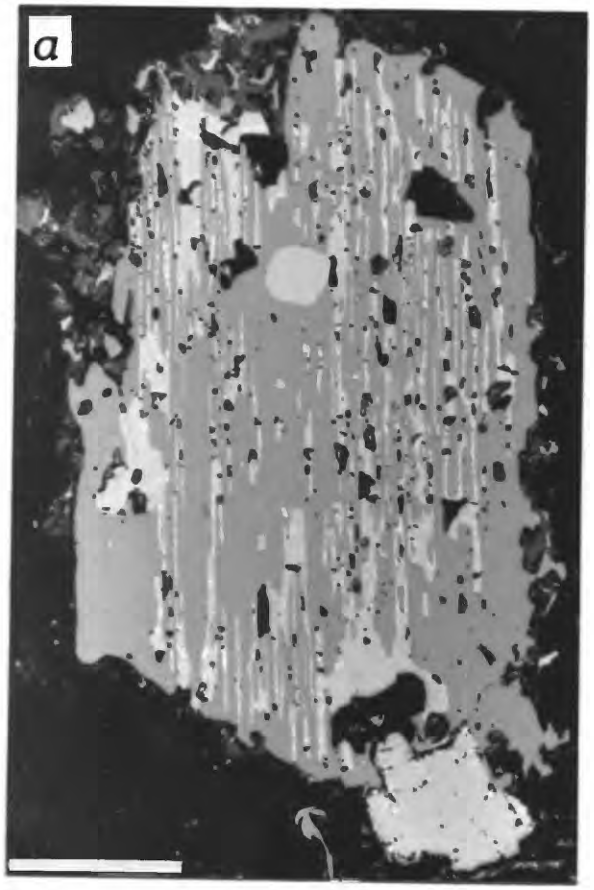
a

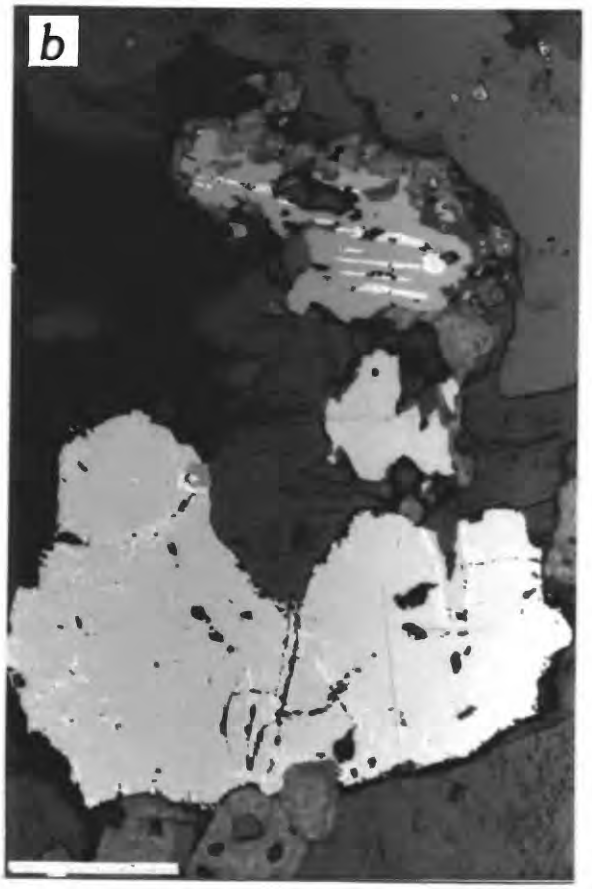
b


c

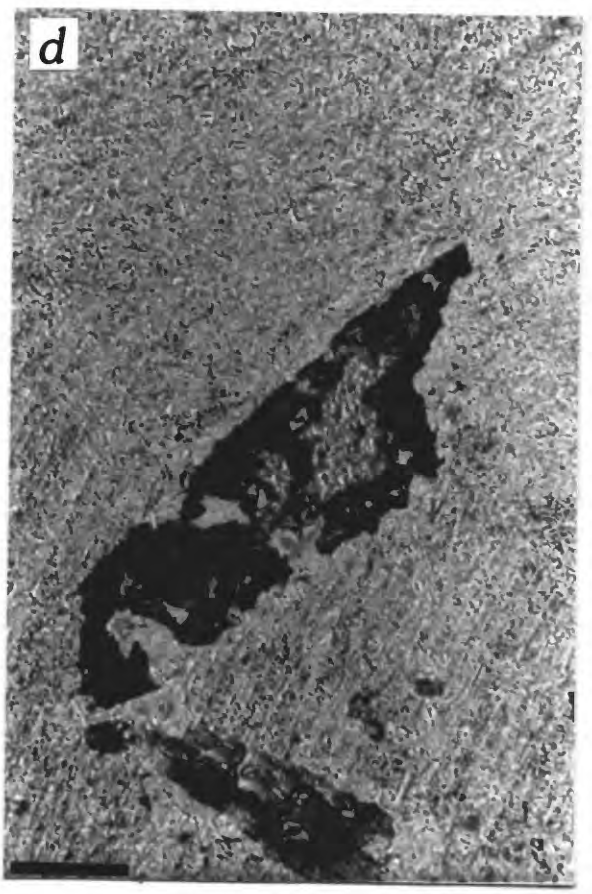
d

PLATE II.4: Photomicrographs of ilmenite-magnetite-sphene intergrowths, continued.

(a) Lozenge-shaped ilmenite aggregate after sphene (darker gray), next to magnetite (lighter gray) containing ilmenite "exsolution" lamellae of types (2) and (3), both punctuated by gahnitic spinel granules (black); magnetite contains minor martite. Rito del Medio granite, sample 81S28. Bar is 100 microns long.

(b and c) Large euhedral sphene grain containing irregular ilmenite grains of differing orientation. Ilmenite is partly unmixed to hematite (thin, light-gray lamellae) and partly oxidized to hematite plus rutile (white and gray mats). Granodiorite of Rio Hondo, sample 84QC31. Bars are 100 microns long.

(d) Irregular rim of sphene around magnetite which contains thin type (2) ilmenite lamellae and minor martite. Granodiorite of Rio Hondo, sample 84QC31. Bar is 100 microns long.

---

(4) A fourth association consists of thin irregular sphene coronas around magnetite (Plate II.4, d) and is found in the granodioritic facies and in the mafic-magmatic enclaves of the Rio Hondo pluton, as well as in the granodiorite of the Red River intrusive complex.

There is little literature on replacement textures involving ilmenite-sphene or magnetite-sphene reactions. Associations (2) and (3) appear to involve partial replacement of ilmenite, with introduction of SiO_2 and CaO (Ramdohr, 1969). This type of replacement has been described as auto-metasomatic, caused by residual liquids (Haggerty, 1976). In association (2) in Virgin Canyon, the irregular sphene rim around ilmenite suggests a late-stage process, that was followed by limited reduction "exsolution" of magnetite from the Fe-enriched ilmenite core. In association (3), the euhedral shape of sphene and the different optical orientations of ilmenite grains suggest contemporaneous crystallization of sphene and ilmenite (with or without magnetite). Minor reaction of ilmenite to sphene could partly account for the common rounded shape of ilmenite grains. Abundant hematite exsolution in ilmenite grains can be explained by high initial content of Fe_2O_3 in ilmenite, or by reaction of ilmenite to sphene (which impoverishes ilmenite in Ti), or both. Association (4) has been described by Haggerty (1976) as resulting from a late-stage process, also metasomatic and involving fluids. In the Questa rocks, associated magnetite is free of Ti and does not usually contain ilmenite "exsolution" products. The sphene coronas around magnetite are therefore considered to be products of Ti exsolution from magnetite under conditions too oxidizing for precipitation of type (5) ilmenite granules.


a

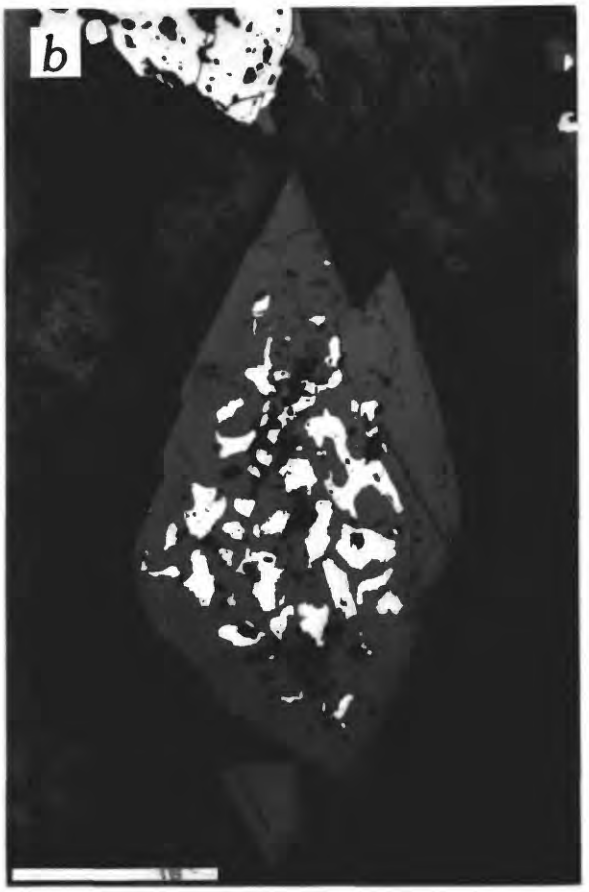
b

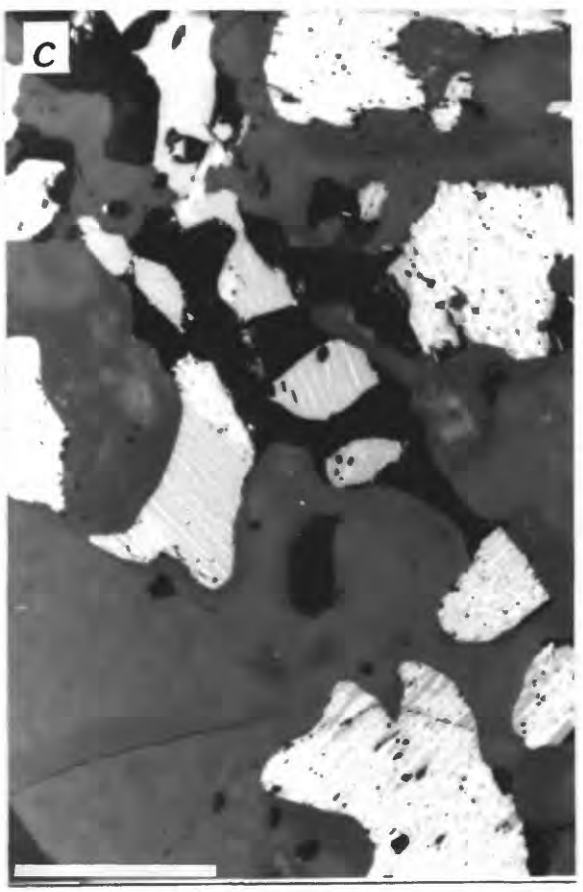
c


d

b) Probably the last to occur are oxidation processes which lead to the formation of hematite plus rutile after ilmenite and hematite after magnetite.

(1) Oxidation of ilmenite to hematite plus rutile has been recognized in different types of rocks. Buddington (1963) refers to "meta-ilmenite" in the Adirondack metamorphic rocks, while Czamanske and Mihalik (1972) describe "irregular, patchy mats" in the granite of the Finnmarka complex, Norway. This reaction may occur at constant or increasing oxygen fugacity as temperature decreases (Robie and Waldbaum, 1968); thus, hematite plus rutile are likely to occur in ilmenite as the stable assemblage at low temperature in an oxidizing environment (Verhoogen, 1962).

As expected in these high-level plutons, oxidation of ilmenite to hematite plus rutile is widespread. Only four specific occurrences of ilmenite are typically free of oxidation: (1) Ilmenite in the peralkaline granites of Virgin Canyon and Canada Pinabete; only locally do samples of the peralkaline granite of Canada Pinabete exhibit trace oxidation of ilmenite to hematite plus rutile. (2) Ilmenite derived by oxidation "exsolution" from magnetite; this ilmenite is free of oxidation, except in type (3) "exsolution" lamellae in the Rio Hondo pluton. (3) Ilmenite exsolved from hematite, most often seen in the Rito del Medio pluton. (4) Ilmenite composing the lozenge-shaped aggregates after sphene in the Virgin Canyon pluton, the Rito del Medio granite, and the Red River intrusive complex.

In all other occurrences, ilmenite is typically partially oxidized. This oxidation is less extensively developed in smaller grains.

(2) It is generally accepted that oxidation of magnetite to hematite (martite) occurs as temperature within the magmatic system decreases (Ramdohr, 1969). It is not clear, however, under what temperature conditions martitization occurs. It is assumed that this temperature is above 400°C (Basta, 1959), because oxidation of magnetite at lower temperature should lead to formation of maghemite (cubic form of Fe_2O_3) instead of hematite. Oxidation to hematite starts preferentially from the edges of the magnetite grains, as well as along cracks and exsolution products; it can also develop preferentially along the (111) planes of magnetite.

Oxidation of magnetite to hematite is a common feature of all granitic plutons associated with Questa caldera. It can be more or less extensive, ranging from cases in which magnetite may contain a few hematite lamellae, to those in which hematite replaces more than half of the magnetite grain. It is often possible to find different degrees of oxidation of magnetite to hematite in the same sample, with no apparent relation to characteristics such as size or shape of the magnetite grains. Among the intracaldera plutons, magnetite is most oxidized in the Virgin Canyon and Canada Pinabete plutons, somewhat less oxidized in the Rito del Medio pluton, and least oxidized in the Cabresto Lake granite. Within the Rio Hondo, Lucero Peak, and Sulphur Gulch plutons, and the Red River intrusive complex, there is only minor oxidation of magnetite to hematite. Magnetite is somewhat more oxidized in the Bear Canyon pluton.

PART II: OCCURRENCE AND CHEMISTRY OF OPAQUE OXIDE MINERALS IN THE QUESTA GRANITIC PLUTONS

Opaque oxide minerals are well represented in all Questa granitic rocks (0.2 to 3.1 volume percent) and have been extensively studied and analyzed in thin section. Magnetite and ilmenite are most abundant; hematite is common and can be primary, but is most often secondary. Opaque oxide textures are often extremely complex and are interrelated with the stabilities of sphene and rutile. Sulfide minerals are present, but usually rare (<0.1%); pyrite is most common, but pyrrhotite is rarely found enclosed in pyrite.

Because of great variability in composition of the opaque oxide minerals in the Questa granitic rocks, a large number of selected analyses are reported for each pluton: 119 magnetite analyses (averaged from 161 analyses) in 80 samples; 210 ilmenite analyses from 68 samples; 24 hematite analyses from 12 samples; 9 ilmenorutile analyses from 4 samples; 2 columbotantalite analyses from 2 samples; and 3 davidite analyses from 1 sample. The analyses are reported in Tables A.1.1 through A.9 of Appendix A.

Opaque oxide minerals were analysed in carbon-coated polished thin sections with an ARL-SEMQ electron microprobe. Analyses were made using an accelerating potential of 15 KV and a sample current of 20 nanoamperes on brass. Synthetic spinel was used as a standard for Mg and Al; synthetic oxides were used for Ti, Mn, Fe, and Nb; gahnite was used for Zn; Si and Ca were analysed using a clinopyroxene as a standard. Si is not reported in the tables because it is always insignificant; Mg and Ca are reported in ilmenite in the Cabresto Lake and the Rio Hondo plutons only, because in other plutons they are not significant. Davidite was also analysed for Y, La, Ce, Pr, Nd, Sm, Dy, Yb, Ta, Th, and U. Correction of raw data was made using the program of Bence and Albee (1968).

Structural formulae for magnetite, ilmenite, and hematite were calculated with a program which estimates Fe^{3+} (Stormer, 1983) and are summarized in Tables II.4 and II.5.

1. VIRGIN CANYON

a) Description

Based on field relations, textures, mineralogy, and whole-rock chemistry, the Virgin Canyon pluton is composed of three units, refered to as the peralkaline, early metaluminous, and later metaluminous granites. In all three units, the most abundant primary opaque minerals are magnetite and ilmenite. Ilmenite can also be secondary, derived by oxidation exsolution from magnetite. Hematite is always present and secondary, either after magnetite or ilmenite.

Opaque oxide minerals constitute 0.9 to 1.2 volume percent of the peralkaline granite. Small phenocrysts, up to 0.8 mm across, are early and crystallized before quartz phenocrysts. Predominant among these phenocrysts, magnetite is usually euhedral and can enclose zircon. Towards the core of the

peralkaline unit, sphene, which is there more abundant, can enclose or be enclosed by magnetite. Types (4) and (5) ilmenite oxidation "exsolution" products in magnetite are common (Plate II.2, d). Magnetite is most often partially oxidized to hematite (martite), this oxidation being most extensive near the outer margin of the peralkaline unit.

Small ilmenite phenocrysts may be isolated or associated with magnetite. Usually euhedral to subhedral, they are contemporaneous with, or later than, magnetite. Near the outer margin of the unit, lozenge-shaped, fine aggregates of ilmenite after sphene can be found, often associated with arfvedsonite; sphene relicts may remain within these aggregates (Plate II.3, d). In more seriate-textured samples, collected near the contact with the early metaluminous granite, ilmenite can be enclosed in irregular sphene rims. In this case, the shape of ilmenite itself is quite irregular and it may contain magnetite lamellae, often partially oxidized to hematite (Plate II.3, a and b). In all cases, ilmenite is free of hematite exsolutions and of oxidation to hematite plus rutile.

In the groundmass, opaque oxides are subhedral and form crystals as small as 0.04 mm across, but ranging up to 0.2 mm; ilmenite is predominant. Magnetite is partially oxidized to hematite and ilmenite is fresh. No sulfide minerals have been found, either isolated or enclosed by opaque oxides.

Opaque oxide minerals constitute 0.75 to 2.0 volume percent of the early metaluminous granite. They form small phenocrysts, up to 1 mm across, as well as smaller crystals, down to 0.01 mm; magnetite is predominant among all sizes. Usually euhedral, it may contain zircon, apatite, and pyrite, and can be enclosed in biotite and quartz phenocrysts (in the porphyritic facies). Ilmenite "exsolution" products are common in magnetite, but less abundant than in the peralkaline granite; such ilmenite is never oxidized. Partial oxidation of magnetite to hematite is less developed than in the peralkaline granite.

Primary isolated ilmenite is usually common, but can be rare in some samples and is much less abundant than in the peralkaline granite. Smaller crystals (less than 0.1 mm across) are euhedral and can be enclosed in biotite or sphene. They rarely contain hematite exsolution droplets and are free of oxidation. Larger euhedral to subhedral ilmenite crystals (more than 0.2 mm long) are associated with magnetite and are contemporaneous with or later than magnetite. They are commonly oxidized to hematite plus rutile.

In the later metaluminous granite, opaque oxide minerals constitute 0.6 to 1.7 volume percent and range in size from 0.02 to 0.8 mm across. Magnetite is euhedral and earlier than or contemporaneous with biotite. It contains ilmenite oxidation products and partial oxidation to hematite is more extensively developed than in the early metaluminous granite. Ilmenite is more abundant than in the early metaluminous granite, but still less abundant than in the peralkaline granite. It can be found as euhedral crystals, enclosed in sphene, biotite, or feldspars, as well as more anhedral crystals partially enclosing magnetite. Ilmenite rarely contains fine hematite exsolution droplets. Ilmenite can also be found as lozenge-shaped aggregates

after sphene and sphene may be surrounded by an ilmenite corona (Plate II.3, c). Primary ilmenite larger than 0.02 mm across commonly is partially oxidized to hematite plus rutile. As in the early metaluminous granite, rare pyrite occurs, enclosed in magnetite or other earlier accessory phases.

b) Chemistry

(1) Magnetite (Tables II.4 and A.1.1)

Magnetite is rather uniform in composition, from grain to grain, within each unit. However, magnetite in the peralkaline granite is quite distinct in composition from magnetite in the two metaluminous granites. The sum (Al_2O_3 + TiO_2 + MnO + ZnO) ranges from 5.5 to 8.2 weight percent in magnetite of the peralkaline granite, from 0.7 to 3.5 weight percent in magnetite of the early metaluminous granite, and from 0.9 to 2.9 weight percent in magnetite of the later metaluminous granite. Ti, Mn, and Zn are more abundant in magnetite of the peralkaline granite, while Al is more characteristic of magnetite in both metaluminous granites.

Magnetite analyses recalculate in terms of Fe_3O_4 (magnetite), Fe_2TiO_4 (ulvospinel), Mn_2TiO_4, Zn_2TiO_4, and $ZnAl_2O_4$ (gahnite) in all three units.

There is a good correlation between Ti and (Fe^{2+}+Mn+Zn-1/2Fe^{3+}) in magnetite of the Virgin Canyon pluton (fig. II.2; r, 1.00). Rare zoning in magnetite of the peralkaline granite shows Fe enrichment and Ti, Mn, and Zn depletion from core to rim.

Discussion—It is well accepted that magnetite contains Ti, dissolved as Fe_2TiO_4 at high temperature, which cannot remain in its structure at lower temperature. Recalculation of magnetite analyses (Table II.4) and good correlation on figure II.2 show that in the Virgin Canyon pluton magnetite contains ulvospinel as well as Mn_2TiO_4, Zn_2TiO_4, and $ZnAl_2O_4$ still dissolved in its structure. The occurrence of Mn- and Zn-rich ilmenite "exsolved" from magnetite shows that Fe_2TiO_4, Mn_2TiO_4, and Zn_2TiO_4 were dissolved in much greater proportions at higher temperature. The rare zoning also suggests that magnetite was becoming more pure as crystallization proceeded. The higher Ti and Mn contents typical of magnetite in the peralkaline granite most probably indicate that reequilibration ceased at higher temperature and/or lower oxygen fugacity than in the metaluminous units (see fig. II.24).

(2) Ilmenite (Tables II.5 and A.1.2)

High Mn content and variability in composition are the two main characteristics of the chemistry of ilmenites in the three units of the Virgin Canyon pluton. High Mn concentration in ilmenite is not unusual in silicic rocks. Occurrences are reported by Snetsinger (1969) in a Sierran adamellite, Elsdon (1975) in the Leinster granite, Ireland, and Czamanske and others (1981) in the Cretaceous-Paleocene batholith of southwestern Japan. High Mn concentration has also been described in high-level plutonic complexes such as the Finnmarka complex, Norway (Czamanske and Mihalik, 1972) and the Pliny Range intrusive complex, New Hampshire (Czamanske and others, 1977). However, Mn concentrations in ilmenite in the Questa granitic rocks typically exceed those reported in these studies.

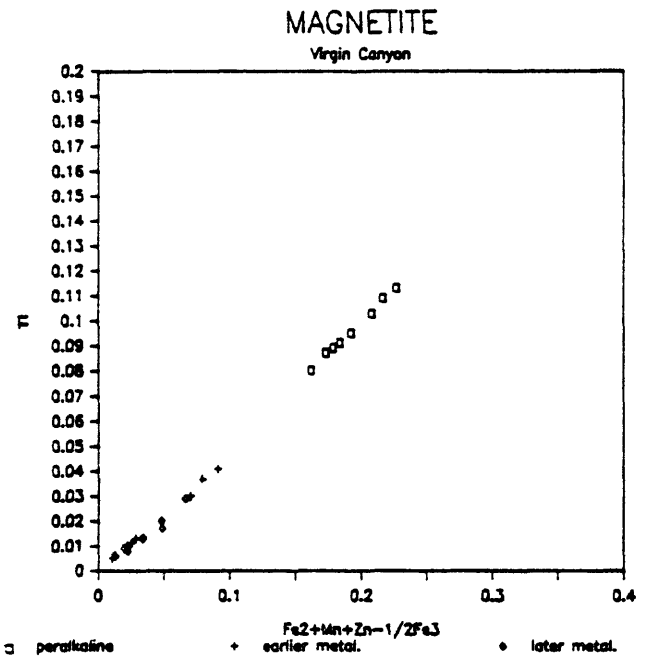

Fig. II.2. Fe2+Mn+Zn-1/2Fe3 against Ti (cations) in magnetite, Virgin Canyon.

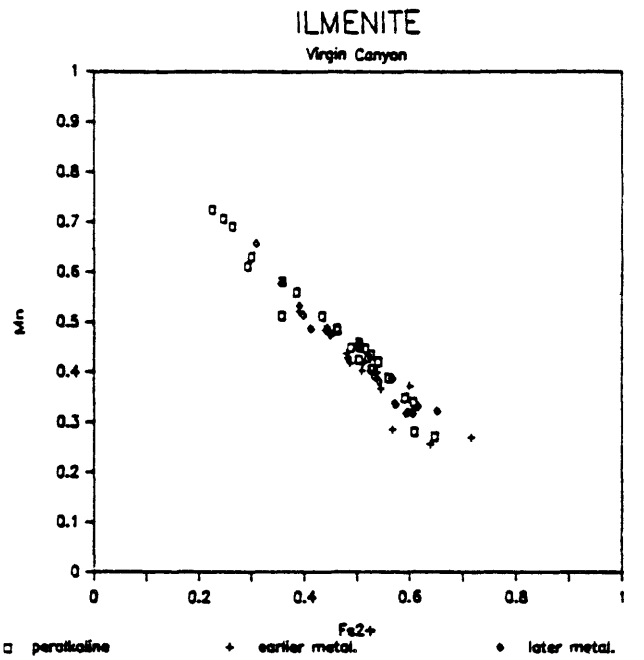

Fig II.3. Fe2 against Mn in ilmenite (cations), Virgin Canyon.

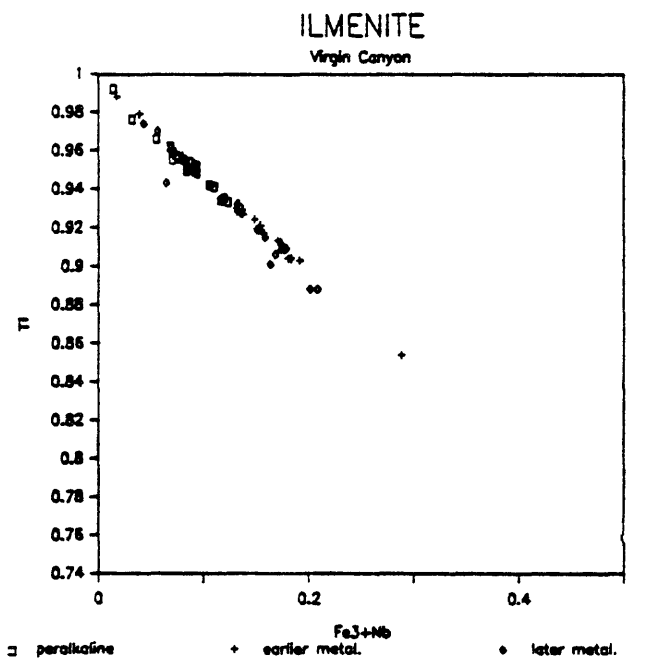

Fig. II.4. Fe3+Nb against Ti (cations) in ilmenite, Virgin Canyon.

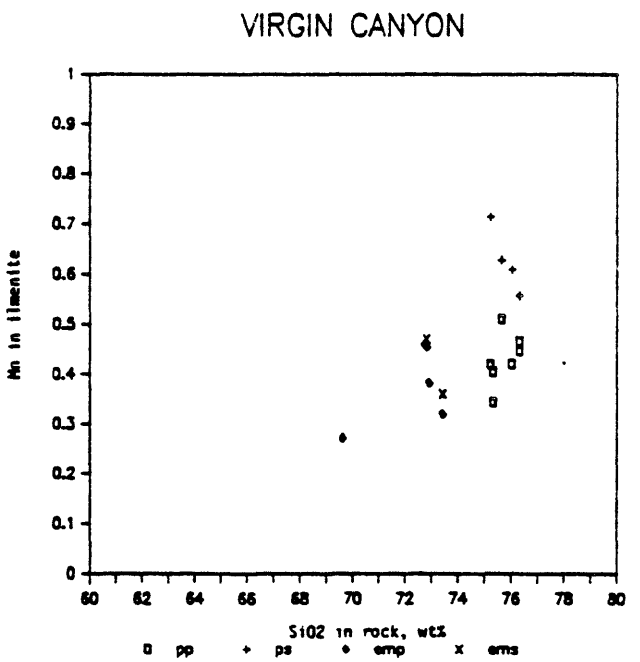

Fig. II.5. SiO2 in host rock (wt%) against Mn in ilmenite (cations), Virgin Canyon; pp, primary ilmenite in peralkaline granite; ps, secondary ilmenite in peralkaline granite; emp, primary ilmenite in early metaluminous granite; ems, secondary ilmenite in early metaluminous granite.

Table II.4: Composition of magnetite in the Questa caldera plutons, in terms of calculated end members (mole percent).

	VIRGIN CANYON								
	Peralkaline			Early metaluminous			Later metaluminous		
	Range of 8		Average	Range of 8		Average	Range of 7		Average
$FeFe_2O_4$	88.50	91.85	90.26	94.70	98.90	97.44	96.10	99.35	97.91
Fe_2TiO_4	1.18	4.85	3.80	0.52	2.05	1.22	0.23	1.15	0.70
Mn_2TiO_4	3.45	6.40	4.80	0.20	2.05	0.68	0.20	1.60	0.59
Zn_2TiO_4	0.68	1.65	1.05	0.00	0.13	0.08	0.03	0.20	0.12
$ZnAl_2O_4$	0.00	0.10	0.07	0.20	0.90	0.39	0.10	0.80	0.57

	CANADA PINABETE						RITO DEL MEDIO		
	Peralkaline			Metaluminous					
	Range of 7		Average	Range of 7		Average	Range of 12		Average
$FeFe_2O_4$	84.15	87.20	85.51	95.25	99.35	97.96	93.80	99.15	96.87
Fe_2TiO_4	7.45	11.33	8.93	0.18	2.53	1.10	0.00@	5.30@	2.11@
Mn_2TiO_4	2.90	6.85	4.52	0.18	1.18	0.34	0.30	1.70	0.61
$MnAl_2O_4$	0.23*	1.10*	0.85*	0.05	0.80	0.16	0.00	0.85	0.26
$ZnAl_2O_4$	0.05	0.15	0.10	0.10	0.80	0.27	0.00	1.25	0.30

	CABRESTO LAKE								
	Granite			Mixed			Biotite-bearing enclaves		
	Range of 8		Average	Range of 3		Average	Range of 4		Average
$FeFe_2O_4$	96.50	99.15	98.48	97.55	98.45	97.97	98.05	99.40	98.85
Fe_2TiO_4	0.38	2.15	0.80	0.73	0.95	0.82	0.10	0.88	0.49
Mn_2TiO_4	0.00	1.75	0.24	0.18	0.60	0.41	0.10	0.45	0.26
$ZnAl_2O_4$	0.00&	0.85&	0.37&	0.20	0.65	0.38	0.05	0.35	0.18

	CABRESTO LAKE			RIO HONDO					
	Amphibole-bearing enclaves			Granodiorite			Granite		
	Range of 2		Average	Range of 9		Average	Range of 7		Average
$FeFe_2O_4$	95.65	98.40	97.03	98.85	99.45	99.19	98.30	99.30	98.94
Fe_2TiO_4	0.95	2.48	1.71	0.00	0.83	0.36	0.10@	1.30@	0.53@
Mn_2TiO_4	0.13	0.15	0.14	0.10	0.25	0.15	0.10	0.35	0.22
$ZnAl_2O_4$	0.20	0.60	0.40	0.00	0.25	0.10	0.00	0.25	0.12

	RIO HONDO						BEAR CANYON	
	Mafic magmatic enclaves			Schlieren	Dikes		82QC8	82QC10
	Range of 2		Average		Latite	Rhyolite	Avg 3	Avg 3
$FeFe_2O_4$	98.85	99.15	99.00	98.90	99.20	90.85	95.45	98.53
Fe_2TiO_4	0.08	0.23	0.15	0.30@	0.25	5.98	3.16	0.80
Mn_2TiO_4	0.08	0.33	0.20	0.25	0.20	1.35	0.48	0.08#
$MnAl_2O_4$							0.28	0.25
$ZnAl_2O_4$	0.30	0.50	0.40	0.30	0.20	0.30*	0.53	0.25

	SULPHUR GULCH				RED RIVER				
	Carapace			Aplite	Gr.dior.	Alk.gr.	Granite	Enclave	Q.dior.
	Range of 8		Average	Avg 2	Avg 3	Avg 2	Avg 4	Avg 2	Avg 3
$FeFe_2O_4$	93.35	98.55	96.68	98.58	99.51	98.83	93.71	96.16	96.05
Fe_2TiO_4	0.28	4.33	1.60	0.74	0.06	0.28	3.81		
Mn_2TiO_4	0.10	1.75	0.71	0.22	0.12	0.38	1.39	0.86	0.88#
$MnAl_2O_4$					0.03*	0.16	0.44	0.28	0.47
$ZnAl_2O_4$	0.10	0.40	0.24	0.25	0.15	0.29	0.40	0.35	0.40

	LUCERO PEAK		
	Range of 5		Average
$FeFe_2O_4$	98.85	99.30	99.12
Fe_2TiO_4	0.00	0.38#	0.26
Mn_2TiO_4	0.00	0.38	0.20
$ZnAl_2O_4$	0.00	0.15	0.07

Notes. * Zn_2TiO_4.
@ $MnFe_2O_4$.
& $MnAl_2O_4$ + $ZnAl_2O_4$, in about equal proportions.
# $FeAl_2O_4$.
For the Cabresto Lake and Rio Hondo plutons, ranges reflect the number of samples; for other plutons ranges reflect the number of analyses.

Variability in ilmenite composition occurs both between and within grains; compositional differences within grains are either related to Fe/Ti or Fe/Mn. Variability in Fe/Ti within grains is due to ilmenite intergrowths with hematite (exsolution) or with hematite plus rutile (oxidation), and is especially evident within ilmenite of both metaluminous granites, in which exsolution and oxidation textures commonly occur. Variability in Fe/Mn within grains is not related to any texture discernible under the microscope at 400X magnification, and may be due to heterogeneous distribution of Fe and Mn in the ilmenite structure.

Compositional differences from one grain to another, largely in Fe^{2+}/Mn, occur in all units of the pluton (r, -0.97; fig. II.3). The differing compositions are partly related to different textural occurrences of ilmenite. In all three units, secondary ilmenite ("exsolved" from magnetite) typically contains more Mn than primary ilmenite. In rare cases, however, one can find primary ilmenite with a higher Mn content than ilmenite after magnetite. Compositional differences also appear within the same textural type; for example, primary ilmenite may have differing Mn contents in a given sample.

Compositional differences distinguish ilmenites in the peralkaline granite from those in the two metaluminous granites; Mn, Ti, Zn, and Nb are more concentrated in ilmenite in the former, while Fe is higher in ilmenite in both metaluminous granites. There is a good negative correlation between Ti and Fe^{3+}+Nb in ilmenite within the three granites (r, -1.00; fig. II.4), ilmenite in the peralkaline granite containing less Fe^{3+} than ilmenite in the two metaluminous granites.

Study of the zoning of several primary, isolated ilmenite grains in both metaluminous granites shows that cores of grains contain more Fe, with Mn and Ti enriched towards their margins; Nb and Zn show no significant changes from core to rim.

In the peralkaline granite, ilmenite intergrown with magnetite contains up to 10 weight percent more Mn than primary ilmenite. Ilmenite aggregates after sphene in the marginal facies have the same Mn content as primary ilmenite. Ilmenite grains surrounded by sphene, typical of the inner part of the unit where the facies has a more seriate texture, have a relatively low Mn content. Within the same sample, analyses of primary ilmenite microphenocrysts and primary grains in the groundmass, show no pattern relating composition to occurrence. Note that in the peralkaline unit there is poor correlation between Mn in primary ilmenite and SiO_2 in the host rock (fig. II.5).

In the early metaluminous granite, highest Mn contents are found in secondary ilmenite (intergrown with magnetite) and lowest Mn contents in primary grains; however, ilmenite "exsolved" from magnetite does not always contain more Mn than primary ilmenite. The positive correlation between contents of Mn in ilmenite and SiO_2 in the host rock is somewhat better than in the peralkaline granite (fig. II.5).

In the later metaluminous granite, as in the peralkaline granite, all ilmenite formed by oxidation "exsolution" from magnetite has a higher Mn content than primary ilmenite or secondary ilmenite aggregates after sphene.

Table II.5. Compositions of significant varieties of ilmenite in the Questa granitic plutons in terms of calculated end members (mole percent).

PLUTON/ Unit	Primary unmixed			Primary homogeneous			Exsolved from magnetite		
VIRGIN CANYON									
Peralkaline granite				Range of 18		Avg	Range of 5		Avg
Fe_2O_3	Not unmixed.			1.1	5.3	3.7	3.2	4.2	3.5
$FeTiO_3$				26.4	64.7	50.2	22.4	35.7	29.5
$MnTiO_3$				27.0	68.5	44.2	51.0	72.3	62.6
Nb_2O_5				0.1	0.8	0.5	0.6	0.7	0.6
ZnO				0.3	2.6	1.4	1.4	9.5	4.2
Early metaluminous granite									
	1 analysis			Range of 10		Avg	Range of 4		Avg
Fe_2O_3	8.5			1.8	14.3	7.5	6.6	7.7	7.0
$FeTiO_3$	50.7			43.6	63.8	51.8	38.8	51.0	45.7
$MnTiO_3$	40.1			25.5	48.3	39.5	41.5	52.0	45.7
Nb_2O_5	0.1			0.1	0.6	0.4	0.1	0.4	0.2
ZnO	0.4			0.2	2.1	0.9	0.4	2.5	1.3
Later metaluminous granite									
	Range of 4		Avg	Range of 5		Avg	Range of 4		Avg
Fe_2O_3	8.5	9.8	8.9	5.0	8.8	7.0	2.7	8.2	5.7
$FeTiO_3$	41.0	59.2	53.6	44.2	61.4	53.7	30.8	39.7	36.2
$MnTiO_3$	31.7	47.8	36.2	31.7	48.7	38.4	51.2	65.5	56.9
Nb_2O_5	0.2	1.1	0.5	0.2	1.0	0.5	0.1	0.5	0.2
ZnO	0.3	0.6	0.5	0.3	0.5	0.4	0.4	1.5	0.8
CANADA PINABETE									
Peralkaline granite				Range of 8		Avg	Range of 2		Avg
Fe_2O_3	Not unmixed.			0.5	5.0	2.4	1.8	2.4	2.1
$FeTiO_3$				45.7	73.8	62.6	64.7	67.8	66.3
$MnTiO_3$				22.8	50.4	33.5	28.0	30.9	29.5
Nb_2O_5				0.6	1.0	0.7	0.3	0.9	0.6
ZnO				0.5	1.8	1.0	1.0	2.3	1.7
Metaluminous granite									
	Range of 6		Avg	Range of 7		Avg	Range of 3		Avg
Fe_2O_3	2.1	8.9	4.4	0.7	10.6	5.1	2.3	6.7	4.3
$FeTiO_3$	54.2	74.1	62.9	42.5	78.0	64.5	38.6	61.0	51.6
$MnTiO_3$	20.3	41.7	31.7	14.8	54.7	28.8	31.6	58.4	43.4
Nb_2O_5	0.4	0.6	0.5	0.3	1.4	0.8	<0.1	0.3	0.1
ZnO	0.2	1.0	0.5	0.1	0.5	0.4	0.5	0.6	0.6

Table II.5.—continued.

PLUTON/ Unit	Primary unmixed			Primary homogeneous			Exsolved from magnetite		
RITO del MEDIO									
	Range of 3		Avg	Range of 5		Avg	Range of 10		Avg
Fe_2O_3	6.0	12.0	9.9	4.0	8.7	5.2	2.5	9.4	5.0
$FeTiO_3$	52.1	63.8	59.5	16.9	73.4	37.3	1.3	27.5	19.8
$MnTiO_3$	23.4	35.6	29.4	16.9	78.0	54.9	61.4	92.7	73.9
Nb_2O_5	0.2	1.1	0.6	0.4	2.0	1.3	0.0	1.4	0.4
ZnO	0.2	0.3	0.3	0.5	0.7	0.6	0.2	1.3	0.6
CABRESTO LAKE									
Granite									
	Range of 9		Avg	Range of 2		Avg	Range of 10		Avg
Fe_2O_3	5.9	20.1	10.1	7.3	8.9	8.1	2.1	8.2	4.8
$FeTiO_3$	57.8	75.0	68.2	65.2	67.8	66.5	42.7	64.9	50.0
$MnTiO_3$	5.7	27.8	19.5	22.3	26.7	24.5	30.2	64.2	44.6
Nb_2O_5	0.1	0.6	0.3	0.2	0.2	0.2	0.0	0.2	0.1
ZnO	0.0	0.4	0.3	0.3	0.4	0.4	0.2	0.8	0.4
Mixed unit									
	Range of 6		Avg	Range of 4		Avg	Range of 3		Avg
FeO_3	10.2	22.0	14.5	6.8	11.0	9.0	3.5	6.2	4.4
Fe_2O_3	59.6	68.0	64.5	61.3	69.5	64.5	51.8	60.2	56.1
$MnTiO_3$	9.4	29.0	19.6	18.7	31.4	25.5	35.0	44.4	38.8
Nb_2O_5	0.1	0.3	0.2	0.1	0.3	0.2	0.0	0.05	<0.05
ZnO	0.2	0.6	0.4	0.2	0.4	0.3	0.3	0.9	0.5
Biotite-bearing enclaves									
	Range of 3		Avg	1 analysis			Range of 3		Avg
Fe_2O_3	13.2	19.9	15.6	8.9			3.9	5.9	5.0
$FeTiO_3$	44.9	73.6	60.3	53.5			35.4	36.7	35.9
$MnTiO_3$	11.2	34.2	23.0	37.2			58.2	59.0	58.6
Nb_2O_5	0.1	0.2	0.2	0.2			<0.1	0.2	0.1
ZnO	0.3	0.5	0.4	0.2			0.2	0.3	0.2
Amphibole-bearing enclaves									
	Range of 4		Avg				Range of 5		Avg
Fe_2O_3	4.2	21.4	12.6	Not analysed.			3.2	6.5	4.7
$FeTiO_3$	72.6	78.2	75.2				53.6	77.6	69.1
$MnTiO_3$	4.6	16.1	10.9				17.6	39.2	25.4
Nb_2O_5	0.15	0.2	0.2				0.0	0.15	0.1
ZnO	0.2	0.4	0.4				0.1	0.3	0.2
RIO HONDO									
Granite									
	Range of 3		Avg	Range of 2		Avg	Range of 4		Avg
Fe_2O_3	2.5	4.1	3.4	0.45	2.65	1.6	1.2	3.3	2.5
$FeTiO_3$	26.0	67.8	53.2	32.0	32.0	32.0	19.0	38.9	30.0
$MnTiO_3$	26.9	67.2	41.3	64.4	65.8	65.1	57.5	79.0	66.4
Nb_2O_5	0.2	0.4	0.2	0.5	0.9	0.7	0.0	0.3	0.1
ZnO	0.2	1.0	0.5	0.2	0.7	0.45	0.0	0.7	0.4

Table II.5—continued.

RIO HONDO

	Granodiorite		Enclaves		
	Primary unmixed Avg of 2	Unmixed, ilmenite phase Avg of 2	Primary unmixed 1 analysis	Unmixed, ilmenite phase Avg of 2	Primary homogeneous 1 analyses
Fe_2O_3	20.2	10.3	10.8	7.5	17.6
$FeTiO_3$	65.7	74.4	76.5	79.2	66.5
$MnTiO_3$	12.5	12.9	10.5	9.7	25.4
Nb_2O_5	0.05	0.05	0.0	<0.05	0.05
ZnO	0.3	0.5	0.3	0.3	0.2

BEAR CANYON

		Primary homogeneous 1 analysis	Exsolved from magnetite Range of 3		Avg
Fe_2O_3	Not analysed.	7.6	4.5	8.9	6.1
$FeTiO_3$		65.9	65.7	74.5	71.0
$MnTiO_3$		24.9	19.6	23.8	21.8
Nb_2O_5		0.8	0.4	0.8	0.6
ZnO		0.3	0.1	0.4	0.2

SULPHUR GULCH

	Carapace					
	Unmixed, ilmenite phase Range of 2		Avg	Primary homogeneous 1 analysis	Exsolved from magnetite Range of 2		Avg
Fe_2O_3	11.5	14.7	13.1	7.6	4.8	6.3	5.5
$FeTiO_3$	48.8	57.2	53.0	59.0	38.9	44.0	41.5
$MnTiO_3$	27.8	35.1	31.5	33.0	49.6	53.1	51.4
Nb_2O_5	0.1	0.15	0.1	0.2	0.0	0.05	<0.05
ZnO	0.1	0.1	0.1	0.1	0.0	0.2	0.1

RED RIVER INTRUSIVE COMPLEX

	Granodiorite			Granite					
				Primary					
	Unmixed, ilmenite phase Range of 3		Avg	homogeneous Range of 3		Avg	Exsolved from magnetite Range of 3		Avg
Fe_2O_3	10.1	11.5	10.6	5.3	6.3	5.9	5.2	7.5	6.1
$FeTiO_3$	79.9	84.0	82.5	49.0	72.9	57.2	42.2	52.6	48.5
$MnTiO_3$	3.8	9.5	6.4	19.8	37.2	30.9	40.9	51.6	44.7
Nb_2O_5	0.05	0.1	0.1	0.4	0.6	0.5	0.1	0.3	0.2
ZnO	0.2	0.2	0.2	0.0	0.2	0.1	0.1	0.7	0.4

	Enclave in granite			Quartz diorite			
	Primary homogeneous Range of 2		Avg	Primary homogeneous Range of 3		Avg	Exsolved from magnetite 1 analysis
Fe_2O_3	6.6	7.4	7.0	11.8	16.7	13.7	9.25
$FeTiO_3$	55.8	56.5	56.2	65.2	71.6	68.1	62.3
$MnTiO_3$	35.2	36.8	36.0	11.1	22.6	19.3	27.4
Nb_2O_5	0.4	0.45	0.4	0.1	0.15	0.1	0.1
ZnO	0.0	0.2	0.1	0.1	0.3	0.2	0.3

LUCERO PEAK

	Primary unmixed Range of 2		Avg	Primary homogeneous Range of 3		Avg	Exsolved from magnetite 1 analysis
Fe_2O_3	8.95	9.05	9.0	1.9	2.8	2.3	1.3
$FeTiO_3$	58.2	61.7	60.0	59.0	66.3	62.6	44.5
$MnTiO_3$	28.0	31.4	29.7	29.2	36.0	33.0	53.4
Nb_2O_5	0.7	0.7	0.7	1.0	1.1	1.0	0.4
ZnO	0.3	0.5	0.4	0.2	0.2	0.2	0.6

Discussion—Study of primary zoning in ilmenite from the Virgin Canyon pluton, which indicates Mn enrichment during crystallization, provides a clue for interpretation of all ilmenite compositions. Mn enrichment in ilmenite during the later stages of magmatic differentiation has commonly been reported. Goldschmidt (1954) suggested that the larger ionic size of Mn causes Mn/Fe and Mn/Mg to increase during differentiation. Buddington (1963) and Buddington and Lindsley (1964) interpret the distribution of Mn between ilmenite and magnetite as controlled by temperature, with Mn enrichment in ilmenite related to decreasing temperature. Oxidation of Fe^{2+} to Fe^{3+} within the crystallizing magma would also promote zoning to higher Mn/Fe in ilmenite. Anderson (1968) and Czamanske and Mihalik (1972) explain this enrichment by fractional oxidation, due to the fact that "...Fe^{2+} is more readily oxidized out of the ilmenite structure than Mn^{2+}."

In the Virgin Canyon ilmenites, Mn enrichment occurred during the crystallization interval, as shown by zoned crystals, and was presumably accompanied by decreasing temperature. The rough correlation between Mn in ilmenite and SiO_2 in the host rock (fig. II.5) supports this interpretation.

Compositional differences observed among primary ilmenites therefore may relate to the time at which the ilmenite crystallized. This is in agreement with microscopic studies which show that primary ilmenite ranges from euhedral to subhedral, as might be expected if it crystallized over an extended period of the crytallization history.

In the peralkaline and later metaluminous granites, ilmenite "exsolved" from magnetite always has a higher Mn content than primary ilmenite and is interpreted to have formed later than primary ilmenite, at a stage when ilmenite was no longer crystallizing directly from the magma. In the early metaluminous granite, primary and secondary ilmenite show overlaping compositions, probably reflecting overlap between primary crystallization of ilmenite and "exsolution" of ilmenite from magnetite.

Although no zoning was observed in primary ilmenite in the peralkaline granite, ilmenite is assumed to have been enriched in Mn with differentiation, because Mn in ilmenite correlates with SiO_2 in the host rock and because ilmenite intergrown with magnetite contains more Mn than primary ilmenite. Mn contents of ilmenite in the peralkaline granite suggest that crystallization of ilmenite microphenocrysts and ilmenite in the groundmass probably occurred over a relatively short time span. Micrography supports the chemical data, ilmenite in the groundmass being typically quite subhedral.

It is of interest that the composition of the ilmenite in aggregates shows, also based on Mn content, that the break-down of sphene at the outer margin of the peralkaline unit occured at a magmatic stage, before the "exsolution" of ilmenite from magnetite. The same interpretation can be made for the later metaluminous granite.

Higher Mn concentrations noted for all varieties of ilmenite in the peralkaline granite are to be expected, as whole-rock Mn/Fe is greater than in the metaluminous granites. Lower Fe^{3+} in ilmenite of the peralkaline granite is consistent with lower fO_2 and higher crystallization temperature for this unit. A greater proportion of ilmenite and lack of hematite exsolution also correlate with lower fO_2 and lower Fe^{3+} in ilmenite of the peralkaline granite.

c) Crystallization history of the opaque oxide minerals

(1) Magnetite and ilmenite are found as primary, early crystallized contemporaneous phases in the peralkaline granite. Because of its more common subhedral (as opposed to euhedral) habit, it may be assumed that ilmenite crystallization extended beyond that of magnetite. During the first stages of ilmenite crystallization and probably because of low oxygen fugacity, early-formed sphene became unstable at the margin of the peralkaline unit and ilmenite replaced it. Later, at a time when ilmenite was no longer directly precipitating from the magma, secondary ilmenite "exsolved" from magnetite by oxidation of its ulvospinel component. This "exsolution" process occured at a temperature at which K_D^{Mn} Ilm/Mt was far greater than 1. At a still later stage, sphene became stable in the core of the unit and started to form after ilmenite. That ilmenite, impoverished in Ti, later "exsolved" excess iron as magnetite. Thus, the oxygen fugacity at that time was high enough to form sphene but was not high enough to produce hematite exsolution from ilmenite. Oxidation of magnetite to hematite, is believed to have taken place at a lower temperature, but above 400°C (Basta, 1959); fO_2 was still low enough that ilmenite was not oxidized to hematite plus rutile.

(2) In the early metaluminous granite, magnetite and ilmenite are primary, early-formed phases. Their crystallization mainly took place between crystallization of earlier accessory phases (zircon, apatite, and pyrite) and later essential phases (biotite, quartz, and feldspars). Based on textural relations, ilmenite probably finished primary crystallization after magnetite.

Primary ilmenite grains more than 0.2 mm long, some containing hematite exsolution products, were subsequently oxidized to hematite plus rutile. Ilmenite "exsolved" from magnetite shows no oxidation to hematite plus rutile, indicating that oxidation of early primary ilmenite occurred prior to oxidation "exsolution" of ilmenite from magnetite. In addition, overlaping formation of late primary ilmenite and secondary ilmenite from magnetite, as deduced from ilmenite compositions, shows that oxidation of ilmenite to hematite plus rutile stopped before the final stages of ilmenite crystallization.

As in the peralkaline granite, oxidation of magnetite to hematite was the last process to occur. However, magnetite and ilmenite compositions, as well as predominance of type (3) "exsolution" in magnetite, show that in other respects the opaque oxides stopped reequilibration at a lower temperature in the early metaluminous granite than in the peralkaline granite.

(3) In the later metaluminous granite the crystallization history of opaque oxide minerals was similar to that in the early metaluminous unit, with two notable differences. First, as shown by the electron microprobe data, there was a more distinct break between primary crystallization of ilmenite and ilmenite "exsolution" from magnetite. Second, there was an early interval of secondary formation of ilmenite after sphene, as found in the marginal facies of the peralkaline unit.

2. CANADA PINABETE

a) Description

The opaque oxide assemblage in the peralkaline granite is that found in the peralkaline granite of the Virgin Canyon pluton and these minerals constitute 0.4 to 1.0 volume percent of the rock. Small phenocrysts can be up to 1 mm long, but are usually around 0.5 mm; opaque oxides in the groundmass are less than 0.1 mm across. Except in one sample where ilmenite is the only oxide phase, primary magnetite and ilmenite are present. Most abundant among the phenocrysts, magnetite is also the more euhedral in shape. It may contain ilmenite oxidation granules (types (4) or (5)), or ferrorutile ("exsolution"?) inclusions. It is always partially oxidized to hematite.

Ilmenite is euhedral to subhedral and is usually free of oxidation. It is more abundant than magnetite in the groundmass. As in the Virgin Canyon pluton, the peralkaline granite does not contain sulfide minerals.

Opaque oxide mineral textures and assemblages in the metaluminous granites of the Canada Pinabete pluton are more diverse than those in the Virgin Canyon pluton. However, late-stage oxidation features such as hematite after magnetite and hematite plus rutile after ilmenite are similar.

Opaque oxide minerals constitute 0.2 to 1.3 volume percent of the metaluminous granites. Grains may be up to 1.6 mm long; however, larger grains are usually between 0.5 and 1 mm across, with smaller grains less than 0.1 mm across. Primary ilmenite occurs both as isolated grains or associated with magnetite and is more poorly formed than magnetite. Ilmenite locally contains fine hematite exsolution lamellae and is sometimes oxidized to hematite plus rutile; it is free of exsolution and oxidation products in magnetite-free samples. Ilmenite is also common enclosed in biotite.

Magnetite is absent in some samples taken from the northern part of the pluton, but where present is more abundant than ilmenite. Usually euhedral, it is always partially, if not completely, oxidized to hematite. Magnetite can be free of ilmenite oxidation "exsolution" products, or it may contain lamellae and/or granules of ilmenite (types (2) to (5), Plate II.2, c); type (3) lamellae are most abundant in samples from the northeastern part of the pluton, which rather closely resemble the early metaluminous granite of Virgin Canyon. Small exsolution granules distributed along type (3) ilmenite "exsolution" lamellae in magnetite are inferred to be gahnite, based on microprobe traverses and magnetite chemistry (Table II.4).

Hematite crystallized locally as a late stage, primary mineral in miarolitic cavities and is more typical of samples from the western margin of the pluton. It may occur as large euhedral crystals (up to 0.8 X 1.8 mm) intergrown with ilmenorutile (Plate II.5, b), or as radiating fibrous aggregates (individual fibers approx 0.03 X 0.7 mm, Plate II.5, c). Hematite-ilmenorutile intergrowths are probably of an exsolution type; hematite is the host phase and ilmenorutile has irregular rounded shapes. In the fine-grained granite which hosts the vugs, primary isolated rutile is more common than primary ilmenite, as might be expected from the oxidized nature of the

system. Late anhedral pyrite (filling cavities?) oxidized to goethite is also typical of these localities. Columbite was found as a small inclusion in a hematite-ilmenorutile intergrowth (Plate II.5, c).

Davidite occurs as crystals up to 0.8 X 1.2 mm in a fine-grained, less vuggy, sample from the western margin of the pluton (Plate II.5, a). It can be homogeneous, or intergrown with ilmenite, rutile, and another unidentified REE-bearing phase.

b) Chemistry

(1) Magnetite (Tables II.4 and A.2.1)

Magnetite chemistry shows the same characteristics as in the Virgin Canyon pluton; it is rather uniform in composition within each unit, and within individual samples. Magnetite in the peralkaline granite is chemically distinct from magnetite in the metaluminous granite in that sums of (Al_2O_3 + TiO_2 + MnO + ZnO) range, respectively, from 7.9 to 11.2 weight percent (avg 8.8), and from 0.4 to 2.7 weight percent (avg 1.1); Ti, Mn, and Zn are more abundant in the peralkaline granite and Al is characteristic of the metaluminous granite. Recalculation of analyses shows that Ti is essentially dissolved as Fe_2TiO_4 and Mn_2TiO_4. In the metaluminous granite, Al is recalculated as $MnAl_2O_4$ and $ZnAl_2O_4$ and gahnite can be found unmixed as fine granules along (111) planes of the magnetite host. There is a good correlation between Ti and (Fe^{2+}+Mn+Zn-1/2Fe^{3+}) (fig. II.6; r, 1.00).

Discussion—From magnetite compositions it can be inferred that magnetite in the peralkaline granite was quenched at higher temperature and/or lower oxygen fugacity than magnetite in the metaluminous granite. Compositions also indicate that magnetite in the peralkaline granite of the Canada Pinabete pluton was quenched at higher temperature and/or lower oxygen fugacity than magnetite in the peralkaline granite of the Virgin Canyon pluton (compare figs. II.6 and II.2; see fig. II.24).

(2) Ilmenite (Tables II.5 and A.2.2)

As in the Virgin Canyon pluton, ilmenite shows a large range of Fe^{2+}/Mn substitution between and within samples, average Mn content being lower in the Canada Pinabete pluton (compare figs. II.7 and II.3). Differences in ilmenite composition within samples of the metaluminous granite primarily reflect occurrence; secondary ilmenite "unmixed" from magnetite contains more Mn than primary ilmenite.

Discussion—By analogy with the Virgin Canyon pluton and in view of the higher Mn content in ilmenite "exsolved" from magnetite, it may be concluded that ilmenite incorporated increasing proportions of Mn as crystallization proceeded in the Canada Pinabete pluton. In the peralkaline granite, primary crystalization of ilmenite was probably followed closely by formation of ilmenite secondary after magnetite (Table A.2.2, sample 84QC7). Ilmenite in the peralkaline granite contains less Fe_2O_3 and thus crystallized at higher temperature and lower fO_2 than that in the metaluminous granite. Lower fO_2 during crystallization also accounts for the generally higher proportion of

PLATE II.5: Photomicrographs of accessory phases, Canada Pinabete and Rito del Medio granites.

(a) Davidite grain containing irregular small darker (altered?) patches. Metaluminous granite of Canada Pinabete, sample 82QC46. Bar is 100 microns long.

(b) Hematite (white) intergrown with ilmenorutile (gray). Shades of medium gray reflect individual grains of ilmenorutile. Vug, metaluminous granite of Canada Pinabete, sample 82QC45. Bar is 100 microns long.

(c) Bladed hematite in vug, containing ilmenorutile (near top, medium gray) and columbite with a metamict core (below center, darker gray). Metaluminous granite of Canada Pinabete, sample 82QC45. Bar is 100 microns long.

(d) Ilmenorutile (light gray) intergrown with columbite (dark gray). Rito del Medio granite, sample 81S31. Bar is 50 microns long.

---

ilmenite in the peralkaline granite, as well as for the occurrence of exsolution-free ilmenite in that unit and in magnetite-free samples of the metaluminous granite.

(3) Hematite and ilmenorutile (Table A.2.3)

Hematite and exsolved ilmenorutile were analyzed in two vugs in sample 82QC45 (Plate II.5, b and c). Hematite contains 0.52 to 5.82 weight percent TiO_2 as the only major constituent other than Fe_2O_3 (92.4 to 98.2 wt%). Ilmenorutile composition (in weight percent) varies considerably from grain to grain: TiO_2, 61.2 to 85.8; FeO, 4.25 to 11.2; and Nb_2O_5, 4.35 to 25.4. Ta is the only other essential constituent; Ta_2O_5 contents are 1.07, 1.26, 1.49, and 0.36 weight percent, respectively, for grains 1, 1', 3, and 6 in sample 82QC45. This ilmenorutile is unusual because of its low Ta content and the fact that Fe/(Nb+Ta) atomic is near 1/1 rather than 1/2 (Palache and others, 1944). There is a positive correlation between Ti in ilmenorutile and Ti in its hematite host (fig. II.9); hematite in vug 2 is richer in Ti than that in vug 1, for the same concentration of Ti in the coexisting ilmenorutile.

Discussion--Exsolution of ilmenorutile rather than ilmenite from hematite shows that Nb and Ti were more concentrated towards the end stages of crystallization. Apparently hematite crystallized as a homogeneous mixed phase of Fe_2O_3 and $(Fe,Ti,Nb)O_6$. With decreasing temperature, the ilmenorutile component unmixed and the large Nb cation was preferentially taken out of the hematite structure, leaving Fe and Ti dissolved as $FeTiO_3$. The differing relation between Ti in coexisting hematite and ilmenorutile in the two vugs suggests that each vug evolved as a closed system with its own distribution coefficient.

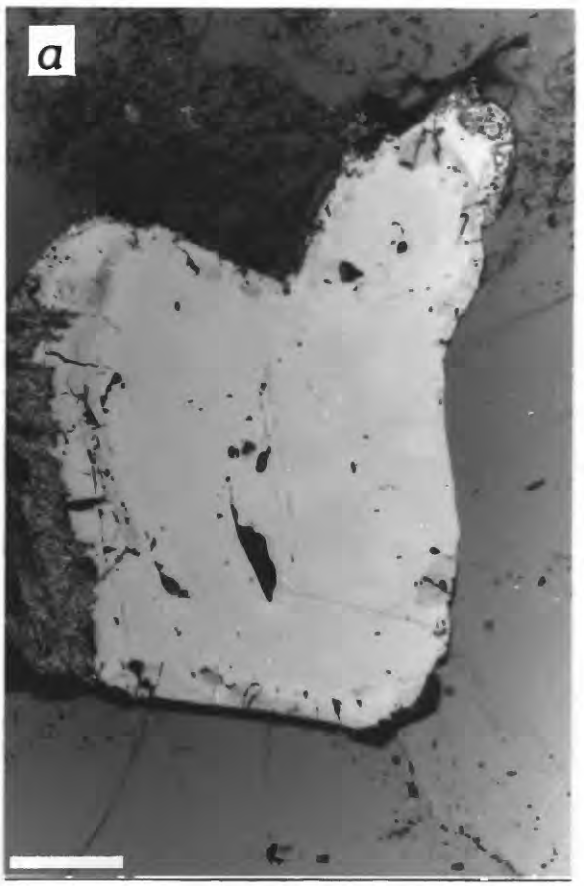
a

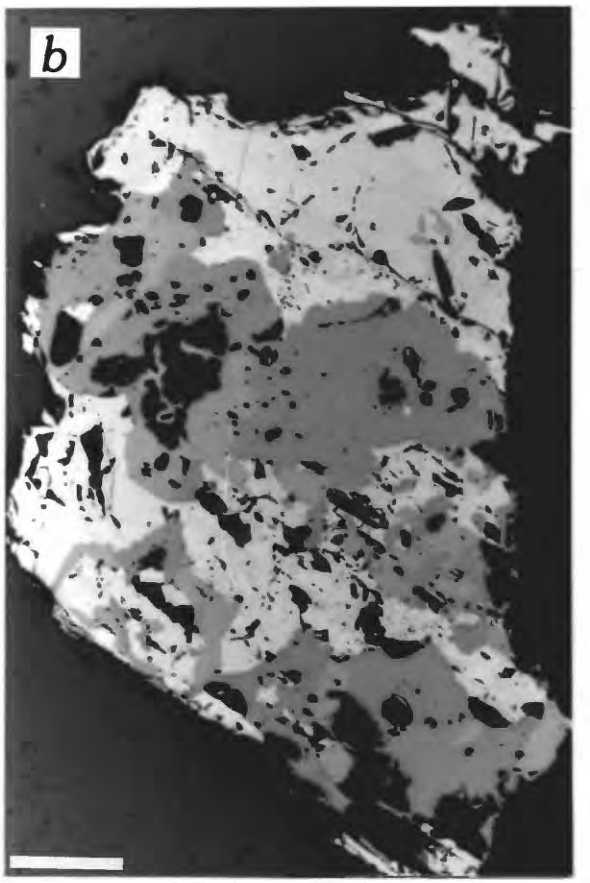
b


c

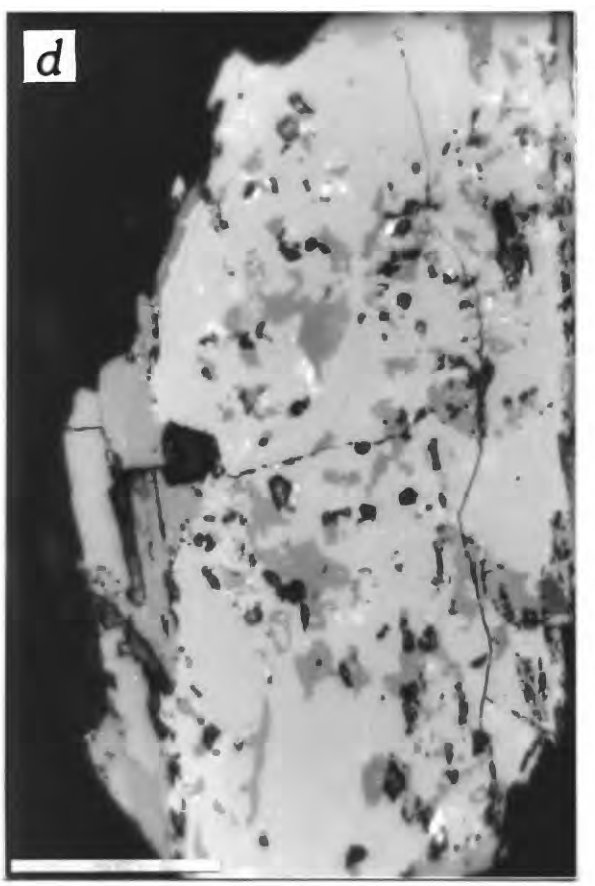
d

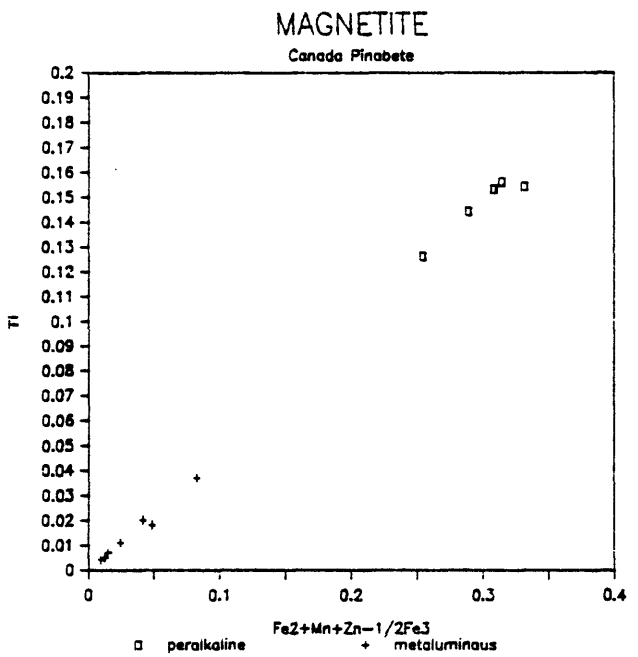

Fig. II.6. Fe2+Mn+Zn-1/2Fe3 against Ti (cations) in magnetite, Canada Pinabete.

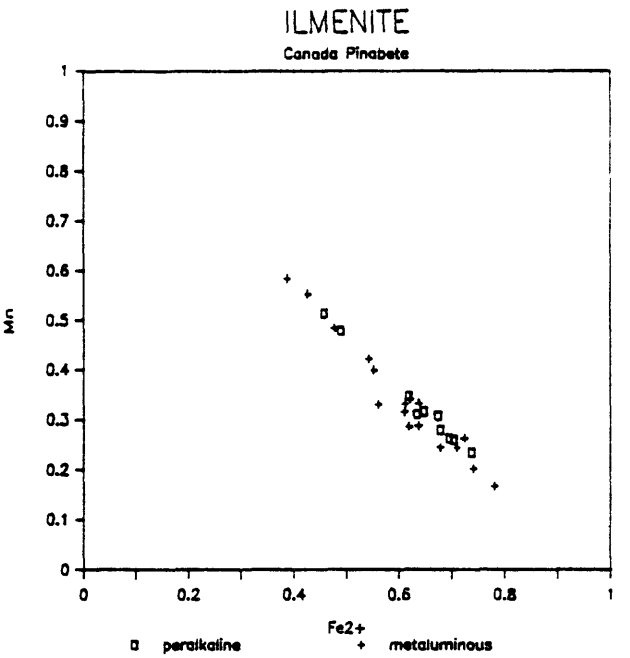

Fig II.7. Fe2 against Mn (cations) in ilmenite, Canada Pinabete.

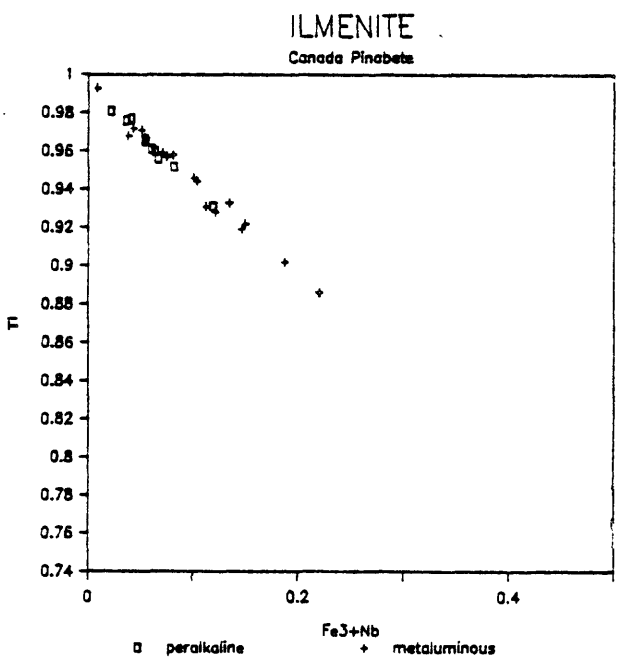

Fig II.8. Fe3+Nb against Ti (cations) in ilmenite, Canada Pinabete.

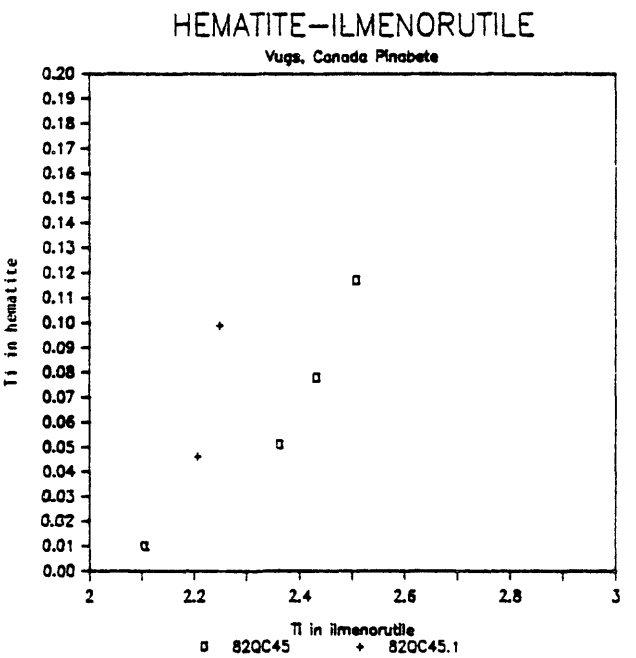

Fig II.9. Ti in ilmenorutile against Ti in hematite (cations), Canada Pinabete.

(4) Columbite (Table A.2.4)

Columbite, found as a small rectangular grain (0.05 x 0.07 mm) with angular shape and a dark core, contains up to 19.2 weight percent ThO_2; its Ti content makes it intermediate to ilmenorutile. The presence of a distinct core and rim suggests that this occurrence of columbite is probably primary and not the result of an exsolution process.

(5) Davidite (Table A.2.4)

Three davidite crystals of slightly different composition were analyzed in sample 82QC46. Characteristic elements other than Ti and Fe are La, Ce, U, Nb, Y, and Mn (between 1.49 and 4.95 oxide wt%); Zn, Ta, Y, and Th are present in lesser amounts (0.46 to 0.99 oxide wt%). Both ilmenite and rutile, intergrown with davidite, have quite high contents of Nb (1.2 to 5.1 wt% Nb_2O_5, not reported in Table A.2.1).

c) Crystallization of the opaque oxide minerals

(1) The crystallization history of opaque oxide minerals in the peralkaline granite of the Canada Pinabete pluton resembles that in the peralkaline granite of the Virgin Canyon pluton. Magnetite is primary, occurring both as phenocrysts and in the groundmass and is more abundant among phenocrysts. Primary ilmenite occurs as phenocrysts and is more abundant than magnetite in the groundmass. The change in the proportions of magnetite and ilmenite between phenocryst and groundmass occurrence suggests that fO_2 decreased during solidification of the unit. "Exsolution" of ilmenite from magnetite took place immediately after, or during the last stages of, crystallization of primary, groundmass ilmenite. Both ilmenite and magnetite compositions indicate that crystallization of the peralkaline unit took place at higher temperature and lower oxygen fugacity than crystallization of the metaluminous unit. As in the Virgin Canyon pluton, late-stage fO_2 was high enough to produce hematite after magnetite, but usually too low to oxidize ilmenite to hematite plus rutile.

(2) Various crystallization histories are reflected by the opaque oxide minerals in the metaluminous unit. In the magnetite-free areas of the pluton where ilmenite is primary, and the only phase present, fO_2 was quite low. In the most characteristic facies of the unit, magnetite and ilmenite occur as the typical primary opaque phases and ilmenite occurs as an "exsolution" product after magnetite. Magnetite and ilmenite compositions indicate lower temperature and higher fO_2 for crystallization of the metaluminous unit than for the peralkaline unit. Ilmenite compositions show, by analogy with the Virgin Canyon pluton, that "exsolution" after magnetite occurred after primary crystallization of ilmenite. Later, conditions became more oxidizing, magnetite was oxidized to hematite and ilmenite to hematite plus rutile.

3. RITO del MEDIO

a) Description

Opaque oxide minerals constitute 0.75 to 1.5 volume percent of the Rito del Medio granite. The main primary phases are magnetite and ilmenite, but hematite also occurs as a primary mineral. A primary intergrowth of ilmenorutile and columbite has been found locally. Opaque oxide minerals crystallized over an extended period of time; they can be euhedral as well as interstitial and also grew in miarolitic cavities.

Magnetite is always the most abundant phase; grains can be up to 1 mm across, but are more often less than 0.6 mm. Euhedral to interstitial, it can be enclosed in feldspars or can host them. Rare pyrite inclusions occur in magnetite. Ilmenite "exsolution" products are common, as lamellae (Plate II.2, a; Plate II.4, a) and granules within or at the edges of magnetite grains. Ilmenite lamellae within magnetite may be associated with small black granules (Plate II.2, a) which are apparently gahnite spinel, based on microprobe detection of enhanced Al and Zn content. Minor partial oxidation to hematite is always present.

Ilmenite is typically less abundant than magnetite, but locally as abundant. It can occur as rather small (0.01 to 0.05 mm long) or larger (up to 0.3 mm) primary crystals. Ilmenite grains can be isolated, enclosed in biotite or feldspar, or occur with magnetite. Ilmenite associated with magnetite, perhaps partly of secondary origin, is subhedral to anhedral and ranges in size from 0.1 mm to 0.3 mm. Hematite exsolution droplets or lenses (Plate II.1, c) and partial oxidation to hematite plus rutile are better displayed in the larger crystals. Late ilmenite is found in cavities as large euhedral crystals (up to 1.8 mm). Ilmenite may also occur as lozenge-shaped aggregates of small grains in different orientations (Plate II.4, a). This type of ilmenite, also described from the Virgin Canyon pluton, is apparently secondary after sphene and is best developed in the Rito del Medio pluton; this secondary ilmenite may contain hematite exsolution lamellae. Rarely, rutile is found with ilmenite in these replacement aggregates.

A peculiar intergrowth of hematite and ilmenite is typical of the Rito del Medio pluton (Plate II.6); an ilmenite core is surrounded by a hematite rim. The ilmenite core contains fine hematite exsolution lamellae, more

---

PLATE II.6: Photomicrographs of "him" association, Rito del Medio granite.

(a-d) "him" association, consisting of magnetite (medium gray) containing type (2) ilmenite "exsolution" lamellae, separated by irregular bands of hematite (light gray) containing ilmenite exsolution lamellae, from ilmenite (darkest gray) containing exsolved hematite. Note isolated grain of ilmenite with hematite rim at lower left in (a). Magnetite contains minor hematite (martite) oxidation. Feathery aggregates in each photograph consist of ilmenite granules, presumably after sphene. (a and d) sample 82QC17;(b and c) sample 82QC18. Bars are 100 microns long.

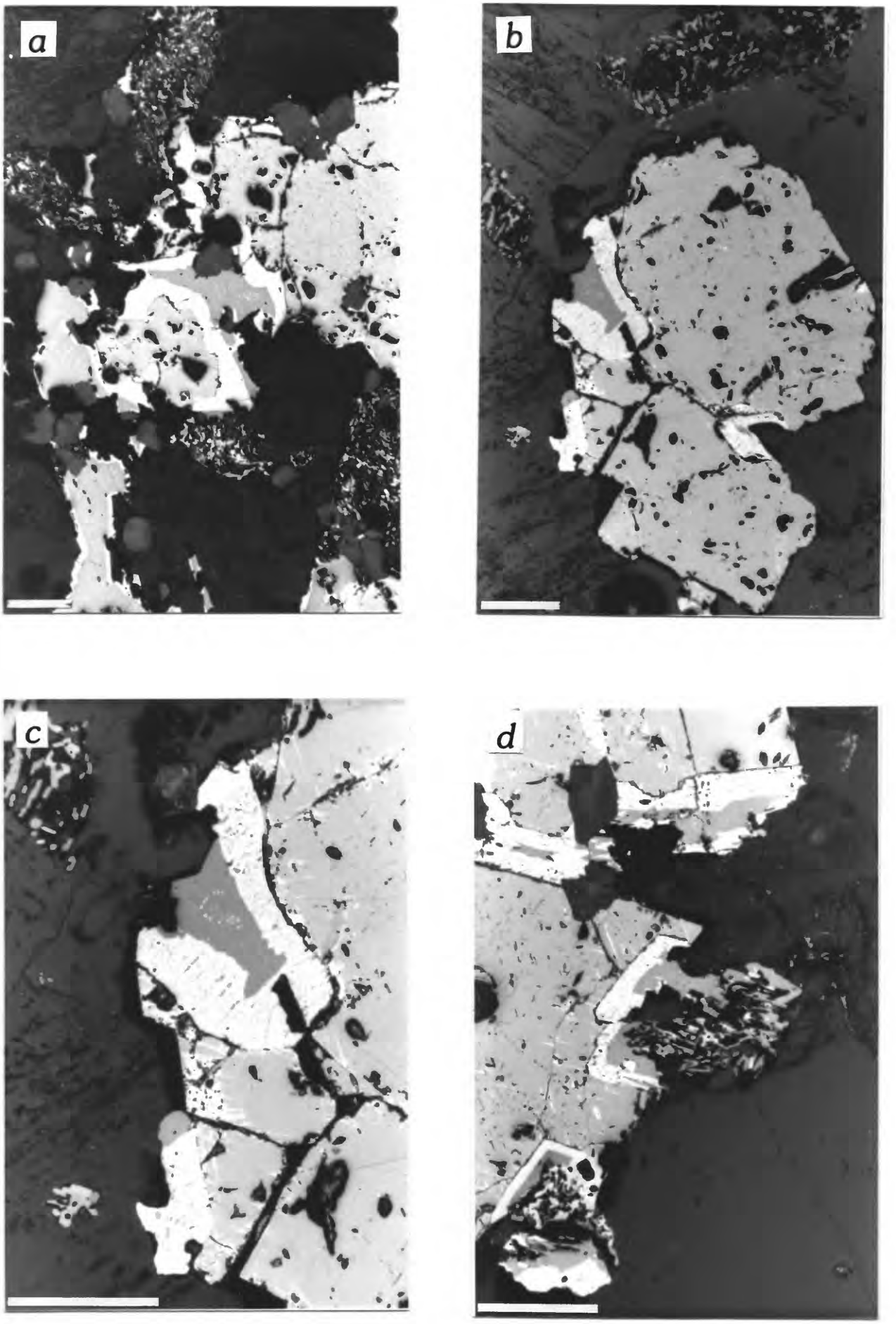
a
b
c
d

concentrated at the center; the hematite rim contains fine, more evenly distributed ilmenite exsolution lenses (Plate II.6, c). Possibly related grains, in which there is no ilmenite core, contain one generation of ilmenite exsolution within hematite. These intergrowths display anhedral shapes, are themselves intergrown with magnetite, and may grade into polycrystalline aggregates of ilmenite (with or without hematite) which often display a lozenge shape and are thus taken to be replacements of sphene (Plate II.6, d). This association will be referred to as "him."

Hematite occurs as early small homogeneous primary grains enclosed in silicates (in samples with "him" associations especially), or as large (up to 0.6 X 1.3 mm), late primary crystals in vugs. Hematite grains in vugs may be complex, composed of cores which contain ilmenite exsolution lamellae and oscillatory zoned rims (Plate II.1, a and b). Hematite can also be secondary after magnetite (oxidation) or ilmenite (exsolution or oxidation).

Ilmenorutile and columbite were found intergrown in a vug in sample 81S31 (Plate II.5, d). The intergrowth is thought to be of an exsolution type, ilmenorutile being the host phase and columbite the exsolved phase. This textural relation has been reported in the Penikoja pegmatite, Somoro, SW Finland (Siivola, 1970).

b) Chemistry

(1) Magnetite (Tables II.4 and A.3.1)

Magnetite in the Rito del Medio granite has a composition quite different from magnetite in the Virgin Canyon and Canada Pinabete plutons. The sum (Al_2O_3 + TiO_2 + MnO + ZnO) ranges from 0.94 to 3.83 weight percent, with Mn being the predominant minor element. Low content of Fe^{2+} relative to Fe^{3+} and high Mn content result in recalculation of magnetite analyses with jacobsite ($MnFe_2O_4$) instead of ulvospinel (Fe_2TiO_4) as the main dissolved constituent. Other constituents such as Mn_2TiO_4, $MnAl_2O_4$ (galaxite), and $ZnAl_2O_4$ (gahnite) are also dissolved, in lesser amounts, in the magnetite.

Discussion—Although no ulvospinel remains in the magnetite structure, ilmenite "exsolution" products reveal that Ti was dissolved in magnetite at higher temperature. Ilmenite "exsolved" from magnetite is Mn rich (64 to 93 mol% $MnTiO_3$) and the amount of Fe_2TiO_4 dissolved in magnetite must have been far lower than the amount of Mn_2TiO_4. Absence of ulvospinel in the magnetite structure probably reflects reequilibration at high fO_2 and low temperature. Excess Fe^{3+} relative to Fe^{2+} also relates to higher fO_2 for the end of reequilibration of magnetite in the Rito del Medio granite.

Gahnite unmixed from magnetite as small granules (identified on the microprobe by enhanced Al and Zn contents) associated with ilmenite "exsolution" lamellae; thus, Al and Zn were more abundant as dissolved constituents in magnetite at higher temperature.

(2) Ilmenite (Tables II.5 and A.3.2)

A wide range in Mn content is the main characteristic of the chemistry of ilmenite in the Rito del Medio granite (17 to 93 mol% $MnTiO_3$); Fe_2O_3 content

varies from 2.5 to 12.1 mole percent. There is a good correlation between Fe^{2+} and Mn (fig. II.10; r, -0.99); analyses which plot farthest from the general slope also show the most Fe_2O_3. The four lowest Mn contents (17 to 36 mol% $MnTiO_3$) are from two samples and represent primary crystallized ilmenite, with or without hematite exsolution lamellae. In all other cases, ilmenite contains at least 51 mole percent pyrophanite.

All ilmenites are characterized by high Nb concentration (up to 3.45 wt% Nb_2O_5). Correlation between Fe^{3+} and Ti (r, -0.91) is much improved by adding Nb to Fe^{3+} (fig. II.11; r, -0.98).

Several characteristics can be pointed out relative to ilmenite compositions within a given sample. (1) Primary ilmenite usually contains less Mn than secondary ilmenite "exsolved" from magnetite. (2) Primary ilmenite with hematite exsolution lamellae contains more Fe_2O_3 (average, 8.4 mol%) than primary ilmenite free of exsolution (average, 5.3 mol%). In the Rito del Medio pluton, analyses of ilmenite containing hematite exsolution products represent an intermediate composition, because the hematite lenses are too fine and widely dispersed to be avoided. (3) Late primary ilmenite, crystallized in vugs, has a higher Mn content than other types of ilmenite in a given sample. (4) Ilmenite in lozenge-shaped aggregates after sphene contains less Mn than ilmenite "exsolved" from magnetite. (5) The only distinguishing feature of ilmenite in "him" associations is low Zn content ($\leq$ 0.08 wt%) relative to all other ilmenites (0.08 to 0.85 wt%; avg, 0.3 wt%).

Discussion—The high Mn content of primary ilmenite found in the vug allows correlation of Mn enrichment in ilmenite with time of crystallization or reequilibration as follows: (1) "Exsolution" of ilmenite from magnetite occurred at a later stage than primary crystallization of ilmenite. (2) Lozenge-shaped aggregates of ilmenite after sphene formed at a magmatic stage, before "exsolution" of ilmenite from magnetite. (3) If Mn content in ilmenite can be related to temperature of formation (Buddington, 1963), ilmenite in the Rito del Medio pluton reflects a lower equilibration temperature than ilmenite in the Canada Pinabete and Virgin Canyon plutons. (4) If Mn content in ilmenite can be related to fO_2 (Czamanske and Mihalik, 1972), ilmenite in the Rito del Medio pluton reflects higher fO_2 than ilmenite in the Canada Pinabete and Virgin Canyon plutons.

(3) Hematite (Table A.3.3)

The composition of hematite is variable not only from one type of occurrence to another, but also within the same type of occurrence. Primary small hematite grains enclosed in felspars are homogeneous, but show compositional variability from one grain to another within a given sample ($Hem_{74}Ilm_{16}Pyr_{10}$ to $Hem_{90.8}Ilm_{8.6}Pyr_{0.6}$). These primary grains of hematite do not contain ilmenite exsolution lamellae.

Because of oscillatory zoning, primary large hematite in vugs is quite variable in composition (Table A.3.3). Crystal 82QC17(8) (Plate II.1, a and b) was studied in detail. The core of the crystal, of composition $Hem_{85.6}Ilm_{13.4}Pyr_{1.0}$, contains broad ilmenite exsolution lamellae of composition $Hem_{3.6}Ilm_{34.2}Pyr_{62.2}$. This core is surrounded by an oscillatory-zoned exsolution-free rim in which composition irregularly becomes more hematite rich outward, as follows (in terms of Hem component): (1) just inside light

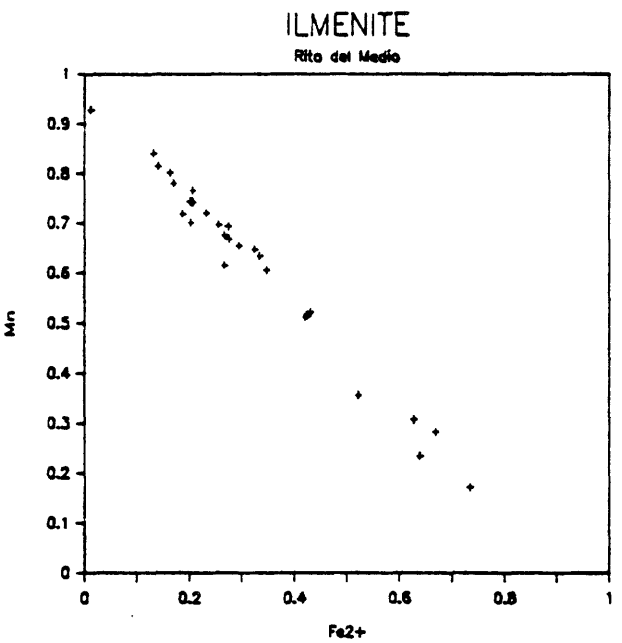

Fig II.10. Fe2 against Mn (cations) in ilmenite, Rito del Medio.

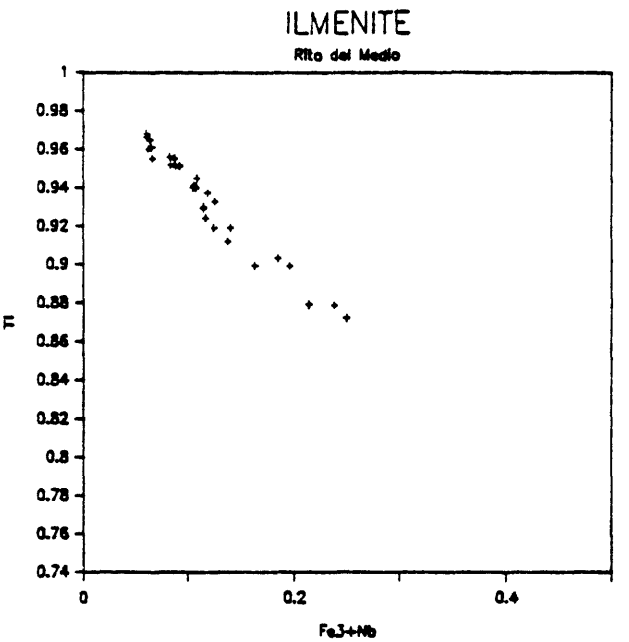

Fig II.11. Fe3+Nb against Ti (cations) in ilmenite, Rito del Medio.

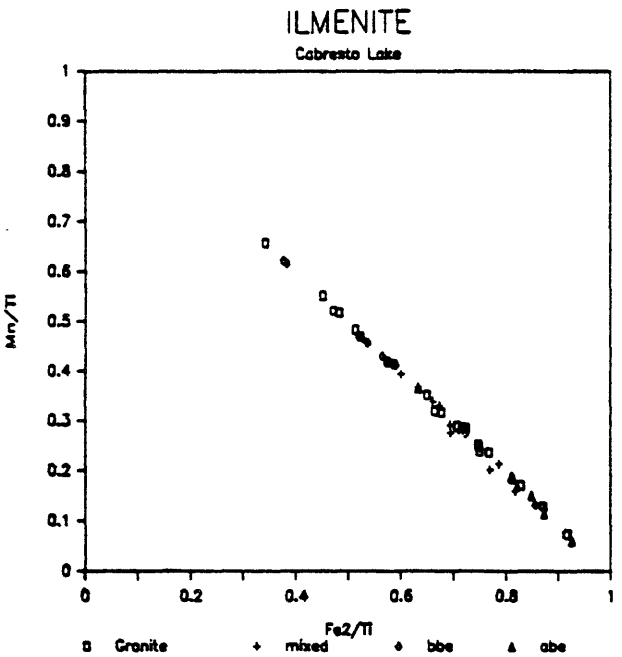

Fig. II.12. Fe2/Ti against Mn/Ti in ilmenite, Cabresto Lake; bbe, biotite-bearing enclaves; abe, amphibole-bearing enclaves.

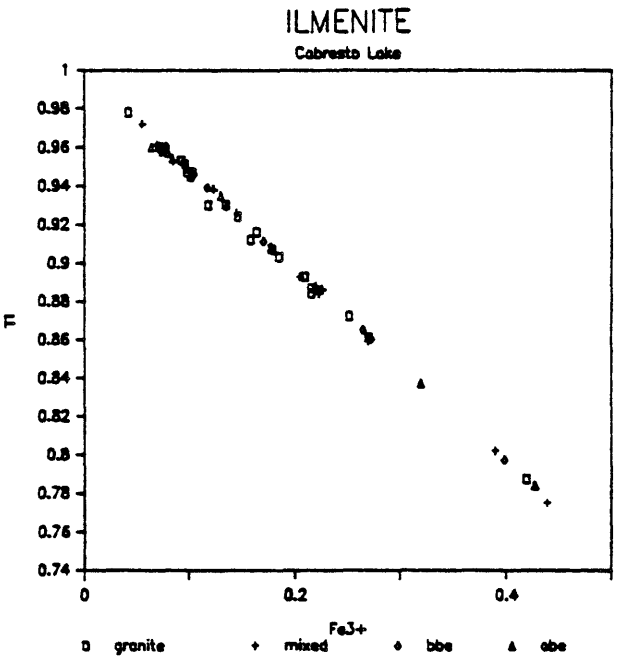

Fig II.13. Fe3 against Ti (cations) in ilmenite, Cabresto Lake; bbe, biotite-bearing enclaves; abe, amphibole-bearing enclaves.

band, $Hem_{85.7-89.6}$; (2) broad light band, $Hem_{94.8}$; (3) just outside band, $Hem_{88.2-89.8}$; and (4) edge of crystal, $Hem_{91.9}$.

Hematite in "him" associations contains the highest proportions of ilmenite and pyrophanite in solution (to 21.7 mol% $FeTiO_3$ and 11.1 mol% $MnTiO_3$), whereas hematite derived from magnetite (martite) is almost pure.

Discussion—The occurrence of primary hematite shows that fO_2 was quite high during crystallization of the Rito del Medio granite. It is possible to relate the composition of hematite to crystallization history. In "him" associations, hematite may contain up to 21.7 mole percent $FeTiO_3$ in solution (to 30.7 mol% $FeTiO_3 + MnTiO_3$). Late hematite in the vug contains up to 12.7 mole percent $FeTiO_3$ (to 14.9 mol% $FeTiO_3 + MnTiO_3$). Appropriately, it can be inferred from these data that hematite in "him" associations stopped reequilibrating at higher temperature and lower fO_2 than hematite in vugs (Spencer and Lindsley, 1981, fig. 4; see fig. II.24). Small primary hematite grains in silicates and hematite in "him" associations are also richer in Ti than hematite in vugs. The low Mn and Ti contents of late secondary hematite derived by oxidation of magnetite are also consistent with Ti impoverishment in hematite with time.

The core of crystal 82QC17(8) crystallized at higher temperature and lower fO_2 than its rim and, as temperature decreased, unmixed part of its Ti content as ilmenite. Hematite with irregularly decreasing Ti content grew around the core, apparently reflecting generally increasing, but variable fO_2. The broad Ti-poor band reflects an unusually sharp and extended increase in oxygen fugacity.

Ilmenorutile and columbite (Table A.3.4)

As for the ilmenorutile in the Canada Pinabete pluton, Ta (not determined) is a minor constituent and Fe/(Nb+Ta) is about 1/1. Columbite is characterized by higher Mn (18.1 wt% MnO) and lower Fe content (2.33 wt% FeO), compared to columbite in the Canada Pinabete granite (7.5 wt% MnO and 11.2 wt% FeO).

Crystallization of such Nb-rich minerals in vugs in high level granites is not surprising and is in agreement with the statement by Kuznetsov (1956) that "...Nb...remains almost entirely in the residual melts...".

4. CABRESTO LAKE

a) Description

Magnetite and ilmenite are the characteristic opaque phases of the predominant, granitic unit of the Cabresto Lake pluton. Primary early minerals, they both crystallized at about the same time as sphene and make up 0.5 to 1.6 volume percent of the rock. Magnetite constitutes about 85 to 92 and ilmenite only 8 to 15 volume percent of the opaque oxides. Magnetite and ilmenite are often intergrown and commonly associated with or enclosed in sphene. They can be enclosed in mafic silicates and less commonly are found as small inclusions (less than 0.01 mm) in feldspar.

Magnetite is typically seen in two sizes: larger crystals are commonly 0.6 mm long and can be 1.4 mm long; a population of smaller crystals ranges down to 0.02 mm across. The larger magnetite grains are euhedral and may contain pyrite, apatite, and sphene. When enclosed by sphene, magnetite retains its euhedral shape. Partial oxidation to hematite (martite) is common, but is much less developed than in the other intracaldera plutons. Oxidation "exsolution" of ilmenite is common as fine type (2), or less abundant, larger type (3) lamellae. Ilmenite can also be "exsolved" as grains that are enclosed in (type (4)), partially enclosed in, or adjacent to (type (5)) magnetite crystals. In those cases ilmenite can be oxidized to a mat of hematite plus rutile.

In addition to intergrowths with magnetite, ilmenite is found in three types of occurrence. It occurs as small (to 0.05 mm) euhedral crystals, either isolated or enclosed in biotite; this ilmenite may contain fine hematite exsolution lamellae, or be homogeneous. A second type of occurrence is as larger anhedral crystals (to 0.15 mm), sometimes including magnetite, or associated with it; this ilmenite is extensively oxidized to hematite plus rutile. Ilmenite grains up to 0.4 mm long also occur enclosed in sphene and have rounded droplet-like shapes. In this case, ilmenite often contains hematite lamellae (exsolution products) and is partially oxidized to hematite plus rutile. Late interstitial pyrite, often altered to goethite, is locally found.

In the mixed unit of the Cabresto Lake pluton, opaque oxides amount to 0.6 to 1.2 volume percent; it seems anomalous that more mafic samples are poorest in opaque oxides (Table I.4.2). Magnetite and ilmenite are typical; ilmenite is a little more abundant than in the granitic facies (more than 20 volume percent of the opaque oxides). Both minerals can be enclosed in sphene, amphibole, and biotite, and as very small grains (less than 0.01 mm) in feldspar. Magnetite contains inclusions such as zircon, apatite, and sphene. As in the granitic facies, magnetite is partially altered to hematite and ilmenite is altered to mats of hematite plus rutile when it is not an oxidation "exsolution" product after magnetite. Coarse type (3) ilmenite "exsolution" lamellae in magnetite are common and more abundant than in the granite. Ilmenite associated with magnetite is common; it contains fine hematite lamellae or is partially oxidized to hematite plus rutile. Isolated ilmenite grains can be up to 0.4 mm long, often contain fine hematite lamellae, and are partially oxidized. Ilmenite enclosed in sphene has the same habit as in the granitic facies and is also unmixed and oxidized. Small grains of magnetite and ilmenite (about 0.02 mm across), associated with small grains of amphibole and biotite, may surround quartz xenocrysts. Rare late interstitial pyrite is altered to goethite.

In biotite-bearing enclaves, opaque oxides usually amount to less than 3 volume percent, except in sample 83QC16; they range in size from 0.05 to 0.5 mm across. The typical primary phases are magnetite and ilmenite; hematite occurs only as a secondary phase, either as an oxidation product after magnetite and ilmenite, or as an exsolution product from ilmenite. Magnetite always constitutes more than 70 volume percent of the opaque minerals. It is euhedral, commonly encloses pyrite, and exhibits fine, long ilmenite "exsolution" lamellae, and rarer broad lamellae (0.005 mm across). Partial oxidation to hematite is minor.

Other than being intergrown with magnetite as an oxidation "exsolution" product, ilmenite has two types of occurrence. It can be found as large subhedral to anhedral crystals, up to 0.8 mm long but more typically 0.1 to 0.4 mm long. These crystals are often oxidized to hematite plus rutile. Ilmenite also occurs as smaller crystals (0.01 to 0.05 mm across), which are mostly homogeneous; however, they may contain hematite exsolution lamellae or hematite plus rutile as oxidation products.

Opaque oxide minerals are quite abundant in amphibole-bearing enclaves (approximately 6 vol%). They typically show two different grain sizes; larger grains range from 0.15 to 0.5 mm long and smaller grains average 0.02 mm. Magnetite is the dominant phase among the larger grains (more than 90 vol%); it is euhedral and encloses pyrite grains. Broad ilmenite lamellae (to 0.01 mm) are more common than in magnetite in biotite-bearing enclaves (Plate II.2, b). Ilmenite rarely forms large euhedral crystals with or without partial oxidation to hematite plus rutile. Ilmenite is also found enclosed in sphene, where it displays rounded shapes and often contains fine hematite exsolution lamellae. Among the smaller grains, magnetite amounts to less than 60 volume percent; it shows the same features as among larger grains. Fine-grained ilmenite is euhedral and rarely shows oxidation to hematite plus rutile; it may contain hematite exsolution lamellae.

b) Chemistry

(1) Magnetite (Tables II.4 and A.4.1)

Magnetite is quite homogeneous in composition and rather pure in all four rock types sampled from the Cabresto Lake pluton. The sum ($Al_2O_3 + TiO_2 + MnO + ZnO$) ranges from 0.42 to 1.93 weight percent in the granitic unit, from 0.84 to 1.57 weight percent in the mixed unit, from 0.40 to 1.15 weight percent in biotite-bearing enclaves, and from 0.77 to 2.10 weight percent in amphibole-bearing enclaves. Magnetite from all four rock types recalculates in terms of Fe_3O_4, Fe_2TiO_4, Mn_2TiO_4, and $ZnAl_2O_4$; magnetite in the granitic unit also contains some $MnAl_2O_4$.

There are only a few slight differences in magnetite composition among the four rock types. (1) Magnetite in both types of enclave contains little Mn. (2) Magnetite in the granitic unit contains the least Zn. (3) Magnetite in the mixed unit and amphibole-bearing enclaves contains the most Al.

Discussion—Low-Ti content in magnetite of the Cabresto Lake pluton reflects reequilibration at low temperature and high fO_2 (see fig. II.24), with no major distinction between the different rock types.

(2) Ilmenite (Tables II.5 and A.5.2)

In contrast to magnetite, ilmenite shows a wide range of compositions relating to Fe^{3+}/Ti and Fe^{2+}/Mn, which can be assessed in figures II.12 and II.13. Most primary ilmenite contains fine hematite exsolution lenses and analyses of such ilmenite reflect an intermediate composition. This partly accounts for the wide range of Fe_2O_3 (2.1 to 22.1 mol%) observed in the four

rock types. The correlation between Ti and Fe^{3+} is excellent (fig. II.13; r, -1.00); and, as opposed to the northern intracaldera plutons, Nb is not a significant element. All four rock types show the same wide range in Fe^{3+}/Ti.

Compositional variability in Fe^{2+}/Mn is shown in figure II.12 where Fe^{2+}/Ti is plotted against Mn/Ti (r, -1.00). Poorer correlation between Fe^{2+} and Mn (r, -0.94) is due to hematite contained in the host ilmenite, causing (Fe^{2+} + Mn) to total much less than 1. The four rock types of the Cabresto Lake pluton do not show the same range in Fe^{2+}/Mn. Ilmenite in both the granitic facies and biotite-bearing enclaves shows great compositional variation, with pyrophanite content ranging, respectively, from 5.8 to 64.4, and 11.4 to 59.2 mole percent. Both the mixed facies and amphibole-bearing enclaves show a smaller variability, with ilmenite compositions in amphibole-bearing enclaves being the most iron-rich. Pyrophanite content ranges from 9.5 to 45.8 mole percent in the mixed facies and from 4.7 to 39.5 mole percent in amphibole-bearing enclaves.

Several features are characteristic of ilmenite chemistry in a given sample. (1) Primary ilmenite containing hematite exsolution lenses always contains more Fe^{3+} than primary homogeneous ilmenite. (2) Secondary ilmenite "exsolved" from magnetite always contains more Mn and Ti, and less Fe^{2+}, Fe^{3+}, and Nb than primary ilmenite. Also, ilmenite in amphibole-bearing enclaves contains less $MnTiO_3$ than ilmenite in biotite-bearing enclaves.

Discussion--Compositions of primary ilmenite show that it probably formed at a higher fO_2 in the Cabresto Lake pluton than in the three northern intracaldera plutons. These data agree with the magnetite analyses in indicating higher fO_2 for their reequilibration. It can be inferred that primary ilmenite formed earlier than ilmenite exsolved from magnetite. This allows three conclusions to be made about evolution in ilmenite chemistry during differentiation of the Cabresto Lake pluton; Fe^{3+}/Ti decreased, Mn/Fe^{2+} increased, and Nb content decreased. Decrease in Fe^{3+} content is the most striking feature because it shows that fO_2 decreased during differentiation.

The initial Fe_2O_3 content in ilmenite is a function of temperature and oxygen fugacity during primary crystallization, while the content of Fe_2O_3 remaining in ilmenite is mainly a function of temperature. In a given sample, ilmenites with differing initial Fe_2O_3 content are interpreted to have crystallized at different times, under slightly different fO_2 and/or temperature conditions. As shown in figure 13 and Table A.4.2, a similar broad range in Fe_2O_3 content is found for ilmenite in all four rock types.

5. RIO HONDO

a) Description

Opaque oxide minerals average 1 to 2 volume percent in the granodioritic facies of the Rio Hondo pluton. The predominant phase, magnetite, is typically free of ilmenite "exsolution" bodies and ranges up to 1 mm across (more typically nearer 0.5 mm) and down to 0.05 mm. Usually euhedral, magnetite can be enclosed in amphibole and biotite and often is partially or

completely enclosed in euhedral sphene. When isolated, magnetite is often surrounded by a narrow rim of sphene (Plate II.4, d). Small grains of pyrite are commonly found enclosed in magnetite. Rare oxidation "exsolution" has produced ilmenite as fine long lamellae, often oxidized to hematite plus rutile. Partial oxidation to hematite is common in magnetite, but not well developed.

Ilmenite is not common and forms less than 5 volume percent of the opaque oxides. Ilmenite most commonly occurs as rounded irregular inclusions in sphene. These inclusions contain one or two sets of hematite exsolution lamellae and are often partially oxidized to hematite plus rutile (Plate II.1, d; Plate II.4, b and c). Ilmenite also occurs as small (less than 0.05 mm) early crystals enclosed in biotite and sometimes in feldspar; these small crystals contain one set of hematite exsolution products. Rare late interstitial pyrite is commonly altered to goethite. Hematite, probably secondary, occurs along biotite cleavages.

In the granitic facies, opaque oxides usually amount to less than 1 volume percent. Magnetite is still predominant, but ilmenite is more common than in the granodiorite. Magnetite can be up to 1 mm long, but is more typically 0.1 to 0.2 mm; it may enclose pyrite, apatite, and zircon. Magnetite is found enclosed by biotite and very small grains (0.01 mm) occur in feldspar. As in the granodioritic facies, magnetite can be enclosed in euhedral sphene; it can also partially enclose sphene. Euhedral to subhedral magnetite commonly contains ilmenite "exsolution" lamellae (fine or broad) or granules. Partial oxidation to hematite is more extensive than in the granodiorite.

Ilmenite occurs as early, euhedral grains. It is commonly enclosed in sphene and, in this case only, is rounded and contains hematite exsolution lamellae. In all cases, ilmenite can be oxidized to hematite plus rutile.

In the mafic-magmatic enclaves of the granodioritic facies, opaque oxide minerals make up 1.6 to 2.9 volume percent of the rock. They mostly occur as inclusions in sphene or associated with mafic silicate clusters (biotite and amphibole); less commonly, they are isolated. Magnetite is again predominant and can be up to 0.8 mm across, but is more typically around 0.2 mm; euhedral to subhedral, it may enclose pyrite. "Exsolution" products are rare; martite is common but many grains are free of oxidation. Magnetite grains are often surrounded by a thin rim of sphene.

Ilmenite occurs as small crystals (to 0.01 mm) enclosed in feldspar, or less often in biotite. These small crystals contain hematite exsolution lamellae. Ilmenite also occurs in sphene, where it is larger, rounded, and contains one or two sets of hematite exsolution lamellae (Plate II.1, d). When enclosed in sphene, it may also be intergrown with magnetite and may be oxidized to hematite plus rutile. Secondary hematite occurs along biotite cleavages. Isolated grains of pyrite may be altered to goethite; rare pyrrhotite is associated with pyrite.

b) Chemistry

(1) Magnetite (Tables II.4 and A.5.1)

Magnetite is nearly pure and similar in composition in the granodiorite, granite, and mafic-magmatic enclaves of the Rio Hondo pluton. The sum (Al_2O_3 + TiO_2 + MnO + ZnO) is always less than 0.85 weight percent and Fe_3O_4 averages 99 mole percent. However, recalculation of magnetite analyses shows a distinction between the three rock types. Although Mn_2TiO_4 and $ZnAl_2O_4$ are present in all three rock types, more Mn and Fe^{3+} and less Ti and Fe^{2+} in magnetite in the granite makes $MnFe_2O_4$ the main dissolved component, whereas magnetite analyses from both other rock types recalculate in terms of Fe_2TiO_4.

Discussion—Magnetite in the granodiorite of the Rio Hondo pluton reequilibrated at low temperature, such that almost all components dissolved at higher temperature have been removed from its structure. In the granodioritic facies and mafic-magmatic enclaves, exsolution apparently took place at relatively high fO_2 because exsolution of the Fe_2TiO_4 component caused sphene rather than ilmenite to precipitate at grain margins. In the granitic facies, however, Fe_2TiO_4 and Mn_2TiO_4 unmixed as Mn-rich ilmenite "exsolution" bodies.

The fact that $MnFe_2O_4$ remains dissolved in magnetite of the granitic facies, whereas Fe_2TiO_4 remains in magnetite of both the granodioritic facies and mafic-magmatic enclaves, may relate to higher $Mn/(Mn+Fe^{2+})$ in the granite. More extensive martitization of magnetite in the granite shows that oxygen fugacity was higher in the granite during the later stages of reequilibration.

(2) Ilmenite (Tables II.5 and A.5.2)

As in all other plutons, ilmenite is quite variable in composition in the Rio Hondo pluton; variability relates to Fe^{2+}/Mn and also, to a greater extent than in other plutons, to Fe^{3+}/Ti. Variability in Fe^{3+}/Ti is due to the fact that most ilmenites analyzed are unmixed on a fine scale (especially ilmenite enclosed in sphene) and analyses often reflect compositions intermediate between those of host ilmenite and exsolved hematite. The correlation between Fe^{3+} and Ti is excellent (fig. II.15; r, -1.00) and not notably influenced by the low Nb content. Figure II.15 shows that ilmenite in the three different rock types contains Fe_2O_3 in different proportions; 7.4 to 22.1 mole percent in the granodiorite, 0.5 to 4.1 mole percent in the granite, and 6.7 to 10.8 mole percent in the mafic-magmatic enclaves.

Poor correlation between Fe^{2+} and Mn in ilmenite in the granodiorite relates to high Fe^{3+}. As in the Cabresto Lake pluton, Fe^{2+}/Ti was plotted against Mn/Ti (fig. II.14; r, -1.00) instead of Fe^{2+} against Mn (r, -0.84). Mn content in ilmenite is distinctly lower in both the granodioritic facies and mafic-magmatic enclaves (5.4 to 25.5 mol% pyrophanite) than in the granitic facies (27.7 to 79.7 mol% pyrophanite).

In a given sample of granite, secondary ilmenite "exsolved" from magnetite contains more Mn than either primary isolated ilmenite or ilmenite enclosed in sphene.

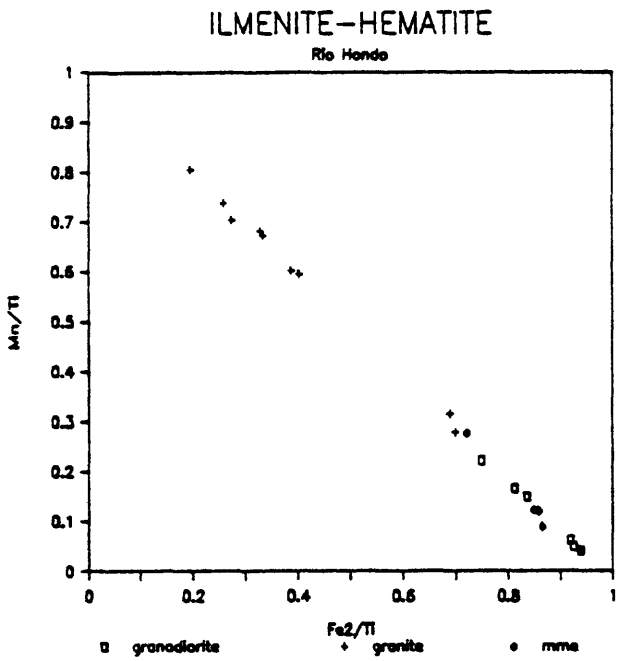

Fig II.14. Fe2/Ti against Mn/Ti in ilmenite, Rio Hondo; mme, mafic magmatic enclaves; black square, hematite.

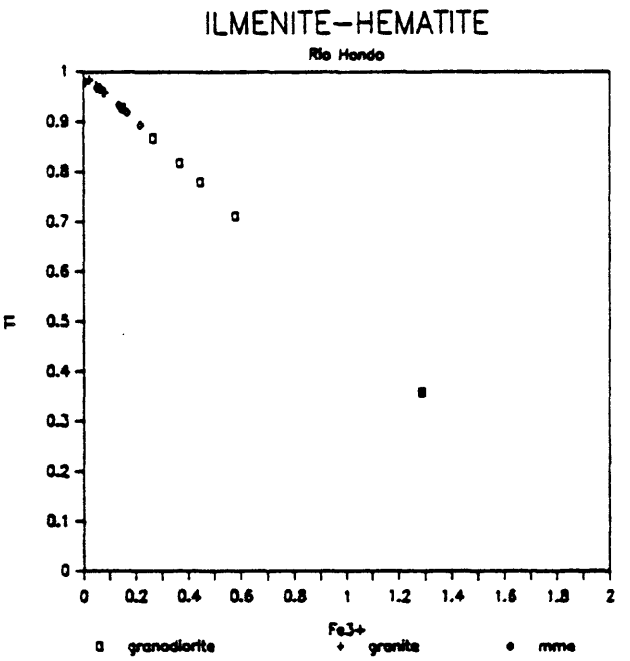

Fig II.15. Fe3 against Ti (cations) in ilmenite and hematite, Rio Hondo; mme, mafic magmatic enclaves; black square, hematite.

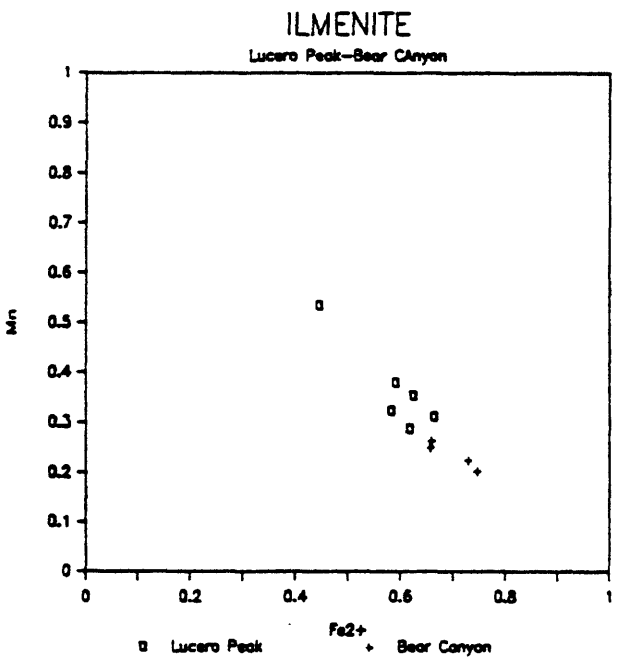

Fig II.16. Fe2 against Mn (cations) in ilmenite, Bear Canyon and Lucero Peak.

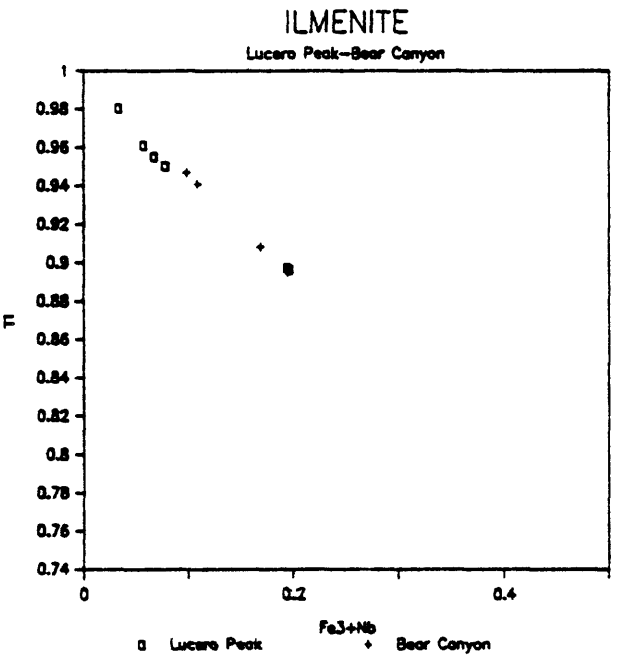

Fig II.17. Fe3+Nb against Ti (cations) in ilmenite, Bear Canyon and Lucero Peak.

Discussion—Ilmenite compositions give information about relative conditions of reequilibration in the three rock types of Rio Hondo. Higher initial Fe^{3+} in ilmenite in the granodiorite reflects higher fO_2 during early stage crystallization of ilmenite in this unit compared to ilmenite in the granite. Ilmenite in mafic-magmatic enclaves stands between these two other facies.

6. BEAR CANYON

a) Description

Magnetite and ilmenite are the main primary opaque phases (approx 70-60/30-40) and constitute 0.6 to 1.3 volume percent of the Bear Canyon granite, as represented by samples 82QC8 and 82QC10.

Magnetite most commonly occurs as rather large grains (up to 0.8 mm across). It rarely contains pyrite inclusions and may be associated with type (5) ilmenite "exsolution" granules. Magnetite is typically oxidized to hematite along fractures in sample 82QC8, but is more typically free of oxidation in sample 82QC10.

Ilmenite can be isolated or occur as grains associated with magnetite; in the latter case, it may partly or totally originate through the type (5) "exsolution" process. Ilmenite grains are usually smaller than magnetite (typically up to 0.1 mm across), but may enclose magnetite grains. Ilmenite is rarely unmixed and in these cases contains small hematite exsolution droplets. Ilmenite is more oxidized to hematite plus rutile in sample 82QC8 than in sample 82QC10.

b) Chemistry (Tables II.4, II.5, and A.6)

The two studied samples of the Bear Canyon pluton contain magnetite and ilmenite of different compositions. In both samples the $MnTiO_3$ component in ilmenite is relatively low for the Questa granitic system.

Magnetite in sample 82QC8 contains more ulvospinel (avg, 3.16 mol% as opposed to 0.80 mol% in 82QC10) and Mn_2TiO_4, while sample 82QC10 contains more $FeAl_2O_4$.

Ilmenite contains more Fe_2O_3 and $MnTiO_3$ in sample 82QC8 (avg, $Hem_{8.3}Ilm_{66.1}Pyr_{25.6}$) than in sample 82QC10 (avg, $Hem_{4.7}Ilm_{74.0}Pyr_{21.3}$). Fe^{2+} plotted against Mn gives a correlation coefficient of -1.00 (fig. II.16). Because of high Nb content ($\geq$ 0.70 wt% Nb_2O_5), Fe^{3+} + Nb was plotted against Ti (fig. II.17; r, -1.00).

Discussion—Relating magnetite and ilmenite data in the fO_2-T-X space projected into the fO_2-T plane (Spencer and Lindsley, 1981, fig. 4; see fig. II.24), shows that oxide compositions in 82QC10 reflect equilibration at lower temperature and fO_2 than those in 82QC8.

7. SULPHUR GULCH

a) Description

Opaque oxide minerals constitute 0.6 to 1.6 volume percent of the carapace unit. Magnetite is the characteristic phase and occurs in the groundmass (down to 0.02 mm across) and as larger crystals (up to 0.7 mm). It may enclose pyrite. Magnetite can be intergrown with either ilmenite (oxidized to hematite plus rutile) or rutile; both types of intergrowth resemble types (4) and (5) "exsolution" intergrowths. Magnetite shows almost no oxidation to hematite.

Ilmenite is not everywhere present. Where it occurs as a primary phase, it is always oxidized to hematite plus rutile and its relations with magnetite show that it crystallized later than magnetite.

Rutile is common and may have formed after ilmenite. Aggregates of rutile grains may also have a lozenge shape, suggestive of sphene replacement, but in such samples there is still fresh euhedral sphene as well. Rare isolated pyrite occurs as grains to 0.2 mm across.

The opaque mineral assemblages are quite different in the source aplite unit. They form 0.3 to 1.5 volume percent of the rock and are characterized by the predominance of euhedral pyrite, as crystals from 0.05 to 0.2 mm across. Rutile is also characteristic, but less abundant than pyrite, and occurs as grains from 0.01 to 0.07 mm across. It is commonly found enclosed in alkali feldspar or biotite.

Only pyrite and rutile are seen in the aplitic facies (1685). The coarser granite facies (82QC55) contains pyrite and rutile as the main phases, minor chalcopyrite (sometimes enclosed in pyrite), and rare small primary hematite and ilmenorutile grains enclosed in silicates. The seriate granite (3438) contains rare lozenge-shaped aggregates of rutile and small (0.05 mm across) anhedral (late) magnetite grains. No ilmenite was found in the source aplite samples.

b) Chemistry

(1) Magnetite (Tables II.4 and A.7.1)

In the carapace unit of the Sulphur Gulch pluton, the sum (Al_2O_3 + TiO_2 + MnO + ZnO) ranges from 0.79 to 3.52 weight percent. These components recalculate in terms of Fe_2TiO_4, Mn_2TiO_4, and $ZnAl_2O_4$. In the source aplite, magnetite contains 0.75 wt% (Al_2O_3 + TiO_2 + MnO + ZnO), which recalculates to the same end-members as in the carapace unit, plus $MnAl_2O_4$.

Discussion—Magnetite compositions probably reflect higher fO_2 and/or lower temperature of reequilibration in the source aplite as compared to the carapace unit.

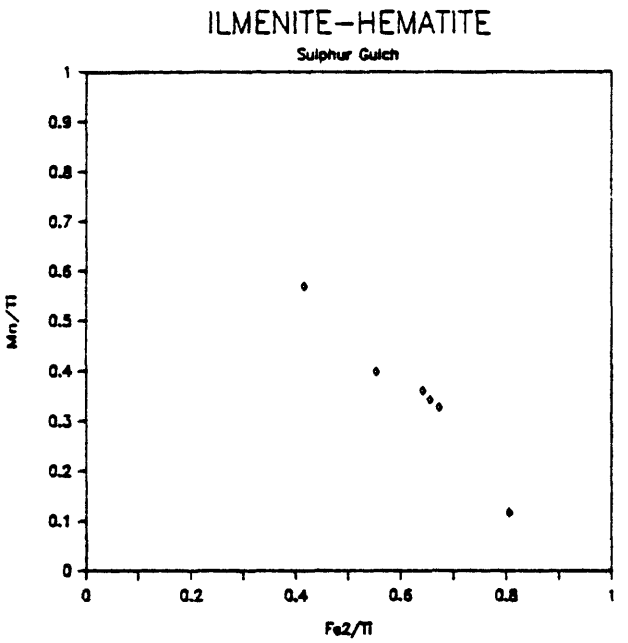

Fig. II.18. Fe2/Ti against Mn/Ti in ilmenite and hematite, carapace unit of Sulphur Gulch; black lozenges, hematite.

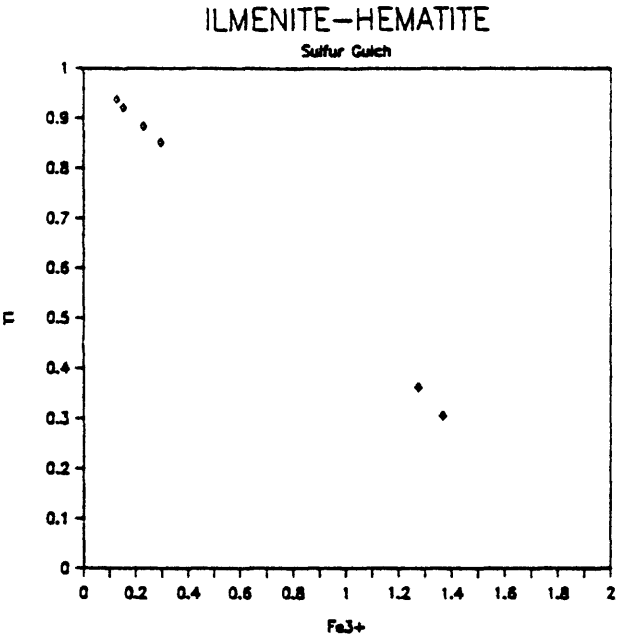

Fig. II.19. Fe3 against Ti (cations) in ilmenite and hematite, carapace unit of Sulphur Gulch; black lozenges, hematite.

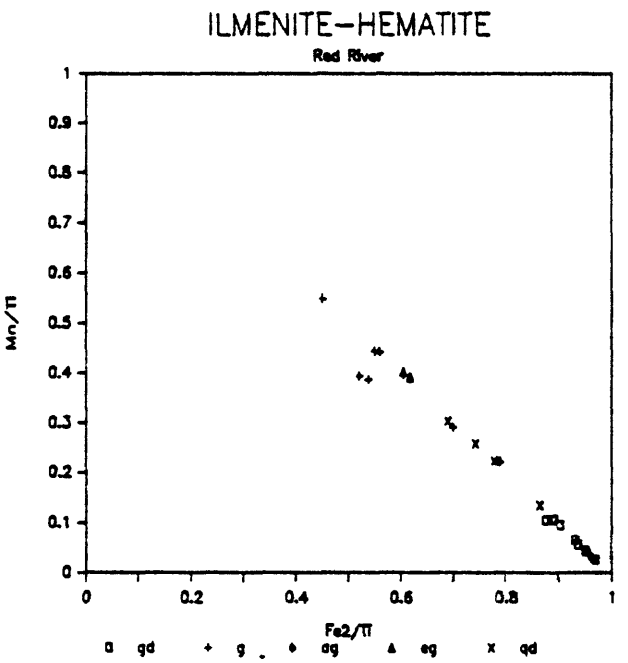

Fig II.20. Fe2/Ti against Mn/Ti in ilmenite and hematite, Red River; gd, granodiorite; g, granite; ag, alkali-feldspar granite; eg, enclave in granite; qd, quartz diorite; black lozenge and squares, hematite.

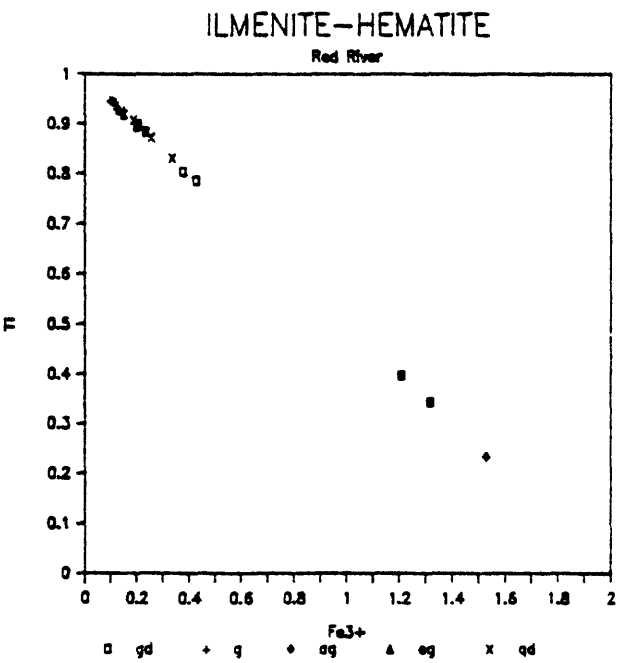

Fig. II.21. Fe3 against Ti (cations) in ilmenite and hematite, Red River; gd, granodiorite; g, granite; ag, alkali-feldspar granite; eg, enclave in granite; qd, quartz diorite; black lozenge and squares, hematite.

(2) Ilmenite, hematite and ilmenorutile (Tables II.5 and A.7.2)

Secondary ilmenite "exsolved" from magnetite contains less Fe_2O_3 and FeO, and more MnO than any primary ilmenite. Fe^{2+}/Ti was plotted against Mn/Ti for ilmenite and hematite (fig. II.18; r, -0.98) instead of Fe^{2+} against Mn (r, -0.92 for ilmenite). Fe^{3+} shows excellent correlation with Ti (fig. II.19; r, -1.00)

The only hematite grain analyzed in the coarse granite of the source aplite unit is nearly pure (0.8 mol% $(Fe,Mn)TiO_3$). Low totals obtained for ilmenorutile may be due to the presence of Ta, which was not determined.

Discussion—Absence of ilmenite and abundance of rutile shows that reequilibration occurred under conditions of higher fO_2 in the source aplite than in the carapace unit. Purity of hematite in the source aplite reflects high fO_2 during its crystallization. Active circulation of hydrothermal fluids during the mineralization process would create conditions of high oxygen fugacity and typically causes ilmenite and sphene to be replaced by rutile. In the carapace unit, lower Fe^{3+} in secondary ilmenite indicates that fO_2 was probably lower during its "exsolution" from magnetite, than during primary crystallization of ilmenite; higher Mn indicates Mn enrichment with differentiation.

8. RED RIVER

a) Description

Both magnetite and ilmenite are primary phases in the granodiorite (82QC44). They constitute 3.1 volume percent of the rock and magnetite is much more abundant than ilmenite (approx 90/10). Magnetite (up to 0.2 mm) is usually euhedral and may contain small chalcopyrite (to 0.02 mm) and pyrrhotite (to 0.008 mm) inclusions. It rarely displays thick ilmenite "exsolution" lamellae, which are always oxidized to hematite plus rutile; slightly more common are thin, irregular sphene coronas. Rarely, magnetite is slightly oxidized to hematite.

Ilmenite may occur as isolated grains and may then be unmixed (containing one set of hematite lamellae) and oxidized to hematite plus rutile. A more common occurrence of ilmenite is enclosed in sphene, in which case it is always unmixed, oxidized, and displays irregular rounded shapes.

Opaque oxide minerals average 1.2 volume percent in the granite of the Red River intrusive complex (82QC43, 85QC36). Magnetite is the most typical phase and is usually euhedral; it may contain pyrite inclusions and is sometimes associated with type (5) ilmenite "exsolution" granules. As in the granodiorite, it is almost never oxidized to hematite.

Ilmenite is more abundant than in the granodiorite and has several modes of occurrence, none of which display hematite exsolution lamellae. It can be found as primary crystals, either isolated or enclosed in biotite, and may be oxidized to hematite plus rutile. Ilmenite also occurs as aggregates of

grains displaying a lozenge shape, presumably after sphene, because it is often possible to find aggregates with relicts of sphene among the irregular ilmenite grains. It is possible to find aggregates containing both ilmenite and rutile grains.

The most distinguishing characteristic of the opaque mineral assemblage in the granite is the presence of pyrite, which is especially abundant near small enclaves rich in biotite and plagioclase.

Opaque oxide minerals constitute 1.7 volume percent of the alkali-feldspar granite (82QC32); they can be euhedral to anhedral. Magnetite occurs as a primary phase and, instead of ilmenite, rutile and hematite are present.

Magnetite can be up to 0.4 mm across, and is only rarely oxidized to hematite. Granules of rutile, which resemble type (5) ilmenite "exsolution" products, are often found intergrown with the margins of magnetite grains. Rutile also occurs as isolated grains. Hematite occurs as small grains enclosed in feldspars.

In the quartz diorite (82QC31, 85QC37b), which appears to be a local variant of the Red River intrusive complex, opaque oxides are quite abundant (3.0 to 3.6 vol%) and comprise a rather homogeneous population of small (0.05 mm) grains of primary magnetite and ilmenite (approx 70/30). Magnetite commonly contains pyrite inclusions, but no ilmenite "exsolution" or oxidation to hematite has been found. Ilmenite is often oxidized to hematite plus rutile.

b) Chemistry

(1) Magnetite (Tables II.4 and A.8.1)

Magnetite has quite distinct compositions in the different units of the Red River intrusive complex. In the granodiorite the sum (Al_2O_3 + TiO_2 + MnO + ZnO) ranges from 0.29 to 0.34 weight percent; these components recalculate in terms of $ZnAl_2O_4$, Mn_2TiO_4, Fe_2TiO_4, and Zn_2TiO_4.

Magnetite in the granite is characterized by significantly higher concentrations of minor elements, such that the sum (Al_2O_3 + TiO_2 + MnO + ZnO) averages 3.4 weight percent; recalculation gives a high content of ulvospinel (3.8 mol%), as well as Mn_2TiO_4, $MnAl_2O_4$, and $ZnAl_2O_4$. Magnetite in the enclaves recalculates to the same components, in about the same proportions as in the granite, but in lesser amount.

In the alkali-feldspar granite magnetite contains 0.39 to 1.30 percent of the minor element oxides, which recalculate in terms of Mn_2TiO_4, $ZnAl_2O_4$, Fe_2TiO_4, and $MnAl_2O_4$.

Magnetite in the quartz diorite contains 0.78 to 2.63 weight percent (Al_2O_3 + TiO_2 + MnO + ZnO), which recalculate in terms of Fe_2TiO_4, $FeAl_2O_4$, $MnAl_2O_4$, and $ZnAl_2O_4$.

Discussion—These data indicate that magnetite in the granite probably stopped reequilibrating at the highest temperature, while magnetite in the granodiorite probably stopped reequilibrating at the lowest temperature.

(2) Ilmenite and hematite (Tables II.5 and A.8.2)

Ilmenite compositions are quite different from one unit to another. Ilmenite in the granodiorite contains the least Mn (<10 mol% $MnTiO_3$) and Nb, and the most Fe^{3+} and Fe^{2+}, compared to that in the granite and the quartz diorite. Ilmenite is always unmixed and integrated analyses of ilmenite-hematite intergrowths show that primary ilmenite contained substantial Fe_2O_3 (18.9 to 21.3 mol% Fe_2O_3).

Ilmenite in the granite is quite variable in $MnTiO_3$ content (20.6 to 51.8 mol%) and relatively constant in Fe_2O_3 content (4.8 to 7.5 mol%). Compositions of primary ilmenite and ilmenite "exsolved" from magnetite are overlapping, showing that ilmenite was probably still crystallizing at the time magnetite was "unmixing" its ulvospinel component as ilmenite. The main characteristic of ilmenite "exsolved" from magnetite in the granite, is its lower Nb content compared to that of primary ilmenite. Ilmenite in the enclaves is quite similar in composition to that in the host granite.

Hematite in the alkali-feldspar granite is characterized by lower Ti content than hematite unmixed from ilmenite in the granodiorite.

In the quartz diorite, ilmenite "exsolved" from magnetite has a composition distinct from that of primary ilmenite; it contains less Fe^{3+} and more Mn.

There is a good correlation between Fe^{2+}/Ti and Mn/Ti (r, -0.99; fig. II.20) in ilmenite and hematite from all units of the pluton. A good correlation (r, -0.99) is also observed between Fe^{3+} and Ti (fig. II.21).

Discussion—Higher Fe_2O_3 content in ilmenite of the granodiorite indicates higher fO_2 during primary crystallization of ilmenite in that unit.

Compared to the other rock types, ilmenite in the granite reflects quite low fO_2 during its primary crystallization. The limited range in Fe_2O_3 content shows that conditions probably remained relatively constant during crystallization and reequilibration of the opaque oxides in the granitic unit.

In the alkali-feldspar granite, lack of ilmenite and presence of hematite with low Ti content attests for the highest fO_2 during crystallization among the different units of the Red River intrusive complex.

Lower Fe^{3+} in secondary ilmenite in the quartz diorite shows that fO_2 was decreasing during crystallization.

9. LUCERO PEAK

a) Description

The Lucero Peak granite contains 0.3 to 0.9 volume percent of opaque minerals. Primary phases are magnetite, ilmenite, and rare pyrite enclosed in magnetite. Magnetite is more abundant than ilmenite and constitutes about 60 volume percent of the opaque oxides. It is mostly euhedral and forms small crystals (less than 0.15 mm) which can be enclosed in biotite and feldspar, as well as larger grains (up to 0.5 mm across) which may enclose pyrite, apatite, zircon, and sphene. Ilmenite "exsolution" products are common as type (3) lamellae and type (5) granules. Minor oxidation to hematite is always present.

Ilmenite forms larger as well as smaller grains than magnetite. Early ilmenite can be as small as 0.01 mm when enclosed in biotite and feldspar, and up to 0.1 mm across in biotite. Ilmenite inclusions in biotite may be either along cleavages or independant of cleavages. Later ilmenite can be up to 1.1 mm long and encloses apatite, zircon, allanite, and magnetite. It is most often associated with magnetite and is the more anhedral phase. This type of ilmenite contains very fine hematite exsolution droplets (less than 0.001 mm across) which are difficult to see even at 400X magnification. Ilmenite often shows partial oxidation to hematite plus rutile.

b) Chemistry

Because of similarity with opaque oxide chemistry in the Bear Canyon pluton, data for opaque oxide minerals in the Lucero Peak pluton are plotted on the same diagram as data for the Bear Canyon pluton.

(1) Magnetite (Tables II.4 and A.9)

Magnetite compositions are similar from one grain to another; the sum (Al_2O_3 + TiO_2 + MnO + ZnO) ranges from 0.35 to 0.72 weight percent and recalculated Fe_3O_4 averages 99.1 mole percent. Trace elements in magnetite recalculate in terms of Fe_2TiO_4, Mn_2TiO_4, $ZnAl_2O_4$, and Zn_2TiO_4.

Discussion—Magnetite in the Lucero Peak pluton has reequilibrated at relatively low temperature and/or high fO_2 and is now quite pure (see fig. II.24). The volume of ilmenite "exolution" products in magnetite is small and the bulk of the minor components apparently migrated from the grains.

(2) Ilmenite (Tables II.5 and A.9)

Ilmenite compositions in the Lucero peak pluton show several notable features. (1) Except for one example of secondary ilmenite "exsolved" from magnetite, ilmenite is rich in Nb (1.2 to 1.9 wt% Nb_2O_5). (2) Homogeneous primary ilmenite in sample 82QC25 contains only 0.7 to 2.9 mole percent Fe_2O_3, whereas ilmenite in sample 82QC15, in which fine hematite exsolution droplets could not be avoided during microprobe analyses, contains 9 mole percent Fe_2O_3. (3) Secondary ilmenite contains more Mn than primary ilmenite (53 mol% as opposed to 33 mol% $MnTiO_3$) and less Fe. Fe^{2+} was plotted against Mn (fig. II.16; r, -0.92). The correlation between Fe^{3+} and Ti (r, -0.98) is improved by adding Nb to Fe^{3+} (fig. II.17; r, -1.00).

Discussion—As in other plutons, ilmenite composition shows Mn enrichment with differentiation. Ilmenite in sample 82QC25 crystallized at lower fO_2 than that in sample 82QC15.

PART III: SUMMARY AND CONCLUSIONS

1. PARAGENESES

Magnetite and ilmenite are the most common opaque minerals in the Questa granitic rocks; except in magnetite-free samples from the Canada Pinabete pluton and in the peralkaline granites of Virgin Canyon and Canada Pinabete, magnetite is predominant over ilmenite. Magnetite is always primary; ilmenite is a characteristic primary mineral but also commonly occurs as a secondary mineral after magnetite (oxidation "exsolution"), hematite (exsolution), or sphene (reaction). Hematite is often present, but is much less common than magnetite and ilmenite. Hematite is most commonly secondary, after magnetite (oxidation) or ilmenite (exsolution or oxidation), but can be primary, both as an early and late-stage mineral.

In the granodiorite and mafic-magmatic enclaves of the Rio Hondo pluton and in the granodiorite of Red River, magnetite is surrounded by a thin rim of sphene; in all other plutons magnetite contains ilmenite oxidation "exsolution" products. Both textures are a result of expulsion of Ti from the magnetite structure; sphene coronas around magnetite apparently formed because oxygen fugacity was too high for ilmenite to form. Magnetite is often oxidized to hematite (martite), oxidation being most pronounced in magnetite from the Virgin Canyon and Canada Pinabete plutons.

Magnetite in the Questa granitic rocks is rather pure, except in the peralkaline granites of Virgin Canyon and Canada Pinabete, where the sum ($Al_2O_3 + TiO_2 + MnO + ZnO$) ranges from 5.5 to 11.2 weight percent, and the granite of Red River, where the sum ($Al_2O_3 + TiO_2 + MnO + ZnO$) averages 4.4 weight percent. The main constituent still dissolved in magnetite is usually Fe_2TiO_4, but in the Rito del Medio pluton and in the granite of Rio Hondo analyses recalculate in terms of $MnFe_2O_4$. In the granite of Rito del Medio, this may be the result of high $Mn/(Mn+Fe^{2+})$ or high fO_2. In the granite of Rio Hondo, fO_2 was probably quite low and the presence of $MnFe_2O_4$ component is probably due to high $Mn/(Mn+Fe^{2+})$ in the residual magma.

The ratio ilmenite/magnetite is greatest in the peralkaline granites of Virgin Canyon and Canada Pinabete and lowest in the granodiorite and mafic-magmatic enclaves of Rio Hondo and the granodiorite of Red River. Unmixing is rare and limited in ilmenite from the Virgin Canyon, Canada Pinabete, and Bear Canyon plutons, while it is rather common and well developed in the Rito del Medio, Cabresto Lake, and Rio Hondo plutons. Ilmenite is commonly oxidized to hematite plus rutile.

Ilmenite in the Questa granitic rocks is characterized by high Mn content. The highest Mn contents are found in ilmenite in the granite of Rito del Medio and the lowest are characteristic of ilmenite in the granodiorite and mafic-magmatic enclaves of Rio Hondo and the granodiorite of Red River. In a given sample, ilmenite "exsolved" from magnetite typically contains more Mn than primary ilmenite. High Fe_2O_3 contents are characteristic of ilmenite in the Cabresto Lake, Rio Hondo, and Sulphur Gulch plutons and in the Red River intrusive complex. Ilmenite in the peralkaline granites of Virgin Canyon and Canada Pinabete is characterized by the highest Zn contents. Nb is most abundant in ilmenite from the northern intracaldera plutons and in the granites of Bear Canyon and Lucero Peak.

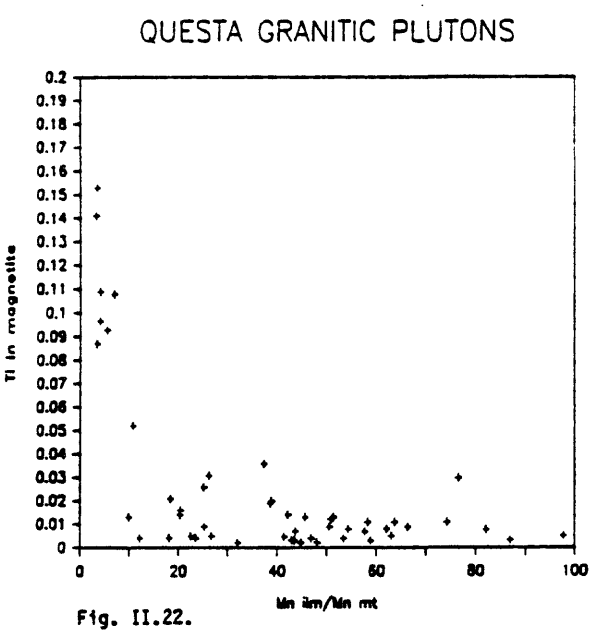

Fig. II.22.

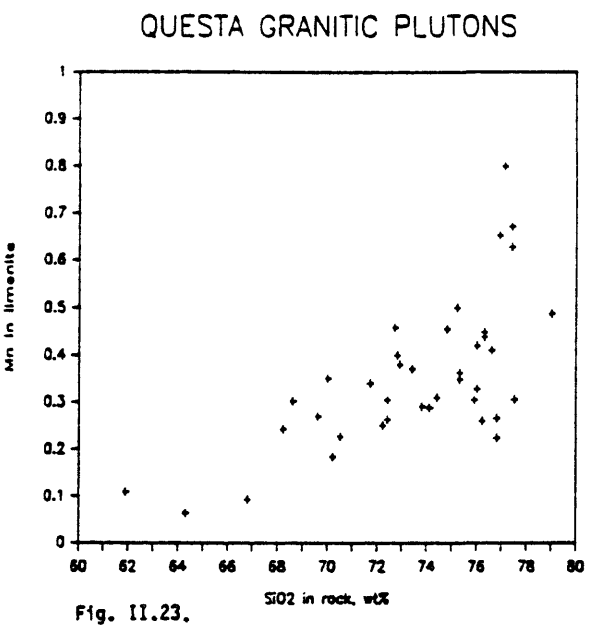

Fig. II.23.

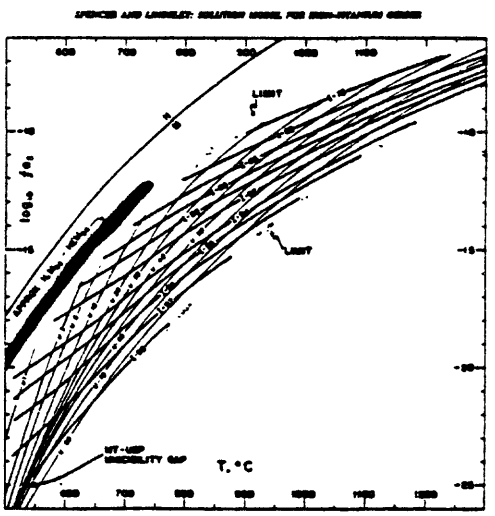

Fig. II.24.

Fig. II.22. Mn in ilmenite over Mn in magnetite against Ti (cations) in magnetite, Questa granitic plutons.

Fig. II.23. Mn (cations) in ilmenite against host-rock SiO_2 (wt%), Questa granitic plutons.

Fig. II.24. T (°C)-$\log_{10} f_{O_2}$ grid for coexisting magnetite-ilmenite pairs, from Spencer and Lindsley (1981). The light stippled fields are estimates of the limits of the model.

In the granite of Rito del Medio and in the alkali-feldspar granite of Red River, hematite is found as small primary grains enclosed in silicates, indicating relatively high oxygen fugacity during early stages of crystallization. In the Canada Pinabete and Rito del Medio plutons, hematite occurs as large crystals in vugs, attesting to high oxygen fugacity during the late stages of crystallization. These large crystals usually contain ilmenite exsolution products, but, in the metaluminous granite of Canada Pinabete, ilmenorutile instead of ilmenite is common, indicating high Nb concentrations during the final stages of crystallization.

Hematite in the Rito del Medio pluton contains the most Mn. Low Mn content characterizes secondary hematite after magnetite (martite), which is also notable for its low Ti content.

A plot of $Mn_{ilmenite}/Mn_{magnetite}$ against Ti in magnetite for the Questa granitic plutons shows two distinct relations (fig. II.22). In the peralkaline granites of Virgin Canyon and Canada Pinabete, $Mn_{ilmenite}/Mn_{magnetite}$ is less than 10 and Ti in magnetite is more than 0.08 cation. In all other Questa granitic rocks $Mn_{ilmenite}/Mn_{magnetite}$ is more than 10 and Ti in magnetite is less than 0.05 cation. The contrast in $Mn_{ilmenite}/Mn_{magnetite}$ is believed to be due to contrast in fO_2, while Ti in magnetite may have been controlled by cooling history as well as fO_2. A plot of Mn in ilmenite against host-rock SiO_2 shows a distinct increase in Mn with differentiation (fig. II.23), as described by Neumann (1974).

2. TEMPERATURE AND OXYGEN FUGACITY

Despite the limited success typically associated with calculations based on Fe, Ti-oxide pairs in plutonic rocks, temperatures and oxygen fugacities have been determined for magnetite-ilmenite pairs (Table II.6; fig. II.25), applying the solution model of Spencer and Lindsley (1981; fig. II.24). The influence of high Mn content in ilmenite (or in magnetite, as in the Rito del Medio pluton) on the model is not well known. The treatment used in the following discussion considers the Mn-bearing component of ilmenite and magnetite to be inert, and the reasonable values calculated suggest that this assumption is not unrealistic. Many oxide pairs in the Questa granitic rocks fall outside the limits of the model, so that temperatures and oxygen fugacities given by the program are even less certain. Discussion of temperature and oxygen fugacity for the Questa granitic rocks, based on oxide mineral pairs, may therefore be of more relative, than absolute, significance, and may relate in part to cooling history.

As discussed earlier, oxide pairs in the peralkaline granites of Virgin Canyon and Canada Pinabete indicate lower fO_2 and higher temperatures than oxide pairs in the metaluminous granites of those plutons (Table II.6; figs. II.25, b and c). Among the three northern intracaldera plutons, the peralkaline granite of Canada Pinabete is characterized by the lowest fO_2 and the Rito del Medio granite contains oxide pairs indicating the lowest temperatures (fig. II.25, c).

Notable is the fact that for individual samples of the peralkaline granite of Virgin Canyon, higher equilibration temperatures are often obtained from calculations based on the composition of ilmenite "exsolved" from

Table II.6. Calculated temperatures and oxygen fugacities for ilmenite-magnetite equilibration.

PLUTON/ Unit	Sample number	*	T, °C	fO_2, $\log_{10}$	Sample number	*	T, °C	fO_2, $\log_{10}$
VIRGIN CANYON								
Peralkaline granite	82QC38	p	576	-21.5	Q83J62	p	582	-21
		m	640	-18	Q83J67	p	604	-20
	83QC29	p	626	-18.5		m	651	-17.5
		m	610	-19.5	Q83J63	p	647	-17.5
Early metaluminous granite	82QC33	m	545	-18.5	82QC41	p	570	-16
	82QC39	p	623	-17	83QC25	p	576	-17.5
Later metaluminous granite	82QC35	p	591	-17	Q83J78	p	605	-16
		m	585	-17.5	Q83J79	p	604	-17
	83QC33	p	560	-18		m	547	-21
		m	573	-17				
CANADA PINABETE								
Peralkaline granite	Q83J94	p	501	-27	84QC7	p	597	-21
						m	550	-24
Metaluminous granite	82QC46	p	465	-25	Q83J81	p	592	-18
		m	473	-24	Q83J82	p	551	-19.5
	82QC47	p	545	-19		m	551	-19.5
RITO del MEDIO								
	82QC16	p	526	-18.5	82QC18	i	534	-19
		m	604	-18		m	536	-18.5
	82QC17	i	501	-21	82QC19	m	596	-16.5
		m	495	-21.5				
CABRESTO LAKE								
Granite	78L172	m	588	-17	83QC10	m	500	-21.5
	82QC51b	p	543	-18	83QC18	m	522	-21
		m	522	-19.5	83QC20	m	527	-20
Mixed	83QC14	p	558	-18.5	85QC12	p	601	-16.5
		m	525	-21		m	572	-18.3
	85QC11	m	519	-22.5				
Biotite-bearing enclave	83QC14	p	570	-17	83QC17	m	573	-18
Amphibole-bearing enclave	83QC12	m	521	-21.5	85QC9	m	595	-18
RIO HONDO								
Granodiorite	84QC31	i	527	-19	84QC32	i	559	-16.5
Granite	82QC5	m	482	-22.5	84QC11	p	475	-22.5
	Q83SL25	ps	472	-23	84QC14	p	360	-34.5
	Q83SL27	ps	435	-25.5		m	426	-26.5
Mafic magmatic enclave	Loc.12.1	i	523	-19				

Table II.6. Calculated temperatures and oxygen fugacities for ilmenite–magnetite equilibration.–Continued

PLUTON/ unit	Sample number	*	T, °C	fO_2, $\log_{10}$	Sample number	*	T, °C	fO_2, $\log_{10}$
BEAR CANYON								
	82QC8	p	626	-17	82QC10	m	521	-21
		m	639	-16				
SULPHUR GULCH								
Carapace	3417	m	628	-17	3440	p	579	-17.5
	3439	i	662	-14.5		i	623	-15
RED RIVER INTRUSIVE COMPLEX								
Granodiorite	82QC44	i	516	-18				
Granite	85QC36	p	630	-17.5	85QC36e#	p	616	-17
		m	636	-17				
Quartz diorite	85QC37	p	640	-15				
		m	616	-16.5				
LUCERO PEAK								
	82QC15	ph	566	-17	82QC25	p	446	-25.5
						m	419	-28

* Mode of occurrence: i, ilmenite phase of unmixed ilmenite; m, ilmenite exsolved from magnetite; p, primary homogenous ilmenite; ph, unmixed primary ilmenite, intermediate composition; ps, ilmenite enclosed in sphene, intermediate composition.
# Enclave in the granite of Red River.

magnetite, as compared to those based on the composition of primary ilmenite (Table II.6). This is related to the higher Fe_2O_3 content of secondary ilmenite; in an oxidizing environment, evolution of the system with decreasing temperature will drive the composition of ilmenite towards higher Fe_2O_3 contents. Clearly, one has to be careful about interpretation of such data. The compositions determined for magnetite are also quite different from their initial compositions, which were richer in ulvospinel; ideally, primary ilmenite should be paired with magnetite containing a greater ulvospinel component.

Based on studies of the system $KAlSi_3O_8$-$NaAlSi_3O_8$-$NaFeSi_2O_6$-SiO_2-H_2O, the liquidus for the peralkaline granite has been estimated at about 744°C (Czamanske and Dillet, in press). At that temperature, ilmenite with low Fe_2O_3 content, such as the primary ilmenite in the peralkaline granite of Virgin Canyon (X_{ilm} = 93.5–96.5), should coexist with magnetite in which ulvospinel content ranges from 40 to 60 mole percent. Thus, in the case of the peralkaline granite of Virgin Canyon, the crystallization path crossed the ilmenite and magnetite composition curves toward higher fO_2 (see fig. II.24). In most other units, ilmenite "exsolved" from magnetite contains less Fe_2O_3, than primary ilmenite.

QUESTA GRANITIC PLUTONS

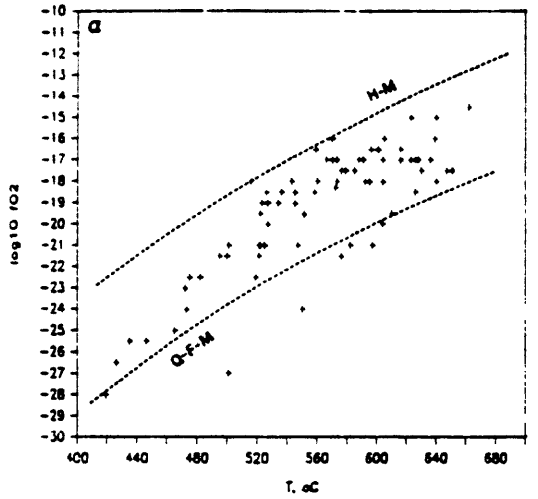

Virgin Canyon

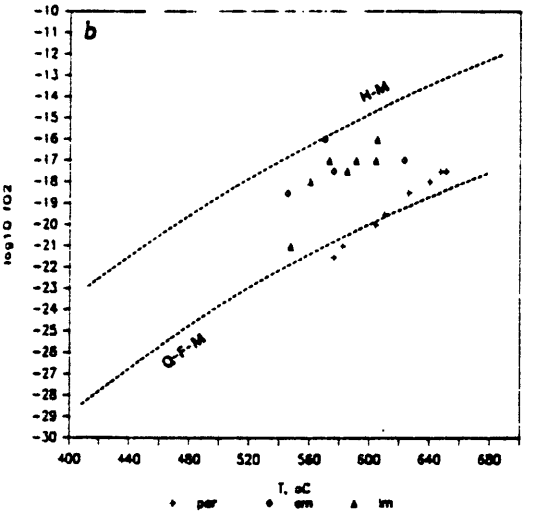

Canada Pinabete–Rito del Medio

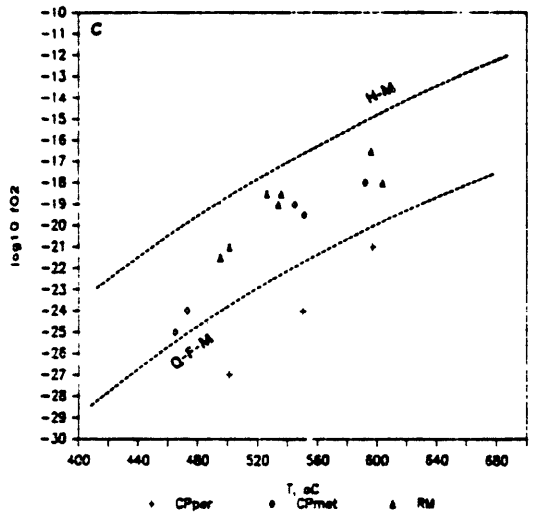

Cabresto Lake

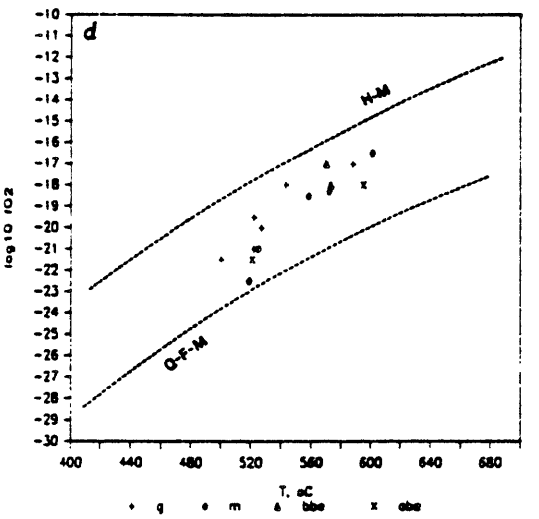

Rio Hondo

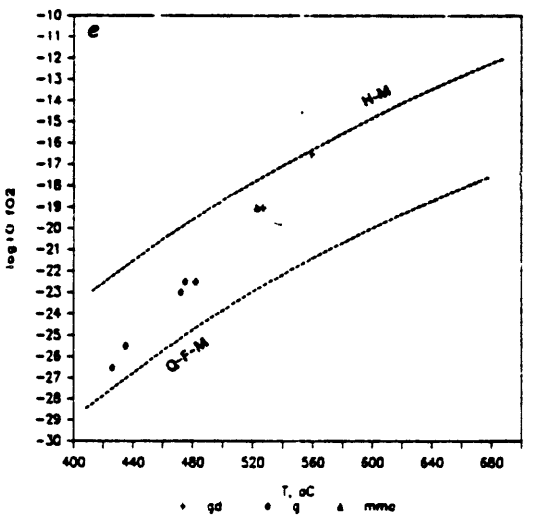

Late mineralized plutons

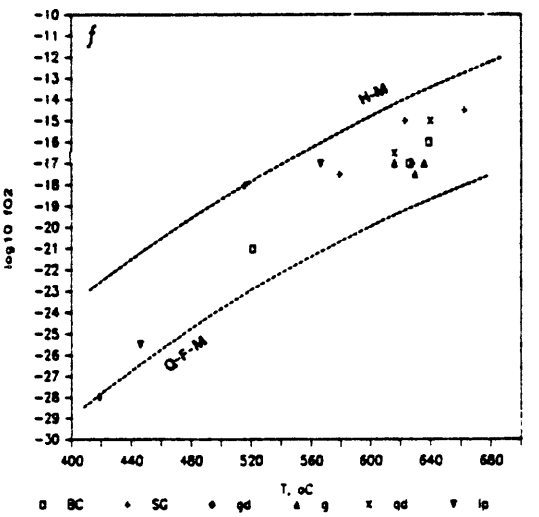

Oxide pairs in all rock types of the Cabresto Lake pluton cluster in the same area in the T-fO_2 diagram, with overlaping ranges of temperature and oxygen fugacity (fig. II.25, d). They fall in the same area as the metaluminous granites of the northern intracaldera plutons. Amphibole-bearing enclaves are characterized by the highest oxide-pair temperatures and the lowest temperatures are indicated for the granite.

Oxide-pair calculations result in a different pattern of temperature and oxygen fugacity for the Rio Hondo pluton (fig. II.25, e), as compared to the Cabresto Lake pluton. Calculations for oxide pairs in the granodiorite and mafic-magmatic enclaves cluster above the fO_2 limit of the model, indicating high fO_2 during equilibration. In constrast, calculations for oxide pairs in the granite plot below the temperature limit of the model and indicate that granite crystallization was characterized by relatively low temperature and oxygen fugacity.

Data for the late mineralized plutons are quite scattered (fig. II.25, f), especially in the case of the Lucero Peak pluton for which oxide pairs in the two studied samples (82QC15 and 82QC25) suggest significantly different conditions of equilibration. Calculations for both samples fall beyond the limits of the model; oxide pairs in 82QC15 indicate high fO_2, while those in 82QC25 indicate low temperature.

The two studied samples from the Bear Canyon pluton may be considered to represent an evolution from 82QC8 down to 82QC10, with T and fO_2 decreasing parallel to the buffer curves; oxide pairs in both samples fall within the limits of the model. The carapace unit of the Sulphur Gulch pluton is characterized by oxide pairs which equilibrated at high temperature and oxygen fugacity. It is probable that oxide compositions (and the dependent calculations) in this heavily mineralized pluton reflect the influence of late mineralizing solutions. In fact, the opaque oxide mineralogy of the source aplite, which contains only minor hematite and magnetite, records conditions of even higher oxygen fugacity.

Fig. II.25. T (^oC) against $\log_{10} fO_2$ for magnetite-ilmenite pairs in the plutons of the Questa granitic system calculated from the model of Spencer and Lindsley (1981). Hematite-magnetite (H-M) and quartz-fayalite-magnetite (Q-F-M) buffer curves after Haas (unpublished data, 1986).

(a) All Questa granitic plutons.

(b) Virgin Canyon pluton. Crosses, peralkaline granite; diamonds, early metaluminous granite; triangles, later metaluminous granite.

(c) Canada Pinabete and Rito del Medio plutons. Crosses, peralkaline granite of Canada Pinabete; diamonds, metaluminous granite of Canada Pinabete; triangles, granite of Rito del Medio.

(d) Cabresto Lake pluton. Crosses, granite; diamonds, mixed; triangles, biotite-bearing enclaves; x's, amphibole-bearing enclaves.

(e) Rio Hondo pluton. Crosses, granodiorite; diamonds, granite; triangles, mafic magmatic enclaves.

(f) Late mineralized plutons. Squares, granite of Bear Canyon; crosses, carapace unit of Sulphur Gulch; diamonds, granodiorite of Red River; triangles, granite of Red River; x's, quartz diorite of Red River; inverted triangles, granite of Lucero Peak.

The granodiorite of the Red River intrusive complex plots in the same area as the granodiorite of the Rio Hondo (high fO_2, rather low T). Oxide pairs in the granite of Red River record a higher temperature than the granodiorite and data for the enclave in the granite plot near other data for the host granite. The quartz diorite is characterized by high fO_2 and the alkali-feldspar granite, which contains primary hematite and does not contain ilmenite, crystallized at even higher fO_2.

3. ILMENITE-HEMATITE SOLVUS

Plotting Fe_2O_3 (mol%) against temperature for ilmenite and hematite in the Questa granitic rocks (figs. II.1 and II.26) shows a rather good fit with the solvus of Kretchsmar and McNutt (1971) and indicates that the solvii (fig. II.1) of Carmichael (1961) and Lindsley (1973) are not applicable to the Questa granitic rocks. Data which plot closest to pure ilmenite are for ilmenite in the peralkaline granites of Virgin Canyon and Canada Pinabete (figs. II.26, b and c). In those two cases, fO_2 was relatively low and only a small amount of Fe_2O_3 entered the ilmenite structure. Moreover, quenching at relatively high temperature gave little opportunity for Fe_2O_3 to unmix. Ilmenite from the metaluminous granites of Virgin Canyon and Canada Pinabete contains more Fe_2O_3, and therefore plots closer to the solvus (figs. II.26, b and c), indicating higher fO_2 for initial ilmenite crystallization. In some cases such ilmenite unmixed because of intersection of the crystallization path with the solvus. Ilmenite from the Rito del Medio pluton, although often unmixed, plots between ilmenite from the peralkaline and metaluminous granites of Virgin Canyon and Canada Pinabete (fig. II.26, c). This may be related to especially high Mn content which may widen the ilmenite limb of the solvus toward more ilmenite-rich compositions. Ilmenite in the different rock types of the Cabresto Lake pluton has similar Fe_2O_3 content and plots near the solvus (fig. II.26, d). Data for the Rio Hondo pluton reflect the large difference in Fe_2O_3 content between ilmenite in the granite and ilmenite in the granodiorite and mafic-magmatic enclaves (fig. II.26, e). Ilmenite from the Bear Canyon and Lucero Peak plutons plots near the solvus (fig. II.26, f). Data for ilmenite in the carapace unit of the Sulphur Gulch pluton and in the Red River intrusive complex are quite scattered; ilmenite plotting farthest from the solvus is unmixed (fig. II.26, f).

Plotting of Fe_2O_3 in hematite for the few analyses obtained (fig. II.1), shows that compositions fall near the hematite limb of the solvus of Kretchsmar and McNutt, with one exception. The analysis represents primary hematite with ilmenite exsolution bodies in a vug in the Rito del Medio granite; it is likely that the intergrowth formed at unusually low temperature, perhaps in association with a hydrothermal vapor phase.

In summary, ilmenite-hematite solid solutions in the Questa granitic rocks plot near the solvus of Kretchsmar and McNutt in a region of low Fe_2O_3 in ilmenite and temperatures between 440 and 660°C. It is not possible to assess the effect of Mn content in ilmenite on the shape of the solvus because of scatter in the data, but the general conformity of the Questa data to the solvus is a strong indication that the Mn-bearing component can be considered inert and that the solvus is correct.

Fig. II.26. Fe_2O_3 (mol%) in ilmenite against T (°C) as calculated by the model of Spencer and Lindsley (1981); dashes, limb of miscibility gap reported by Kretchsmar and McNutt (1971). Titles and legends of figures are the same as in fig. II.25.

QUESTA GRANITIC PLUTONS

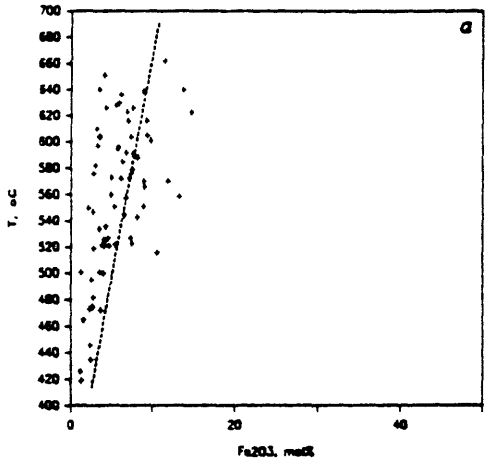

Virgin Canyon

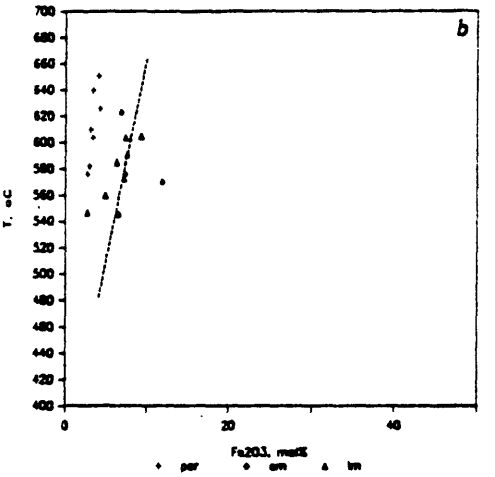

Canada Pinabete–Rito del Medio

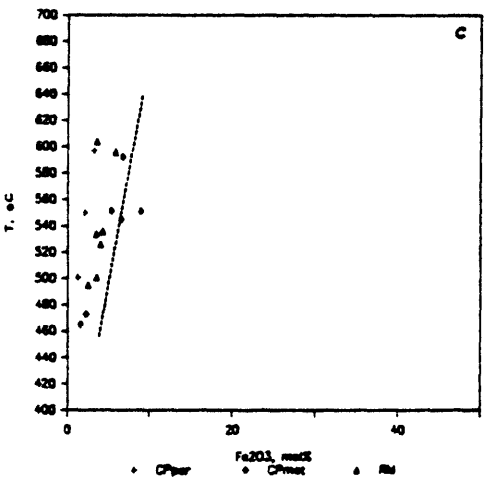

Cabresto Lake

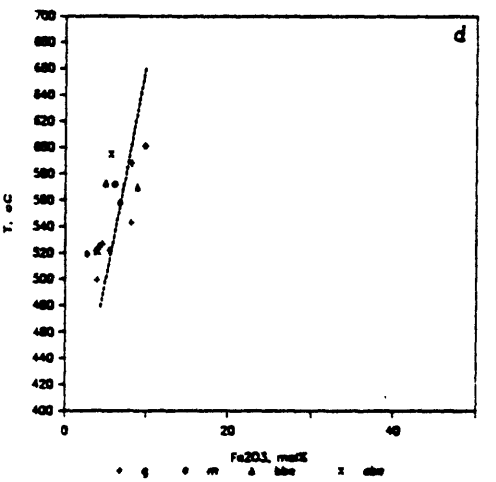

Rio Hondo

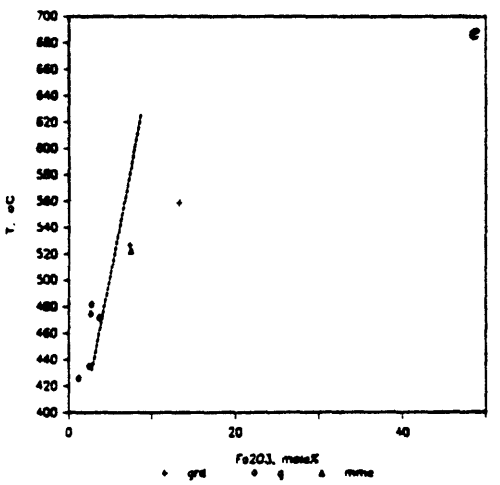

Late mineralized plutons

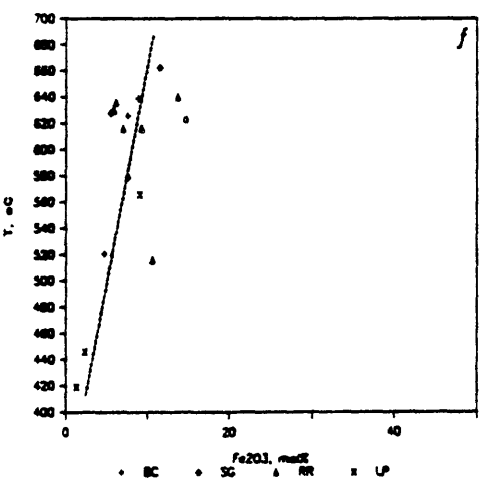

4. OCCURRENCE OF SPHENE

Sphene-magnetite-quartz assemblages indicate relatively high oxygen fugacities in siliceous magmas. It has been suggested that intrinsic oxygen fugacity is related to tectonic setting and that more highly oxidized magmas are associated with compressive tectonics and convergent plate boundaries. Among the Questa granitic rocks, the Rio Hondo pluton contains the most sphene; differentiation of the Rio Hondo magma, based on its calc-alkaline character and chemical similarities to pre-caldera intermediate volcanic rocks, was probably related to compressive tectonics. However, primary sphene is ubiquitous in the Questa granitic rocks, indicating that granitic magmas in a rifting environment can be characterized by high intrinsic oxygen fugacities. Czamanske and Wones (1973) concluded that late interstitial sphene in the granodiorite of the Finnmarka complex, Norway was produced by an oxidizing magmatic trend in that system, which is located within the Oslo graben. Based on the paragenesis of sphene, the Questa magmatic system, located adjacent to the Rio Grande Rift, was more oxidized than any other system known to us.

Sphene is abundant in the granitic rocks of the Questa area that contain less than 70 weight percent SiO_2, and occurs as a primary phase in nearly all of the granites and granite porphyries that contain 75 to 77 weight percent SiO_2.

The occurrences of sphene are of particular interest; it can be primary, secondary after or in place of ilmenite, or reacted to ilmenite or rutile. Notable are the relations of sphene in the peralkaline granite of Virgin Canyon. At the outer margin of the unit, early sphene has been replaced by ilmenite (Plate II.3, d), probably at an early-magmatic stage as indicated by ilmenite composition. Toward the interior of the unit, sphene continued to be stable and even formed irregular rims around ilmenite grains (Plate II.3, a and b). Sphene may show reaction to both ilmenite (Plate II.4, a) and rutile in the Rito del Medio pluton, indicating exposure to earlier reducing, and

---

PLATE II.7: Photomicrographs of occurrences of sphene.

(a) Sphene grain recording a period of contemporaneous ilmenite growth. Granodiorite of Red River, sample 85QC38. Bar is 1 mm long.

(b) Euhedral sphene in 70.2 weight percent SiO_2 granite porphyry. Carapace unit of Sulphur Gulch, sample 3439. Bar is 0.5 mm long.

(c) Sphene partly reacted to rutile in 72.4 weight percent SiO_2 granite porphyry. Carapace unit of Sulphur Gulch, sample 3440. Bar is 0.2 mm long.

(d) Rutile aggregate after sphene in 77.0 weight percent SiO_2 aplite. Source aplite unit of Sulphur Gulch, sample 1685. Bar is 0.2 mm long.

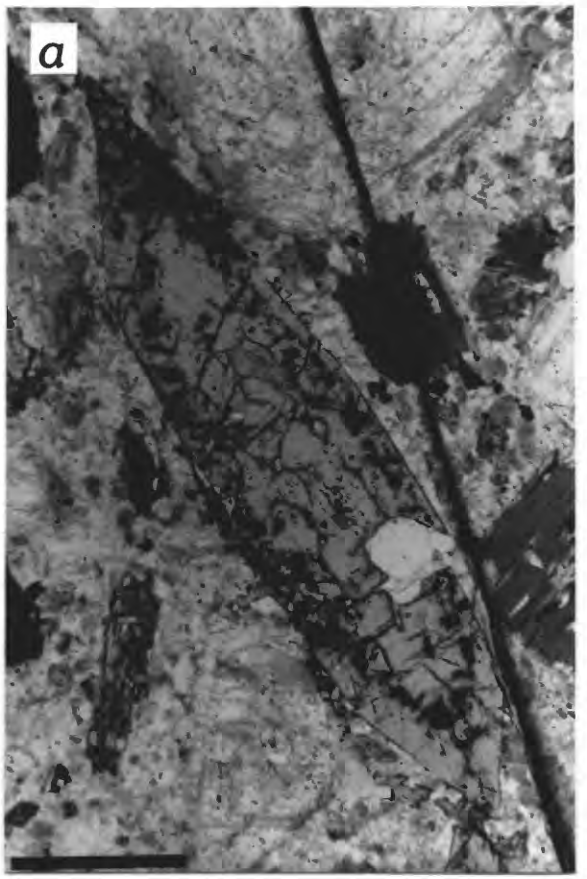
a


b

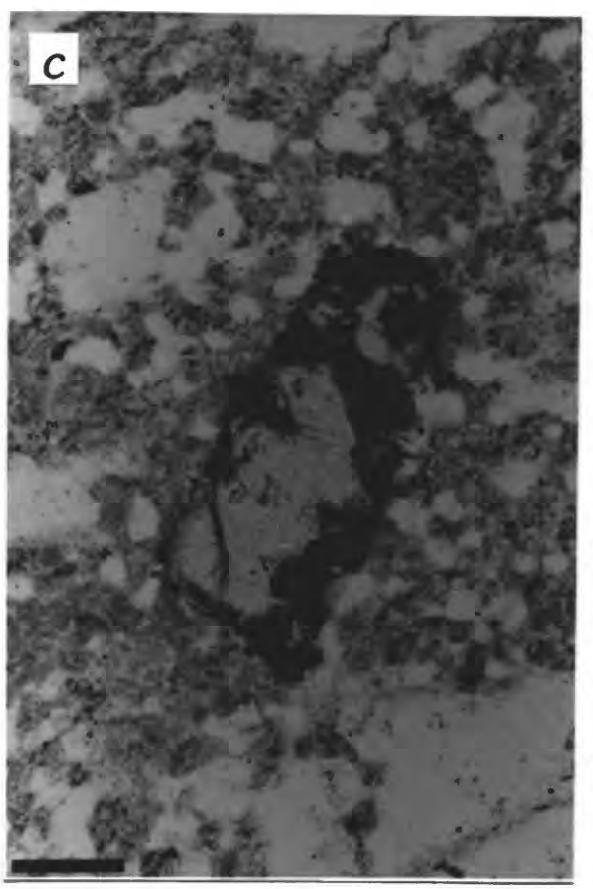
c

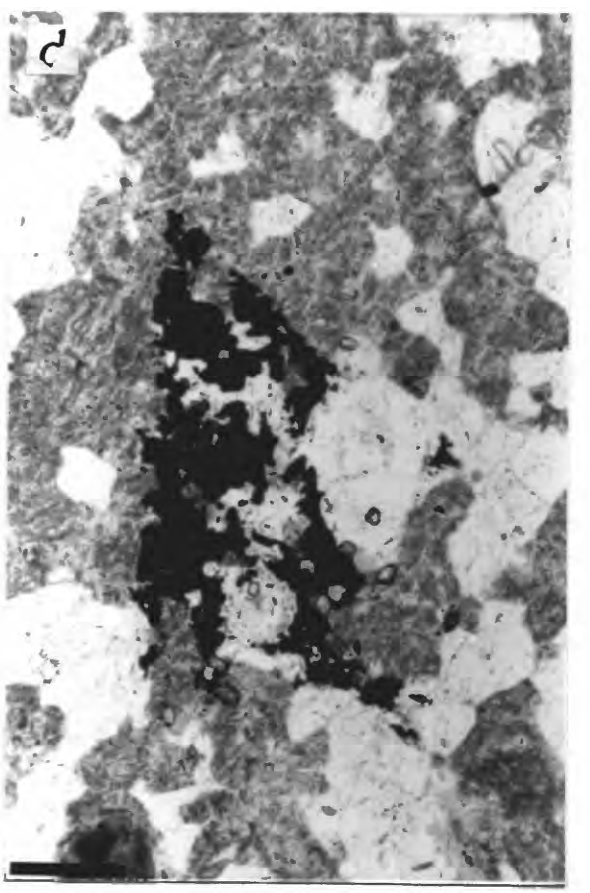
d

later oxidizing trends. In the carapace unit of the Sulphur Gulch pluton, sphene has undergone progressive reaction to rutile. Within the carapace unit, the reaction can be related to host-rock SiO_2 content and groundmass texture; euhedral sphene is characteristic of 70.2 weight percent SiO_2 porphyry (Plate II.7, b), sphene partly reacted to rutile is found in 72.4 weight percent SiO_2 porphyry (Plate II.7, c), and rutile aggregates after sphene occur in 77.0 weight percent SiO_2 aplite (Plate II.7, d). This relation may be in part due to greater circulation of oxidizing hydrothermal solutions in the more siliceous porphyries.

In the Cabresto Lake and Rio Hondo plutons and in the granodiorite from the Red River intrusive complex, euhedral sphene containing ilmenite is common, and in some cases represents the only occurrence of ilmenite. Such texture is thought to be the result of contemporaneous crystallization of sphene and ilmenite during part of the crytallization history (Plate II.7, a).

Sphene coronas around magnetite are found in the granodiorite and mafic-magmatic enclaves of the Rio Hondo pluton and in the granodiorite of the Red River intrusive complex (Plate II.4, d). These coronas apparently formed by precipitation of Ti which was exsolved from magnetite under conditions of relatively high oxygen fugacity.

Altough Fe,Ti-oxide mineral pairs often allow precise estimates of oxygen fugacity and temperature for volcanic rocks, retrograde recrystallization of primary Fe,Ti-oxide minerals often makes it difficult to estimate oxygen fugacities during the early crystallization history of plutonic rocks, as has been documented above. However, the relation between oxygen fugacity and temperature can be calculated for such reactions as:

$$CaFeSi_2O_6 + FeTiO_3 + O_2 = CaTiSiO_5 + Fe_3O_4 + SiO_2,$$

as indicated in figure II.27. The presence of Fe_2O_3 and substantial amounts of $MnTiO_3$ in the Questa ilmenites will cause the reaction curves involving ilmenite to fall at even higher oxygen fugacities than those indicated in figure II.27.

The many complex relations between ilmenite and sphene in the Questa granitic rocks indicates that oxygen fugacities in the crystallizing magmas fluctuated across a reaction curve involving these two minerals. One may assume that the data of Lipman (1971) provide a more realistic approximation to this reaction curve in a siliceous melt than the various simplified reaction curves of figure II.27. If so, oxygen fugacities in the Questa magmas are indicated to have been in the range of $fO_2 = 10^{-14}$ to 10^{-15} at 700°C and 10^{-17} to 10^{-18} at 600°C. It is notable that these estimates are in reasonable accord with the temperatures and oxygen fugacities indicated by the Fe,Ti,Mn-oxide pairs (fig. II.25). This is another indication that abundant Mn does not interfere dramatically with oxide-pair calculations and that such calculations for high-level plutonic rocks may be meaningful.

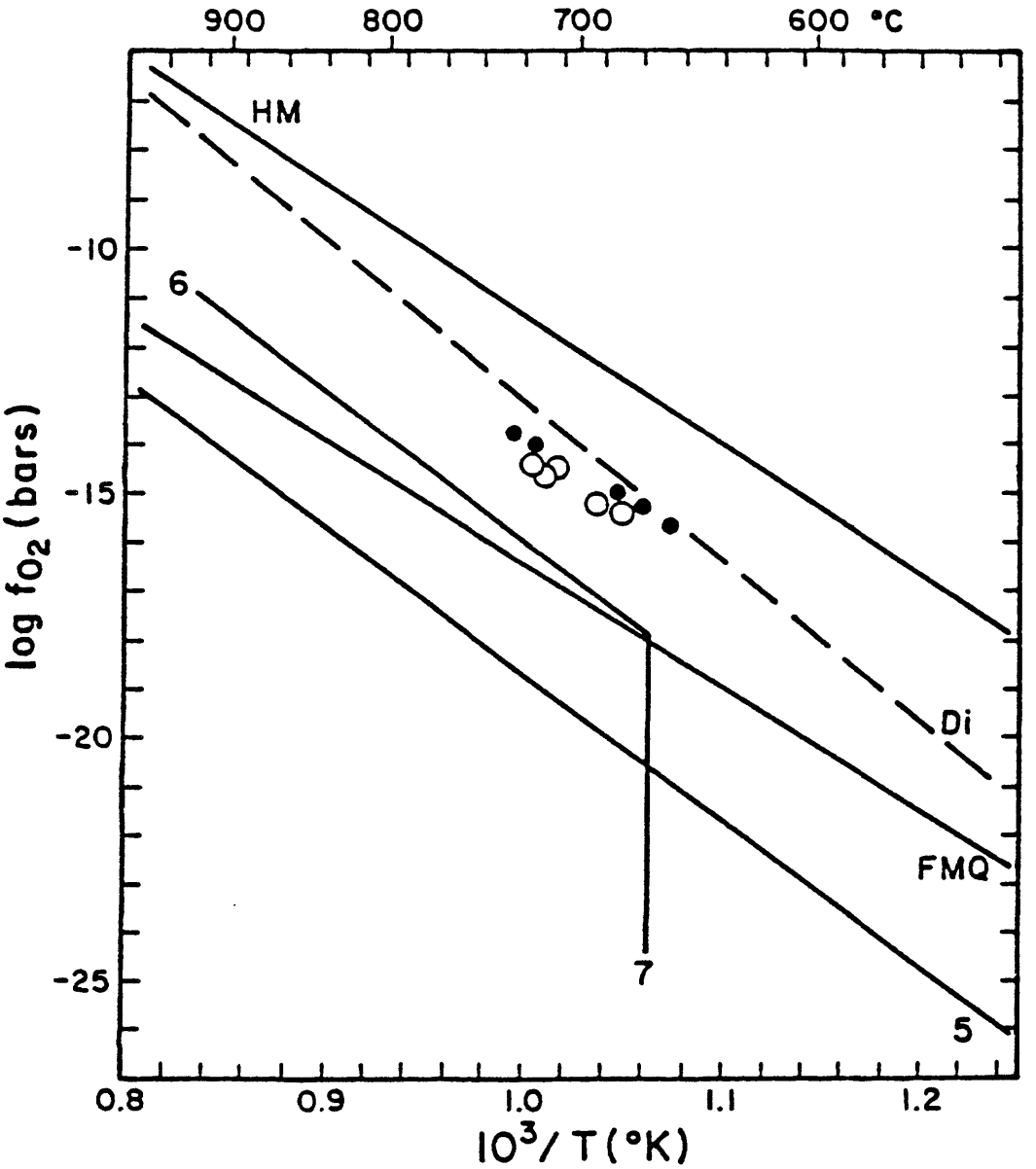

Fig II.27. $\log_{10}$ fO_2-1/T plot indicating the stability of several mineral assemblages: HM, Fe_2O_3-Fe_3O_4; FMQ, Fe_2SiO_4-Fe_3O_4-SiO_2; 5, $CaSiO_3$-$FeTiO_3$-$CaTiSiO_5$-Fe_3O_4; 6, $CaFeSi_2O_6$-$FeTiO_3$-$CaTiSiO_5$-Fe_3O_4-SiO_2; 7, $CaTiSiO_5$-Fe_2SiO_4-$CaFeSi_2O_6$-$FeTiO_3$; Di, $CaMgSi_2O_6$-$FeTiO_3$-$CaTiSiO_5$-Fe_3O_4-SiO_2. Circles represent fO_2-T determined for pyroxene-ilmenite-bearing silicic tuffs; dots represent sphene-magnetite-bearing silicic tuffs from the same sequence (Lipman, 1971).

Page 118 follows

CHAPTER III

Mafic Silicates

PART I: MAFIC SILICATES IN PERALKALINE ROCKS

OCCURRENCE

1. VIRGIN CANYON

Mafic silicates constitute 1.9 to 3.6 volume percent of the peralkaline granite. The main phases are alkali amphibole and sodic pyroxene; tetrasilicic mica and biotite are conspicuous in some samples, but much less abundant (<0.4 vol%). Occurrence and proportion of mafic silicate phases have been studied in a cross-section through the 30-m-thick peralkaline unit on Venado Peak.

Alkali amphibole is present throughout the cross-section and its abundance increases from the outer margin (1.5 vol% in 83QC30) toward the inner contact of the unit (1.9 vol% in 83QC29 and 2.2 vol% in 82QC38). In porphyritic samples, alkali amphibole is found as phenocrysts (to 4 mm long, but more commonly 0.5 to 2 mm long) as well as a groundmass constituent (0.02 to 0.08 mm). In seriate-textured samples from near the contact with the early metaluminous granite, arfvedsonite grain size ranges from 0.05 to 0.2 mm across.

At the outer margin of the unit (83QC30), alkali amphibole phenocrysts have a general ovoidal shape with irregular margins. They are pleochroic from light to dark blue, may be twinned, and do not show zoning. Towards their cores they may contain tetrasilicic mica laths in random orientation. Small anhedral alkali amphibole grains occur in the groundmass and usually average 0.02 mm across.

Toward the middle of the unit (83QC29) alkali amphibole phenocrysts may be twinned; they are often zoned, displaying a rounded "dusty" looking core surrounded by a clear irregular rim (Plate III.1, a). The cores are brownish to bluish, the rims dark blue to light blue or brownish green. Contacts between the cores and rims are relatively abrupt, not gradational. The cores often contain tetrasilicic mica laths in random orientation. In some cases, the whole core may be replaced by tetrasilicic mica (Plate III.1, b). Alkali amphibole also occurs in aggregates with tetrasilicic mica, opaque oxide minerals, and occasionally biotite and sodic pyroxene (Plate III.1, d). Small alkali amphibole grains in the groundmass are subhedral to anhedral and range from 0.05 to 0.08 mm.

In seriate-textured samples (82QC38) alkali amphibole more than 0.15 mm across can be zoned in the same manner as just describded. Tetrasilicic mica may occur in the "dusty" cores (Plate III.1, c). There are no conspicuous aggregates.

Sodic pyroxene is most abundant in samples from the middle of the unit (0.7 to 1.9 vol%) and is rare in seriate-textured samples taken nearest the early metaluminous granite ($\leq$ 0.3 vol%). The amount of sodic pyroxene seems to be related to the amount of tetrasilicic mica, and is highest in samples where aggregates are typical.

At the contact with the country rock, sodic pyroxene occurs mostly as euhedral grains (usually around 0.1 mm across, but to 0.2 X 0.4 mm) in clusters with polycrystalline quartz. A second occurrence is as smaller (0.05 mm) subhedral grains in a radiating association with hematite. There is no sodic pyroxene in the groundmass.

In samples toward the middle of the unit, sodic pyroxene is found as subhedral to anhedral, deep green to brown yellow phenocrysts (to 0.9 mm, but usually smaller). Less commonly it occurs as more euhedral grains in clusters with polycrystalline quartz. Sodic pyroxene is also found as small (0.05 to 0.1 mm) interstitial grains in the groundmass.

Rare sodic pyroxene in samples taken from near the contact with the early metaluminous granite is anhedral, up to 0.2 mm across, and is found associated with quartz, opaque oxide minerals, or alkali amphibole; it seems to have grown later than alkali amphibole (Plate III.1, c).

Tetrasilicic mica is most abundant in samples from the middle of the peralkline unit (around 0.3 vol%). In these samples, it occurs both as laths (0.05 to 0.1 mm) across the "dusty" rounded cores of alkali amphibole (Plate III.1, b), and in aggregates (to 1 X 1.6 mm) with alkali amphibole, opaque oxide minerals, biotite, and sodic pyroxene (Plate III.1, d). In samples taken from the outer margin of the unit or near the early metaluminous granite, tetrasilicic mica occurs only in the cores of alkali amphibole (Plate III.1, c); it ranges from 0.02 mm across in the former locality to 0.05 to 0.08 mm in the latter locality.

Biotite is typical except at the outer margin of the unit. In samples from the interior of the unit it occurs in mafic aggregates (Plate III.1, d) or as large well-formed crystals (0.8 X 1.1 mm). The large crystals have irregular margins and can have a thin lighter rim. They are associated with alkali feldspar clusters or enclosed in alkali feldspar phenocrysts, and contain inclusions of ilmenite, rutile, and apatite. In samples nearest the early metaluminous granite, biotite occurs as large (0.4 X 1 mm), complexly zoned crystals with irregular rims.

PLATE III.1: Photomicrographs of mafic silicates in the peralkaline granite of Virgin Canyon.

(a) Zoned alkali amphibole grains showing a dusty rounded (more calcic) core and a rather irregular clear (sodic) rim; inclusions are sphene; sample 82QC38.1. Bar is 0.5 mm long.

(b) Euhedral alkali amphibole crystal extensively replaced by tetrasilicic mica; sample Q83J67. Bar is 1 mm long.

(c) Zoned alkali amphibole hosting tetrasilicic mica and overgrown by acmite (A); to right, ilmenite replacement of sphene; sample 82QC34. Bar is 0.5 mm long.

(d) Aggregate of tetrasilicic mica (upper arm), biotite (lower arm), arfvedsonite, and acmite; sample 82QC34. Bar is 0.5 mm long.

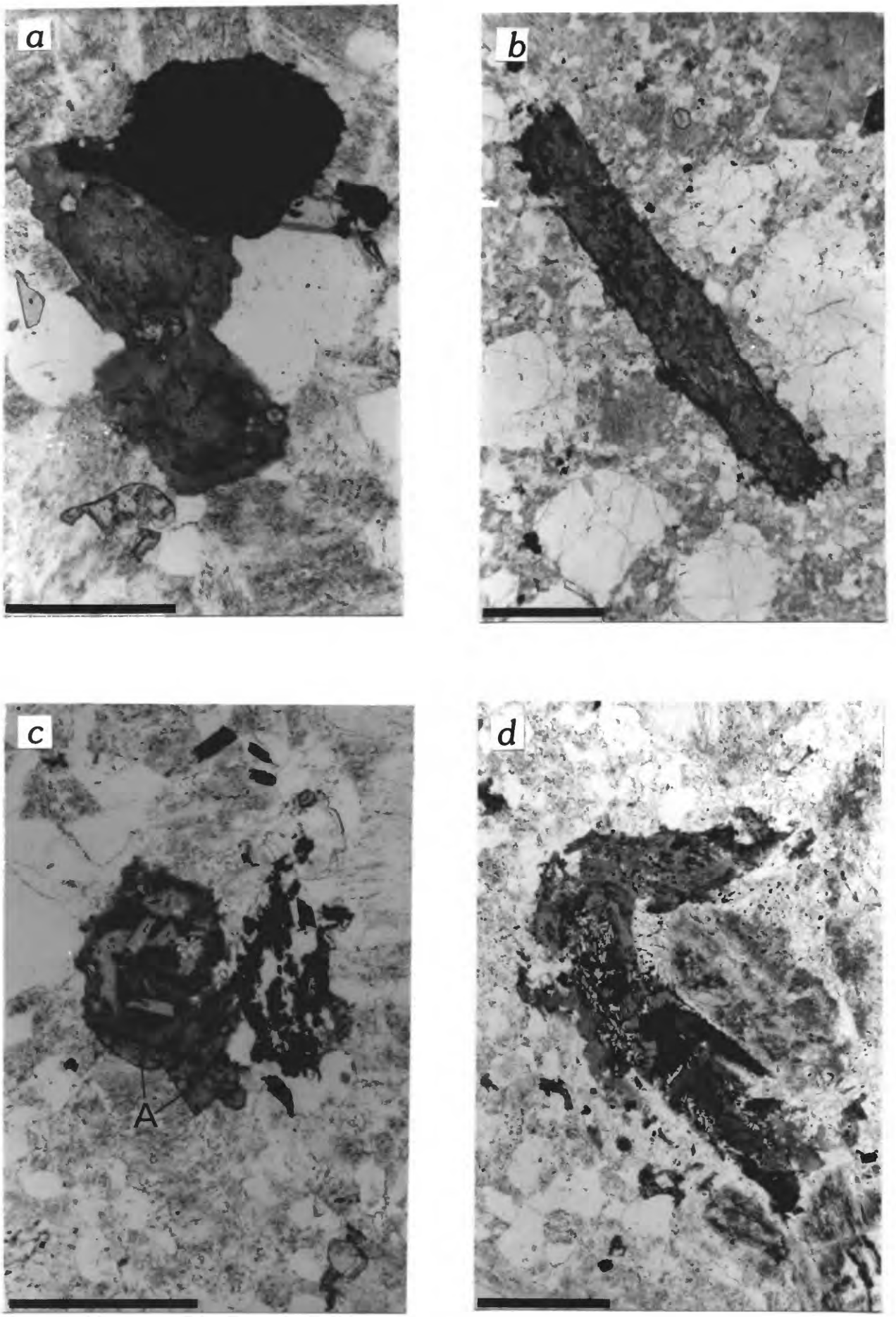
a
b
c
A
d

2. CANADA PINABETE

Alkali amphibole is the characteristic mafic silicate phase in the peralkaline granite of the Canada Pinabete pluton and constitutes 2.0 to 3.8 volume percent. Sparse sodic pyroxene occurs as small (0.05 mm) euhedral to subhedral grains associated with quartz, opaque oxide minerals, or alkali amphibole. Tetrasilicic mica is rare; it was found in an aggregate with alkali amphibole and biotite, and one lath (0.04 mm across) was found in an alkali amphibole crystal.

Alkali amphibole occurs as clusters (to 1.2 X 2.4 mm) of euhedral to subhedral grains (0.2 mm), or as single small phenocrysts (0.3 X 0.5 mm). It shows a very dark blue to greenish pleochroism, and can be zoned with a darker, slightly "dusty" core. Alkali amphibole also occurs in the groundmass as grains ranging from 0.05 to 0.1 mm across.

3. AMALIA TUFF, PERALKALINE RHYOLITE, AND NORTHERN DIKES

The only mafic silicate which occurs in the Amalia Tuff is an altered, brown to red, equant amphibole (0.06 to 0.10 mm), whose chemistry relates it to alkali amphibole.

In the peralkaline rhyolite, alkali amphibole occurs as subhedral to euhedral grains 0.005 to 0.02 mm across in the groundmass, where discrete rare crystals of tetrasilicic mica are also found. Occasionally, larger crystals of alkali amphibole and tetrasilicic mica range up to 0.1 X 0.2 mm. Larger amphibole grains display the more irregular shapes characteristic of the peralkaline granite in the Virgin Canyon pluton. There is no sodic pyroxene.

In the northern peralkaline dikes, mafic silicates are quite rare as well. Early biotite may be surrounded by a reaction rim of chlorite plus iron oxides. In one of the northern dike samples, 5 grains of tetrasilicic mica (to 0.05 mm across) have grown within biotite. Alkali amphibole and sodic pyroxene were found in several thin sections.

CHEMISTRY

Mafic silicates in the peralkaline rocks were analyzed for nine major elements using an ARL-SEMQ electron microprobe. Elements analyzed and standards used were as follows: Al, Ca, Mg, and Si, Kakanui hornblende; Na and Fe, crocidolite; K, biotite; Mn and Ti, synthetic oxides. All mafic silicate phases were analyzed using the same standards. Selected grains were reanalyzed by an 11-element procedure which also utilized synthetic fluor-phlogopite and natural sodalite as standards for F and Cl. Each analysis represents 4 to 10 points per grain or distinct part of a zoned grain; each point represents a counting interval of 10 seconds. Oxide analyses were computed using an online version of the Bence-Albee data-reduction scheme (1968).

On the basis of amphibole abundance and lack of alteration to tetrasilicic mica, two samples were selected for preparation of alkali amphibole separates to measure FeO/Fe_2O_3, H_2O, and F (Table III.1). Extreme care was taken with the separations, which ultimately required use of Clerici solution and "timed sinks" in pure methylene iodide to remove ilmenite and composite amphibole-ilmenite grains. The data in Tables III.1 and III.2 suggest that the separates are good.

Table III.1. Partial chemical analyses of amphibole separates from the Questa granitic rocks (weight percent).

PLUTON/ Unit	Sample number	F	H_2O^+	FeO	FeO^T	$Fe^{2+}/(Fe^{2+} + Fe^{3+})$
VIRGIN CANYON						
Peralkaline granite	Q83J63	2.16	0.85	8.84	18.00	0.51
CANADA PINABETE						
Peralkaline granite	84QC7	1.54	0.84	16.76	28.87	0.40
CABRESTO LAKE						
Granite	82QC51b	0.73	1.47	9.18	12.35	0.74
RED RIVER INTRUSIVE COMPLEX						
Granodiorite	82QC44	0.31	2.24	8.01	10.85	0.74
RIO HONDO						
Granodiorite	Q83J59	0.34	2.11	8.22	10.64	0.77
	Q84J6	0.34	1.89	9.84	13.37	0.74

1. ALKALI AMPHIBOLE CHEMISTRY

A total of 103 alkali amphibole analyses were obtained by electron microprobe, representing 76 grains in 24 samples, including 1 of the Amalia Tuff, 1 of the peralkaline rhyolite, 6 from the northern dikes, 3 from the Canada Pinabete pluton, and 13 from the Virgin Canyon pluton. Early and late amphibole compositions were measured for 17 grains in 11 samples of the Virgin Canyon and Canada Pinabete plutons. Unless otherwise noted, the following figures and discussion refer to the 89 analyses obtained for samples from these two plutons and the northern dikes. Overall compositional ranges among these 89 analyses are (weight percent): SiO_2, 48.2 to 53.8; Al_2O_3, 0.32 to 2.35; FeO^T, 10.5 to 34.2; MgO, 0.47 to 14.6; CaO, 0.04 to 9.40; Na_2O, 4.55 to 8.84; K_2O, 0.45 to 1.46; TiO_2; 0.09 to 1.44; MnO, 1.68 to 5.75; and F (26 grains), 2.7 to 5.6. Much of this range is represented in the analyses of Table III.2. Note that if F content has been measured, the totals in Table III.2 include F and have been corrected.

Table III.2. Electron microprobe analyses and structural formulae for alkali amphibole.

	Amelia Tuff	Peralk. rhy.		Virgin Canyon pluton								
	82L42A	Q83J124		83QC30	83QC29,12		82QC38.1,9		82QC34,2		Q83J62,1	
	(3)*	(2)	(9)	(2)	early	late	early	late	early	late	early	late
SiO_2	51.5	50.3	51.1	51.6	50.9	53.0	50.8	52.4	51.1	52.2	51.2	51.4
Al_2O_3	2.07	0.87	0.77	1.34	1.55	1.10	2.25	1.12	2.24	1.23	2.22	1.39
FeO^T	12.6	25.1	22.2	22.9	17.5	19.4	10.5	19.5	11.4	18.7	12.6	22.6
MgO	14.0	3.11	4.72	4.02	8.28	7.41	14.4	8.36	14.6	8.40	12.5	5.93
CaO	7.09	1.03	0.86	0.16	3.49	0.86	8.21	2.30	6.20	1.66	5.06	0.72
Na_2O	3.96	8.45	8.66	8.38	7.34	7.66	5.75	7.10	5.36	7.23	6.77	8.01
K_2O	0.79	0.77	0.85	1.34	1.26	1.20	0.79	1.20	0.74	1.17	0.85	1.11
TiO_2	0.48	0.60	0.66	0.35	0.42	0.49	0.56	0.39	0.44	0.44	0.48	0.56
MnO	3.69	6.25	6.30	5.70	4.33	4.59	2.94	3.74	3.40	3.88	3.90	3.71
F	n.m.	n.m.	n.m.	3.2	5.6	3.5	4.9	3.2	3.5	2.9	4.9	2.7
Total	96.90**	96.48	96.12	98.94	99.31	98.85	99.64	99.07	98.16	97.66	99.14	98.28
Si	7.566	7.808	7.875	7.907	7.742	7.962	7.476	7.847	7.546	7.887	7.610	7.826
Al	0.359	0.159	0.125	.093	0.258	0.038	0.391	0.153	0.390	0.113	0.389	0.174
Fe^{3+}	0.075	0.033	-	-	-	-	0.133	-	0.064	-	0.001	-
Al	-	-	0.015	0.149	0.020	0.157	-	0.045	-	0.106	-	0.076
Fe^{3+}	0.713	1.335	1.200	1.494	1.134	1.242	0.525	1.243	0.653	1.204	0.797	1.466
Fe^{2+}	0.760	1.891	1.660	1.441	1.092	1.197	0.635	1.199	0.691	1.159	0.769	1.413
Mg	3.067	0.720	1.085	0.919	1.878	1.660	3.160	1.867	3.215	1.893	2.771	1.347
Mn	0.460	0.822	0.823	0.740	0.558	0.585	0.367	0.475	0.426	0.497	0.491	0.479
Ti	0.053	0.070	0.077	0.040	0.048	0.055	0.062	0.044	0.049	0.050	0.054	0.064
Sum M1-M3	5.000	4.838	4.860	4.783	4.730	4.896	4.749	4.873	5.000	4.909	4.882	4.845
X oct.	0.053	-	-	-	-	-	-	-	0.034	-	-	-
Ca	1.116	0.171	0.142	0.026	0.569	0.138	1.294	0.369	0.981	0.269	0.806	0.117
Na	0.831	1.829	1.858	1.974	1.431	1.862	0.706	1.631	0.985	1.731	1.194	1.883
Na	0.297	0.714	0.729	0.515	0.733	0.369	0.935	0.430	0.550	0.387	0.757	0.482
K	0.148	0.153	0.167	0.262	0.245	0.230	0.148	0.229	0.139	0.226	0.161	0.216
Sum A	0.445	0.867	0.896	0.777	0.978	0.599	1.083	0.659	0.689	0.613	0.919	0.698

TABLE III.2. continued

	Virgin Canyon pluton						Canada Pinabete pluton				Northern dikes	
	Q83J63,4		Q83J63,3		84QC21,1		Q83J94		82QC49	84QC7	Q83J70+76	Q83J48+71
	early	late	early	late	early	late	early(2)	late(2)	(4)	(3)	(2)	(2)
SiO_2	48.2	51.9	52.3	52.1	51.9	50.9	52.3	51.2	51.8	50.2	51.6	50.0
Al_2O_3	2.26	1.75	1.94	1.45	1.50	0.32	1.30	1.22	1.12	1.39	1.10	0.87
FeO^T	11.9	14.8	15.2	20.7	13.8	30.8	19.7	22.3	23.6	27.8	20.4	27.5
MgO	12.4	11.0	10.8	8.31	11.2	1.24	7.79	5.68	2.55	2.50	6.30	0.60
CaO	9.40	4.35	3.45	1.85	4.03	0.77	1.19	1.19	0.20	0.90	1.28	0.08
Na_2O	5.26	6.41	6.39	6.93	6.53	6.30	7.94	7.63	8.64	7.73	8.00	8.21
K_2O	1.34	1.04	1.09	1.12	1.06	0.45	1.12	1.16	1.22	1.12	1.12	1.31
TiO_2	0.40	0.37	0.47	0.41	0.36	0.09	0.57	0.64	0.70	0.83	0.56	1.25
MnO	3.70	4.33	4.25	3.21	4.85	3.28	4.09	4.43	4.28	4.02	4.12	5.23
F	n.m.	n.m.	3.2	2.9	n.m.	n.m.	3.3	2.8	n.m.	n.m.	n.m.	n.m.
Total	95.54	96.79	98.61	98.94	96.02	95.90	98.83	98.12	95.22	97.80	95.44	96.34
Si	7.335	7.722	7.761	7.800	7.771	7.982	7.890	7.865	8.087	7.772	7.946	7.906
Al	0.406	0.278	0.239	0.200	0.229	0.018	0.110	0.135	-	0.228	0.054	0.094
Fe^{3+}	0.259	-	-	-	-	-	-	-	-	-	-	-
Al	-	0.029	0.101	0.056	0.036	0.041	0.121	0.086	0.206	0.026	0.146	0.068
Fe^{3+}	0.513	0.937	0.962	1.319	0.880	2.056	1.042	1.202	1.294	1.511	1.103	1.527
Fe^{2+}	0.743	0.904	0.925	1.273	0.849	1.983	1.443	1.663	1.788	2.089	1.524	2.110
Mg	2.814	2.441	2.390	1.855	2.501	0.290	1.753	1.301	0.594	0.577	1.447	0.141
Mn	0.477	0.546	0.535	0.407	0.616	0.436	0.523	0.577	0.566	0.528	0.538	0.701
Ti	0.046	0.041	0.052	0.046	0.041	0.011	0.065	0.074	0.082	0.097	0.065	0.149
Sum M1-M3	4.593	4.898	4.965	4.956	4.923	4.817	4.947	4.903	4.530	4.828	4.823	4.696
X oct.	-	-	-	-	-	-	-	-	-	-	-	-
Ca	1.532	0.693	0.548	0.297	0.646	0.129	0.192	0.196	0.033	0.149	0.211	0.014
Na	0.468	1.307	1.452	1.703	1.354	1.871	1.808	1.804	1.967	1.851	1.789	1.986
Na	1.084	0.542	0.386	0.308	0.541	0.044	0.514	0.468	0.648	0.469	0.599	0.531
K	0.260	0.197	0.206	0.214	0.203	0.090	0.216	0.227	0.243	0.221	0.220	0.264
Sum A	1.344	0.739	0.592	0.522	0.744	0.134	0.730	0.695	0.891	0.690	0.819	0.795

* Number of analyses averaged.
** Totals corrected for F = 0; Cl $\leq$ 0.04 wt%.

Distribution of cations according to the standard amphibole formula was accomplished with the program provided by Rock and Leake (1984) based on 23 oxygen ions. Values indicated for Fe^{3+} and Fe^{2+} cations in Table III.2 are those obtained by applying the two measured values of $Fe^{2+}/(Fe^{2+}+Fe^{3+})$ of Table III.1 to all samples from each respective pluton. Additionally, for purposes of uniform data comparison in figures and based on comparable total iron content, Fe^{T} in amphiboles from the Amalia Tuff and the peralkaline rhyolite was proportioned as in the Virgin Canyon pluton; for amphiboles from the northern dikes, Fe^{T} was proportioned as in the Canada Pinabete pluton.

As evidenced in Table III.2, systematic variation in the composition of these alkali amphiboles is caused predominately by variation in Si, Al, Fe, Mg, Ca, and Na; the most significant substitution appears to be $Na^{M4}+Fe$ for Mg+Ca. The analyses of Table III.2 are typical in showing that although SiO_2 weight percentage shows no regular pattern of change from early to late amphibole, the fraction of Si cations in the structural formula increases in all but one case. This apparent anomaly is due to the heavy atomic weight of Fe, which invariably increases in concentration. During evolution of the Questa alkali amphiboles, total Al and Al^{IV} contents typically decrease. For more calcic compositions there may be insufficient Si+Al to fill the tetrahedral sites and in 12 cases Fe^{3+IV} is indicated. The amphiboles rarely contain more than 0.150 Al^{VI} cation (avg 0.089 cation).

The alkali amphiboles at Questa have several notable compositional characteristics, including high Mn content, low Ti content, relatively constant K content, and high Na/Fe. In these respects they are most similar to alkali amphiboles in alkali granites of the Oslo area (Neumann, 1976). Mn contents of the Questa alkali amphiboles are higher than for any other alkali amphiboles known, except those of the Oslo area, but are relatively uniform. High Mn content may simply relate to the fact that in these peralkaline rocks, Mn enters only the minor phases amphibole and ilmenite. The average host rock content of 0.11 weight percent MnO can be accounted for by 1.5 percent of alkali amphibole containing 4 weight percent MnO and 0.3 percent of ilmenite containing 20 weight percent MnO. Ti is relatively uniform and minor (avg 0.061 cation) in the alkali amphiboles; Ti content correlates well with Fe^{3+} in samples from the Canada Pinabete pluton, but this correlation is not found for other samples. K is not well related to another element or to amphibole zoning. Excluding the few more riebeckitic analyses, K accounts for 14 to 41 percent of A-site occupancy (avg 0.221 cation).

A plot of $Ca+Al^{IV}+Fe^{3+IV}$ against Si+Na+K (fig. III.1) shows that alkali amphiboles in the peralkaline granite of Virgin Canyon and Canada Pinabete follow an exceptionally well-defined, continuous, and extensive evolutionary trend (e.g., compare Giret and others, 1980 and Strong and Taylor, 1984). This diagram and the nomenclatural aspect of the Rock and Leake program, indicate that the majority of the amphibole compositions can be characterized as manganoan ferrian richterite, manganoan magnesio-arfvedsonite, and manganoan arfvedsonite. Following the distinction made by Strong and Taylor, note that with rare exception (e.g. Table III.2, grain 82QC21,1; fig. III.1, points 17 and 21) the evolutionary path followed can be characterized as magmatic-subsolidus, rather than oxidizing. That is, as demonstrated by the classic work of Ernst (1962), the A-site is occupied in magmatic amphiboles.

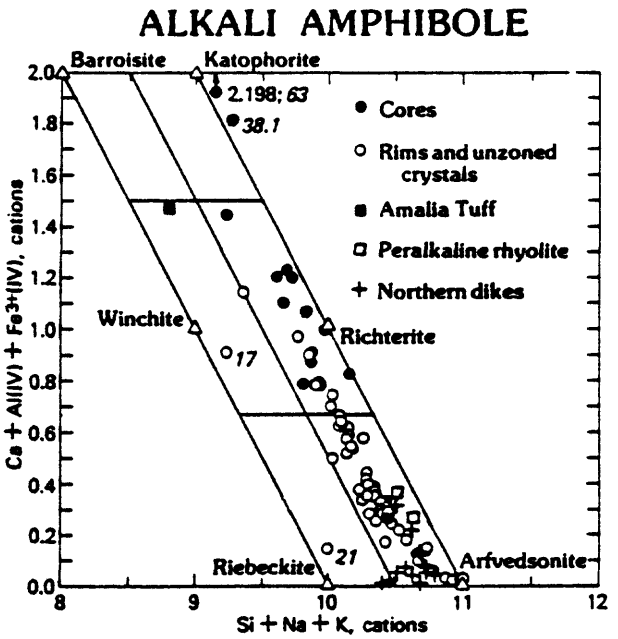

Fig. III.1.

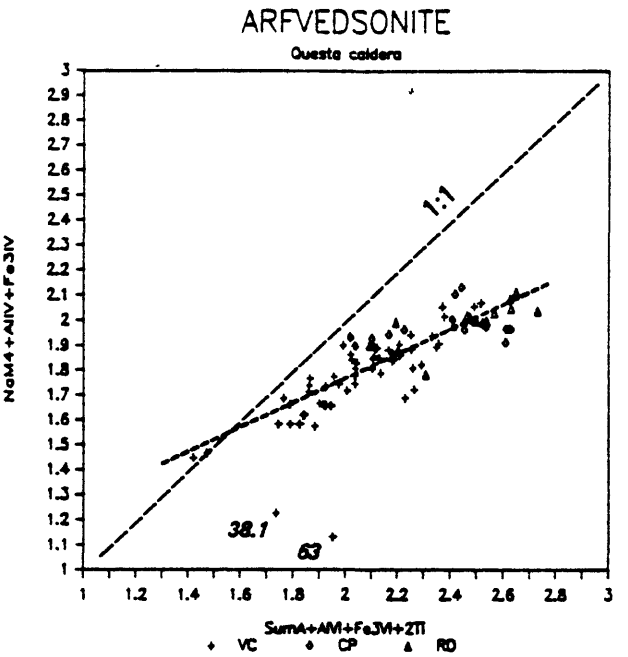

Fig. III.2.

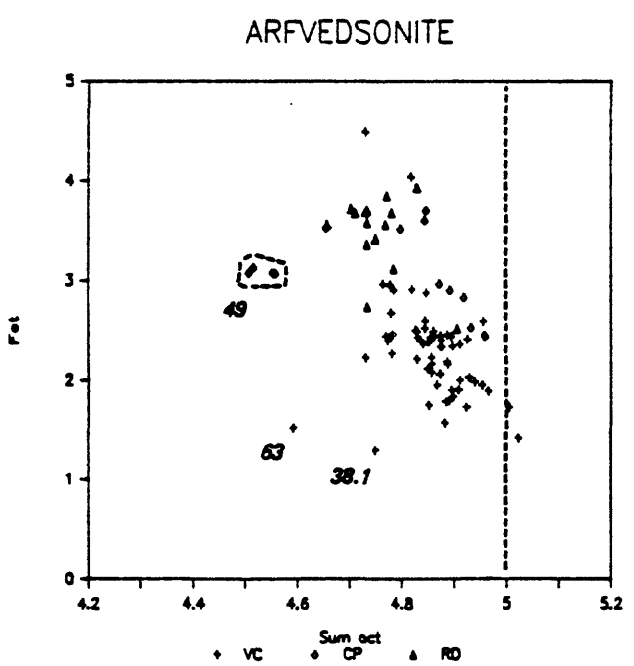

Fig. III.3.

Fig. III.1. Si+Na+K against $Ca+Al^{IV}+Fe^{3+IV}$ for zoned and unzoned alkali amphiboles in the peralkaline units of the Questa magmatic system. Indicated on this and other figures are two calcic core compositions (63,4c and 38.1,9c) and two riebeckitic compositions (17,1 and 21,1r) that deviate notably from the general trend. Fields are from Giret and others (1980) after the classification of Leake (1978).

Fig. III.2. Total A-site occupancy+$Al^{VI}+Fe^{3+VI}$ +2Ti against $Na^{M4}+Al^{IV}+Fe^{3+IV}$ (cations) for the alkali amphiboles. Long-dashed line, 1:1 correlation; short-dashed line, statistical best fit, excluding points 38.1 and 63. Crosses, peralkaline granite of Virgin Canyon; diamonds, peralkaline granite of Canada Pinabete; and triangles, peralkaline northern dikes.

Fig. III.3. Total octahedral-site occupancy against total Fe (cations) for alkali amphiboles. Reference line at full octahedral-site occupancy. Symbols as in fig. III.2.

As might have been anticipated from their sites of emplacement, amphiboles in the Amalia Tuff and the northern dikes are somewhat more oxidized. Somewhat surprising in view of the appearance of figure III.1 is the fact that structural formulae for early and late alkali amphibole compositions (Table III.2) show that A-site occupancy has invariably diminished from core to rim as the result of reduction in Na^{A}.

The simplest clino-amphibole formula can be written $[]Ca_2(Fe^{2+},Mg)_5Si_8O_{22}(OH)_2$. Substitutions involving ions of lesser or greater charge are balanced in diverse ways (e.g., Czamanske and Wones, 1973, p. 360). However, consideration of this basic formula shows that charge can only be decreased by replacement of Ca by Na in the M4 site or of Si by Al or Fe^{3+}. Conversely, charge is increased by addition of Na or K to the A site and Al, Fe^{3+}, or Ti^{4+} to the octahedral strip. Figure III.2 shows that with two notable exceptions (excluded from the regression line) these substitutions follow an offsetting relation ($r = 0.87$). Because Fe^{3+} figures prominently in this plot, it is important to note that averaged data for samples Q83J63 and 84QC7, for which $Fe^{2+}/(Fe^{2+} + Fe^{3+})$ was measured, fall on the regression line. The plot indicates that charge-reducing substitutions are over compensated by a factor of about 1.6, and that vacancies must exist in the octahedral strip. Because average values for A-site occupancy (0.758), Al^{VI} cations (0.089), and Ti cations (0.061) are relatively constant and/or low, the generation of vacancies must relate principally to the presence of Fe^{3+}. This relation is further explored in figure III.3 in which octahedral-strip occupancy is plotted against Fe^{T}; a plot of octahedral-strip occupancy against Na is quite similar.

A series of correlation plots (fig. III.4 to III.8) has been chosen to portray the substitutional characteristics of the alkali amphiboles at Questa. Because two measurements of $Fe^{2+}/(Fe^{2+} + Fe^{3+})$ have been ascribed to the entire data set, as much of the data analysis as possible is based on plots that do not involve Fe^{2+}, Fe^{3+}, or total octahedral-site occupancy. Table III.3 shows, however, that neither octahedral-site or A-site occupancy will be drastically affected by significant changes in $Fe^{2+}/(Fe^{2+} + Fe^{3+})$.

A number of the plots show that alkali amphiboles in the sample suite from the Virgin Canyon pluton tend to form a more coherent group within the total data set. For samples from the northern dikes, this may reflect variable interaction and alteration of the relatively thin body in the shallow environment of emplacement. For samples from the Canada Pinabete pluton this may well reflect the inadequacy of applying one determination of $Fe^{2+}/(Fe^{2+} + Fe^{3+})$ when parts of the pluton have crystallized under conditions of differing fO_2, as evidenced by the presence of some samples which are magnetite-free and contain only ilmenite. One such sample (82QC49, Table III.2), contains alkali amphibole which, on average, contains 0.23 less octahedral cations than any other sample of the pluton. On figure III.3 the four alkali amphibole analyses representing sample 82QC49 are labeled "49." Also often distinct from the general trend are the two most calcic core compositions (82QC38.1,9c and Q83J63,4c) and the two most riebeckitic compositions (84QC17,1 and 84QC21,1r); these analyses are labeled in several figures by the last digits of the sample numbers. Uniformly in all figures, Virgin Canyon samples are represented by crosses, Canada Pinabete samples by diamonds, and northern dike samples by triangles.

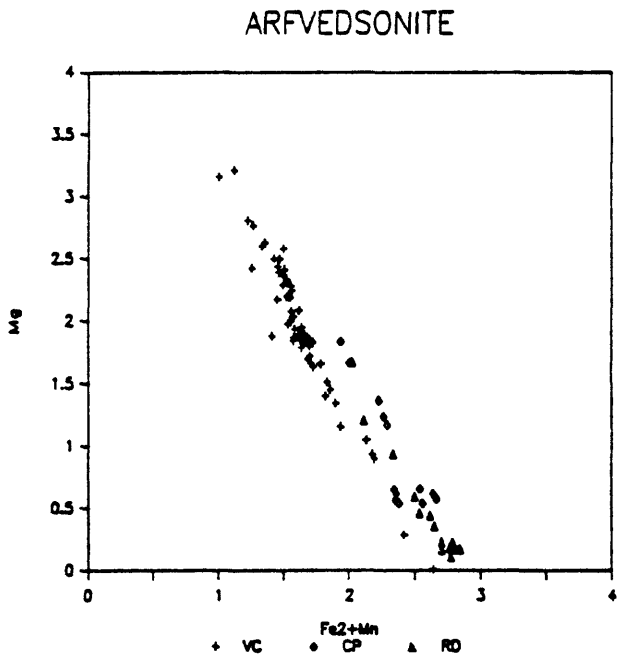

Fig. III.4. Fe^{2+} + Mn against Mg (cations) for alkali amphiboles (r = −0.97). Symbols as in fig. III.2.

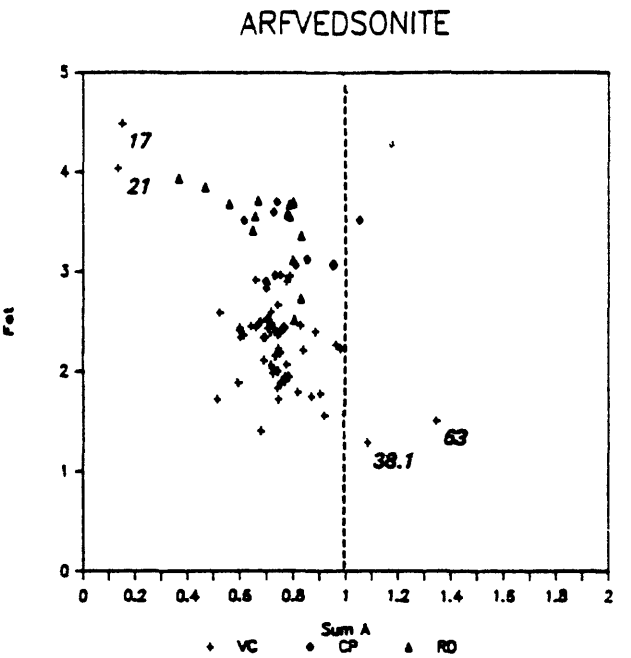

Fig. III.5. Total A-site occupancy against total Fe (cations) for alkali amphiboles. Reference line at full A-site occupancy. Symbols as in fig. III.2.

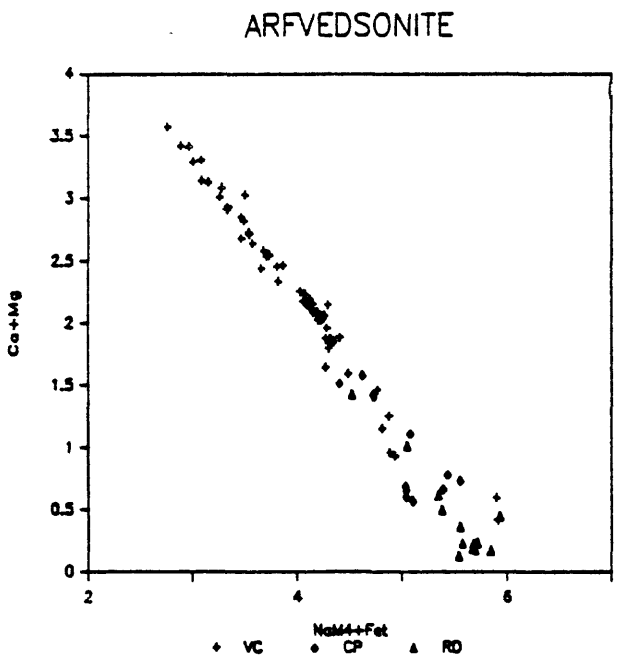

Fig. III.6. Na^{M4}+total Fe against Ca+Mg (cations) for alkali amphiboles (r = −0.99). Symbols as in fig. III.2.

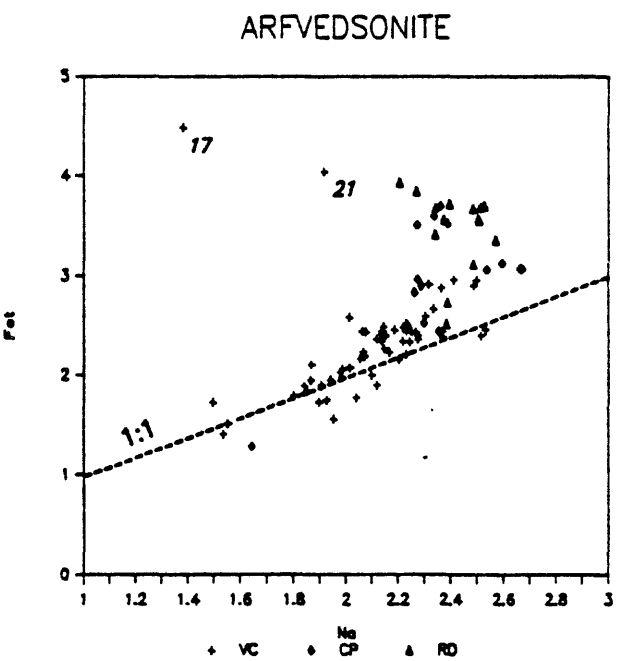

Fig. III.7. Total Na against total Fe (cations) for alkali amphiboles. 1:1 correlation line shown for reference. Symbols as in fig. III.2.

Table III.3. Comparison of structural formulae calculated by the Rock and Leake program, analysis 84QC7 (3).

	Micro-probe	Est. Fe_2O_3, 24(O,OH,F)	Est. Fe_2O_3, 23(O)	Calc. Fe_2O_3, 24(O,OH,F)	Calc. Fe_2O_3, 23(O)
SiO_2	50.2	7.835	7.774	7.887	7.878
Al_2O_3	1.39	0.256	0.254	0.258	0.257
FeO^T	27.8	-	-	-	-
Fe_2O_3	-	1.521	1.509	1.215	0.912
FeO	-	2.106	2.089	2.435	2.735
MgO	2.50	0.582	0.577	0.586	0.585
CaO	0.90	0.150	0.149	0.151	0.151
Na_2O	7.73	2.339	2.321	2.354	2.352
K_2O	1.12	0.223	0.221	0.225	0.224
TiO_2	0.83	0.097	0.097	0.098	0.098
MnO	4.02	0.532	0.528	0.535	0.535
F	1.54	0.760	-	0.765	-
H_2O	0.84	0.876		0.881	
$Fe^{2+}/(Fe^{2+} + Fe^{3+})$		0.581	0.581	0.667	0.750
Sum M1-M3		4.929	4.828	5.014	5.000
Sum A		0.712	0.691	0.730	0.727

Resolution of the most important substitutional schemes in the alkali amphiboles at Questa is a difficult process because much more is involved than substitution of Si+Na+K for $Ca+Al^{IV}+Fe^{3+IV}$, which does not involve the M1-M3 sites. The simplest substitution involving the M1-M3 sites is that between Mg and Fe^{2+}+Mn (fig.III.4). The correlations between Mg and Fe^{2+} or Mg and Fe^{2+} +Mn ($r = -0.97$; fig. III.4) are excellent; the fact that a change of 3.2 Mg cations correlates with a change of only 1.7 cations of Fe^{2+} + Mn indicates that Mg is also being replaced by Fe^{3+} as alkali amphibole crystallization evolves. In fact, the excellent correlation ($r = -0.98$) between Fe^T and Mg approaches 1:1. Mn shows no correlation with Fe or Mg.

Because these alkali amphiboles contain a high proportion of Fe^{3+} and because the late-formed amphibole in zoned grains contains somewhat fewer A-site cations, one might be tempted to ascribe importance to the $[]+Fe^{3+}$ for Na^A+Fe^{2+} (riebeckitic) substitution. However, figure III.5 shows that, excluding 2 analyses which have a more distinct riebeckitic composition, there is no diminution in A-site occupancy (avg 0.758 cation) with increase in Fe^T. This plot is little affected by assumptions regarding Fe oxidation state

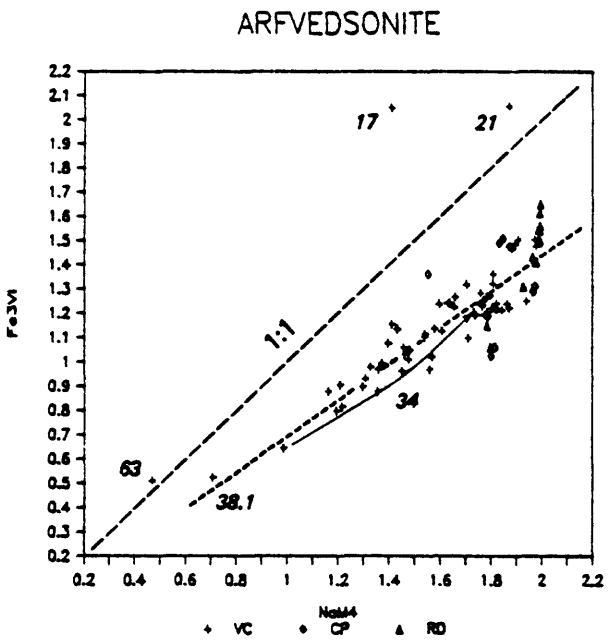

Fig. III.8.

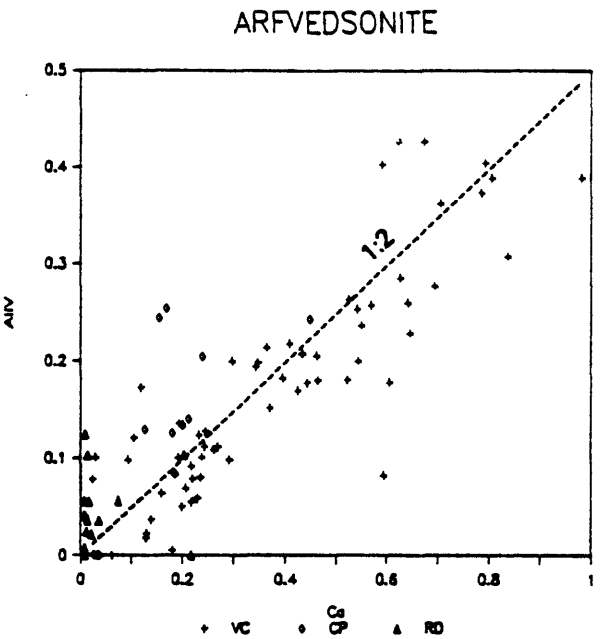

Fig. III.9.

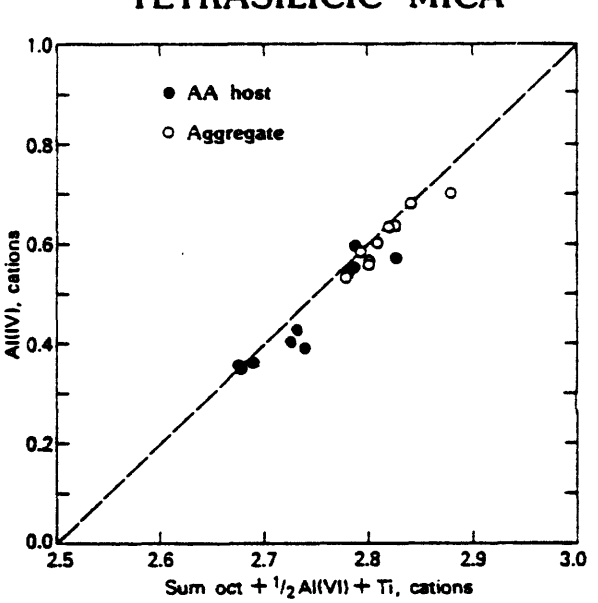

Fig. III.10.

Fig. III.8. Na^{M4} against Fe^{3+VI} (cations) for alkali amphiboles. Long-dashed line, 1:1 correlation; short-dashed line, statistical best fit, excluding points 17, 21, 38.1, and 63. Arrow connects data for core and rim of grain 84QC34,2 (Table III.2). Symbols as in fig. III.2.

Fig. III.9. Ca against Al^{IV} (cations) in alkali amphiboles. 1:2 correlation line shown for reference. Symbols as in fig. III.2.

Fig. III.10. Al^{IV} cations against "effective octahedral-site occupancy" for tetrasilicic micas. Dashed line represents perfect compensation. Dots, mica replacing alkali amphibole; circles, mica in mafic aggregate.

(Table III.3). A plot of Na^{A} against Fe^{T} is virtually identical except that Na^{A} averages 0.537 cation. Conspicuous distinction of the riebeckitic compositions on this and figures III.7 and III.8 supports the conclusion that this is not an important trend in these amphiboles.

As shown by figure III.6, the dominant substitution in the alkali amphiboles at Questa is $Na^{M4}+Fe^{T}$ for Ca+Mg (r = -0.99). The slope of the data set indicates that loss of Ca+Mg is not totally compensated by $Na^{M4}+Fe$, a fact which we interpret to reflect the creation of vacancies in the M1-M3 octahedral sites. A plot of $Na^{M4}+Fe^{T}$ against Mg is virtually identical below 1.75 Mg cations, but drops below the linear trend at higher Mg contents because all Ca is removed when $Na^{M4}+Fe^{T}$ reaches 4.5 cations.

A plot of $Na^{M4}+Fe^{3+VI}$ against Ca+Mg shows that the $Na-Fe^{3+}$ couple accounts for approximately one-half of the loss in Ca+Mg, the remainder being accounted for by Fe^{2+}.

Relations between Na and Fe contents are illustrated in figures III.7 and III.8. Figure III.7 shows that at lower Na and Fe contents the elements are well related, but that Fe content increases more rapidly than Na content; higher Fe^{T} contents are poorly related to Na content. Figure III.8 suggests that the appropriate correlation is Na^{M4} with Fe^{3+VI} (r = 0.87). Core and rim compositions for amphibole grain 84QC34,2 (Table III.2) are connected by an arrow for illustrative purposes. The best-fit to the data indicates that 0.3 to 0.5 of the Na^{M4} cations can be considered to be coupled with Na^{A}, in accord with richteritic coupling. The fact that there is more $Na^{M4}-Na^{A}$ coupling in the more iron-rich amphiboles relates to fact that they contain notably fewer trivalent tetrahedral-site cations coupled with Na^{A}. Excess charge due to Al and Ti in the M1-M3 sites is essentially balanced by K^{A} (Table III.2).

Figure III.9 indicates that Al^{IV} and Ca contents roughly obey a relation of 1:2 in alkali amphibole from the Virgin Canyon pluton. Fabries (1978, fig. 7) considers a 1:2 ratio between Al^{IV} and Ca to be typical of the alkali amphibole fractionation trend in oversaturated alkaline rocks. Falling well off the trend of figure III.9 are the points representing analyses 82QC38.1,9c and Q83J63,4c; they lie, respectively at Al^{IV}=0.390, Ca=1.295 and Al^{IV}=0.406, Ca=1.533. Corresponding octahedral-strip occupancies of 4.748 and 4.591 and A-site occupancies of 1.083 and 1.344 suggest that Ca may occupy octahedral sites in these amphiboles (see Hawthorne, 1976). There is no relation between Al^{IV} and Na^{A} or total A-site occupancy.

The substitutional schemes most often suggested as characterizing alkali amphiboles are $Ca+Al^{IV}$ for Si+(Na,K) and $Na^{A}+Fe^{2+}$ for $[]+Fe^{3+}$. Only Fabries (1978) has argued for substitutions of the type $Na^{M4}+R^{3+}$ for $Ca+R^{2+}$, which seems to be dominant at Questa.

2. TETRASILICIC MICA CHEMISTRY

Strictly speaking, tetrasilicic micas are those in which the tetrahedral sites are fully occupied by Si. Their synthesis was first reported by Seifert and Schreyer (1965), who later studied their stability and relation to phlogopite (Seifert and Schreyer, 1971). Apparently because of certain ceramic and catalytic properties, there is substantial literature, largely in

Table III.4. Electron microprobe analyses and structural formulae for tetrasilicic mica and biotite.

	TETRASILICIC MICA										BIOTITE					
		Peralk. rhy.		Peralkaline porphyry							Peralkaline porphyry					
	Robert and Maury	Q83J124		82QC30	82QC29			82QC38.1		82QC34	82QC29		82QC38.1		82QC34	
		12A	1A	(2)	4b	4a	3	(2)	1b	(2)	core	rim	core	rim	(3)	6
SiO_2	47.3	43.1	43.9	49.0	49.2	45.5	44.2	46.1	44.0	45.7	39.2	41.8	37.0	41.8	39.1	36.3
Al_2O_3	4.96	6.04	5.87	5.02	5.33	7.18	7.88	7.60	7.73	6.85	14.2	12.4	13.4	11.1	11.2	13.0
FeO^T	17.1	21.5	17.5	9.54	8.81	12.5	14.8	10.8	13.8	12.0	13.5	10.8	16.1	11.1	16.5	19.0
MgO	4.30	5.75	9.03	14.3	15.8	13.3	12.7	16.0	15.8	14.6	13.9	15.9	12.1	16.2	12.1	9.80
Na_2O	1.02	0.64	0.81	0.26	0.33	0.23	0.31	0.33	0.31	0.30	0.33	0.30	0.38	0.35	0.35	0.34
K_2O	8.89	9.03	9.13	10.2	9.93	9.81	9.70	10.2	9.94	9.57	9.77	9.97	9.60	9.53	9.51	9.27
TiO_2	2.44	1.89	1.62	0.89	0.88	1.60	2.19	1.42	1.17	1.84	3.16	2.46	4.62	2.64	2.64	3.81
MnO	9.89	5.05	4.86	4.35	2.47	2.77	1.39	1.40	0.77	2.10	0.52	0.44	1.35	1.66	2.54	2.90
F	4.4	n.m.	n.m.	7.9	7.7	6.2	6.0	6.4	5.6	5.9	4.5	4.9	3.4	4.7	3.7	2.7
Total	98.49*	93.00	92.74	98.14	97.21	96.48	96.64	97.56	96.76	96.38	97.60	97.23	96.99	97.43	96.56	96.56
Si	3.643	3.462	3.463	3.643	3.637	3.447	3.362	3.411	3.319	3.437	2.901	3.063	2.799	3.073	2.985	2.802
Al	0.357	0.538	0.537	0.357	0.363	0.553	0.638	0.589	0.681	0.563	1.099	0.937	1.195	0.927	1.008	1.183
Fe^{3+}	-	-	-	-	-	-	-	-	-		-	-	0.006	-	0.007	0.015
Al	0.094	0.034	0.008	0.083	0.101	0.088	0.069	0.074	0.007	0.044	0.139	0.134	-	0.036	-	-
Fe^{3+}	-	-	-	-	-	-	-	-	-	-	0.205	0.163	0.244	0.168	0.252	0.287
Fe^{2+}	1.103	1.444	1.154	0.593	0.545	0.792	0.942	0.668	0.871	0.755	0.630	0.499	1.768	0.515	0.749	0.925
Mg	0.494	0.689	1.062	1.585	1.741	1.502	1.440	1.765	1.777	1.637	1.533	1.737	1.364	1.776	1.377	1.128
Ti	0.141	0.114	0.096	0.050	0.049	0.091	1.125	0.079	0.066	0.104	0.176	0.136	0.263	0.146	0.152	0.221
Mn	0.645	0.344	0.325	0.274	0.155	0.178	0.090	0.088	0.049	0.134	0.033	0.027	0.086	0.103	0.164	0.190
Sum oct.	2.477	2.624	2.645	2.585	2.591	2.651	2.666	2.674	2.770	2.674	2.716	2.696	2.725	2.744	2.739	2.751
Na	0.152	0.100	0.124	0.037	0.047	0.034	0.046	0.047	0.045	0.044	0.047	0.043	0.056	0.050	0.052	0.051
K	0.928	0.925	0.919	0.967	0.936	0.948	0.941	0.963	0.957	0.918	0.922	0.932	0.926	0.894	0.926	0.913
F	1.08	-	-	1.86	1.80	1.49	1.44	1.50	1.34	1.40	1.05	1.14	0.81	1.09	0.89	0.67

* Totals corrected for F=O; CaO $\leq$ 0.03 and Cl $\leq$ 0.04 wt%. Totals for biotites also include iron proportioned to Fe_2O_3 and FeO as in structural formulae.

Japanese journals, on their characteristics (e.g., Grossman, 1972; Toraya and others, 1976; Morikawa and others, 1983). To date, however, only one other example of naturally occurring tetrasilicic mica has been documented. Robert and Maury (1979) describe a Mn-rich mica from the Charlannes comendite in the Mont-Dore massif, France, which contains only 0.36 Al^{IV} cations (as recalculated in the same way as for other micas in this study, Table III.4). Because the compositions of tetrasilicic mica occurring in the peralkaline granite at Questa are less Mn rich and represent a reasonably extensive range in Mg/Fe, the Questa occurrence is of significant interest.

Representative analyses from a set of 19 analyses in 8 samples of peralkaline granite are tabulated in Table III.4 along with corresponding structural formulae based on a standard mica recalculation scheme (11 oxygen ions). Also shown in Table III.4 are analyses of tetrasilic mica from the peralkaline rhyolite and representative analyses of the earlier biotite that has been partly replaced by tetrasilicic mica in the peralkaline granite. The tetrasilicic mica analyses were recalculated on the assumption that all iron is ferrous; Robert and Maury report that Fe^{3+} is minor in the Mont-Dore mica. Assignment of $Fe^{2+}/(Fe^{2+} + Fe^{3+})$ in the biotite was made on the basis of two measured values for compositionally identical biotite separated from samples of the early and later metaluminous granites of Virgin Canyon; values of 0.750 and 0.758 were averaged to 0.754.

Compositional ranges for the 19 analyses of tetrasilicic mica from the peralkaline granite are (weight percent): SiO_2, 43.0–49.2; Al_2O_3, 4.90–7.91; FeO^T, 7.15–18.1; MgO, 9.87–17.5; CaO, 0.00–0.07; Na_2O, 0.18–0.37; K_2O, 9.31–10.2; TiO_2, 0.85–2.41; MnO, 0.77–4.36; F, 5.1–7.9; and Cl, 0.00–0.04. Four analyses from the peralkaline rhyolite extend some of these ranges as follows: SiO_2 down to 39.9; FeO^T up to 28.5; MgO down to 3.27; Na_2O up to 0.81; K_2O down to 9.01; and MnO up to 5.05 weight percent.

Among the 19 analyses of tetrasilicic mica in peralkaline granite, Si cations in the tetrahedral site range from 3.30 to 3.65; in contrast, a search of the literature by Seifert and Schreyer (1971) revealed no reported phlogopite analysis in which Si exceeded 3.18 cations. Although Seifert and Schreyer (1971) demonstrated that $KMg_{2.5}Si_4O_{10}(OH)_2$ and $KMg_3AlSi_3O_{10}(OH)_2$ are linked by a ternary range of solid solutions, the Questa analyses show Al^{IV} content to range between 0.35 and 0.70 cation in tetrasilicic mica and 0.90 to 1.19 cations in the earlier biotite. As might be anticipated, Al^{VI} is also quite low, averaging 0.064 cation.

A plot of the sum of the octahedral cations+$1/2Al^{VI}$+Ti against Al^{IV} (fig. III.10) is designed to relate the increased charge in the tetrahedral sites caused by diminished Al content, to the overall charge decrease in the octahedral sites. In the octahedral sites there is poor correlation between Fe and Mn, which range, respectively, from 0.441 to 1.185 and 0.049 to 0.275 cations. However, Mg (1.151–1.923 cations) shows good inverse correlation with Fe+Mn ($r = -0.93$). There is also good correlation between Ti and Fe^{2+} ($r = 0.90$). Not readily explicable are rather regular decreases in Al^{VI} with increasing Al^{IV}, or in Al^{VI} and Mn with increasing octahedral-site occupancy.

The tetrasilicic micas are quite fluorine rich, as was the Mont-Dore occurrence. Among the 19 structural formulae calculated for tetrasilicic mica, F cations range from 1.20 to 1.86 and average 1.53. Fluorine generally decreases with increasing Fe content, as expected from the work of Rosenberg and Foit (1977). The same relation is found in the coexisting biotites,

which, however, contain significantly less F (0.67 to 1.14 cations). Although Seifert and Schreyer (1971) found that pure $KMg_{2.5}Si_4O_{10}(OH)_2$ is stable to 620°C at 1 kb fluid pressure, it becomes less stable with increased Fe content and at lower pressures. The extensive Japanese literature deals almost exclusively with fluorine end-member compositions which are stable at 1 atm, and it seems likely that natural tetrasilicic micas will be rich in fluorine.

The 19 analyses include 11 groups of grains hosted in alkali amphibole and 8 groups of grains in mafic aggregates. Respective average compositions of tetrasilicic mica in amphibole, as opposed to aggregates, are (weight percent): SiO_2, 47.7 and 44.7; Al_2O_3, 6.29 and 7.33; TiO_2, 1.19 and 1.81; FeO^T, 9.69 and 13.6; MnO, 2.41 and 1.79; MgO, 15.7 and 12.9; Na_2O, 0.28 and 0.32; K_2O, 9.85 and 9.66; F, 7.0 and 5.9. For both populations, reasonably good correlations exist within individual samples between Mg, Mn, and Ti in tetrasilicic mica and in alkali amphibole. The most SiO_2-rich samples of peralkaline granite contain tetrasilicic mica with the highest content of Si cations and therefore the most octahedral site vacancies. Thus, tetrasilicic mica in aggregates, which contains less Si than tetrasilicic mica enclosed in alkali amphibole, is interpreted to have formed at an earlier stage. The chemistry of the tetrasilicic mica may also be related to the chemistry of the alkali amphibole host.

3. SODIC PYROXENE CHEMISTRY

Forty-seven analyses of sodic pyroxene were obtained from 14 representative samples of the peralkaline granite. In contrast to alkali amphibole, no significant zoning was found. An indication of the range of compositions found is presented in Table III.5 and the full data set is plotted in figures III.11, III.12, and III.13. Total measured ranges are (weight percent): SiO_2, 51.7-53.0; Al_2O_3, 0.25-1.12; $Fe_2O_3^T$, 29.0-33.7; MgO, 0.00-1.08; CaO, 0.02-4.75; Na_2O, 10.1-13.2; TiO_2, 0.16-1.94; MnO, 0.17-2.03. Ideal acmite has the composition SiO_2, 52.02; Fe_2O_3, 34.56; Na_2O, 13.42. The data in Table III.5 represent average compositions for sodic pyroxene in six samples, the three taken to span the peralkaline unit in Virgin Canyon, two from the northern dikes, and one from the Canada Pinabete pluton. The analyses of Table III.5 show that sodic pyroxene in samples from the dikes tends to be richer in Ti and poorer in Mn.

Pyroxene analyses were recalculated following the scheme of Papike and others (1974) which maintains calculation on the basis of 6 oxygen anions, but assigns Fe^{2+} until a charge-balancing equation is satisfied. On this basis, Si cations range from 2.005 to 2.042 and average 2.017; octahedral-site occupancies range from 1.959 to 1.995 and average 1.983 cations (Si cations in excess of 2.000 are included in these values).

The range of sodic pyroxene compositions in terms of acmite and "other components" is shown in figure III.11. As indicated, the compositions of pyroxene in the three samples which span the peralkaline screen in the Virgin Canyon pluton, span the range of measured compositions. Deviation from the reference lines in figures III.11, and III.12, as well as calculation of Si cations in excess of 2.000, are the indications of octahedral-site vacancies or low Na_2O values. Note that in the two plots, Si cations in excess of 2.000 have been included in the octahedral-site summations.

Table III.5. Averaged electron microprobe analyses, with structural formulae, for sodic pyroxene.

	Virgin Canyon pluton			Canada Pinabete pluton	Northern dikes	
	83QC30 (2)	83QC29 (3)	83QC38 (3)	82QC49 (3)	Q83J72 (3)	Q83J76 (3)
SiO_2	53.0	52.2	52.1	52.8	52.9	52.4
Al_2O_3	0.36	0.30	0.39	0.35	0.91	0.41
$Fe_2O_3^T$	33.1	32.2	29.2	32.2	32.4	31.8
MnO	0.47	1.55	1.72	0.44	0.23	1.01
MgO	0.01	0.43	1.05	0.01	0.01	0.09
TiO	0.22	0.21	0.63	0.62	0.94	1.36
CaO	0.12	1.81	4.65	0.13	0.04	0.74
Na_2O	13.1	11.8	10.2	12.5	13.1	12.4
Total	100.38*	100.50	99.94	99.05	100.53	100.21
Si	2.020	2.008	2.018	2.037	2.014	2.024
Al	0.016	0.014	0.018	0.017	0.041	0.019
Fe^{3+}	0.939	0.855	0.711	0.882	0.872	0.831
Fe^{2+}	0.011	0.079	0.140	0.054	0.057	0.093
Mn	0.015	0.051	0.056	0.014	0.007	0.033
Mg	0.001	0.025	0.061	0.001	0.001	0.005
Ti	0.006	0.006	0.018	0.018	0.027	0.040
Ca	0.005	0.075	0.193	0.005	0.000	0.004
Na	0.968	0.880	0.766	0.935	0.967	0.929
Sum oct.**	1.981	1.993	1.981	1.963	1.986	1.978

* For all Fe as Fe_2O_3; $K_2O \leq 0.03$.
** Includes Si in excess of 2.000.

Figure III.12 shows that the excess charge in the M2 site is not totally balanced by Na in M1. In this plot the four most deviant points relate to magnetite-free sample 82QC49 in which the measured values of Na_2O are atypically low (Table III.5).

Plots based on the pyroxene structural formulae show that there are no relations between Ca and Al, Ca and Ti, Mg and Ti, or Fe and Ti contents. As shown by figure III.13, the $CaMgSi_2O_6$, $CaFeSi_2O_6$, and $CaMnSi_2O_6$ end members account for the Ca in these pyroxenes; Ca and Mg are related on a 3:1 basis ($r = 0.99$). The two somewhat distinct trends shown by the plot reflect almost exclusively the fact that there is a group of 18 analyses for which Fe^{2+} increases from 0.00 to 0.09 cation while Ca remains below 0.01 cation. Mn content ranges only up to 0.07 cation. The acmitic component of these pyroxenes is so dominant that whereas calculated Fe^{2+} and Mn increase according to a reasonably good relation, a similarly good correlation exists between increasing Mn and decreasing Fe^{T} contents.

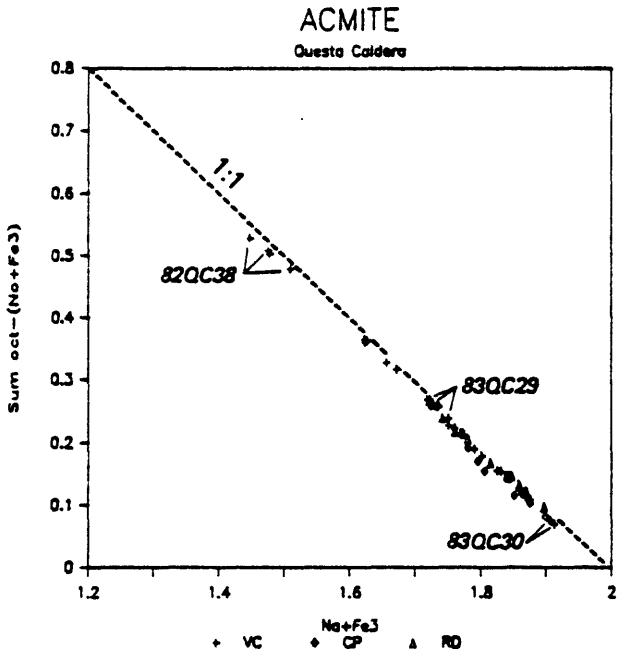

Fig. III.11.

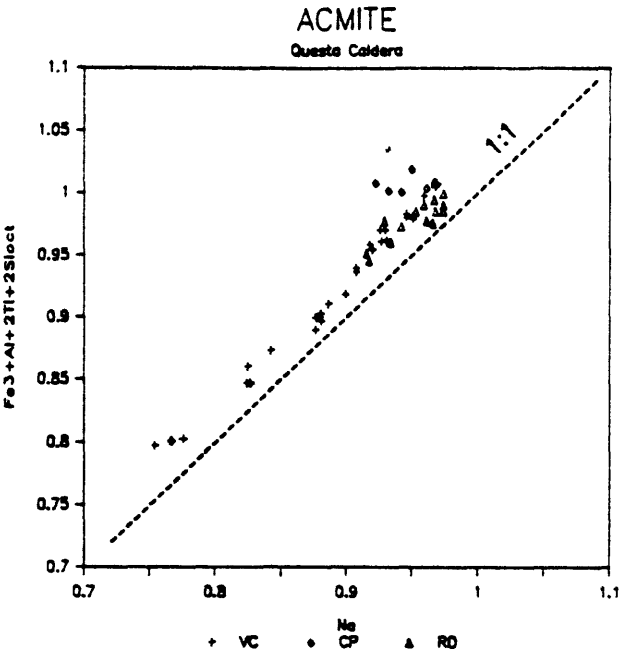

Fig. III.12.

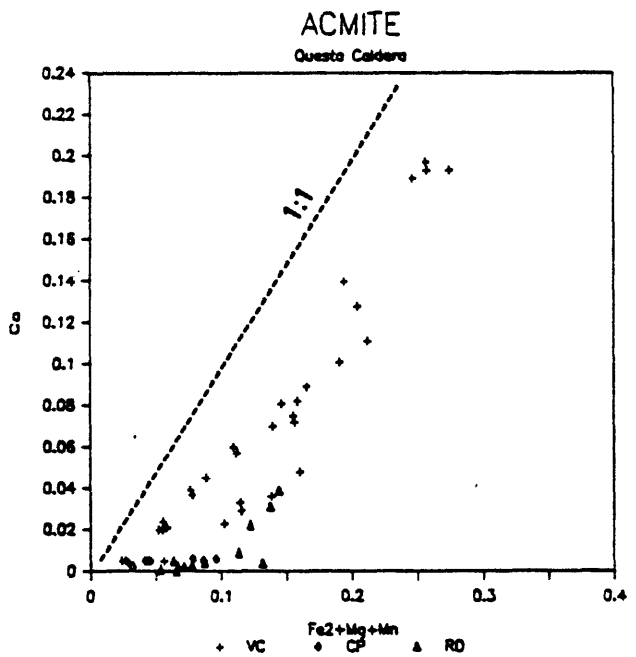

Fig. III.13

Fig. III.11. Range of composition for sodic pyroxenes (cations) in terms of acmite and "other components." Sample numbers shown are for Virgin Canyon section. 1:1 correlation line shown for reference. Symbols as in fig. III.2.

Fig. III.12. Na (cations) against "effective trivalent octahedral-site occupancy" for sodic pyroxenes. 1:1 correlation line shown for reference. Symbols as in fig. III.2.

Fig. III.13. Fe^{2+} + Mg+Mn against Ca (cations) for sodic pyroxenes. 1:1 correlation line shown for reference. Symbols as in fig. III.2

Mao (1971), Wood and Henderson (1978), and Smyth (1980) have discussed the occurrence of vacancies in the M1 and M2 sites of pyroxenes. They, and others, have shown that vacancies are favored by high alumina content, high pressure, and high activity of SiO_2. In the high-SiO_2-activity environment of the peralkaline units at Questa, vacancies are prominent in alkali amphiboles and tetrasilicic mica. It is equivocal as to whether they exist in the sodic pyroxenes, but the possibility should be further explored. A significant consideration is that because Si fills the tetrahedral sites, there is no opportunity for charge balancing between the tetrahedral and octahedral sites.

CONCLUSIONS

The mafic-mineral assemblage of the high-level, high-silica peralkaline granites at Questa is entirely compatible with knowledge of other high-level granitic plutons in rifting environments and with experimental studies on alkali amphiboles, tetrasilicic mica, and acmite. Alkali granite from the Oslo area, as represented by samples 144, 260, and 743 of Neumann (1976), is of similar composition to the peralkaline granites and contains alkali amphibole and sodic pyroxene of nearly indistinguishable composition.

Ernst (1962) has shown that riebeckite-arfvedsonite is stable up to 610°C at 500 bars fluid pressure at fO_2 defined by the quartz-fayalite-magnetite buffer and Bailey (1969) has shown that acmite is stable at 700°C and 2kb over the total range of fO_2 bounded by the iron-wustite and hematite-magnetite buffers. Bailey concluded that arfvedsonitic amphibole is the stable phase under severely reducing conditions and that mixed assemblages of arfvedsonite-acmite may indicate a lower degree of peralkalinity in the magma or a slightly higher fO_2. He noted also that fluctuating crystallization of acmite and arfvedsonite "... may have been controlled simply by fluctuating oxidation conditions in the magma." A most interesting aspect of our study is that the assemblage acmite-arfvedsonitic amphibole has formed at relatively high fO_2 due to stabilization of the alkali amphibole by substitution of F, Mg, and Mn. These substitutions also account for the presence of these iron-rich alkali amphiboles in the peralkaline rhyolite and high-level porphyry, environments of low fluid pressure in which Ernst (1962, p.732) predicted these amphiboles would be unstable. The relatively high $Fe^{3+}/(Fe^{2+} + Fe^{3+})$ determined for the alkali amphiboles at Questa is consistent with their crystallization along a relatively oxidizing buffer curve involving ilmenite and sphene.

Charles (1975, 1977) has established that richterite and ferrorichterite have extensive ranges of magmatic stability at temperatures above those of arfvedsonitic amphiboles. As temperature fell and peralkalinity increased due to feldspar crystallization (Thompson and MacKenzie, 1967), the stable alkali amphibole shifted to significantly less calcic and magnesian compositions, with relatively modest increase in Na content. Biotite first reacted slightly to form a thin Al-depleted rim and then started to break down to fluor-tetrasilicic mica which is stable at low pressure. Tetrasilicic mica also replaced early, more calcic alkali amphibole, but crystallized in equilibrium with alkali amphibole characterized by relatively high $Fe^{3+}/(Fe^{2+} + Fe^{3+})$ and octahedral-site vacancies.

PART II: BIOTITE AND CALCIC AMPHIBOLE

OCCURRENCE

1. VIRGIN CANYON

Biotite is the only mafic silicate present in the early and later metaluminous granites of Virgin Canyon. It constitutes 1.3 to 3.6 volume percent of the early metaluminous granite. In the porphyritic facies, nearest the peralkaline unit, biotite is found both as phenocrysts (up to 0.5 X 1.8 mm) and in the groundmass (<0.2 mm across). Pleochroism is from light green or yellow-brown to dark-green brown. Phenocrysts have a general euhedral to subhedral shape, with irregular margins; they often enclose apatite, opaque oxides, and rarely zircon. Biotite can be found enclosed in plagioclase or alkali feldspar. Phenocrysts are commonly zoned, with an irregular darker core in sharp contact with a lighter rim (Plate III.2, a). They may show an irregular reaction rim with feldspars. Biotite in the groundmass is rather anhedral and is usually free of inclusions.

In the more equigranular facies, biotite ranges from 0.1 mm across to 0.6 X 3.6 mm. Biotite characteristics are essentially the same as in the porphyritic facies (color, zoning, inclusions, reaction rims with feldspars, enclosed in feldspars), however its shape is usually more euhedral. Rarely, chlorite formed after biotite. Biotite occurs as long plates (Plate III.2, b) in samples from near the contact with the later metaluminous granite.

Biotite is less abundant in the later metaluminous granite (1.0 to 1.4 vol%); it ranges from 0.01 mm across up to 0.4 X 1.7 mm. It can be euhedral to anhedral, with a reaction rim against plagioclase or alkali feldspar. Biotite can be enclosed in feldspars. Pleochroism is the same as in the early metaluminous granite. Inclusions (apatite, opaque oxides, rare zircon) are not abundant. Biotite is also found as aggregates of grains or as radiating aggregates (filling small cavities). Although not commonly chloritized, it is more so than in the early metaluminous granite.

2. CANADA PINABETE

In finer grained samples biotite is rather sparse (0.7 to 1.3 vol%). It is present as rather small (to 0.3 mm across), subhedral to anhedral grains, light yellow-brown to darker green-brown. They may be zoned, with a dark irregular core and a lighter rim. These grains may contain rare inclusions of apatite, opaque oxides, and zircon. Less commonly biotite occurs as thin plates, up to 0.25 X 2.8 mm in sections perpendicular to (001).

Muscovite is common as radiating grains in cavities, usually 0.3 to 0.5 mm long, and also occurs in the rock (0.1 to 0.2 mm long).

In coarser grained samples, biotite is more abundant (1.6 to 3.0 vol%). Biotite is subhedral to anhedral, ranges in size from 0.1 to 0.5 mm across, and can be up to 2 mm long. Crystals are often zoned and show a dark

irregular core in sharp contact with a lighter colored rim. Pleochroism is the same as in the finer grained facies. Biotite may contain inclusions of apatite and opaque oxides. The two magnetite-free samples (82QC48 and Q83J88) are characterized by large interstitial biotite grains, which seem to have crystallized after plagioclase and quartz (Plate III.2, c). In 82QC48 some crystals show irregular zoning with a lighter core and a darker rim. Also notable in this sample is the presence of amphibole which is rather anhedral and may enclose biotite (Plate III.3, c).

3. RITO del MEDIO

Biotite and muscovite are the typical mafic silicates in the granite of Rito del Medio. Except in the border facies near Precambrian rocks, biotite constitutes less than 0.5 volume percent. It is less abundant than muscovite in equigranular samples and more abundant than muscovite in granophyric samples.

Biotite is rather subhedral, locally with irregular margins. It is pleochroic from light brown to darker brown, sometimes with a more distinct green color. Its size is quite typically around 0.15 mm, locally up to 0.2 X 1 mm. Zoning exists but is not sharp; rims are lighter than cores. Inclusions are not abundant and apatite is most common. Biotite can be found enclosed in plagioclase, alkali feldspar, and quartz.

Near the contact with Precambrian andesite, biotite is locally more abundant (>1 vol%). There, it is unzoned and forms thin sheets which look like needles in thin section perpendicular to (001) (Plate III.2, c). These needles can be up to 3 mm long and only 0.04 mm wide. The (001) section of these biotites is wider (0.5 mm).

PLATE III.2: Photomicrographs of occurrences of biotite in the Questa granitic plutons.

(a) Zoned biotite showing sharp contact between darker, more iron-rich core and lighter, more magnesium-rich rim. Early metaluminous granite of Virgin Canyon, sample 82QC40. Bar is 0.5 mm long.

(b) Long plates of biotite in a polygonal arrangement in quenched granite. Early metaluminous granite of Virgin Canyon, sample Q83J78A2. Bar is 1 mm long.

(c) Late interstitial biotite. Magnetite-free granite of Canada Pinabete, sample 82QC48. Bar is 0.5 mm long.

(d) Euhedral cleavage flake of mica containing biotite core and muscovite rim. Vug, Rito del Medio granite. Bar is 1 mm long.

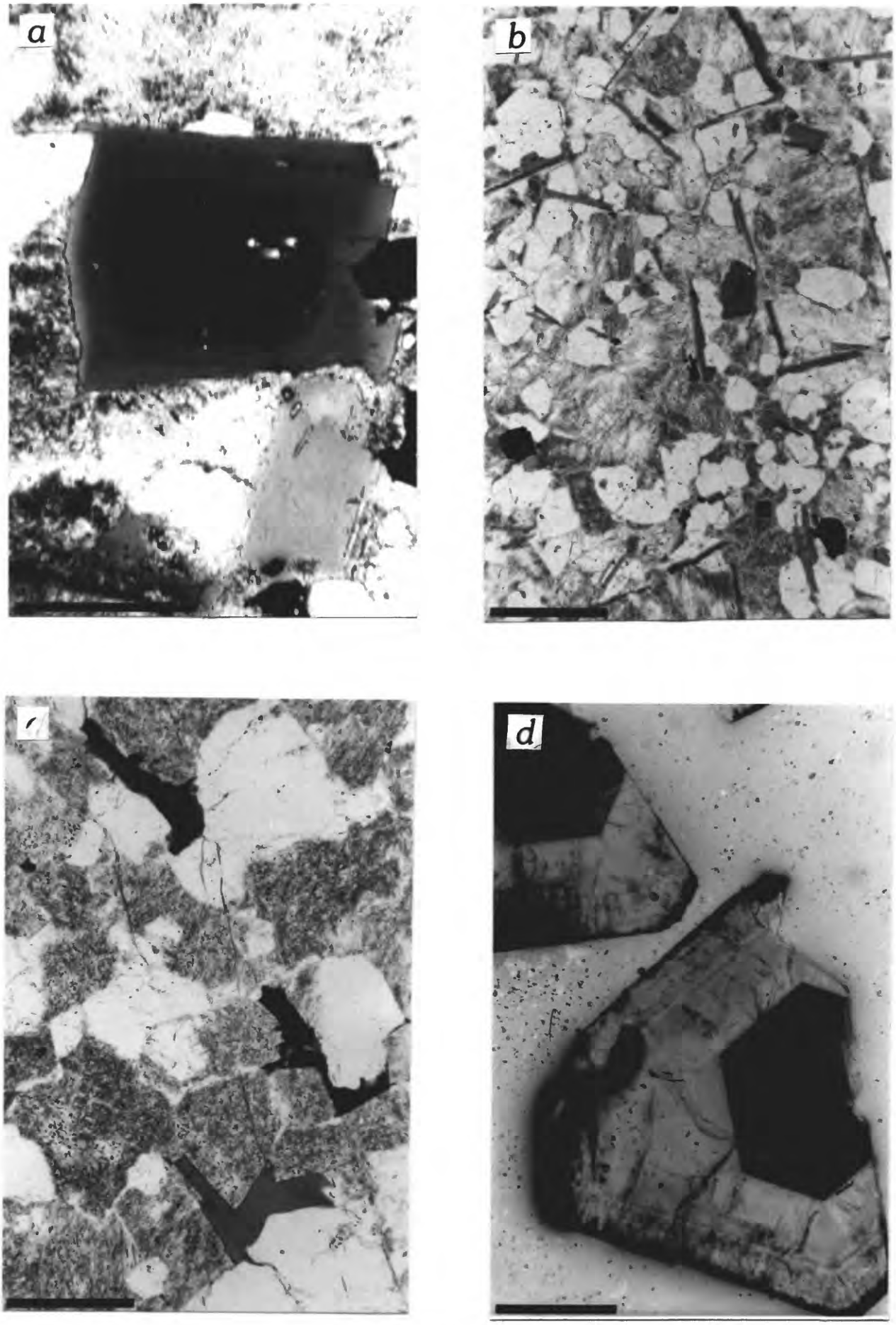
a
b
c
d

Muscovite occurs most commonly in cavities, but in equigranular samples it occurs in the rock as well. Outside the cavities muscovite is subhedral and may or may not show irregular margins. It looks fresh and primary, and can be enclosed in quartz or feldspar; grains are typically a few tenths of a millimeter long. Muscovite in cavities has two types of occurrence; as radiating aggregates (rosettes) commonly up to 2 mm across and 1.5 mm high, or as "books" to 4 mm thick perpendicular to (001) and 3 mm across parallel to (001). Such crystals are free of inclusions, but may contain a biotite core (Plate III.2, d).

4. CABRESTO LAKE

Biotite and amphibole are both present in the typical facies of the granite of Cabresto Lake. In the border facies, both near the Weary Willie mine and south of Cabresto Creek, biotite is the only mafic silicate present, except for some rare remnants of amphibole in 83QC17.

Biotite constitutes 3.2 to 4.8 volume percent of the typical facies. It is euhedral to subhedral, occasionally anhedral, especially in sections parallel to (001). It contains many inclusions; apatite is most abundant, opaque oxides are common, and zircon is more rare. Globular sphene is rarely partially enclosed in biotite. Biotite is pleochroic from light brown to darker orange-brown and ranges in size from 0.1 mm across up to 2.8 X 3.5 mm. Biotite can locally be found in clots. It is commonly altered to chlorite.

Biotite forms 1.5 to 2.5 volume percent of the border facies and occurs both as phenocrysts (up to 0.5 X 1.5 mm) and in the groundmass (down to 0.05 mm across). It is rarely zoned, with a darker indistinct core. Biotite can be enclosed in plagioclase or quartz phenocrysts. It is commonly partially chloritized. Apatite inclusions are common and abundant. In samples from south of Cabresto Creek, fine-grained biotite also occurs in aggregates with quartz. The aggregates have a lozenge shape and can be up to 1.6 mm across Plate III.3, a).

PLATE III.3: Photomicrographs of occurrences of biotite and amphibole in the Questa granitic plutons.

(a) Lozenge-shaped aggregate of biotite and quartz. Border facies of the granite of Cabresto Lake, sample 83QC18. Bar is 0.5 mm long.

(b) Reaction rim between biotite and feldspar. Granodiorite of Rio Hondo, sample 82QC26. Bar is 0.5 mm long.

(c) Interstitial amphibole containing biotite inclusions (lighter). Magnetite-free granite of Canada Pinabete, sample 82QC48. Bar is 0.5 mm long.

(d) Fresh, well-formed biotite grains enclosed in euhedral amphibole. Granodiorite of Rio Hondo, sample 82QC26. Bar si 0.5 mm long.

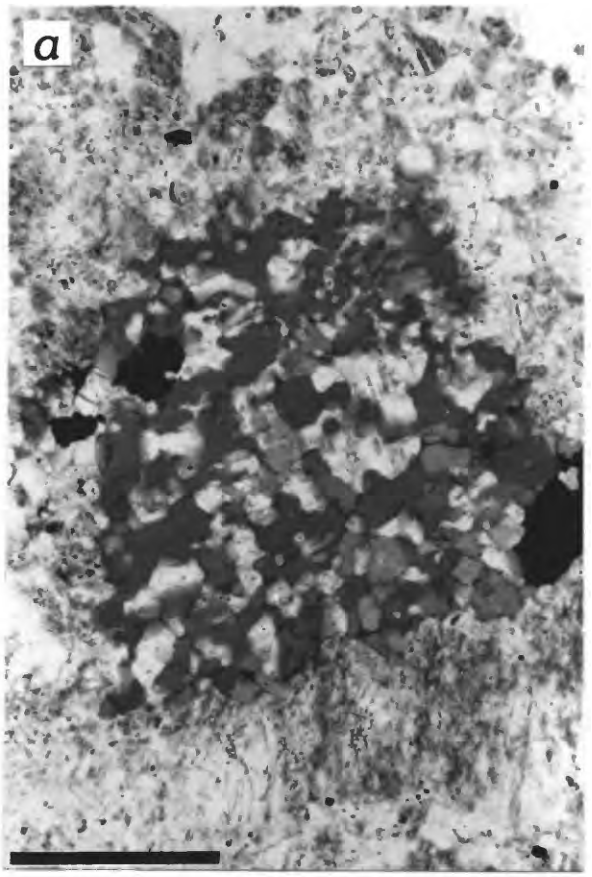
a

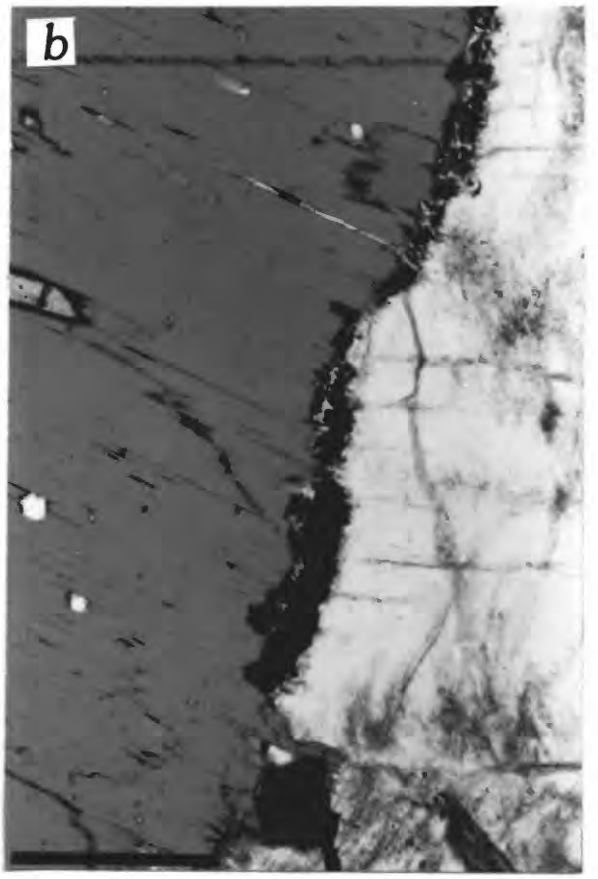
b


c

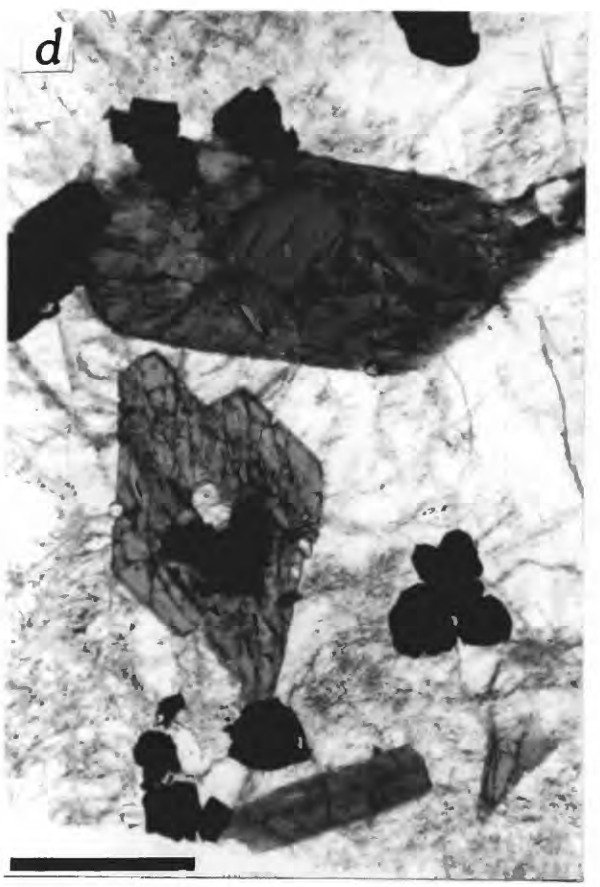
d

Amphibole is characteristic of the typical facies. It is not abundant (always <1 vol%) and forms large euhedral crystals (to 3.2 mm across in lozenge-shaped sections, 1.3 X 4.8 mm for elongated sections), as well as smaller grains (0.4 mm across). Amphibole is slightly pleochroic with light green colors. It contains many inclusions such as apatite, sphene, opaque oxides, zircon, and biotite (Plate III.3, d). Amphibole is often chloritized along cleavages, and margins can be reacted to chlorite and biotite.

Both biotite and amphibole occur in the mixed facies; biotite is more abundant in more silicic samples (<10 vol% mafic minerals), while amphibole is more abundant in more mafic samples (>10 vol% mafic minerals).

Biotite forms euhedral to subhedral phenocrysts (to 1.2 X 2.2 mm) as well as small grains in the groundmass (0.03 mm across); pleochroism is from light yellow-brown to darker orange-brown. Biotite can be zoned with a darker irregular core, but the zoning is not as sharp as in the metaluminous granites of Virgin Canyon and Canada Pinabete. Phenocrysts contain common inclusions of apatite, opaque oxides, and zircon.

Amphibole is found as very euhedral phenocrysts (to 1.3 X 3 mm) containing sphene, apatite, opaque oxides, and biotite. Biotite may also occur along cleavages. Amphibole phenocrysts can be zoned with a dusty core surrounded by a clear rim. Pleochroism is from light yellow-green to darker green. Amphibole occurs in the groundmass as well, as nice euhedral crystals (0.05 mm across).

Both biotite and amphibole are found as small crystals surrounding large quartz xenocrysts.

In biotite-bearing enclaves in the typical facies of the granite (82QC51b) biotite is subhedral, rarely zoned, and relatively free of inclusions; it is typically 0.05 mm across. In biotite-bearing enclaves in the border facies of the granite (83QC16 and 83QC17) biotite grains are larger (0.2 to 0.3 mm across) and commonly chloritized. In biotite-bearing enclaves in the mixed facies (83QC14) biotite and a little amphibole are present. Biotite is usually anhedral and 0.2 mm across, often chloritized. Amphibole is smaller (0.1 mm across) and rather euhedral.

In amphibole-bearing enclaves amphibole is predominant. It occurs as small (0.2 X 0.6 mm) rather rounded phenocrysts, often containing opaque oxides. The phenocrysts can be isolated or in clots with plagioclase or biotite. Amphibole also occurs in the groundmass, as small elongated (0.03 X 0.2 mm) rather euhedral grains. Biotite can be up to 0.6 mm across as phenocrysts, and down to 0.03 mm in the groundmass; phenocrysts contain apatite inclusions and are zoned.

5. RIO HONDO

Biotite and amphibole are typical mafic silicate phases in the granodiorite of Rio Hondo. Biotite amounts 4 to 7 volume percent. It can be found as large (to 2 X 4 mm) euhedral to subhedral phenocrysts, as well as small crystals (0.1 mm across); reaction rims against feldspars are common (Plate III.3, b). Biotite does not show any zoning and is not commonly chloritized; it is pleochroic from light orange to dark brown and commonly contains inclusions of apatite, opaque oxides, sphene, and zircon.

Amphibole is often more abundant than biotite (3 to 10 vol%). It can range in size from small (0.2 mm across) euhedral crystals to large (lozenge-shaped sections to 2.8 X 5.6 mm), very euhedral, light yellow-green to darker grass-green phenocrysts. Inclusions are common; apatite is less abundant and opaque oxides are more abundant than in biotite. Biotite is commonly enclosed in amphibole (Plate III.3, d) and can occur locally as a core to relatively small (0.2 X 1.2 mm) amphibole grains. Amphibole also occurs in clots with opaque oxides; clots can be up to 4 mm across, amphibole 0.1 to 0.2 mm across.

In the silicic granite, biotite is the only mafic silicate; it constitutes 1.5 to 2.5 volume percent of the rock. Its color is usually more orange than in the granodiorite, sometimes greenish as in samples taken near the contact with the Precambrian roof rocks. Euhedral to subhedral biotite ranges from 4 mm long down to 0.2 mm across; 0.07 mm in the groundmass of porphyritic samples located near the roof zone. Zoning is rare and usually characterized by a lighter thin rim; there can be a reaction rim against feldspars. Inclusions of apatite, sphene, opaque oxides, and zircon are common. Chlorite after biotite is rather common, sometimes replacing whole grains. Rarely biotite has been found in clots with opaque oxides.

Biotite plus amphibole may total more than 30 volume percent in mafic-magmatic enclaves; biotite is always predominant over amphibole (15 to 30 and 1 to 20 vol% respectively). Biotite occurs as small (0.6 X 1.6 mm) subhedral phenocrysts, but is mainly found as a subhedral to anhedral groundmass mineral (0.04 to 0.1 mm). Pleochroism is the same as in the granodiorite (light orange to dark brown). Inclusions of apatite are the most common. In some cases, minor reaction to chlorite has occurred. In the amphibole-poor enclave (82QC28), biotite occurs as clots as well as grains in the groundmass (0.1 to 0.3 mm) and inclusions of acicular apatite are common.

Amphibole, except in 82QC28, forms 11 to 20 volume percent of the enclaves. It can be found as anhedral, rather rounded, grass-green to brown-green phenocrysts (1.2 X 1.7 mm). Inclusions are of sphene, opaque oxides, and minor biotite. Amphibole also occurs as clots of small grains (0.08 mm across) with opaque oxides, and in the groundmass as more euhedral crystals 0.04 to 0.1 mm across.

Study of a schlieren shows that the morphology of biotite and amphibole is quite different from that in mafic-magmatic enclaves. Both minerals occur as euhedral large crystals (to 2 X 3.8 mm for amphibole, to 1 X 2 mm for biotite) and as smaller grains, usually around 0.2 mm across. Reaction rims between feldspar and biotite are well developed.

6. BEAR CANYON

Biotite constitutes 0.6 to 1.9 volume percent of the Bear Canyon granite. It is light yellow to light green to brown, usually subhedral, and ranges in size from 0.08 mm across to 0.6 X 1.4 mm. It is often zoned with a darker irregular core, or with darker patches within a lighter grain. Inclusions of apatite and opaque oxides are common, and fine needles of rutile are also found.

7. SULPHUR GULCH

In the carapace unit as well as in the source aplite, mafic silicates are mostly reacted to chlorite, sericite, and calcite. A few remnants of biotite still exist in the cores of former phenocrysts (to 1.4 X 2.4 mm) or as smaller crystals.

8. RED RIVER

Biotite and amphibole amount to 15 volume percent in the granodiorite of the Red River intrusive complex. As in the granodiorite of Rio Hondo, amphibole (9.2 vol%) is more abundant than biotite (5.6 vol%). Biotite forms large (1.7 X 2.6 mm) as well as small (to 0.1 mm), euhedral to subhedral, light yellow-brown to orange-brown crystals. Biotite is not zoned and is often altered to chlorite. Inclusions of apatite and opaque oxides are common, and feldspars are also enclosed in biotite.

Amphibole is found as light to bright green, subhedral to euhedral, crystals, as large as 0.8 X 2.8 mm and as small as 0.1 mm across. It is rarely zoned with a dusty core. Inclusions are opaque oxides and biotite, more rarely apatite.

The granite of Red River contains only biotite (2 to 8 vol%), in two types of occurrence. One is as subhedral to anhedral crystals, 0.1 mm across to 0.5 X 1.4 mm. Larger crystals can be zoned with a darker irregular core and a lighter rim, and contain inclusions of apatite and opaque oxides. Smaller crystals are usually larger than the size of the groundmass and can be found enclosed in feldspars. The second occurrence is as aggregates (to 1.4 X 3.8 mm) of laths (to 0.1 mm) with quartz (Plate III.3, a). In both cases, biotite is rather orange in color.

The alkali-feldspar granite contains little biotite (0.6 vol%) as yellow-brown to green to darker orange-brown subhedral crystals which range from 0.1 mm across to 0.4 X 0.8 mm; no zoning is noticeable. Biotite may contain apatite, opaque oxides, and zircon.

The quartz diorite contains more than 10 volume percent biotite as the only mafic silicate. It occurs as long plates, or as more blocky crystals, both as small subhedral phenocrysts (0.2 X 2 mm) and rather anhedral grains in the groundmass (0.05 X 0.5 for long crystals, 0.1 X 0.3 for others). None of the types of biotite is zoned. Inclusions of apatite and opaque oxides are characteristic.

In the small enclaves in the granite, biotite occurs as long (to 0.4 X 6 mm) broken plates or as subhedral to anhedral crystals 0.1 to 0.6 mm across. Zoning is common and often irregular; pleochroism is from light yellow-brown to slightly green to darker orange-brown. Typical inclusions are opaque oxides and apatite.

9. LUCERO PEAK

Biotite is the only mafic silicate in the Lucero Peak granite and amounts to 1.2 to 2.6 volume percent; it is mostly subhedral and ranges in size from 0.1 mm across to 2.2 X 2.4 mm. Pleochroism is from light brown-yellow to light green to green-brown. Biotite can be zoned with a quite indistinct darker core, and it is rarely altered to chlorite. Apatite, opaque oxides, allanite, and zircon are found as inclusions, sphene can be partially enclosed in biotite.

BIOTITE CHEMISTRY

The 150 biotite analyses which constitute the data base for the following discussion represent an even larger group of 345 individual analyses (Table III.6); the reduction in number was accomplished by averaging analyses of grains of essentially identical composition within an individual sample. This extraordinary number of analyses, obtained from 90 samples, was considered essential to fully appreciate and document the variation in biotite chemistry among the nine plutons, especially because all but the Bear Canyon and Lucero Peak plutons are characterized by multiple facies or units and because biotite displays compositional zoning in many samples. All discussion and plots in this report represent either the data set of 150 analyses, or that portion of this data set presented in Table III.7.

Biotite separates were made from 22 samples, representing those facies of each pluton for which high quality separates could be obtained; analyses for F, H_2O^+, FeO, and FeO^T are presented in Table III.8. With four notable exceptions $Fe^{2+}/(Fe^{2+}+Fe^{3+})$ ranges from 0.75 to 0.87. Measured values of $Fe^{2+}/(Fe^{2+}+Fe^{3+})$ listed in Table III.8 were applied to values for total iron measured with the electron microprobe. Because of biotite zoning, this procedure represents an approximation even when a ratio is applied to analyses for the same sample from which the separate was obtained. Because biotite of core composition is predominant in most samples, measured $Fe^{2+}/(Fe^{2+}+Fe^{3+})$ is considered most appropriate to core compositions. Application of a single or average ratio to all analyses from a facies or pluton has generally been straightforward and is considered superior to allowing assignment of $Fe^{2+}/(Fe^{2+}+Fe^{3+})$ by a charge-balancing recalculation scheme. Unusual applications of these measured ratios are discussed individually.

Table III.6. Indication of unit representation for biotite analyses.

PLUTON/ Unit	FULL DATA SET Samples	Analyses	Number in 150
VIRGIN CANYON			
Peralkaline granite	3	10	3,8*
Early metaluminous granite	9	65	9,20
Late metaluminous granite	5	12	5,10
Rhyolite dike	1	4	1,1
NNE-trending dike	1	2	1,1
Ring dike	1	1	1,1
CANADA PINABETE			
Typical granite	12	50	11,22
Magnetite-free granite	3	12	3,10
RITO del MEDIO			
Typical granite	5	18	5,9
Border facies	2	8	2,3
CABRESTO LAKE			
Typical granite	4	13	4,6
Border facies	3	12	3,5
Mixed	1	5	1,1
Biotite-bearing enclaves	3	5	3,4
Amphibole-bearing enclaves	1	5	1,2
RIO HONDO			
Granodiorite	9	26	9,9
Granite	6	22	6,8
Enclave in granodiorite	4	13	4,4
Schlieren in granodiorite	1	5	1,1
Quartz latite dike	1	5	1,1
BEAR CANYON	2	7	2,3
SULPHUR GULCH			
Carapace	2	4	2,3
Source aplite	4	6	4,6
RED RIVER INTRUSIVE COMPLEX			
Granodiorite	1	3	1,1
Granite	2	10	2,5
Alkali-feldspar granite	2	9	2,2
Enclave in granite	1	2	1,1
Quartz diorite	1	4	1,1
LUCERO PEAK	2	7	2,2

* Number of samples, number of analyses.

Table III.7. Representative electron microprobe analyses and structural formulae for biotites in the Questa granitic rocks.

	Peralkaline granite				VIRGIN CANYON PLUTON Early metaluminous granite			Rhyolite dike	Late metaluminous granite	
	83QC29		82QC38.1							
	Core 11**	Rim 11	Core 6	Rim 6	Core (3,6)***	Rim (4,11)	Late (2,5)	83QC31 (4)	Core (4,5)	Rim (4,5)
SiO_2	39.2	41.8	37.0	41.8	36.7	40.4	41.2	41.6	37.6	40.1
Al_2O_3	14.2	12.4	13.4	11.1	13.4	12.2	11.2	11.4	13.2	12.3
TiO_2	3.16	2.46	4.62	2.64	3.79	1.68	0.90	1.32	3.17	2.02
Fe_2O_3	3.69	2.95	4.40	3.04	4.15	3.44	3.07	3.16	4.32	3.58
FeO	10.2	8.14	12.1	8.37	11.6	9.66	8.64	8.86	11.6	9.68
MnO	0.52	0.44	1.35	1.66	1.69	1.48	1.69	0.66	1.58	1.38
MgO	13.9	15.9	12.1	16.2	13.7	16.8	18.4	18.4	14.3	16.8
Na_2O	0.33	0.30	0.38	0.35	0.40	0.31	0.35	0.10	0.38	0.27
K_2O	9.77	9.97	9.60	9.53	8.94	9.65	9.79	9.92	9.27	9.84
F	4.5	4.9	3.4	4.7	4.0	4.8	4.4	-	4.2	4.8
Cl	0.04	0.03	0.04	0.03	0.08	0.06	0.04	-	0.07	0.04
	94.97*	94.36	94.95	94.69	94.37	95.24	95.24	95.42	95.42	95.97
Si	2.901	3.063	2.799	3.073	2.799	2.970	3.027	3.035	2.817	2.943
Al^{IV}	1.099	0.937	1.195	0.927	1.201	1.030	0.970	0.965	1.166	1.057
Fe^{3+IV}	-	-	0.006	-	-	-	0.003	-	0.017	-
Al^{VI}	0.139	0.134	-	0.036	0.004	0.028	-	0.016	-	0.007
Fe^{3+VI}	0.205	0.163	0.244	0.168	0.238	0.190	0.161	0.174	0.227	0.198
Fe^{2+}	0.630	0.499	0.768	0.515	0.740	0.594	0.531	0.541	0.727	0.594
Mg	1.533	1.737	1.364	1.776	1.489	1.841	2.015	2.001	1.597	1.838
Ti	0.176	0.136	0.263	0.146	0.217	0.093	0.050	0.072	0.179	0.112
Mn	0.033	0.027	0.086	0.103	0.109	0.092	0.105	0.041	0.100	0.086
Sum oct.	2.716	2.696	2.725	2.744	2.798	2.838	2.868	2.845	2.846	2.835
Na	0.047	0.043	0.056	0.050	0.059	0.044	0.050	0.014	0.055	0.038
K	0.922	0.932	0.926	0.894	0.870	0.905	0.918	0.923	0.886	0.921
F	1.05	1.14	0.98	1.09	0.97	1.12	1.02	-	0.99	1.12
Fe/(Fe+Mg)	0.353	0.276	0.427	0.278	0.396	0.299	0.258	0.263	0.378	0.301

* Not including F and Cl.

** Identification of grain analyzed.

*** Number of samples, analyses represented by average.

Table III.7--continued.

	CANADA PINABETE PLUTON									
	Typical granite			Magnetite-free granite						
			84QC1	82QC48			Q83J88			
	Core (3,9)	Rim (3,8)	(7)	Stage 1	Stage 2(3)	Stage 3(2)	Core 4	Rim 4	Core 2	Rim 2
SiO_2	37.2	40.2	40.2	40.5	38.1	39.3	38.4	37.2	35.4	38.0
Al_2O_3	13.1	11.8	11.9	12.0	11.9	12.3	11.7	11.8	13.4	12.1
TiO_2	3.33	1.97	1.35	2.01	2.21	2.15	1.67	1.75	3.54	1.83
Fe_2O_3	3.65	2.89	2.71	4.69	7.22	5.39	6.30	8.06	9.11	6.29
FeO	13.1	10.4	9.81	11.3	17.3	13.0	15.1	19.4	21.9	16.8
MnO	1.23	1.06	2.74	0.90	0.78	0.83	1.76	1.94	2.14	1.78
MgO	13.6	16.8	15.6	15.6	9.35	13.9	11.3	6.85	2.38	9.10
Na_2O	0.31	0.24	0.31	0.33	0.19	0.32	0.33	0.20	0.13	0.19
K_2O	9.43	9.70	9.83	9.57	9.13	9.52	9.27	8.92	8.68	9.17
F	4.3	5.3	-	3.5	1.6	3.7	4.1	1.4	2.6	3.3
Cl	0.08	0.09	-	0.07	0.28	0.12	0.05	0.32	0.08	0.10
	94.95	95.06	94.45	96.90	96.18	96.71	95.83	96.12	96.68	95.26
Si	2.817	2.977	3.011	2.961	2.913	2.914	2.927	2.903	2.791	2.935
Al^{IV}	1.169	1.023	0.989	1.034	1.072	1.075	1.051	1.086	1.209	1.065
Fe^{3+IV}	0.014	-	-	0.005	0.015	0.011	0.022	0.011	-	-
Al^{VI}	-	0.007	0.061	-	-	-	-	-	0.037	0.037
Fe^{3+VI}	0.194	0.161	0.153	0.253	0.400	0.290	0.339	0.462	0.541	0.366
Fe^{2+}	0.830	0.644	0.614	0.690	1.107	0.803	0.964	1.263	1.444	1.085
Mg	1.535	1.854	1.742	1.700	1.066	1.537	1.284	0.797	0.280	1.048
Ti	0.190	0.110	0.076	0.111	0.127	0.120	0.096	0.103	0.210	0.106
Mn	0.079	0.066	0.174	0.056	0.051	0.052	0.114	0.128	0.143	0.116
Sum oct.	2.841	2.843	2.820	2.810	2.751	2.802	2.797	2.753	2.655	2.759
Na	0.046	0.034	0.045	0.047	0.028	0.046	0.049	0.030	0.020	0.028
K	0.911	0.916	0.939	0.893	0.891	0.901	0.901	0.888	0.873	0.904
F	1.03	1.24	-	0.81	0.39	0.87	0.99	0.35	0.65	0.81
Fe/(Fe+Mg)	0.403	0.303	0.306	0.358	0.588	0.418	0.508	0.685	0.876	0.581

Table III.7—continued.

	RITO del MEDIO PLUTON						
	Typical				Border facies		
	82QC16		82QC17		82QC19		82QC22
	Core (4)	Rim	Core (3)	Rim	Core (2)	Rim (2)	(4)
SiO_2	39.4	40.7	39.7	40.8	38.8	40.2	39.5
Al_2O_3	14.9	13.9	14.8	15.9	12.9	12.5	11.9
TiO_2	1.95	1.28	1.92	1.16	1.97	1.42	2.40
Fe_2O_3	2.24	1.96	2.24	1.99	2.24	1.98	4.86
FeO	10.1	8.84	10.1	9.01	10.1	8.92	8.13
MnO	2.87	2.53	3.41	3.63	2.62	2.43	0.97
MgO	12.2	14.3	11.7	11.0	15.7	16.8	17.7
Na_2O	0.39	0.32	0.33	0.30	0.39	0.33	0.33
K_2O	9.85	10.1	9.91	9.99	9.76	9.79	9.31
F	5.6	6.0	5.7	-	5.9	6.2	3.4
Cl	0.05	0.02	0.04	-	0.05	0.03	0.06
	93.90	93.93	94.11	93.78	94.48	94.37	95.10
Si	2.961	3.031	2.983	3.045	2.911	2.987	2.907
Al^{IV}	1.039	0.969	1.017	0.955	1.089	1.013	1.032
Fe^{3+IV}	-	-	-	-	-	-	0.061
Al^{VI}	0.281	0.250	0.294	0.444	0.052	0.082	-
Fe^{3+VI}	0.127	0.110	0.127	0.112	0.126	0.111	0.208
Fe^{2+}	0.634	0.550	0.634	0.562	0.633	0.554	0.500
Mg	1.367	1.587	1.310	1.224	1.756	1.861	1.942
Ti	0.110	0.072	0.108	0.065	0.111	0.079	0.133
Mn	0.183	0.160	0.217	0.229	0.167	0.153	0.060
Sum oct.	2.702	2.729	2.690	2.636	2.845	2.840	2.843
Na	0.057	0.046	0.048	0.043	0.057	0.048	0.047
K	0.945	0.959	0.950	0.951	0.934	0.928	0.874
F	1.33	1.41	1.35	-	1.40	1.46	0.79
Fe/(Fe+Mg)	0.358	0.294	0.367	0.355	0.302	0.263	0.284

Table III.7—continued.

	CABRESTO LAKE PLUTON									
	Granite					Mixed	Biotite-bearing enclave		Amphibole-bearing enclave	
	Typical	82QC10		Border facies		82QC14			83QC12	
		Core	Rim	Early	Late		Early	Late	Core	Rim
	(2,5)	(2)	(3)	(2,5)	(2,4)	(5)	(2,2)	(2,3)	(2)	(3)
SiO_2	38.9	37.9	40.1	38.8	40.2	38.1	38.1	39.4	37.3	38.2
Al_2O_3	12.8	13.3	11.9	12.6	11.7	12.7	13.3	12.4	13.4	12.8
TiO_2	3.58	4.04	2.97	2.64	2.07	3.65	3.38	3.02	4.10	3.42
Fe_2O_3	3.43	3.41	2.89	3.15	2.78	3.30	3.50	3.15	3.54	3.32
FeO	11.3	11.2	9.50	10.3	9.10	10.8	11.5	10.4	11.6	10.9
MnO	0.65	0.64	0.56	0.89	0.84	0.54	0.81	0.70	0.51	0.45
MgO	15.4	15.2	17.4	16.7	18.0	15.9	15.3	17.1	15.3	16.2
Na_2O	0.21	0.28	0.16	0.24	0.22	0.17	0.16	0.18	0.20	0.16
K_2O	9.73	9.57	9.80	9.50	9.69	9.77	9.54	9.68	9.59	9.76
F	1.9	2.3	2.5	3.5	3.9	1.9	1.6	2.0	1.9	2.1
Cl	0.12	0.13	0.16	0.13	0.11	0.14	0.12	0.15	0.17	0.17
	96.00	95.54	95.28	94.82	94.60	94.93	95.59	96.03	95.54	95.21
Si	2.871	2.812	2.945	2.885	2.970	2.841	2.830	2.890	2.777	2.839
Al^{IV}	1.113	1.163	1.031	1.104	1.019	1.116	1.164	1.072	1.176	1.121
Fe^{3+IV}	0.016	0.025	0.025	0.011	0.011	0.043	0.006	0.038	0.047	0.040
Al^{VI}	-	-	-	-	-	-	-	-	-	-
Fe^{3+VI}	0.174	0.165	0.135	0.165	0.144	0.142	0.190	0.136	0.151	0.146
Fe^{2+}	0.697	0.697	0.584	0.640	0.562	0.675	0.714	0.638	0.724	0.678
Mg	1.694	1.681	1.905	1.851	1.982	1.768	1.694	1.870	1.698	1.795
Ti	0.199	0.225	0.164	0.148	0.115	0.205	0.189	1.167	0.230	0.191
Mn	0.041	0.040	0.035	0.056	0.053	0.034	0.051	0.043	0.032	0.028
Sum oct.	2.821	2.808	2.823	2.871	2.867	2.824	2.844	2.892	2.835	2.838
Na	0.030	0.040	0.023	0.035	0.032	0.025	0.023	0.026	0.029	0.023
K	0.916	0.906	0.918	0.901	0.913	0.930	0.904	0.906	0.911	0.925
F	0.44	0.54	0.58	0.82	0.91	0.45	0.38	0.46	0.45	0.49
Fe/(Fe+Mg)	0.340	0.345	0.281	0.303	0.263	0.327	0.348	0.293	0.352	0.325

Table III.7—continued.

	RIO HONDO PLUTON								
	Granodiorite		Granite			Enclave		Schlieren	Qtz. latite dike
	(9,25)	Range of 9	84QC11	84QC13	82QC30	(4,13)	Range of 4	(5)	Q83J100
SiO_2	37.5	37.2-38.2	37.9	38.3	40.0	37.5	37.3-37.7	37.2	37.5
Al_2O_3	13.3	12.6-14.0	12.4	13.3	11.9	13.7	13.4-14.0	13.9	13.4
TiO_2	3.66	3.32-4.26	3.16	2.76	2.04	3.35	3.06-3.60	3.04	3.49
Fe_2O_3	3.96	3.66-4.28	5.89	2.98	4.25	4.05	3.96-4.14	4.08	3.94
FeO	12.6	11.6-13.3	10.7	11.8	9.18	12.9	12.6-13.2	13.0	12.6
MnO	0.30	0.21-0.44	1.28	0.98	1.22	0.27	0.16-0.33	0.48	0.25
MgO	14.3	13.8-15.0	13.6	15.0	16.1	14.2	13.9-14.6	13.9	14.6
Na_2O	0.12	0.08-0.14	0.12	0.11	0.09	0.10	0.08-0.12	0.09	0.11
K_2O	9.55	9.33-9.76	9.58	9.89	9.32	9.71	9.64-9.75	9.61	9.70
F	0.9	0.7-1.3	-	2.9	-	0.8	-	-	-
Cl	0.11	0.06-0.23	-	0.03	-	0.09	-	-	-
	95.90		94.63	95.12	94.10	96.31		95.30	95.59
Si	2.810		2.861	2.863	2.978	2.800		2.794	2.799
Al^{IV}	1.175		1.103	1.137	1.022	1.200		1.206	1.201
Fe^{3+IV}	0.015		0.036	-	-	-		-	-
Al^{VI}	-		-	0.035	0.022	0.006		0.025	0.004
Fe^{3+VI}	0.208		0.299	0.168	0.238	0.228		0.231	0.238
Fe^{2+}	0.790		0.676	0.739	0.572	0.806		0.819	0.740
Mg	1.597		1.531	1.672	1.787	1.581		1.556	1.489
Ti	0.206		0.179	0.155	0.114	0.188		0.172	0.217
Mn	0.019		0.082	0.062	0.077	0.017		0.031	0.109
Sum oct.	2.835		2.767	2.831	2.810	2.825		2.834	2.789
Na	0.017		0.018	0.016	0.013	0.014		0.013	0.059
K	0.913		0.923	0.943	0.885	0.925		0.921	0.870
F	0.21		-	0.69	-	0.19		-	-
Fe/(Fe+Mg)	0.388		0.398	0.352	0.312	0.395		0.403	0.396

Table III.7--continued.

	BEAR CANYON PLUTON			SULPHUR GULCH PLUTON				
	Granite			Carapace		Source aplite		
	82QC10		82QC8	3417		3438	82QC55	
	Core(2)	Rim	(3)	Core(2)	Rim		Core	Rim(2)
SiO_2	37.6	39.7	40.6	38.5	38.7	37.6	38.9	41.2
Al_2O_3	13.9	12.8	11.7	13.0	12.7	13.2	13.5	11.4
TiO_2	2.93	1.83	1.58	3.15	2.03	2.80	2.01	1.61
Fe_2O_3	2.75	2.28	2.19	2.34	2.12	2.54	2.22	1.96
FeO	14.6	12.1	11.6	12.4	11.3	13.5	11.8	10.4
MnO	1.31	1.14	0.84	0.66	0.58	1.03	0.57	0.48
MgO	12.5	15.4	16.5	15.8	17.5	14.3	15.2	17.4
Na_2O	0.12	0.12	0.17	0.18	0.11	0.22	0.34	0.26
K_2O	9.89	9.91	9.64	9.84	9.43	9.58	9.46	9.80
F	2.8	3.5	4.6	-	-	-	-	-
Cl	0.03	0.03	0.05	-	-	-	-	-
	95.60	95.28	94.82	95.87	94.47	94.77	94.00	94.51
Si	2.838	2.953	3.015	2.856	2.887	2.844	2.919	3.047
Al^{IV}	1.162	1.047	0.985	1.137	1.113	1.156	1.081	0.953
Fe^{3+IV}	-	-	-	0.007	-	-	-	-
Al^{VI}	0.075	0.075	0.039	-	0.004	0.021	0.114	0.041
Fe^{3+VI}	0.156	0.128	0.122	0.124	0.119	0.145	0.125	0.109
Fe^{2+}	0.924	0.756	0.722	0.769	0.705	0.854	0.741	0.643
Mg	1.407	1.708	1.827	1.747	1.946	1.612	1.700	1.918
Ti	0.166	0.102	0.088	0.176	0.114	0.159	0.113	0.090
Mn	0.084	0.072	0.053	0.041	0.037	0.066	0.036	0.030
Sum oct.	2.812	2.840	2.852	2.864	2.925	2.857	2.830	2.831
Na	0.018	0.017	0.024	0.026	0.016	0.032	0.049	0.037
K	0.953	0.940	0.913	0.931	0.898	0.925	0.906	0.925
F	0.67	0.82	1.08	-	-	-	-	-
Fe/(Fe+Mg)	0.434	0.341	0.316	0.340	0.298	0.383	0.337	0.282

Table III.7—continued.

	RED RIVER INTRUSIVE COMPLEX						LUCERO PEAK PLUTON	
	Granodiorite	Granite		Alk.-feld. granite	Enclave	Quartz diorite	Granite	
	82QC44	85QC36		82QC32C	82QC43I	82QC31	82QC15	82QC25
	(3)	Early(5)	Late	(6)	(2)	(4)	(3)	(4)
SiO_2	36.9	39.1	40.5	39.6	39.1	38.3	39.4	39.2
Al_2O_3	13.5	12.3	11.6	12.2	13.0	14.5	12.2	12.8
TiO_2	4.33	3.00	1.98	1.56	2.72	3.60	1.95	2.10
Fe_2O_3	2.59	2.47	2.03	2.61	2.25	2.39	2.08	2.24
FeO	13.6	11.5	9.47	11.3	9.98	11.1	12.3	13.3
MnO	0.23	1.04	1.00	1.95	0.62	0.48	1.35	1.86
MgO	14.4	15.9	18.2	15.0	17.6	14.8	15.0	14.0
Na_2O	0.12	0.23	0.25	0.24	0.36	0.22	0.17	0.11
K_2O	9.72	9.56	9.60	9.85	9.79	9.17	9.88	9.69
F	0.70	-	-	5.7	-	-	4.4	3.4
Cl	0.17	-	-	0.06	-	-	0.03	0.03
	95.39	95.10	94.63	94.31	95.42	94.56	94.33	95.30
Si	2.772	2.911	2.988	2.983	2.876	2.844	2.970	2.941
Al^{IV}	1.195	1.079	1.009	1.017	1.124	1.156	1.030	1.059
Fe^{3+IV}	0.033	0.010	0.003	-	-	-	-	-
Al^{VI}	-	-	-	0.067	0.004	0.113	0.053	0.073
Fe^{3+VI}	0.113	0.128	0.110	0.148	0.125	0.134	0.118	0.126
Fe^{2+}	0.852	0.715	0.584	0.709	0.614	0.686	0.777	0.834
Mg	1.612	1.764	2.002	1.685	1.930	1.638	1.685	1.566
Ti	0.245	0.168	0.110	0.088	0.150	0.201	0.111	0.118
Mn	0.015	0.066	0.063	0.124	0.039	0.030	0.086	0.118
Sum oct.	2.837	2.841	2.869	2.821	2.862	2.802	2.831	2.836
Na	0.017	0.033	0.036	0.035	0.051	0.032	0.025	0.016
K	0.931	0.908	0.904	0.947	0.919	0.869	0.950	0.927
F	0.17	-	-	1.36	-	-	1.05	0.81
Fe/(Fe+Mg)	0.382	0.326	0.258	0.337	0.277	0.334	0.347	0.380

Table III.8. Partial chemical analyses of biotite separates from the Questa granitic rocks (weight percent).

PLUTON/ Unit	Sample number	F	H_2O^+	FeO	FeO^T	$Fe^{2+}/(Fe^{2+} + Fe^{3+})$
VIRGIN CANYON						
Early metaluminous granite	83QC25	2.64	1.64	11.40	15.05	0.76
Late metaluminous granite	82QC35	2.63	2.11	11.47	15.30	0.75
CANADA PINABETE						
Typical granite	81S40	2.67	1.76	11.91	15.30	0.78
	81S43	2.33	1.74	12.80	16.08	0.80
	Q83J86	3.52	0.87	9.82	12.24	0.83
	84QC1	3.67	1.26	11.02	13.76	0.80
Magnetite-free granite	Q83J88	1.46	2.86	18.34	25.21	0.73
RITO del MEDIO						
Typical granite	81S28	3.63	1.12	10.94	13.12	0.83
Border facies	82QC22	2.42	2.41	8.08	12.42	0.65
CABRESTO LAKE						
Granite	82QC51b	1.18	3.41	12.52	15.95	0.79
RIO HONDO						
Granodiorite	Q83J59	0.62	2.97	12.54	16.72	0.75
	Q83J101	-	-	13.34	16.85	0.79
	Q84J6	0.57	3.50	14.17	17.75	0.80
Granite	82QC30	2.13	3.09	10.35	14.66	0.71
	84QC11	1.76	3.92	11.09	16.59	0.67
	84QC13	2.31	2.89	12.47	15.30	0.82
BEAR CANYON	82QC8	2.60	1.64	12.54	14.66	0.86
RED RIVER INTRUSIVE COMPLEX						
Granodiorite	82QC44	0.56	3.51	13.17	15.43	0.85
Granite	82QC43	2.23	2.02	10.07	12.11	0.83
	85QC36	2.34	2.01	12.28	14.66	0.84
Alkali-feldspar granite	82QC32C	3.12	1.44	11.38	13.76	0.83
LUCERO PEAK	82QC15	2.84	1.83	12.62	14.53	0.87

Oxide weight percentages based on the electron microprobe analyses were reduced to structural formulae based on calculation to 11 oxygen ions. The data presented in Table III.7 were rather subjectively derived from the data set of 150 analyses in an attempt to represent, with the fewest number of analyses, the most significant aspects of biotite chemistry for each pluton and as many analyses as possible. Most often this process involved: 1) recognition of typical, intermediate, and aberrant compositions; 2) elimination of intermediate compositions; and 3) further judicious averaging, often involving analyses from several samples.

A) DESCRIPTION

The range in biotite composition is quite large, but compositions are broadly similar in the different granitic units associated with Questa caldera. High Mg content is characteristic; Fe/(Fe+Mg) ranges from 0.25 to 0.52, except in magnetite-free samples of the Canada Pinabete pluton where this ratio ranges from 0.36 to 0.88. All biotite compositions fall between the Ni-NiO and Fe_3O_4-Fe_2O_3 buffer curves in the ternary diagram used by Wones and Eugster (1965) to represent biotite compositions in terms of the end members $KFe^{2+}_3AlSi_3O_{10}(OH)_2$-$KMg_3AlSi_3O_{10}(OH)_2$-$KFe^{3+}_2AlSi_3O_{12}(H_{-1})$.

1. VIRGIN CANYON, CANADA PINABETE, AND RITO del MEDIO

The occurrence of biotite in the northern intracaldera plutons is of particular interest because of its association with tetrasilicic mica in the peralkaline granites of Virgin Canyon and Canada Pinabete, and primary muscovite in the Rito del Medio pluton and the metaluminous granite of Canada Pinabete. Biotite in these three intracaldera plutons is almost always zoned, with more Fe-rich cores surrounded by broad more Mg-rich rims (Plate III.2, a). Si, Mg, K, and F contents typically increase, while Al, Fe, Ti, and Na contents decrease from core to rim. Mn content does not vary in a regular way from core to rim; however, averages of core and rim compositions show a tendancy for Mn to decrease from core to rim. Notable is the fact that late rims on biotite are broader and better developed in the northern intracaldera plutons, which were emplaced at the highest structural levels. Biotite in the three northern intracaldera plutons is characterized by the highest measured contents of MnO (to 3.63 wt%), Na_2O (to 0.59 wt%), and F (to 6.8 wt%). F content is highest in the Rito del Medio granite (5.6 to 6.8 wt%), and lowest in magnetite-free samples of the Canada Pinabete pluton (2.5 to 3.6 wt%), and in sample 82QC22 from the Rito del Medio pluton (avg 3.4 wt%). Cl content is usually low (avg <0.08 wt%) except for several analyses from magnetite-free samples of the Canada Pinabete pluton in which it reaches 0.30 weight percent.

In the peralkaline granite of Virgin Canyon, the stable mafic mineral assemblage is alkali amphibole, sodic pyroxene, and tetrasilicic mica. Early formed biotite and richteritic amphibole cores are being replaced by tetrasilicic mica. Two types of biotite occur, small crystals in aggregates and larger crystals up to 2 mm across in the porphyry groundmass. The larger crystals commonly have thin rims of more Mg-rich composition than the cores;

biotite in aggregates is similar in composition to the cores, but contains about 1.5 weight percent more MnO. In sample 83QC29, however, a larger host crystal has the composition of the cores of other crystals, while a smaller inclusion has the composition of the typical rims. Biotite in the northern peralkaline dikes contains more Na_2O (avg 0.55 wt%) and less K_2O (avg 9.02 wt%) than biotite in the peralkaline granite of Virgin Canyon.

Biotite in the early and later metaluminous granites of Virgin Canyon is of indistinguishable composition, quite similar to that of biotite phenocrysts in the peralkaline granite. The rims of biotite grains in the early and late metaluminous granites (Plate III.2, a) are much better developed, however, and their compositions extend to lower TiO_2 contents. The most "evolved", late biotite compositions measured in the early metaluminous granite contain significantly less Al, Ti, and Fe and more Mg than typical biotite rims. They are quite similar to biotite compositions measured in samples of a 5 m-wide rhyolite dike (82QC31) which cuts the peralkaline granite between samples localities 83QC30 and 83QC29. Biotite (Table III.7) and whole rock (Table II.10) compositions, as well as minor element data suggest that the dike represents an auto-intrusion of the metaluminous magma.

Biotite in magnetite-free samples of the Canada Pinabete pluton is characterized by high Fe, and low Si, Mg, and F contents compared to that in magnetite-bearing samples. Zoning of biotite in magnetite-free samples may follow the typical trend from Fe-rich cores to Fe-poor rims, but, in these samples alone, among all studied samples of the Questa granitic rocks, the reverse can also be found. Three stages of chemical evolution have been found in single biotite grains in sample 82QC48, whereas grains displaying the two opposing zoning trends are more typical in sample Q83J88. Second-stage biotite contains less Si, Mg, K, and F, and more Fe, and Ti than first- or third-stage biotites, which are of rather similar composition. MnO content is typically in the range 1.00 to 1.60 weight percent in biotite from the Canada Pinabete pluton, but concentrations to 2.79 weight percent have been measured. Magnetite-free, amphibole-bearing sample 82QC48 contains biotite with an unusually low MnO content (0.78-0.90 wt%) while other magnetite-free samples contain above average MnO. MnO content typically drops approximately 0.2 weight percent from core to rim of zoned grains, and shows a good correlation with La contents of biotite separates, a measure of differentiation. For biotites containing 7.8, 14.8, 30.9, and 83 ppm La, respective average MnO contents are 1.50, 1.78, 1.94, and 2.73 weight percent.

Biotite in the main facies of the Rito del Medio pluton is characterized by higher Al, Mn, K, and F contents than biotite in any other rock type in the Questa area. Rock chemistry (Table I.10) provides little indication of why biotite chemistry in the Rito del Medio pluton should be unique among the Questa granites. Other unique characteristics of the Rito del Medio pluton, such as the abundance of miarolitic cavities, abundant coarse muscovite in those cavities, and the presence of quartz-feldspar quench textures suggest that aspects of mode of emplacement and evolution of volatiles were important in controlling biotite chemistry as well as these other characteristics. As indicated in Table III.7, Al content may either increase or decrease from core-to-rim of biotite in typical Rito del Medio granite. Biotite in samples taken from within 20 m of the Precambrian roof has a rather different composition from that in the main facies of the pluton; it contains less Al and K, more Fe, and has a lower $Fe^{2+}/(Fe^{2+} + Fe^{3+})$ (Table III.7).

2. CABRESTO LAKE AND RIO HONDO

Compared to biotite compositions in the northern intracaldera plutons, biotite in the typical granite of the intracaldera Cabresto Lake pluton is characterized by higher contents of TiO_2 (2.45 to 4.04 wt%) and Cl (0.10 to 0.17 wt%), and lower contents of MnO (0.56 to 0.92 wt%), Na_2O (0.16 to 0.28 wt%), and F (1.6 to 4.0 wt%). Biotite compositions are virtually indistinguishable in the typical granite, mixed unit, and two types of enclaves found in the Cabresto Lake pluton. Rare zoning exhibits the same pattern as in the northern intracaldera plutons; cores are richer in Fe, Al, Ti, Mn, and Na; rims are enriched in Mg, Si, K, and F. Biotite in the granite is marked by slightly higher F and Na compared to the three other rock types. Biotite in the border facies of the granite, which is more SiO_2 rich and contains no amphibole, contains less Ti, more Mg and Mn, and significantly more F than biotite in the other units. Biotite in aggregates with quartz, characteristic of samples of the border facies of the granite, contains more Mg, Si, K, and F and less Fe, Al, Ti, and Mn than coexisting biotite. Rare zoning in biotite phenocrysts indicates that biotite in these aggregates crystallized after all other biotites.

Biotite in the granodiorite and mafic-magmatic enclaves of the Rio Hondo pluton is characterized by unusually low contents of MnO (0.21-0.48 wt%) and F (0.8-1.3 wt%); in biotite from the granite MnO ranges between 0.9 and 2.1 weight percent and F between 2.0 and 4.2 weight percent. Biotite in the granodiorite is typically not zoned and compositions are rather uniform within samples, as well as from one sample to another. Biotite compositions in the granodiorite, in mafic-magmatic enclaves, in schlieren, and in a quartz latite dike cutting the granodiorite are indistinguishable. The average composition of biotite in the granite is higher in Mg, Si, Mn, and F and lower in Fe, Al, and Ti than the average composition in these more mafic rocks. As shown in Table III.8, $Fe^{2+}/(Fe^{2+}+Fe^{3+})$ is unusually variable among analysed biotite separates from the granite of Rio Hondo. Values of 0.67 and 0.82 were obtained for equigranular samples 84QC11 and 84QC13 taken, respectively, 200 m and 50 m from a contact with Precambrian rocks in Columbine Creek canyon, while the ratio is 0.71 for auto-brecciated, silicified sample 82QC30 taken some 400 m to the north of 84QC13, at the northern tip of the Rio Hondo pluton. $Fe^{2+}/(Fe^{2+}+Fe^{3+})$ values of 0.75, 0.79, and 0.80 obtained for biotite from the granodiorite, suggest that the unusual samples are 84QC11 and 82QC30. Redetermination of ferrous iron confirmed the reported values; variation in $Fe^{2+}/(Fe^{2+}+Fe^{3+})$ in these relatively closely spaced samples is most probably due to proximity to the upper contact of this large pluton. Biotite is zoned in only one of 6 granite samples; in the rims, Fe, Al, Ti, Mn, and K are depleted and Mg, Si, and F are enriched. Samples which represent a cross-section through the margin of the granitic facies suggest that toward the contact, biotite is enriched in F and Mn and depleted in Ti.

3. LATE MINERALIZED PLUTONS

In contrast to the other plutons, portions of the late mineralized intrusions contain Mo mineralization and substantial amounts of pyrite, and have undergone biotite-destructive hydrothermal alteration. Adequate biotite

could not be separated from altered rocks of the Sulphur Gulch pluton, but because biotite composition is similar for the Bear Canyon and Sulphur Gulch plutons and because the plutons have been shown to have subsurface connection, $Fe^{2+}/(Fe^{2+}+Fe^{3+})$ measured on sample 82QC8 from the Bear Canyon pluton has been applied to the Sulphur Gulch biotite analyses.

At similar SiO_2 content there are few significant differences among the biotites from the late mineralized plutons. Where measured, zoning follows the same trends as in other Questa plutons, SiO_2 and MgO increase while Al_2O_3, TiO_2, and FeO decrease. Biotite from the Sulphur Gulch pluton has a relatively low MnO content. Na_2O contents are low in the Bear Canyon and Lucero Peak plutons and in the carapace unit of the Sulphur Gulch pluton. Biotite compositions in sample 82QC10 from the Bear Canyon pluton were evoling toward those of sample 82QC8.

The compositions of biotite in the various units of the Red River intrusive complex show good relation to host rock SiO_2 content (see Table I.10). In the progression granodiorite—granite—alkali-feldspar granite, TiO_2 content of biotite drops from 4.33 to 1.56 weight percent, while MnO and F contents increase, respectively, from 0.23 to 1.95 and 0.7 to 5.7 weight percent. The unusually low F content of biotite in the granodiorite is similar to that of biotite in the granodiorite of the Rio Hondo pluton. Biotite in enclaves in the granite has a slightly different composition from biotite in the granite; biotite in the enclaves contains more Al and less Mn; Si and Al contents are similar to those of early biotite in the granite, while Ti, Fe, and Mg are similar to those of late biotite in the granite. Biotite in the alkali-feldspar granite is not zoned and is characterized by high concentration of MnO (1.99 wt%) and F (5.7 wt%). Biotite in the Lucero Peak pluton is also unzoned and is virtually indistinguishable in composition from that in the alkali-feldspar granite of Red River.

Fig. III.14. $Al^{IV}+Fe^{3IV}$ (cations) against "effective octahedral site occupancy" for biotite in the Questa granitic plutons. Crosses, northern intra-caldera plutons; diamonds, Cabresto Lake and Rio Hondo plutons; triangles, late mineralized plutons.

Figs. III.15 to III.17. $Al^{IV}+Fe^{3IV}$+interlayer vacancies against "effective octahedral-site occupancy" for biotite in the northern intracaldera plutons (fig. III.15), the Cabresto Lake and Rio Hondo plutons (fig. III.16), and the late mineralized plutons (fig. III.17).

Fig. III.15. Squares, peralkaline granite of Virgin Canyon; crosses, early metaluminous granite of Virgin Canyon; diamonds, later metaluminous granite of Virgin Canyon; triangles, typical metaluminous granite of Canada Pinabete; x's, magnetite-free granite of Canada Pinabete; inverted triangles, granite of Rito del Medio.

Fig. III.16. Squares, granite of Cabresto Lake; crosses, mixed unit of Cabresto Lake; diamonds, enclaves in Cabresto Lake units; triangles, granodiorite of Rio Hondo; x's, granite of Rio Hondo; inverted triangles, mafic magmatic enclaves in the granodiorite of Rio Hondo.

Fig. III.17. Crosses, granite of Lucero Peak; diamonds, granite of Bear Canyon; triangles, units and rock types of Red River; x's, carapace unit and source aplite of Sulphur Gulch.

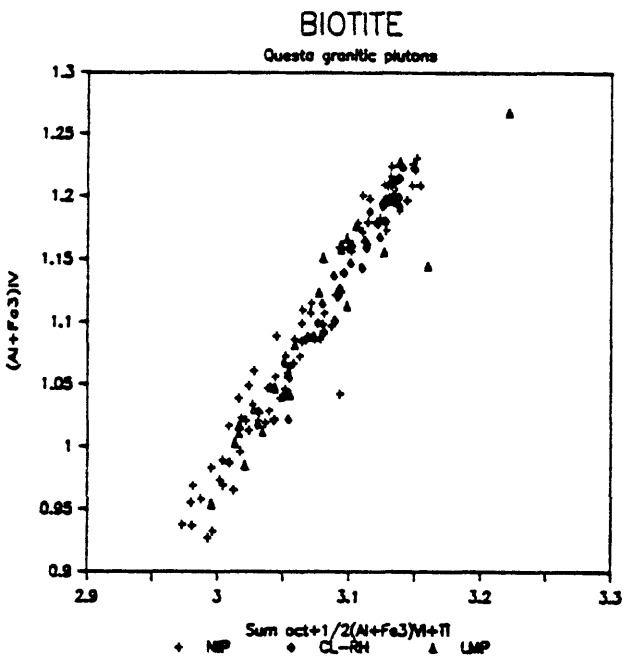

Fig. III.14.

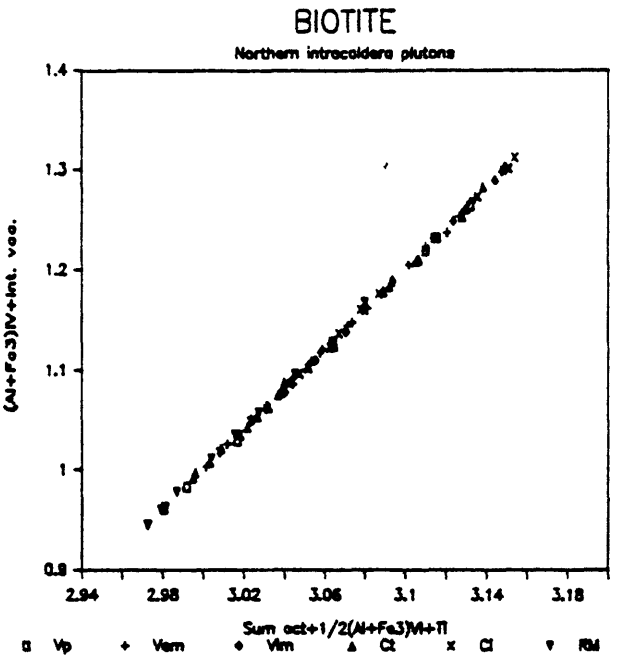

Fig. III.15.

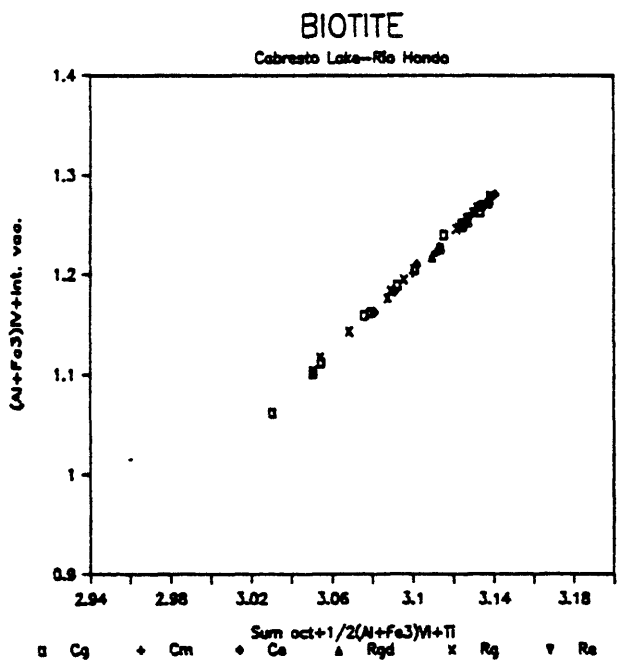

Fig. III.16.

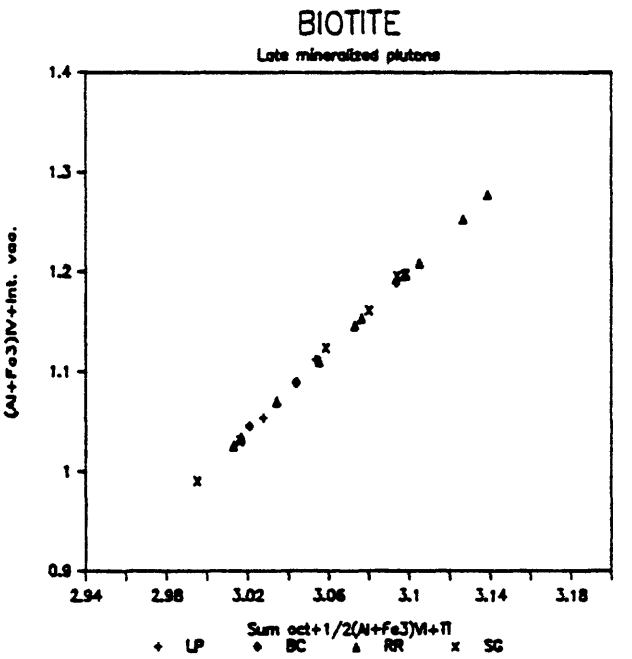

Fig. III.17.

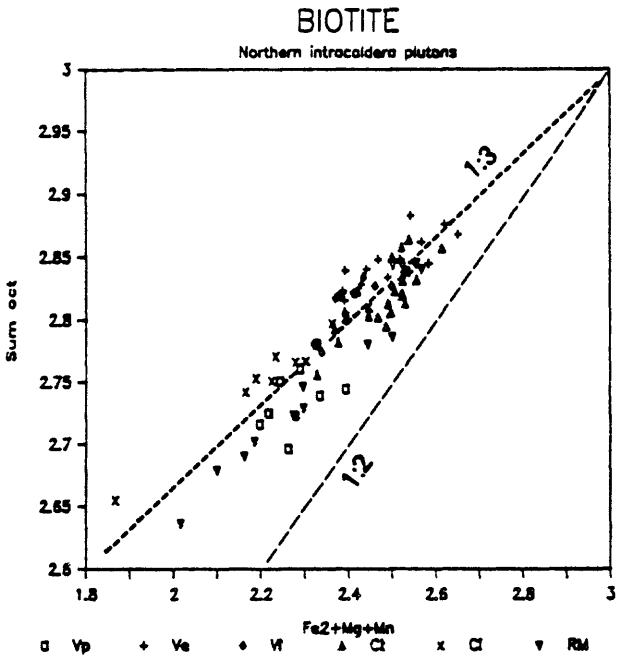

Fig. III.18.

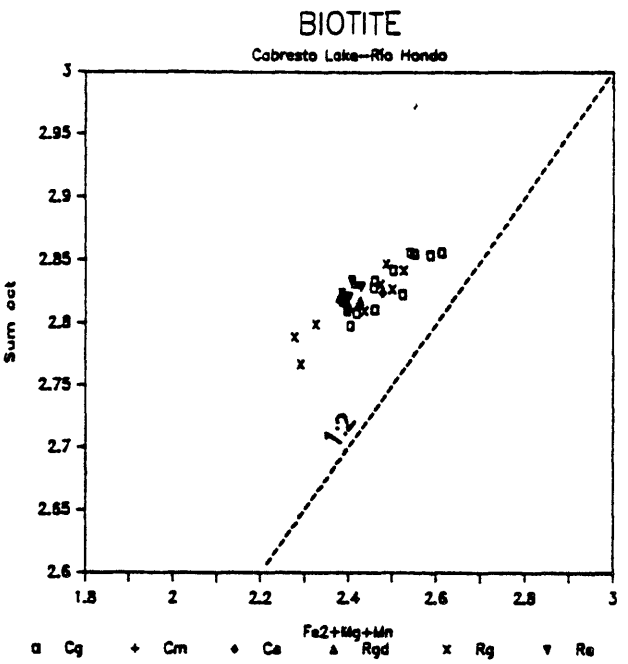

Fig. III.19.

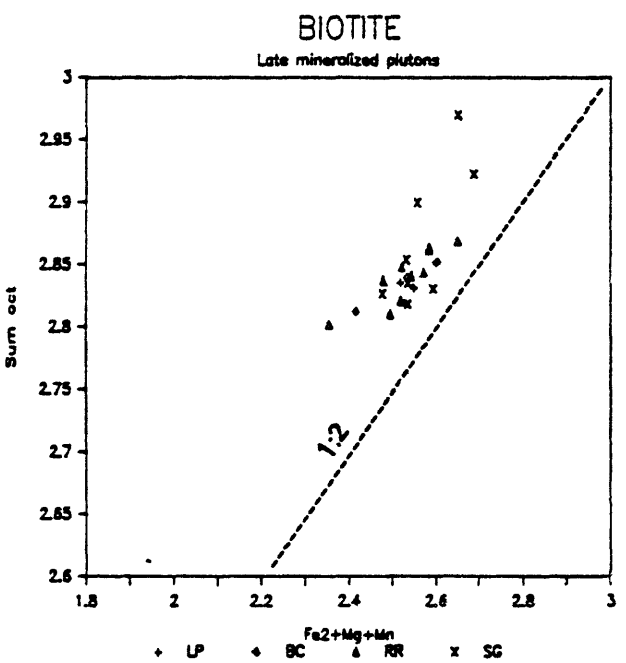

Fig. III.20.

Figs. III.18 to III.20. Fe^{2+}+Mg+Mn (cations) against the sum of the octahedral cations for biotite in the northern intracaldera plutons (fig. III.18), the Cabresto Lake and Rio Hondo plutons (fig. III.19), and the late mineralized plutons (fig. III.20). 1:2 and 1:3 correlation lines shown for reference. Symbols as in figs. III.15 to III.17.

B) DISCUSSION

Consideration and comparison of biotite chemistry is simplified by using data from calculated structural formulae. These data may be used in two ways; as calculated, to indicate the degree of filling of structural sites, or corrected for ionic charge, to indicate mechanisms of charge balancing within and between structural sites. An example of the latter approach, a plot of the sum of the octahedral cations+1/2($Al^{VI}+Fe^{3+VI}$)+Ti against $Al^{IV}+Fe^{3+IV}$ shows a rather good correlation (fig. III.14). However, the correlation is not 2:1 as it should be and the data show considerable scatter; addition of the interlayer vacancies to $Al^{IV}+Fe^{3+IV}$ gives a much better correlation with a slope of 2:1 (figs. III.15, III.16, and III.17). This shows that vacancies occur in the interlayer site and that substitutions of R^{3+} or R^{4+} for R^{2+} in the octahedral sites compensate for substitution of R^{3+} for R^{4+} in the tetrahedral sites, as well as replacement of K or Na by vacancies in the interlayer sites. In most cases, the octahedral sites contain less than 3 cations, but more than 6 positive charges, and the tetrahedral and interlayer sites show a charge deficiency. In the peralkaline granite of Virgin Canyon and in the Rito del Medio granite, some biotite rim compositions are transitional toward tetrasilicic mica, with more than 3 Si cations in the tetrahedral sites and less than 6 charges in the octahedral sites (fig. III.15).

Biotite in the Cabresto Lake pluton typically contains Fe^{3+} in octahedral sites and no Al^{VI}. As in the northern intracaldera plutons, the correlation between the sum of the octahedral cations+1/2($Al^{VI}+Fe^{3+VI}$)+Ti and $Al^{IV}+Fe^{3+IV}$ (fig. III.14) is much improved by adding the interlayer vacancies to the trivalent tetrahedral cations (fig. III.16). Biotite compositions in the mixed unit and in the biotite-bearing enclaves of the Cabresto Lake pluton show more excess charge in the octahedral sites than does biotite in the granite. The same relation occurs in the Rio Hondo pluton; biotite in the granodiorite and in mafic-magmatic enclaves has more excess charge in the octahedral sites than biotite in the granite.

Plots of the sum of the octahedral cations+1/2($Al^{VI}+Fe^{3+VI}$)+Ti against $Al^{IV}+Fe^{3+IV}$ or $Al^{IV}+Fe^{3+IV}$+interlayer vacancies for the late mineralized plutons show the same relations as in the other plutons (figs. III.14 and III.17).

There is good correlation of 1:3 to 1:2 between Fe^{2+}+Mg+Mn and the sum of the octahedral cations in biotite for all plutons (figs. III.18, III.19, and III.20). A 1:3 relation is appropriate for occurrence of the substitution $1.5R^{2+} = R^{3+} + 0.5[]$. However, biotite in the Questa granitic rocks contains a significant amount of Ti (0.050 to 0.263 cations) whose substitution in the octahedral sites must be written $2R^{2+} = R^{4+} + 1.0[]$, requiring a 1:2 relation between R^{2+} and sum of the octahedral cations. Further consideration of figures III.18, III.19, and III.20 shows that for many analyses there is an "excess" of R^{3+} and R^{4+} cations in the octahedral sites which must result in excess charge. Apparently, the excess R^{3+} and R^{4+} cations balance the deficit present on the tetrahedral and interlayer sites, as already discussed in reference to figures III.15 to III.17. A plot of Fe^{2+}+Mg+Mn against the sum of the octahedral cations for biotite in the Cabresto Lake and Rio Hondo plutons (fig. III.19) shows that a greater proportion of the samples have

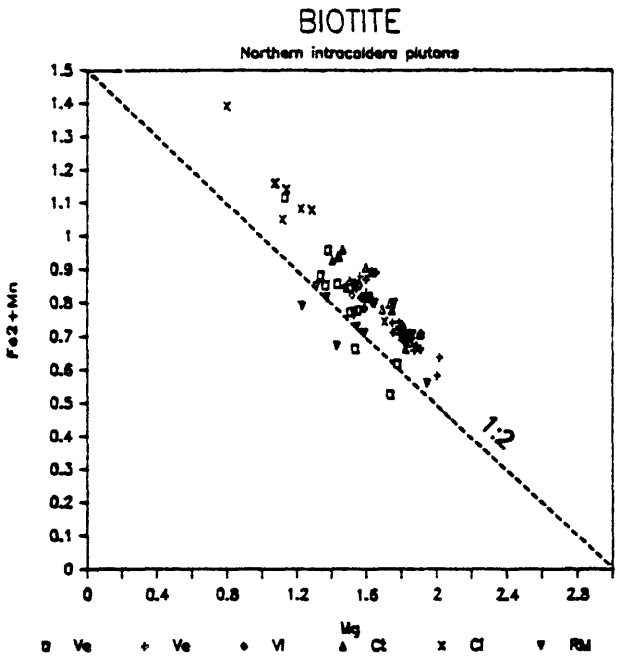

Fig III.21. Mg against Fe^{2+}+Mn (cations) for biotite in the northern intracaldera plutons. Symbols as in fig. III.15.

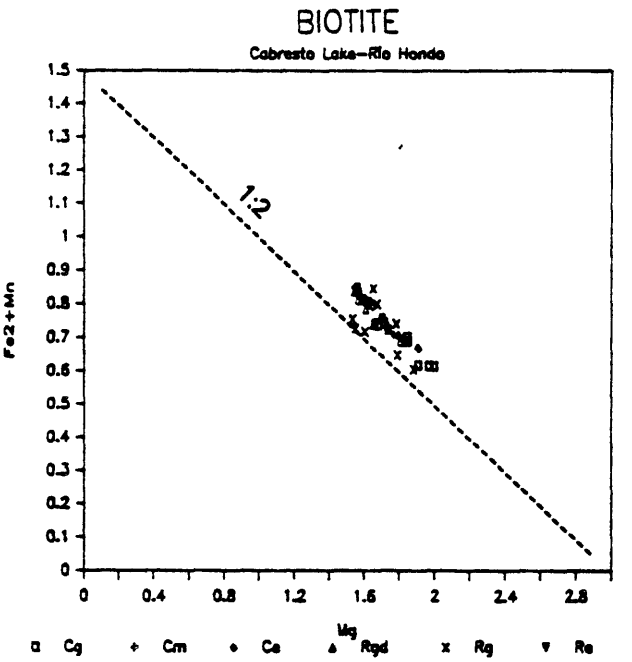

Fig III.22. Mg against Fe^{2+}+Mn (cations) for biotite in the Cabresto Lake and Rio Hondo plutons. Symbols as in fig. III.16.

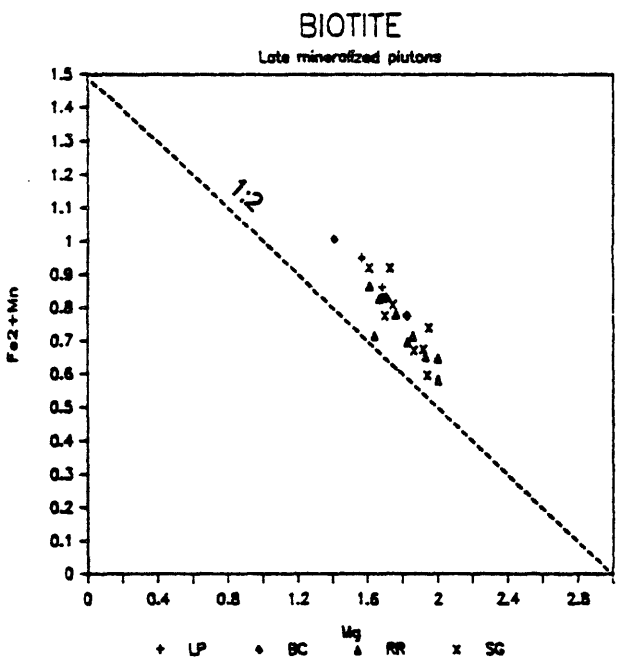

Fig. III.23. Mg against Fe^{2+}+Mn (cations) for biotite in the late mineralized plutons. Symbols as in fig. III.17.

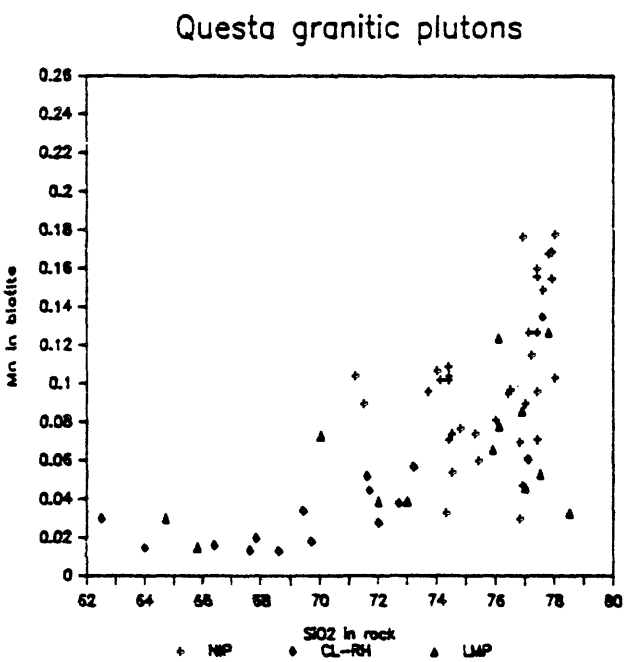

Fig. III.24. Mn in biotite (cations) against host-rock SiO_2 (wt%) for the Questa granitic plutons.

excess charge in the octahedral sites than for biotite in the northern intracaldera plutons. Although not clearly shown in the plot of $Fe^{2+}+Mg+Mn$ against the sum of the octahedral cations for biotite in the late mineralized plutons (fig. III.20), biotite in the most mafic rocks (granodiorite and quartz diorite of Red River) and early crystallized biotite (cores in the Bear Canyon granite) is characterized by more excess charge in the octahedral sites than biotite in more silicic units or late-formed biotite.

There is a fair 1:2 negative correlation between Mg and $Fe^{2+}+Mn$ for the Virgin Canyon and Canada Pinabete plutons (fig. III.21). This suggests that Mg substitutes not only for Fe^{2+} but also for Fe^{3+}, Al, and Ti in the octahedral sites. Study of biotite zoning suggests that these substitutions may also occur with differentiation. Notable is the lack of good relation between Mg and Fe^{2+} for biotites in the Rito del Medio pluton, and the occurrence of a much better relation between Mg and $Fe^{2+}+Mn$.

A plot of Mg against $Fe^{2+}+Mn$ (fig. III.22) for biotite in the Cabresto Lake and Rio Hondo plutons is tighter than that for biotite in the northern intracaldera plutons. Biotite compositions in the Cabresto Lake pluton are typically more Mg rich.

The relation between Mg and $Fe^{2+}+Mn$ for biotite in the late mineralized plutons is the same as for the other plutons, the range of composition being larger than in the Cabresto Lake and Rio Hondo plutons.

A plot of Mn in biotite against whole-rock SiO_2 content for the Questa granitic plutons (fig. III.24) is quite similar to the plot of Mn in ilmenite against whole-rock SiO_2 content, and indicates Mn enrichment in biotite with differentiation.

C) OXYGEN FUGACITY-TEMPERATURE RELATIONS

Biotite compositions can be interpreted in light of the experiments of Wones and Eugster (1965) which provide a means of roughly estimating fO_2 during crystallization of biotite by plotting Fe^{3+}, Fe^{2+}, and Mg end-members. Wones and Eugster (1965, fig. 4) also show that Fe/(Fe+Mg) in biotite is related to oxidation, more Mg-rich biotites reflecting higher oxidation states (fig. III.26).

Biotite data for all units of the Virgin Canyon, Canada Pinabete, and Rito del Medio plutons fall between the Ni-NiO and Fe_3O_4-Fe_2O_3 buffers in the Fe^{3+}-Fe^{2+}-Mg end-member diagram (fig. III.25). Figure III.25 shows that the most Fe-rich biotites of the peralkaline granite of Virgin Canyon reflect lower fO_2 than the least Fe-rich biotites in the early metaluminous granite. This is in agreement with the compositions of the opaque oxide minerals which show that fO_2 was lower during crystallization of the peralkaline granite than during crystallization of the metaluminous granites. Biotite in magnetite-free samples of the Canada Pinabete pluton is distinctly Mg-poor, yet $Fe^{2+}/(Fe^{2+}+Fe^{3+})$ in this biotite is lower than that in magnetite-bearing samples, causing analyses to plot nearer the Fe_3O_4-Fe_2O_3 buffer. The high proportion of Fe^{3+} in these biotites may be due to the fact that in the

absence of magnetite, biotite is the only phase which accommodates ferric iron. The Mg-poor composition of the biotite and lack of magnetite both indicate low oxygen fugacity during crystallization of magnetite-free samples. Magnetite-free samples of the Canada Pinabete pluton appear to be localized in a few small areas which are interpreted to represent pipes through which H_2 gas escaped from lower levels in the crystallizing pluton.

Biotite in typical samples of the Rito del Medio pluton plots closest to the Ni-NiO buffer curve. Lower $Fe^{2+}/(Fe^{2+}+Fe^{3+})$ in biotite from sample 82QC22 places it nearer the Fe_3O_4-Fe_2O_3 buffer, reflecting a significant difference in fO_2 between the contact zone and the main facies of the pluton.

Comparison of the three plots in figure III.25 shows that biotites from the Virgin Canyon pluton plot nearer the Fe_3O_4-Fe_2O_3 buffer, biotites from the Rito del Medio pluton plot nearer the Ni-NiO buffer, and data for magnetite-bearing samples of the Canada Pinabete pluton fall in between. However, figure III.26, which is based on Fe/(Fe+Mg) and may more truely reflect fO_2, shows that biotite in the Rito del Medio pluton probably crystallized at higher oxygen fugacity than biotite in the Canada Pinabete and Virgin Canyon plutons. Thus, the representation of figure III.26 and the opaque oxide mineral data are in agreement and indicate that oxygen fugacity was highest during crystallization of the Rito del Medio granite and lowest during crystallization of the peralkaline granite of Virgin Canyon.

Biotite compositions for both the Cabresto Lake and Rio Hondo plutons fall between the Ni-NiO and Fe_3O_4-Fe_2O_3 buffers (fig. III.25) in the diagram of Wones and Eugster (1965). Scatter in the Rio Hondo data is caused by the wide variability in $Fe^{2+}/(Fe^{2+}+Fe^{3+})$, as previously discussed.

Biotite compositions fall near the Ni-NiO buffer in the Wones and Eugster ternary diagram (1965) for all of the late mineralized plutons (fig. III.25).

The experiments of Wones and Eugster also allow interpretation of the reverse zoning (more Mg-rich rims), best developed in biotite in the northern intracaldera plutons. Such zoning indicates constant or increasing oxygen fugacity as temperature decreased during crystallization of biotite; that is, crystallization of biotite was not oxygen-buffered. In the case of oxygen-buffered crystallization, fO_2 decreases with temperature, following the buffer curves (fig. III.26; Wones and Eugster, 1965, fig. 4). The sharp change in composition in biotite in the northern intracaldera plutons indicates an abrupt increase in oxygen fugacity at some time in the crystallization history. Such a trend has been reported in other igneous systems, such as in the Ben Nevis igneous complex, Scotland (Haslam, 1968), the Finnmarka complex, Norway (Czamanske and Wones, 1973), and the Baie-des-moutons syenitic complex, Quebec (Lalonde and Martin, 1983).

Fig. III.25. Data for biotite in the Questa granitic plutons plotted in terms of the ternary system $KFe_3^{2+}AlSi_3O_{10}(OH)_2$-$KMg_3AlSi_3O_{10}(OH)_2$-$KFe_3^{3+}AlSi_3O_{12}(H_{-1})$. Dashed lines indicate compositions of biotites stable along the buffers Fe_3O_4-Fe_2O_3 and Ni-NiO. After Wones and Eugster (1965).

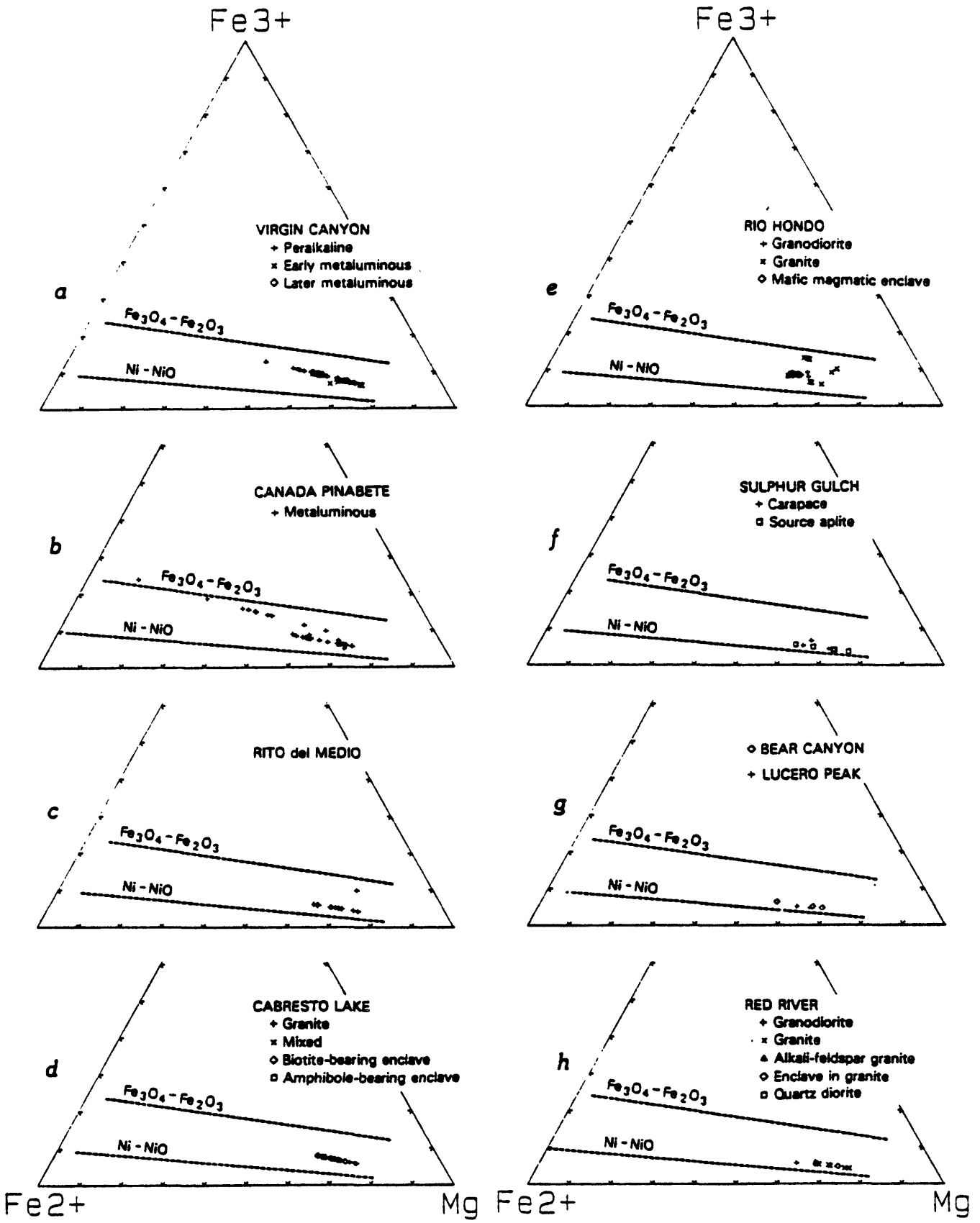
Fe3+
a
VIRGIN CANYON
+ Peralkaline
× Early metaluminous
◇ Later metaluminous
Fe3O4 - Fe2O3
Ni - NiO
b
CANADA PINABETE
+ Metaluminous
c
RITO del MEDIO
d
CABRESTO LAKE
+ Granite
× Mixed
◇ Biotite-bearing enclave
□ Amphibole-bearing enclave
e
RIO HONDO
+ Granodiorite
× Granite
◇ Mafic magmatic enclave
f
SULPHUR GULCH
+ Carapace
□ Source aplite
g
◇ BEAR CANYON
+ LUCERO PEAK
h
RED RIVER
+ Granodiorite
× Granite
▲ Alkali-feldspar granite
◇ Enclave in granite
□ Quartz diorite
Fe2+
Mg

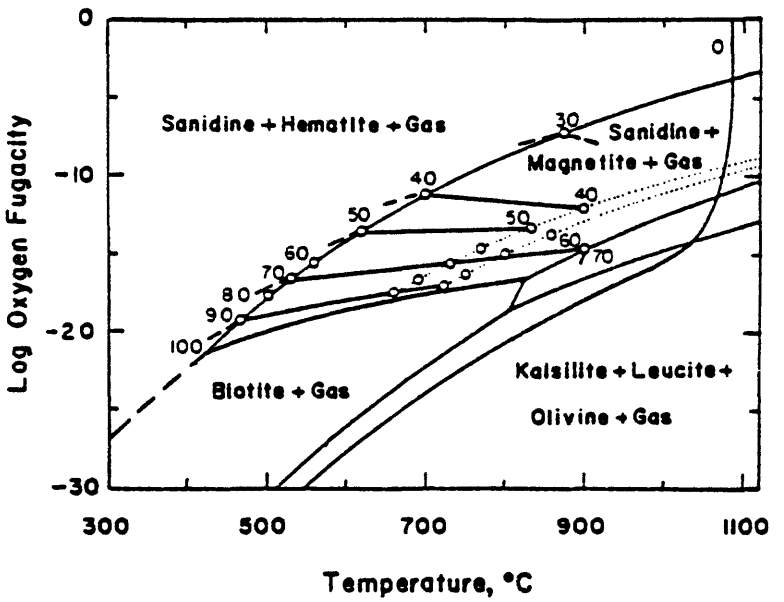

Fig. III.26. Projection of biotite equilibria from the Fe/(Fe+Mg) axis onto the T (°C)-$\log_{10} fO_2$ plane at 2070 bars total pressure. From Wones and Eugster (1965).

Notable in the peralkaline granite of Virgin Canyon and in magnetite-free samples of the Canada Pinabete pluton are records of reducing trends, indicated by more Mg-rich compositions occurring in the cores of grains (Canada Pinabete) or more Mg-rich biotite grains enclosed in larger, more Fe-rich biotite grains (Virgin Canyon). While these textures are less evident than the ilmenite replacement of sphene, both features are in accord.

More Mg-rich biotite compositions in the Cabresto Lake pluton and in the granite of Rio Hondo reflect higher fO_2 during their crystallization than prevailed during crystallization of the granodiorite of Rio Hondo. Rare zoning in biotite, as found in the granite and amphibole-bearing enclaves of the Cabresto Lake pluton and in the granite of Rio Hondo indicates a constant or increasing fO_2 as temperature decreased during biotite crystallization. Absence of zoning, as found in biotite-bearing enclaves of the Cabresto Lake pluton and in mafic-magmatic enclaves in the Rio Hondo pluton reflects the rapid crystallization to be expected in these quenched mafic bodies. Large unzoned biotite grains reflect constant oxygen fugacity during their crystallization. In the Rio Hondo pluton, Fe/(Fe+Mg) in biotite relates well to host-rock SiO_2 content; Mg content of biotite increased with differentiation. This suggests that biotite did not acquire its composition during late magmatic reequilibration processes and that oxygen fugacity was not buffered, but constant or increasing.

Since the classic paper of Wones and Eugster (1965) it has become common place to use calculations of biotite stability to better understand environments of magmatic crystallization. For a number of years, upper limits of biotite stability have been calculated with a revised equation developed in Czamanske and Wones (1973):

$$-1/2\log fO_2 = (7409/T) + 4.25 - \log f_{H_2O} + 3\log X_{Fe}2+ + 2\log X_{OH} - \log a_{KAlSi_3O_8} - \log a_{Fe_3O_4},$$

where T is in ^{o}K; $X_{Fe}2+$ is the number of ferrous iron atoms in the biotite formula divided by three, the total number of octahedral sites; and X_{OH} is equal to the molecular ratio OH/(OH+F).

Waldbaum and Thompson (1969, fig. 3b) have conveniently shown that the activity of $KAlSi_3O_8$ is about 0.6 for temperatures between 600° and 800°C and mole fractions of $KAlSi_3O_8$ between 0.25 and 0.75. Because normative An is less than 1 percent in many of the Questa granites (Table I.10), one can use values of normative Or and Ab to estimate original alkali feldspar compositions. Nine samples containing less than 1 mole percent An yield $X_{KAlSi3O8}$ of 0.45±0.01, with two higher values at 0.52 (82QC30) and 0.55 (82QC22); thus, a value of 0.6 has been used for the activity of $KAlSi_3O_8$ in all calculations. Based on a geologic reconstruction by Lipman (1984, fig. 15), a reasonable assumption is that present levels of exposure correspond to pressures during crystallization of about 700, 1000, and 1500 bars, respectively, for plutons that crystallized within the caldera, along the southern ring fracture, and south of the caldera. Because an aqueous fluid phase appears to have evolved during crystallization of several of the plutons, one may assume that PH_2O was equal to total pressure. Burnham and others (1969) show that over the temperature range 640° to 740°C, values of fH_2O average 564, 746, and 1027 bars, respectively, for PH_2O of 700, 1000, and 1500 bars. Mole fraction of Fe_3O_4 in magnetite is typically measured as 0.98; it is unclear what the activity of magnetite was during biotite crystallization. For the calculations used in figure III.27, a_{Fe3O4} was assumed to be 0.98 for magnetite-bearing granites and in the range 0.2 to 0.6 for the magnetite-free granite of Canada Pinabete. If, for example, one prefers to assume that during biotite crystallization ulvospinel content was 0.4 and a_{Fe3O4} was 0.6 in magnetite-bearing granites, then the curves plotted in figure III.27 for magnetite-bearing granites would be uniformely lowered by 0.42 log units in fO_2. It is appropriate to emphasize that the relations of figure III.27 should be viewed as indications of relative, rather than absolute biotite stability.

The hematite-magnetite and quartz-fayalite-magnetite buffer curves of figure III.27 have been located on the basis of recent data regressions by J. L. Hass, Jr. (U.S. Geological Survey, unpublished data). The curve shown for sphene-ilmenite is based on extrapolation of the data of Lipman (1971; see fig. II.27) obtained from a study of iron-titanium oxide phenocrysts in a sequence of sphene-bearing and sphene-free high-silica tuffs. It is considered to well represent the fO_2-T environment about which the Questa granitic system often fluctuated.

Appropriately, the relations of figure III.27 show that the majority of Questa biotites are stable in association with sphene. Plotted as "Rim and Core, Virgin Canyon" are stability curves based on biotite rim and core

compositons in sample 83QC25 of the early metaluminous granite. The separation between these upper stability limit curves of about 0.6 log fO_2 is created entirely by the difference of 0.06 in $X_{Fe}2+$ between core and rim compositions. This difference is near the average for biotite zoning in 13 other samples from the Virgin Canyon and Canada Pinabete plutons. Typically, therefore, it would appear that the late oxidizing event which caused Mg-enrichment in biotite rims involved an increase in log fO_2 of about 0.6.

Largely because of its relatively high fluorine content, biotite in the Rito del Medio granite is stable at somewhat higher fO_2. This is in keeping with the opaque oxide mineralogy of this pluton, which also indicates it to be one of the more oxidized granites. Fluorine-rich samples of the Canada Pinabete pluton contain biotite of similar stability and, similarly, contain late primary hamatite. In contrast, relatively low fluorine content causes the biotite in the granite of Rio Hondo to have a calculated upper stability limit at significantly lower oxygen fugacities.

Because of relatively restricted ranges in log fH_2O, $X_{Fe}2+$, X_{OH}, $a_{KAlSi3O8}$, and a_{Fe3O4} involved in the calculations, upper stability limit curves for most of the biotites in Table III.7 fall between the curves calculated for zoned biotite in the Virgin Canyon pluton. It is noteworthy that a differential of 500 bars in fH_2O causes a shift of only 0.27 in the log fO_2 for calculated stability curves.

Thus, the notably different stability limit of biotite in magnetite-free samples of the Canada Pinabete pluton stands in sharp contrast to those for the other Questa biotites. The markedly lower stability limit of this biotite is caused predominantely by its high Fe^{2+} content and secondarily by relatively low fluorine content. These calculations of biotite stability provide one of the most tangible illustrations of the unusal conditions associated with crystallization of the magnetite-free parts of the Canada Pinabete pluton.

AMPHIBOLE CHEMISTRY

The 28 reported amphibole analyses represent 63 individual analyses from 24 samples from the Questa granitic plutons (Tables III.9 and III.10). $Fe^{2+}/(Fe^{2+}+Fe^{3+})$ determined on 4 amphibole separates (1 from the granite of Cabresto Lake, 2 from the granodiorite of Rio Hondo, and 1 from the granodiorite of Red River) are quite similar and range from 0.749 to 0.757 (Table III.1). For these three plutons, recalculation of amphibole analyses was made using the Rock and Leake program (1984), based on 23 oxygen ions, with the appropriate $Fe^{2+}/(Fe^{2+}+Fe^{3+})$. An amphibole separate could not be obtained from the only sample containing amphibole in the Canada Pinabete pluton (82QC48) and Fe^{2+} and Fe^{3+} were assigned by the Rock and Leake program. It is probably significant that this, the only one of 25 studied samples of the Canada Pinabete pluton which contains amphibole, is a magnetite-free rock.

A common feature of amphibole in all plutons is filling of the M1-M3 sites to a total of 5 cations, Mn and in rare cases Fe^{2+} being assigned to the M4 sites (Tables III.9 and III.10).

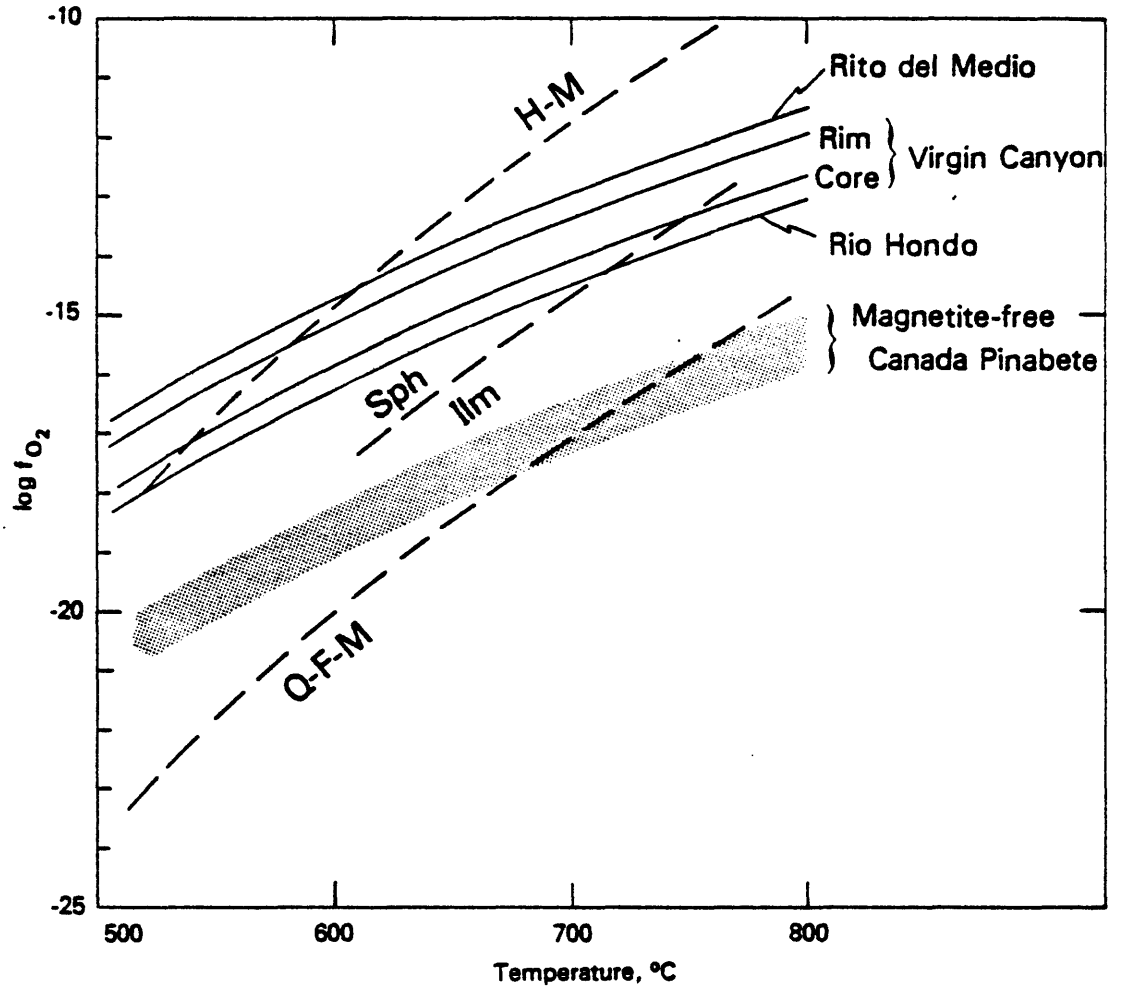

Fig. III.27. Upper stability limits of selected biotites from Questa granitic rocks in terms of temperature and oxygen fugacity, and in relation to selected buffer curves. See text for explanation.

Compositions of amphibole are plotted in a diagram of Si+Na+K against $Ca+Al^{IV}+Fe^{3+IV}$ where the fields of Giret and others (1980) are shown (fig. III.28). The terminology of Leake (1978) indicates that amphibole in the Questa granitic plutons are of hornblende or actinolitic hornblende composition, while the fields of Giret and others indicate hornblende to actinolitic composition. This discrepancy is due to assumption of full M4-site occupancy by Ca for construction of the fields of Giret and others.

As would be expected, amphibole compositions in the Canada Pinabete granite are quite different from those in the three other plutons. Amphibole formed late in the crystallization history and is of ferro-hornblende composition (Leake, 1978), with Fe/(Fe+Mg)>0.77. Si, Mg, and Ca are lower, and Na, Cl, Fe, and Mn are higher than in amphibole in the less silicic, magnetite-bearing units of the other plutons.

Table III.9. Representative electron microprobe analyses and structural formulae for amphiboles in the Canada Pinabete and Cabresto Lake plutons and in the granodiorite of Red River.

	CANADA PINABETE		CABRESTO LAKE						RED RIVER INTRUSIVE COMPLEX	
	Granite		Granite		Mixed		Biotite bearing enclave	Amphibole bearing enclave	Granodiorite	
	82QC48		Core	Rim	Core	Rim			82QC44	
	10	9	(2)	(2)					Core(4)	Rim(2)
SiO_2	43.7	46.0	49.8	48.6	48.8	50.0	49.4	49.5	51.1	48.8
Al_2O_3	5.90	5.52	4.80	5.38	5.01	4.66	4.47	4.79	3.84	5.39
TiO_2	1.02	0.82	0.93	1.08	1.10	1.01	0.85	0.96	0.65	1.06
Fe_2O_3	-	-	3.37	3.49	3.37	3.09	3.11	3.23	3.26	3.64
FeO	31.3^T	27.4^T	8.77	9.06	8.77	8.02	8.10	8.40	8.27	9.23
MnO	1.52	3.06	1.16	1.07	1.03	0.92	1.16	0.96	0.45	0.45
MgO	2.43	4.54	15.8	15.2	15.6	16.0	16.1	16.0	16.5	15.3
CaO	9.26	9.31	11.2	11.2	11.0	11.3	11.3	11.4	11.2	12.5
Na_2O	1.86	1.86	1.73	1.84	1.64	1.42	1.44	1.38	0.84	1.07
K_2O	0.81	0.73	0.59	0.66	0.60	0.51	0.49	0.56	0.36	0.54
F	1.0	-	1.4	1.5	1.2	1.2	1.0	1.2	0.5	0.4
Cl	0.22	-	0.05	0.06	0.05	0.05	0.05	0.06	0.04	0.06
	97.80*	99.24	98.15	97.58	96.92	96.93	96.42	97.18	96.47	97.98
Si	6.886	7.003	7.194	7.091	7.142	7.260	7.233	7.198	7.381	7.119
Al^{IV}	1.097	0.991	0.806	0.909	0.858	0.740	0.767	0.802	0.619	0.881
Fe^{3+IV}	0.017	0.006	-	-	-	-	-	-	-	-
Al^{VI}	-	-	0.012	0.017	0.007	0.058	0.005	0.020	0.035	0.046
Fe^{3+VI}	1.015	1.082	0.366	0.383	0.371	0.338	0.343	0.354	0.354	0.400
Fe^{2+}	3.090	2.399	1.059	1.105	1.073	0.973	0.991	1.021	0.986	1.110
Mg	0.571	1.031	3.404	3.307	3.405	3.465	3.516	3.470	3.554	3.328
Mn	0.203	0.394	0.058	0.069	0.023	0.056	0.051	0.030	-	-
Ti	0.121	0.094	0.101	0.119	0.121	0.110	0.094	0.105	0.071	0.116
Sum M1-M3	5.000	5.000	5.000	5.000	5.000	5.000	5.000	5.000	5.000	5.000
Mn	-	0.001	0.084	0.063	0.105	0.057	0.093	0.088	0.055	0.056
Fe	-	-	-	-	-	-	-	-	0.012	0.015
Ca	1.563	1.518	1.733	1.751	1.725	1.758	1.773	1.776	1.826	1.828
Na	0.437	0.481	0.183	0.186	0.170	0.185	0.134	0.136	0.107	0.101
Na	0.131	0.068	0.301	0.344	0.295	0.215	0.275	0.253	0.128	0.202
K	0.163	0.142	0.109	0.123	0.112	0.094	0.092	0.104	0.066	0.101
Sum A	0.294	0.210	0.410	0.457	0.407	0.309	0.367	0.357	0.194	0.303
Fe/(Fe+Mg)	0.878	0.772	0.295	0.310	0.298	0.274	0.275	0.284	0.276	0.314

* Sums do not include F and Cl.

Table III.10. Representative electron microprobe analyses and structural formulae for amphiboles in granodiorite of the Rio Mondo pluton and a cross-cutting quartz latite dike.

	Granodiorite														Quartz latite dike		
	82QC26		82QC28		84QC31			82QC12					Q83J59	Q84J6	82QC2	Q83J100		
	Core, 5	Rim, 5	Host (4)	Enclave (3)	Host Core	Host Rim	Enclave	Host (3)	Enclaves (4)			Schlieren (4)	(2)	(2)	4	(2)	(3)	Grndm.
									Range									
SiO_2	46.1	48.0	50.5	49.7	47.8	50.4	50.1	47.6	48.1	44.6	50.9	48.1	51.4	50.2	51.2	46.4	47.9	48.9
Al_2O_3	7.43	5.81	4.08	4.80	6.14	4.23	4.60	6.23	6.13	8.01	3.90	6.01	3.62	4.85	3.65	7.05	6.19	5.38
TiO_2	1.35	1.04	0.69	0.81	0.94	0.58	0.63	1.15	1.06	1.60	0.38	0.99	0.65	0.73	0.32	1.30	1.07	0.88
Fe_2O_3	4.05	3.67	3.28	3.47	3.64	2.98	3.39	3.86	3.91	4.40	3.47	3.80	2.75	3.76	3.42	3.94	3.69	3.47
FeO	11.2	10.1	9.05	9.58	10.0	8.22	9.35	10.6	10.8	12.1	9.58	10.5	8.43	9.42	9.43	10.9	10.2	9.58
MnO	0.41	0.37	0.51	0.54	0.51	0.52	0.49	0.58	0.55	0.50	0.52	0.61	0.46	0.60	0.80	0.43	0.44	0.45
MgO	13.3	14.7	15.7	15.0	14.6	16.0	15.5	13.9	13.8	11.9	15.4	14.0	16.9	15.0	15.6	13.6	14.4	15.0
CaO	11.5	11.5	11.8	11.7	11.6	11.7	11.8	11.6	11.9	11.6	12.0	11.6	11.6	11.9	11.8	11.6	11.6	11.8
Na_2O	1.46	1.30	1.01	1.05	1.17	0.89	0.93	1.17	1.00	1.45	0.60	1.04	0.95	0.91	0.86	1.44	1.31	1.13
K_2O	0.84	0.64	0.43	0.50	0.58	0.37	0.42	0.64	0.63	0.93	0.48	0.62	0.36	0.47	0.35	0.77	0.64	0.58
F	0.4	0.4	0.5	-	0.4	0.5	0.5	-	-	-	-	-	0.6	-	0.6	-	-	-
Cl	0.09	0.06	0.03	-	0.04	0.02	0.03	-	-	-	-	-	0.05	-	0.01	-	-	-
	97.64*	97.13	97.05	97.15	96.98	95.89	97.21	97.33	97.88	97.09	97.23	97.27	97.12	97.84	97.43	97.43	97.44	97.17
Si	6.809	7.047	7.339	7.247	7.025	7.316	7.281	7.001	7.036	6.683	7.393	7.065	7.412	7.261	7.419	6.853	7.018	7.144
Al^{IV}	1.191	0.953	0.661	0.753	0.975	0.684	0.719	0.999	0.964	1.317	0.607	0.935	0.588	0.739	0.581	1.147	0.982	0.856
Al^{VI}	0.103	0.053	0.038	0.073	0.089	0.040	0.070	0.082	0.094	0.099	0.061	0.106	0.028	0.089	0.043	0.081	0.088	0.071
Fe^{3+}	0.450	0.406	0.359	0.381	0.403	0.362	0.371	0.427	0.430	0.496	0.379	0.420	0.298	0.409	0.373	0.438	0.407	0.382
Fe^{2+}	1.368	1.207	1.099	1.168	1.204	1.071	1.131	1.307	1.318	1.521	1.163	1.287	0.969	1.139	1.142	1.341	1.241	1.170
Mg	2.929	3.219	3.403	3.262	3.200	3.464	3.359	3.049	3.010	2.659	3.336	3.066	3.634	3.236	3.371	2.996	3.146	3.268
Mn	-	-	0.026	0.027	-	-	-	0.008	0.031	0.045	0.019	0.012	-	0.048	0.036	-	-	0.012
Ti	0.150	0.115	0.075	0.089	0.104	0.063	0.069	0.127	0.117	0.180	0.042	0.109	0.071	0.079	0.035	0.144	0.118	0.097
Sum M1-M3	5.000	5.000	5.000	5.000	5.000	5.000	5.000	5.000	5.000	5.000	5.000	5.000	5.000	5.000	5.000	5.000	5.000	5.000
Mn	0.051	0.046	0.037	0.040	0.064	0.064	0.060	0.064	0.037	0.019	0.045	0.064	0.056	0.026	0.062	0.054	0.055	0.044
Fe	0.010	0.033	-	-	0.028	0.036	0.005	-	-	-	-	-	0.047	-	-	-	0.006	-
Ca	1.820	1.809	1.837	1.828	1.826	1.819	1.837	1.828	1.865	1.862	1.867	1.825	1.792	1.844	1.832	1.836	1.821	1.847
Na	0.119	0.112	0.126	0.132	0.082	0.081	0.098	0.108	0.098	0.119	0.088	0.111	0.105	0.130	0.106	0.110	0.118	0.109
Na	0.299	0.258	0.159	0.165	0.251	0.169	0.164	0.226	0.186	0.302	0.081	0.185	0.161	0.125	0.136	0.302	0.254	0.211
K	0.158	0.120	0.080	0.093	0.109	0.069	0.078	0.120	0.118	0.178	0.089	0.116	0.066	0.087	0.065	0.145	0.120	0.108
Sum A	0.457	0.378	0.239	0.258	0.360	0.238	0.242	0.346	0.304	0.480	0.170	0.301	0.227	0.212	0.201	0.447	0.374	0.319
Fe/(Fe+Mg)	0.384	0.338	0.300	0.322	0.338	0.298	0.310	0.363	0.367	0.431	0.316	0.358	0.266	0.324	0.310	0.373	0.345	0.322

* Sum do not include F and Cl.

Amphiboles in the Cabresto Lake and Rio Hondo plutons and in the Red River intrusive complex are quite similar in composition and range from magnesio-hornblende to actinolitic hornblende (Leake, 1978). As might be expected for more siliceous host rocks, Ca is less abundant and Mn, Na, and F are more abundant in amphibole in the Cabresto Lake pluton. Spot analyses across large amphibole crystals reveal zoning which is not apparent under the microscope.

The range of composition of amphibole in the Cabresto Lake pluton is rather small. Zoning is characteristic of the granitic and mixed units; weak zoning trends are toward Si and Mg impoverishment in the granite and enrichment in the mixed unit. In both cases, changes in Al, Fe, Na, K, and Ti contents are opposite to those of Si and Mg. The compositions of amphibole in the two types of enclave are remarkably similar to those in the host rocks, indicating magmatic equilibrium.

Amphibole compositions cover a larger range in the Rio Hondo pluton. This range is roughly related to SiO_2 content of the host rock, with Si in amphibole increasing as host-rock SiO_2 content increases. There is also a rough positive correlation between Fe/(Fe+Mg) in amphibole and host-rock SiO_2 content. Si and Mg increase with host-rock SiO_2 content and from core to rim in zoned crystals, while Fe, Al, Ti, Na, and K decrease. Increase in Mg content is rather unusual in an igneous environment and is yet another indication of the late oxidizing trend that characterized crystallization in these plutons. Typically there is iron enrichment in amphibole as host-rock SiO_2 content increases (Wones and Gilbert, 1982). Mn content increases with differentiation, but is not related to zoning; Ca content is rather constant. Overall, there is a trend from magnesio-hornblende in Si-poor rocks and in cores of zoned crystals, to actinolitic hornblende in Si-rich rocks and in rims of zoned crystals. Compositions of amphiboles in mafic-magmatic enclaves fall in the range defined by amphiboles in the granodiorite. In the quartz latite dike, groundmass amphibole is enriched in Mg compared to amphibole in phenocrysts.

Fig. III.28. Si+Na+K against $Ca+Al^{IV}+Fe^{3+IV}$ (cations) for calcic amphiboles in the Questa granitic plutons. Fields are from Giret and others (1980) after the classification of Leake (1978). Crosses, magnetite-free granite (82QC48) of Canada Pinabete; diamonds, granite, mixed unit, and enclaves of Cabresto Lake; triangles, granodiorite, enclaves, and quartz latite dike of Rio Hondo; x's, granodiorite of Red River.

Fig. III.29. Si (cations) against Fe/(Fe+Mg) for calcic amphiboles in the Questa granitic plutons. Symbols as in fig. III.28.

Fig. III.30. $Al^{VI}+Fe^{3+VI}+2Ti+$sum of A-site cations against $Al^{IV}+Fe^{3+IV}+Na^{M4}$ for calcic amphiboles in the Questa granitic plutons. 1:1 correlation line shown for reference. Symbols as in fig. III.28.

Fig. III.31. Mg (cations) against $Mn+Fe^{2+}$ in octahedral sites for calcic amphibole in the Questa granitic plutons. 1:1 correlation line shown for reference. Symbols as in fig. III.28.

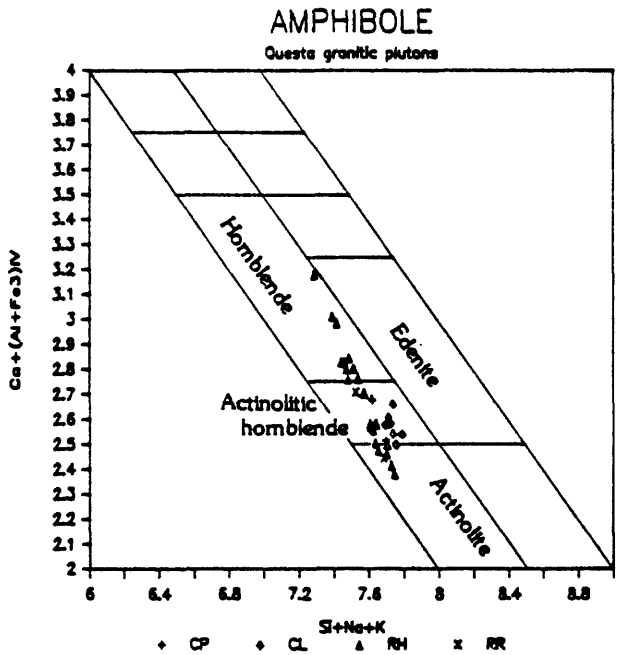

Fig. III.28.

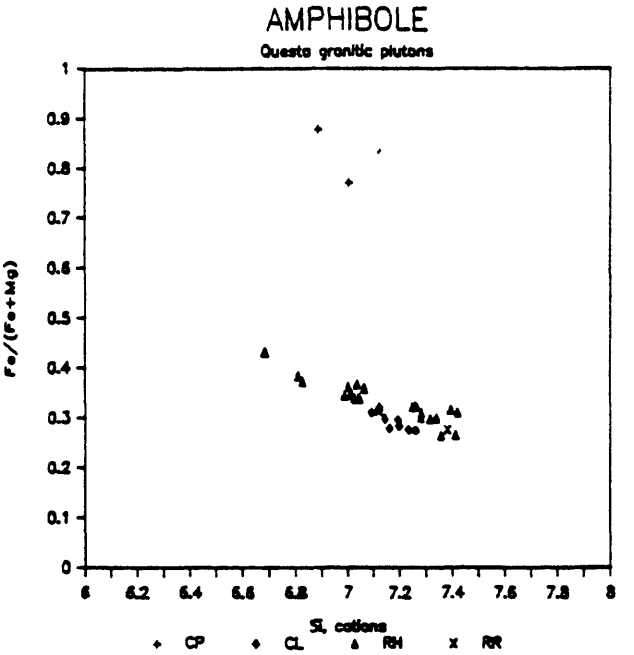

Fig. III.29.

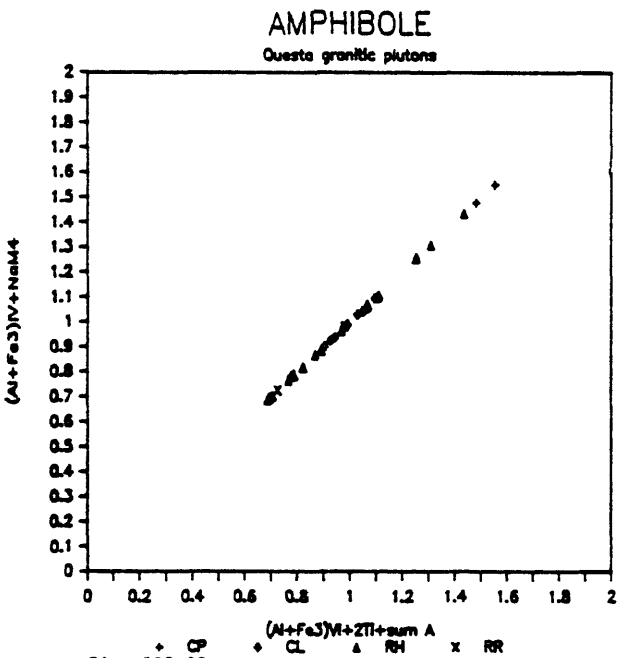

Fig. III.30.

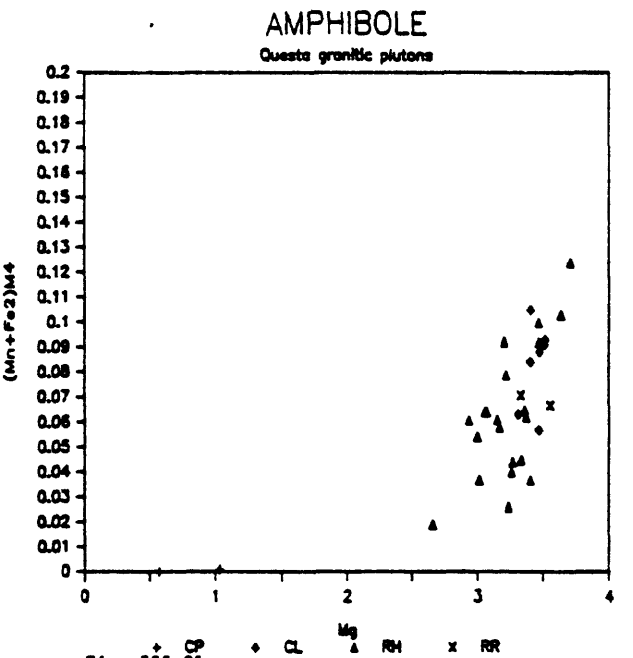

Fig. III.31.

Amphibole in the granodiorite of the Red River intrusive complex shows the same zoning as that in the granite of the Cabresto Lake pluton, with actinolitic-hornblende cores and magnesio-hornblende rims. It is appreciably lower in Na_2O and F content.

There is good negative correlation between Si cations and Fe/(Fe+Mg) in amphibole from the Cabresto Lake and Rio Hondo plutons and the Red River intrusive complex (fig. III.29). Amphibole in the Canada Pinabete pluton falls in a different area, well off this trend. The relation between Si and Fe/(Fe+Mg) in amphibole in the Rio Hondo pluton is the same as that in the Finnmarka complex, Norway (Czamanske and Wones, 1973; Wones and Gilbert, 1982).

The simplest clino-amphibole formula can be written $[]Ca_2(Fe^{2+},Mg)_5Si_8O_{22}(OH)_2$. Substitutions involving ions of lesser or greater charge are balanced in diverse ways (e.g., Czamanske and Wones, 1973, p. 360). However, consideration of this basic formula shows that charge can only be decreased by replacement of Ca by Na in the M4 site or of Si by Al or Fe^{3+}. Conversely, charge is increased by addition of Na or K to the A site and Al, Fe^{3+}, or Ti to the octahedral sites.

A plot of Mg against Fe^{2+} shows a good negative correlation with a slope of about 4:7 and an intercept of about 3.1 Fe^{2+} cations at 0.0 Mg cation ; data for amphibole in the Canada Pinabete pluton plot on the same trend. A plot of Mg cations against $Fe^{2+}+Al^{VI}+Fe^{3+VI}+Ti+Mn$ cations (not shown) indicates an excellent correlation with a slope of -1. This shows that Mg substitutes for Fe^{3+}, Al, Ti, and Mn as well as for Fe^{2+} in the M1-M3 sites and that the M1-M3 sites are fully occupied (see also Tables III.9 and III.10). Because the M1-M3 sites are fully occupied for all amphibole compositions found in the Questa granitic rocks, these sites contain an excess total charge that must be balanced by substitutions in other sites. A plot of $Al^{VI}+Fe^{3+VI}+2Ti+A$-site occupancy against $Al^{IV}+Fe^{3+IV}+Na^{M4}$ shows an excellent positive correlation with a slope of 1 (fig. III.30), indicating that charge balance is well maintained in these amphiboles. For amphiboles in the Questa granitic rocks $Mn+Fe^{2+}$ occupancy of the M4 sites increases with increasing Mg content (fig. III.31).

CORRELATION BETWEEN BIOTITE AND AMPHIBOLE CHEMISTRY

A plot of $Fe^{2+}/(Fe^{2+}+Mg)$ in biotite against $Fe^{2+}/(Fe^{2+}+Mg)$ in amphibole (fig. III.32) shows that the pairs in the granite of Cabresto Lake and in the granodiorites of Rio Hondo and Red River share a common trend. The slope is about 1 and biotite is slightly iron enriched compared to amphibole. The distribution is the same as that described by Speer (1984) for a number of igneous rocks. The pairs from the Questa granitic rocks plot toward the magnesian-rich end of Speer's plot. The pairs from the Canada Pinabete granite plot far off that trend, show substantial iron enrichment in amphibole compared to biotite, and no relation between $Fe^{2+}/(Fe^{2+}+Mg)$ in amphibole and that in biotite. These features are probably not related to differences in

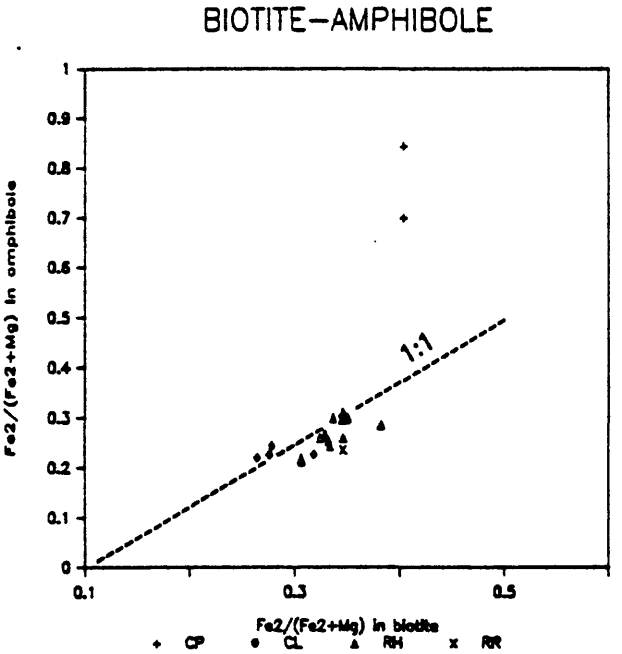

Fig. III.32. $Fe^{2+}/(Fe^{2+}+Mg)$ in biotite against $Fe^{2+}/(Fe^{2+}+Mg)$ in amphibole for the Questa granitic plutons. 1:1 correlation line shown for reference. Symbols as in fig. III.28.

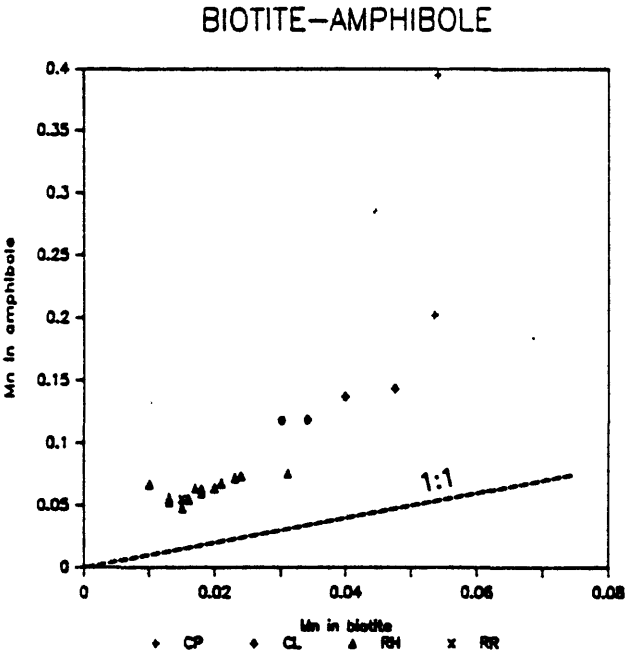

Fig. III.33. Mn in biotite against Mn in amphibole (cations) for the Questa granitic plutons. 1:1 correlation line shown for reference. Symbols as in fig. III.28.

magma chemistry, but to the low oxygen fugacity characteristic of the magnetite-free amphibole-bearing sample from the Canada Pinabete pluton; they may also indicate that amphibole and biotite are not in equilibrium in the rock.

The distribution coefficient, defined as $(Mg/Fe)_{biotite}/(Mg/Fe)_{amphibole}$ ranges from 0.62 to 0.89 for amphibole-biotite pairs in the granite of Cabresto Lake and the granodiorites of Rio Hondo and Red River. This is close to the range of 0.66 to 1.1 reported by Speer (1984) for biotite and amphibole pairs in igneous rocks. The pairs in the Canada Pinabete granite have far different distribution coefficients (3.7 and 7.9) due to iron enrichment in amphibole and Mg enrichment in biotite.

The distribution of Mn between biotite and amphibole (fig. III.33) is typical for igneous rocks, in that Mn is concentrated in amphibole over biotite (Speer 1984, fig. 6). The proportion $Mn_{amphibole}/Mn_{biotite}$ is relatively constant between 2.5 and 4.3, except for two values of 7.3 (Canada Pinabete) and 6.7 (biotite-rich enclave in the Rio Hondo pluton). The slope for the pairs in the Questa granitic rocks is about 3:1; the highest Mn contents are found in the Canada Pinabete sample.

An interesting feature of the relation between amphibole and biotite is the common presence of well-formed crystals of biotite enclosed in amphibole (Plate III.3, d). In all of the Questa granitic rocks that contain amphibole, early-formed biotite is present as inclusions in amphibole. This order is the opposite of that defined by Bowen (1922) for a liquid with a starting basaltic composition which undergoes fractional crystallization.

Wones and Gilbert (1982) relate the order of crystallization of amphibole and biotite to the reaction:

$$NaCa_2Fe_4AlSi_6Al_2O_{22}(OH)_2 + KAlSi_3O_8 + SiO_2 = NaAlSi_3O_8 + CaAl_2Si_2O_8 + CaFeSi_2O_6 + KFe_3AlSi_3O_{10}(OH)_2;$$

low activities of $KAlSi_3O_8$ and SiO_2 shift the reaction to the left (crystallization of amphibole followed by crystallization of biotite), and low f_{H_2O} and moderate K_2O shift the reaction to the right (biotite crystallizes first).

SUMMARY AND CONCLUSIONS

Except in magnetite-free samples of the Canada Pinabete granite, Fe/(Fe+Mg) in biotite is less than 0.5, corresponding to a quite high Mg content for biotite in siliceous granites.

$Fe^{2+}/(Fe^{2+}+Fe^{3+})$ for biotite is quite similar in all plutons (Table III.6) and all biotite compositions plot between the Ni-NiO and Fe_3O_4-Fe_2O_3 buffer curves in the Fe^{3+}-Fe^{2+}-Mg diagram of Wones and Eugster (1965). However, as shown by the opaque oxide chemistry, oxygen fugacity was quite different in the different plutons, the lowest fO_2 being characteristic of the peralkaline granites and the highest characteristic of the granodiorites. Decrease in Fe/(Fe+Mg) indicates an oxidation trend (Wones and Eugster, 1965) during crystallization of biotite in most units of the Questa granitic plutons.

Biotite composition is related both to host rock chemistry and to occurrence. High SiO_2 rocks contain biotite with high F, Mn, Mg, and Si contents; more mafic rocks contain biotite with higher Al, Fe, and Ti contents. Biotite in the three northern intracaldera plutons is marked by an unusually broad, sharply bounded rim of Mg-rich composition, indicating an abrupt and sustained increase in oxygen fugacity. Opposing zoning trends in biotite in magnetite-free samples of the Canada Pinabete pluton show that oxygen fugacity was fluctuating during crystallization. In the other plutons, zoned grains are not as common as homogeneous grains but, when present, show the same oxidation trend as in the northern intracaldera plutons.

Amphibole is also characterized by high Mg content (Mg>Fe) except in the sample from the Canada Pinabete pluton in which Fe>Mg. All amphiboles are characterized by full occupancy of the M1-M3 sites. Zoning in amphibole in the Rio Hondo pluton indicates Si and Mg enrichment with differentiation; however zoning in amphibole from the Cabresto Lake granite and the Red River granodiorite is in the opposite sense, with Si and Mg impoverishment during differentiation.

page 180 follows

Conclusion

CHAPTER IV

This study deals with the nine granitic plutons emplaced shortly after the formation of Questa caldera (28 Ma) in the southern Sangre de Cristo Mountains of northern New Mexico. Three plutons with alkaline affinities were emplaced in the northern part of the caldera. The Virgin Canyon and Canada Pinabete plutons include a peralkaline and two metaluminous granitic units. The Rito del Medio pluton, emplaced slightly later, contains only metaluminous granite. Two plutons were subsequently emplaced within (Cabresto Lake, calc-alkaline monzonitic) and south of (Rio Hondo, calc-alkaline granodioritic) the caldera. A few million years later, three plutons intruded the southern margin of the caldera. These are the Bear Canyon (medium-K calc-alkaline) and the Sulphur Gulch (medium- to high-K calc-alkaline) plutons and the Red River intrusive complex (medium- to high-K calc-alkaline). Finally, the Lucero Peak pluton was emplaced south of the Rio Hondo pluton and has calc-alkaline granodioritic affinities.

Detailed study of the mineralogy of the granitic rocks has established trends of chemical evolution and allowed assessment of relative temperatures and oxygen fugacities during crystallization of these different plutons.

The Fe,Ti,Mn-oxide minerals, sphene, and rutile occur in an unprecedented variety of assemblages in the Questa granitic rocks. Relations among these minerals clearly indicate that during emplacement and crystallization, oxygen fugacities within the plutons often changed significantly from those which characterized the magmas at depth and suggest that crystallization took place over an extended time interval. Accessory minerals as well as calcic amphibole chemistry, often indicate that reversals in the trend of change in oxygen fugacity took place during crystallization.

Strong evidence that the entire magmatic system at Questa was characterized by high intrinsic oxygen fugacity is provided by the abundance of early-formed sphene in all rocks of granodioritic composition, and the occurrence of sphene in high silica granitic rocks. Indeed, the high proportion of Fe_2O_3 in ilmenite in the granodiorite of Rio Hondo and the fact that the proportion of ilmenite to magnetite is only 1 to 20, suggest that oxygen fugacity was nearly above the ilmenite stability field.

Most often, reequilibration of opaque oxide pairs took place between the Q-F-M and H-M buffer curves. However, the alkali-feldspar granite of Red River, where ilmenite is absent and hematite and rutile are typical, was characterized by higher fO_2; fO_2 also became quite high during the late stages of crystallization in the Canada Pinabete and Rito del Medio granites, where primary hematite is characteristic in vugs. Opaque oxide minerals in the peralkaline granites of Virgin Canyon and Canada Pinabete formed under even more reducing conditions, below the stability of magnetite.

Chemistry of the opaque oxide minerals shows that oxygen fugacity must have been fluctuating during their crystallization and reequilibration in most of the Questa granitic rocks.Responding to changes in oxygen fugacity within the crystallizing magmas, the assemblage primary sphene + ilmenite was affected in many ways.

1) When oxygen fugacity remained high, sphene remained stable. Large sphene grains containing disoriented ilmenite granules prove that during limited intervals, sphene and ilmenite crystallized contemporaneously in the granite of Cabresto Lake and the granodiorites of Rio Hondo and Red River. Ti expelled from magnetite was precipitated as sphene. Sphene rims ilmenite in seriate-textured samples of the peralkaline granite of Virgin Canyon.

2) If oxygen fugacity fell, sphene was replaced by ilmenite. Lozenge-shaped aggregates of small, irregular ilmenite grains characterize the outer margin of the peralkaline granites of Virgin Canyon, as well as the granites of Red River and Rito del Medio. Characteristic of all but the Rito del Medio granite is lack of both hematite exsolution lamellae in ilmenite and ilmenite with high Fe^{3+} content. In the Rito del Medio granite, ilmenite replacement of sphene is the only indication of a relatively reducing interlude which ocurred between the time of incorporation of early hematite in silicates and the growth of late hematite in vugs.

3) In the late, oxidizing regime of active hydrothermal circulation, sphene was unstable and was replaced by rutile, often in association with primary hematite. Rutile is found in the granite of Rito del Medio, the source aplite and carapace units of the Sulphur Gulch pluton, and the alkali-feldspar granite of Red River.

More subtle indications of relative oxygen fugacity among units and fluctuation in oxygen fugacity during varying stages of crystallization are given by the Fe^{3+} contents of ilmenite. Lowest Fe_2O_3 contents are found in the granite of Rio Hondo and highest in the quartz diorite of Red River.

Czamanske and Wones (1973) proposed that high-level granitic magmas can become internally oxidized if exsolved water dissociates and H_2 gas is lost. While other studies have invoked a similar interpretation to explain Mg-enrichment trends in mafic silicates minerals, H_2 gas migration provides appealing solutions to various complexities in Fe,Ti-oxide and sphene relations in the Questa granitic rocks. H_2 gas migration through the magma provides a convenient explanation for the localized magnetite-free areas of the Canada Pinabete pluton, as well as for several instances in which minerals in the marginal parts of a pluton record a more reduced state.

1) The marginal peralkaline granites of the Virgin Canyon and Canada Pinabete plutons record lower fO_2 conditions than the inner, metaluminous granites, as evidenced by a) a greater proportion of ilmenite, b) lower concentrations of Fe^{3+} in primary ilmenite, and c) replacement of sphene by ilmenite. Moreover, the proportion of ilmenite to magnetite is greater in the groundmass than among the phenocrysts.

2) As opposed to the typical facies, ilmenite in the magnetite-free samples of the metaluminous granite of Canada Pinabete is free of hematite exsolution lamellae.

3) Fe^{3+} concentrations in primary homogeneous ilmenite are lower in the granite of Rio Hondo than in the granodiorite.

Opaque oxide pairs also indicate differences in crystallization temperature between the different units of the Questa granitic system. The peralkaline granites of Virgin Canyon and Canada Pinabete contain oxide pairs which reequilibrated at the highest temperatures among the Questa granitic plutons, and rather high temperatures are given by oxide pairs in the southern caldera margin intrusions.

Except for a few samples, values of $Fe^{2+}/(Fe^{2+}+Fe^{3+})$ for biotite separates in a variety of units of the Questa granitic plutons are rather uniform and indicate that biotite crystallized at oxygen fugacities limited by the Ni-NiO and H-M buffer curves. Comparison of opaque oxide and biotite data show that for the peralkaline granites there was a general increase in fO_2 from the time of opaque oxide crystallization. Study of zoning in

biotite shows that fO_2 was often still increasing during its crystallization, except in rare cases such as the peralkaline granites of Virgin Canyon and Canada Pinabete, or the magnetite-free granite of Canada Pinabete. Study of zoning in amphibole, however, shows oxidizing (Rio Hondo) as well as reducing (Cabresto Lake and Red River) trends during its crystallization; this, as well as opaque oxide chemistry, shows the fluctuating character of oxygen fugacity in these high-level granitic plutons.

Ilmenite, biotite and amphibole are typically Mn-rich in all Questa granitic rocks. The highest Mn contents are found in the alkaline types. Analyses of ilmenites and biotites reveal significant Mn enrichment with differentiation.

These characteristics of opaque oxide and mafic silicate mineral compositions together with geochemical data (Johnson, 1986) make the Questa magmatic system exceptionally interesting to study. Its emplacement encompasses the time of change from a compressional to an extensional tectonic regime, during the late Oligocene and early Miocene. The compressional tectonic regime is believed to be related to a double subduction system underneath northwestern America. The extensional regime, as exemplified by the opening of the Rio Grande Rift, was related to a right-transcurrent fault system between the American and western Pacific plates after intersection of the East Pacific Rise with the mid-Tertiary continental margin trench. The change in tectonic regime was accompanied by a change in associated magmatism, from calc-alkaline to alkaline compositions, which reflects tapping of a different source.

Petrographic and chemical studies indicate the coexistence of two rock series among the Questa granitic rocks, corresponding to two series of magmas in the Questa magmatic system. One series has calc-alkaline affinities and comprises the Cabresto Lake, Rio Hondo, Bear Canyon, and Lucero Peak plutons, as well as the granodiorite and quartz diorite of Red River. Most of these units belong to the calc-alkaline granodioritic (medium K) trend defined by Lameyre and Bowden (1982). However, the granite of Cabresto Lake belongs to the calc-alkaline monzonitic (high K) trend and its border facies is intermediate to metaluminous rocks associated with the alkaline trend. Their trace-element distribution (HREE depleted, no Eu anomalies, high Sr, Nb + Y against Rb) is typical of subduction-related magmatism (VAG of Pearce and others, 1984).

The other series is of alkaline composition and comprises the peralkaline granites of Virgin Canyon and Canada Pinabete as well as their "associated" metaluminous granites whose mode parallels the aluminous trend in alkaline provinces. The Rito del Medio granite is interpreted to be a somewhat unusual member of this aluminous, alkaline trend. These rocks are HREE enriched with strong negative Eu anomalies and are Sr depleted (feature characteristic of within-plate magmatism. The distribution of Nb + Y compared to Rb relates them to within-plate granites (WPG of Pearce and others, 1984) .

The plutons that belong to the calc-alkaline series (such as the Rio Hondo pluton) were emplaced after those of the alkaline series. Thus, time of emplacement and rock geochemistry are not in accord with a transition from a compressional to an extensional tectonic regime. The later-emplaced calc-alkaline pluton of Rio Hondo is interpreted to have differentiated, at an earlier stage, from a calc-alkaline magma related to the subduction. The

later-emplaced alkaline plutons are interpreted to have differentiated later, from an alkaline magma related to within-plate magmatism.

It is possible to relate the location of the plutons with their depth of emplacement, the basal Tertiary surface being about 2 km higher in the south than in the north. This is interpreted as the result of post-Miocene tilting, which could be related to the rise of these light magmas through the crust. As indicated by opaque oxide pairs, the northern intracaldera plutons are derived from hotter magmas which could rise faster and higher in the crust than the cooler Rio Hondo magma. Higher temperature can also explain why the peralkaline magmas were more contaminated by crustal material than the calc-alkaline magmas.

Petrographic and geochemical data show, therefore, that the granitic rocks of the Questa magmatic system exemplify the rapid change in tectonic regime from compressional to extensional. Such associations of alkaline and calc-alkaline granitic rocks, reflecting changes in tectonic regime and sources, have been described in other areas in the world.

In the Arabian Shield, Harris (1985) describes alkaline complexes of two types. One type contains only alkaline rocks and is clearly related to within-plate magmatism, derived from upper mantle sources. The other type (Jabel Sayid complex) contains calc-alkaline and alkaline components. The calc-alkaline granitoids show geochemical characteritics of arc-related magmatism, and the alkaline granitoids have within-plate geochemical characteristics.

In the Adrar des Iforas (Ba and others, 1985; Liégeois and Black, 1986) one low-K calc-alkaline, two high-K calc-alkaline, and an alkaline trend are distinguished. Trace-element data relate the calc-alkaline granitoids to volcanic-arc or syn-collision magmatism, and the alkaline granitoids to within-plate magmatism (Liégeois and Black, 1986, after Pearce and others, 1984).

As in the Jabel Sayid complex of the Arabian Shield and in the Adrar des Iforas, the Questa granitic system is devoid of silica-undersaturated rocks. The three provinces postdate a period of active subduction, which was followed by a period of oblique collision in the Adrar des Iforas. The switch from calc-alkaline to alkaline magmatism is usually rapid, over a period estimated at less than 10 Ma in the Adrar des Iforas and less than 2 Ma in the Questa magmatic system.

Harris (1985) and Liégeois and Black (1986) consider the formation of such complexes to occur in a changing environment which allows tapping from different sources. The calc-alkaline magmas are generated from a mantle source hydrated by the underlying plunging plate. The alkaline magmas seperated from a more primitive non-hydrated mantle source. In the Adrar des Iforas, as in the Questa granitic rocks, $^{87}Sr/^{86}Sr$ initial indicates more participation of continental crust for the alkaline rocks than for the calk-alkaline rocks.

Petrographic and geochemical similarities of Questa with the Adrar des Iforas and the Jabel Sayid complex indicate two mantle sources for the Questa magmatic system. In the Adrar des Iforas, Liégeois and Black (1986) propose a model "whereby asthenospheric mantle originally underlying the subducted plate has risen to shallow depth beneath the continental lithosphere after the rupture of the cold plunging plate".

page 186 follows

Bibliography

Appendix

REFERENCES

Anderson, A. T., 1968, Oxidation of the LaBlache Lake titaniferous magnetite deposit, Quebec: Journal of Geology, v. 76, p. 528-547.

Atwater, T., 1970, Implications of plate tectonics for the Cenozoic tectonics of western North America: Geological Society of America Bulletin, v. 81, p. 3513-3536.

Ba, H., Black, R., Benziane, B., Diombana, D., Hascoet-Fender, J., Bonin, B., Fabre, J., and Liégeois, J. P., 1985, La province des complexes annulaires alcalins sursaturés de l'adrar des Iforas, Mali: Journal of African Earth Sciences, v. 3, p. 123-142.

Bailey, D. K. 1969, The stability of acmite in the presence of H_2O: American Journal of Science, v. 267-A, p. 1-16.

Baker, D. R., 1955, Geology of the Edison area, Sussex County, New Jersey: Princeton, New Jersey, Princeton University, Ph.D. thesis.

Basta, E. S., 1959, Some mineralogical relationships in the system Fe_2O_3-Fe_3O_4 and the composition of titanomaghemite: Economic Geology, v. 54, p. 698-719.

Basta, E. S., 1960, Natural and synthetic titanomagnetites (the system Fe_3O_4-Fe_2TiO_4-$FeTiO_3$): Neues Jahrbuch fur Mineralogie Abhandlungen, v. 94, p. 1017-1048.

Bence, A. E., and Albee, A. L., 1968, Empirical correction factors for the electron microanalysis of silicates and oxides: Journal of Geology, v. 76, p. 382-403.

Bonin, B., 1972, Le complexe granitique subvolcanique de la région de Tolla-Cauro (Corse): Thêse 3e cycle, Paris VI, publiée en 1973 par Laboratoire Géologique ENS, No. 7, 127 p.

Bonin, B., 1977, Les complexes granitiques subvolcaniques de Corse: caratéristiques, signification et origine: Sociétie geologique de France Bulletin, v. 19, p. 865-871.

Bowen, N. L., 1922, The reaction principle in petrogenesis: Journal of Geology, v. 30, p. 177-198.

Brett, R., 1964, Experimental data from the system Cu-Fe-S and their bearing on exsolution textures in ores: Economic Geology, v. 59, p. 1241-1269.

Buddington, A. F., 1963, Distribution of MnO between coexisting ilmenite and magnetite, in Subramanian, A. P., and Balakrishna, S., eds., Advancing frontiers in geology and geophysics—a volume in honor of M. S. Krishnan: Hyderabad, India, Indian Geophysical Union, p. 233-248.

Buddington, A. F., Fahey, J., and Vlisidis, A., 1963, Degree of oxidation of Adirondack iron oxide and iron-titanium oxide minerals in relation to petrogeny: Journal of Petrology, v. 4, p. 138-169.

Buddington, A. F., and Lindsley, D. H., 1964, Iron-titanium oxide minerals and synthetic equivalents: Journal of Petrology, v. 5, p. 310-357.

Burnham, C. W., Holloway, J. R., and Davis, N. F., 1969, Thermodynamic properties of water to 1,000°C and 10,000 bars: Geological Society of America Special Paper 132, 96 p.

Burton, B. P., 1985, Theoretical analysis of chemical and magnetic ordering in the system Fe_2O_3-$FeTiO_3$: American Mineralogist, v. 70, p. 1027-1035.

Cantagrel, J. M., Didier, J., and Gourgaud, A., 1984, Magma mixing: origin of intermediate rocks and "enclaves" from volcanism to plutonism: Physics of Earth and Planetary Interiors, v. 35, p. 63-76.

Carmichael, C. M., 1961, The magnetic properties of ilmenite-haematite crystals: Proceedings of the Royal Society, ser. A, v. 263, p. 508-530.

Charles, R. W., 1975, The phase equilibria of richterite and ferrorichterite: American Mineralogist, v. 60, p. 367-374.

Charles, R. W., 1977, The phase equilibria of intermediate compositions on the pseudobinary $Na_2CaMg_5Si_8O_{22}(OH)_2$-$Na_2CaFe_5Si_8O_{22}(OH)_2$: American Journal of Science, v. 277, p. 594-625.

Christiansen, R. L., and Lipman, P. W., 1972, Cenozoic volcanism and plate tectonic evolution of the western United States, Part II, Late Cenozoic: Philosophical Transactions of the Royal Society of London, v. 271, p. 249-284.

Cordell, L., 1978, Complete Bouguer anomaly map of the Taos basin section of the Rio Grande Rift, New Mexico: U. S. Geological Survey Open-File Map 78- 317.

Czamanske, G.K., and Dillet, Brigitte, in press, Alkali amphibole, tetrasilicic mica, and sodic pyroxene in peralkaline siliceous rocks, Questa caldera, New Mexico: American Journal of Science.

Czamanske, G. K., Ishihara, S., and Atkin, S. A., 1981, Chemistry of rock-forming minerals of the Cretaceous-Paleocene batholith in southwestern Japan and implications for magma genesis: Journal of Geophysical Research, v. 86, p. 10431-10469.

Czamanske, G. K., and Mihalik, P., 1972, Oxidation during magmatic differentiation, Finnmarka complex, Oslo area, Norway: Part 1, The opaque oxides: Journal of Petrology, v. 13, p. 493-509.

Czamanske, G. K., and Wones, D. R., 1973, Oxidation during magmatic differentiation, Finnmarka complex, Oslo area, Norway: Part II, The mafic silicates: Journal of Petrology, v. 14, p. 349-380.

Czamanske, G. K., Wones, D. R., and Eichelberger, J. C., 1977, Mineralogy and petrology of the intrusive complex of the Pliny Range, New Hampshire: American Journal of Science, v. 277, p. 1073-1123.

Didier, J., and Roques, M., 1959, Sur les enclaves des granites du Massif Central francais: Comptes rendus Académie des Sciences, v. 248, p. 1839-1841.

Edwards, A. B., 1954, Textures of the ore minerals and their significance: Australasian Institute of Mining and Metallurgy, 242 p.

Elsdon, R., 1975, Manganoan ilmenite from the Leinster granite, Ireland: Mineralogical Magazine, v. 40, p. 419-421.

Ernst, W. G., 1962, Synthesis, stability relations, and occurrence of riebeckite and riebeckite-arfvedsonite solid solutions: Journal of Geology, v. 70, p. 689-736.

Fabriès J., 1978, Les types paragéné des amphiboles sodiques dans le roches magmatiques: Bulletin de Minéralogie, v. 101, p. 155-165.

Giret, A., Bonin, B., and Leger, J., 1980, Amphibole compositional trends in oversaturated and undersaturated alkaline plutonic ring-complexes: Canadian Mineralogist, v. 18, p. 481-495.

Goldich, S. S., Ingamells, C. O., Suhr, N. H., and Anderson, D. H., 1967, Analyses of silicate rock and mineral standards: Canadian Journal of Earth Sciences, v. 4, p. 747-755.

Goldschmidt, V. M., 1954, Geochemistry: Oxford, The Clarendon Press, 730 p.

Grossman, D. G., 1972, Machinable glass-ceramic based on tetrasilicic mica: American Chemical Society Journal, v. 55, p. 446-449.

Haggerty, S. E., 1976, Opaque mineral oxides in terrestrial igneous rocks, in Oxide Minerals: Mineralogical Society of America Short Course Notes, v. 3, p. Hg 101-300.

Haggerty, S. E., Borley, G. D., and Abbott, M. J., 1966, Iron-titanium oxides in a suite of alkaline volcanic rocks from Tenerife: International Mineralogical Association General Meeting, 5th, Cambridge, U.K.

Hagstrum, J. T., Lipman, P. W., and Elston, D. P., 1982, Paleomagnetic evidence bearing on the structural development of the Latir volcanic field near Questa, New Mexico: Journal of Geophysical Research, v. 87, p. 7833-7842.

Hagstrum, J. T., and Lipman, P. W., 1986, Paleomagnetism of the structurally deformed Latir volcanic field, northern New Mexico: Relations to formation of the Questa caldera and development of the Rio Grande Rift: Journal of Geophysical Research, v. 91, p. 7383-7402.

Harker, A., 1909, The natural history of igneous rocks: New York, MacMillan, 384 p.

Harris, N. B. W., 1985, Alkaline complexes from the Arabian Shield: Journal of African Earth Sciences, v. 3, p. 83-88.

Haslam, H. W., 1968, The crystallization of intermediate and acid magmas at Ben Nevis, Scotland: Journal of Petrology, v. 9, p. 84-104.

Hatherton, T., and Dickinson, W. R., 1969, The relationship between andesitic volcanism and seismicity in Indonesia, the Lesser Antilles, and other island arcs: Journal of Geophysical Research, v. 74, p. 5301-5310.

Hawthorne, F. C., 1976, The crystal chemistry of the amphiboles. V. The structure and chemistry of arfvedsonite: Canadian Mineralogist, v. 14, p. 346-356.

Hildreth, W. E., 1981, Gradients in silicic magma chambers—implications for lithospheric magmatism: Journal of Geophysical Research, v. 86, p. 10153-10192.

James, R. S., and Hamilton, D. L., 1969, Phase relations in the system $NaAlSi_3O_8$-$KAlSi_3O_8$-$KAlSi_3O_8$-$CaAl_2Si_2O_8$-SiO_2 at 1 kilobar water vapor pressure: Contributions to Mineralogy and Petrology, v. 21, p. 111-141.

Jarosewich, E. J., Nelen, J. A., and Norberg, J. A., 1980, Reference samples for electron microprobe analysis: Geostandards Newsletter, v. 4, no. 1., p. 257.

Johnson, C. J., 1986, The Questa magmatic system: petrologic, chemical, and isotopic variations in cogenetic volcanic and plutonic rocks of the Latir volcanic field and associated intrusives, northern New Mexico: Stanford California, Stanford University, Ph.D. thesis.

Kretchsmar, U. H., and McNutt, R. H., 1971, A study of the Fe-Ti oxides in the Whitestone anorthosite, Dunchurch, Ontario: Canadian Journal of Earth Sciences, v. 8, p. 947-959.

Kuznetsov, V. I., 1956, Data on chemical analyses of minerals of the series columbite-tantalite: Geochemistry, v. 8, p. 801-811.

Lalonde, A. E., and Martin, R. F., 1983, The Baie-des-Martens syenitic complex, La Tabatière Quebec. II. The ferromagnesian minerals: Canadian Mineralogist, v. 21, p. 81-91.

Lameyre, J., and Bowden, P., 1982, Plutonic rock type series: Discrimination of various granitoid series and related rocks: Journal of Volcanology and Geothermal Resources, v. 14, p. 169-186.

Laughlin, A. W., Rehrig, W. A., and Mauger, R. L., 1969, K-Ar chronology and sulfur and strontium isotope ratios at the Questa mine, New Mexico: Economic Geology, v. 64, p. 903-904.

Leake, B. E., 1978, Nomenclature of amphiboles: American Mineralogist, v. 63, p. 1023-1052.

Leonardson, R. W., Dunlop, G., Starquist, V. L., Bratton, G. P., Meyer, J. W., Osborne, L. W., Atkin, S. A., Molling, P. A., Moore, R. F., and Olmore, S. D., 1983, Preliminary geology and molybdenum deposits at Questa, New Mexico, in The genesis of Rocky Mountain ore deposits: Changes with time and tectonics: Proceedings of a Symposium, Denver Region Exploration Geologists Society, Denver, Colorado, p. 151-155.

Liégeois, J. P., and Black, R., in press, Alkaline magmatism subsequent to collision in the Pan-African belt of the Adrar des Iforas (Mali).

Lindsley, D. H., 1962, Investigations in the system FeO-Fe_2O_3-TiO_2: Carnegie Institution of Washington Year Book 61, p. 100-106.

Lindsley, D. H., 1973, Delimitation of the hematite-ilmenite miscibility gap: Geological Society of America Bulletin, v. 84, p. 657-661.

Lipman, P. W., 1971, Iron-titanium oxide phenocrysts in compositionally zoned ash-flow sheets from southern Nevada: Journal of Geology, v. 79, p. 438-456.

Lipman, P. W., 1981, Volcano-tectonic setting of Tertiary ore deposits, southern Rocky Mountains, in Dickinson, W. R., and Payne, W. D., eds., Relation of tectonics to ore deposits in the southern cordillera: Arizona Geological Society Digest, v. 14, p. 199-213.

Lipman, P. W., 1983, The Miocene Questa caldera, northern New Mexico: Relation to batholith emplacement and associated molybdenum mineralization, in The genesis of Rocky Mountain ore deposits: Changes with time and tectonics: Proceedings of a Symposium, Denver Region Exploration Geologists Society, Denver, Colorado, p. 133-147.

Lipman, P. W., 1984, The roots of ash flow calderas in western North America: Windows into the tops of granitic batoliths: Journal of Geophysical Reserch, v. 89, p. 8801-8841.

Lipman, P. W., and Mehnert, H. H., 1975, Late Cenozoic basaltic volcanism and development of the Rio Grande depression in the southern Rocky Mountains: Geological Society of America Memoir 144, p. 119-154.

Lipman, P. W., Mehnert, H. H., Naeser, C. W., 1986, Evolution of the Latir volcanic field, northern New Mexico, and its relation to the Rio Grande Rift, as indicated by potassium-argon and fission track dating: Journal of Geophysical Research, v. 91, p. 6329-6345.

Lipman, P. W., Prostka, H. J., and Christiansen, R. L., 1972, Cenozoic volcanism and plate-tectonic evolution of the western United States, Part I: Philosophical Transactions of the Royal Society of London, v. 271, p. 217-248.

Lipman, P. W., and Reed, J. C., in press, Geologic map of the Latir volcanic field and adjacent areas, northern New Mexico: U.S. Geological Survey Miscellaneous Investigations Map.

Luth, W. C., 1969, The systems $NaAlSi_3O_8$-SiO_2 and $KAlSi_3O_8$-SiO_2 at 20 kb and the relationship between H_2O content, PH_2O, and P_{total} in granitic magmas: American Journal of Science, v. 267-A, p. 325-341.

Luth, W. C., Jahns, R. H., and Tuttle O. F., 1964, The granite system at pressures of 4 to 10 kilobars: Journal of Geophysical Research, v. 69, p. 759-773.

Mao, H. K., 1971, The system jadeite ($NaAlSi_2O_6$)-anorthite ($CaAl_2Si_2O_8$) at high pressures: Carnegie Institute of Washington Year Book 69, p. 163-168.

Miyashiro, A., 1977, Nature of alkalic volcanic rock seris: Contributions to Mineralogy and Petrology, v. 66, p. 91-104.

Morikawa, Y., Yasuda, A., Morooka, Y., and Ikawa, T., 1983, Catalytic activities of metal-ion-exchanged forms of fluoro-tetrasilicic mica for the reaction of butanes: Chemical Letters, no. 12, p. 1911-1912.

Neumann, E.-R., 1974, The distribution of Mn^{2+} and Fe^{2+} between ilmenites and magnetites in igneous rocks: American Journal of Science, v. 274, p. 1074-1088.

Neumann, E.-R., 1976, Compositional relations among pyroxenes, amphiboles and other mafic phases in the Oslo Region plutonic rocks: Lithos, v. 9, p. 85-109.

Papike, J. J., Cameron, K. L., and Baldwin, K., 1974, Amphiboles and pyroxenes: Characterization of other than quadrilateral components and estimates of ferric iron from microprobe data: Geological Society of America Abstracts with Program, v. 6, p. 1053-1054.

Pearce, J. A., Harris, N. B. W., and Tindle, A. G., 1984, Trace element discrimination diagrams for the tectonic interpretation of granitic rocks: Journal of Petrology, v. 25, p. 956-983.

Price, G. D., 1981, Subsolidus phase relations in the titanomagnetite solid solution series: American Mineralogist, v. 66, p. 751-758.

Ramdohr, P., 1980, The ore minerals and their intergrowths: Pergammon Press, International Series in Earth Sciences, 2nd edition, 1207 p.

Reed, J. C., Lipman, P. W., and Robertson, J. M., 1983, Geologic map of the Latir Peak and Wheeler Peak wildernesses and Columbine-Hondo wilderness study area, Taos County, New Mexico: U.S. Geological Survey Miscellaneous Field Investigations Map MF-1750-B.

Rittmann, A., 1953, Magmatic character and tectonic position of the Indonesian volcanoes: Bulletin of Volcanology, v. 14, p. 45-58.

Robert, J.-L., and Maury, R. C., 1979, Natural occurrence of a (Fe,Mn,Mg) tetrasilicic potassium mica: Contributions to Mineralogy and Petrology, v. 68, p. 117-123.

Robie, R. A., and Waldbaum, D. R., 1968, Thermodynamic properities of minerals and related substances at 298.15°K (25.0°C) and one atmosphere (1.013 bars) pressure and at higher temperature: U.S. Geological Survey Bulletin 1259.

Rock, N. M. S., and Leake, B. E., 1984, The international mineralogical association amphibole nomenclature scheme: Computerization and its consequences: Mineralogical Magazine, v. 48, p. 211-27.

Rosenberg, P. E., and Foit, F. F., Jr., 1977, Fe^{2+} - F avoidance in silicates: Geochimica et Cosmochimica Acta, v. 41, p. 345-346.

Rumble, D., 1971, Fe-Ti oxide minerals and the behavior of oxygen during regional metamorphism: Carnegie Institution of Washington Year Book 70, p. 157-185.

Seifert, F., and Schreyer, W., 1965, Synthesis of a new mica, $KMg_{2.5}[Si_4O_{10}](OH)_2$: American Mineralogist, v. 50, p. 1114-1118.

Seifert, F., and Schreyer, W., 1971, Synthesis and stability of micas in the system K_2O-MgO-SiO_2-H_2O and their relations to phlogopite: Contributions to Mineralogy and Petrology, v. 30, p. 196-215.

Shannon, J. R., Walker, B. M., Carten, R. B., and Geraghty, E. P., 1982, Unidirectional solidification textures and their significance in determining relative ages of intrusions at the Henderson Mine, Colorado: Geology, v. 10, p. 293-297.

Siivola, J., 1970, Ilmenorutile and struverite from Penikoja, Somero, southwest Finland: Geological Society of Finland Bulletin, v. 42, p. 33-36.

Smyth, J. R., 1980, Cation vacancies and the crystal chemistry of breakdown reactions in kimberlitic omphacites: American Mineralogist, v. 65, p. 1185-1191.

Snetsinger, K. G., 1969, Manganoan ilmenite from a Sierran adamellite: American Mineralogist, v. 54, p. 431-436.

Speer, J. A., 1984, Micas in igneous rocks, in Micas: Mineralogical Society of America Short Course Notes, v. 8, p. 299-356.

Spencer, K. J., and Lindsley, D. H., 1981, A solution model for coexisting iron-titanium oxides: American Mineralogist, v. 66, p. 1189-1201.

Steven, T. A., 1975, Middle Tertiary volcanic fields in the Rocky Mountains: Geological Society of America Memoir 144, p. 75-94.

Stormer, J. C., Jr., 1983, The effects of recalculation on estimates of temperature and oxygen fugacity from analyses of multicomponent iron-titanium oxides: American Mineralogist, v. 68, p. 586-594.

Streckeisen, A. L., 1976, To each plutonic rock its proper name: Earth Science Reviews, v. 12, p. 1-33.

Strong, D. F., and Taylor, R. P., 1984, Magmatic-subsolidus and oxidation trends in composition of amphiboles from silica-saturated peralkaline igneous rocks: Tschermaks Mineralogische und Petrographische Mitteilungen, v. 32, p. 211-222.

Thompson, R. N., and MacKenzie, W. S., 1967, Feldspar-liquid equilibria in peralkaline acid liquids: An experimental study: American Journal of Science, v. 265, p. 714-734.

Toraya, H., Iwai, S., Marumo, F., Daimon, M., and Kondo, R., 1976, The crystal structure of tetrasilicic potassium fluor mica, $KMg_{2.5}Si_4O_{10}F_2$: Zeitschrift fur Kristallographie, v. 144, p. 42-52.

Tuttle, O. F., and Bowen, N. L., 1958, Origin of granite in the light of experimental studies in the system $NaAlSi_3O_8$-$KAlSi_3O_8$-SiO_2-H_2O: Geological Society of America Memoir 74, 153 p.

Tweto, O., 1975, Laramide (late Cretaceous-early Tertiary) orogeny in the southern Rocky Mountains: Geological Society of America Memoir 144, p. 1-44.

Verhoogen, J., 1962, Oxidation of iron-titanium oxides in igneous rocks: Journal of Geology, v. 70, p. 168-181.

Vernon, R. H., 1983, Restite, xenoliths, and microgranitoid enclaves in granites: Royal Society of New South Wales Journal and Proceedings, v. 116, p. 77-103.

Vincent, E. A., Wright, J. B., Chevalier, R., and Mathieu, S., 1957, Heating experiments on some natural titaniferous magnetites: Mineralogical Magazine, v. 31, p. 624-665.

Waldbaum, D. R., and Thompson, J. B., Jr., 1969, Mixing properites of sanidine crystalline solutions. IV. Phase diagrams from equations of state: American Mineralogist, v. 54, p. 1274-1298.

Wones, D. R., and Eugster, H. P., 1965, Stability of bioitite: Experiment, theory, and applications: American Mineralogist, v. 50, p. 1228-1272.

Wones, D. R., and Gilbert, M. C., 1982, Amphiboles in the igneous environment in Amphiboles: Petrology and experimental phase relations: Mineralogical Society of America, Short Course Notes, v. 9B, p. 355-390.

Wood, B. J., and Henderson, C. M. B., 1978, Compositions and unit-cell parameters of synthetic non-stoichiometric tschermakitic clinopyroxenes: American Mineralogist, v. 63, p. 66-72.

Wright, J. B., 1959, Some further heating experiments on natural titaniferous magnetites, Mineralogical Magazine, v. 32, p. 32-37.

Wyllie, P. J., Cox, K. G., and Biggar, G. M., 1962, The habit of apatite in synthetic systems and igneous rocks: Journal of Petrology, v. 3, p. 238-243.

Yund, R., and McCallister, R. H., 1970, Kinetics and mechanisms of exsolution: Chemical Geology, v. 6, p. 5-30.

APPENDIX A: ELECTRON MICROPROBE ANALYSES AND STRUCTURAL FORMULAE FOR IRON TITANIUM OXIDE MINERALS

Explanation for tables A.1.1, 2.1, 3.1, 4.1, 5.1, 6, 7.1, 8.1, and 9: Electron microprobe analyses and structural formulae for magnetite.

* refers to number of analyses averaged.

(*) refers to grain identification.

Explanation for tables A.1.2, 2.2, 3.2, 3.3, 4.2, 5.2, 6, 7.2, 8.2, and 9: Electron microprobe analyses and structural formulae for ilmenite and hematite.

(*) refers to grain identification

p, primary homogeneous ilmenite or hematite.

ph, primary ilmenite containing hematite exsolution products; analysis represents intermediate or integrated composition.

phi, primary ilmenite containing hematite exsolution products; analysis of ilmenite phase.

phh, primary ilmenite containing hematite exsolution products; analysis of hematite phase.

pi, primary hematite containing ilmenite exsolution products; analysis represents intermediate or integrated composition.

pii, primary hematite containing ilmenite exsolution products; analysis of ilmenite phase.

pih, primary hematite containing ilmenite exsolution products; analysis of hematite phase.

ps, ilmenite-hematite intergrowth enclosed in euhedral sphene; analysis represents intermediate or integrated composition.

psi, ilmenite-hematite intergrowth enclosed in euhedral sphene; analysis of ilmenite phase.

psh, ilmenite-hematite intergrowth enclosed in euhedral sphene; analysis of hematite phase.

him, ilmenite or hematite in the "him" association, Rito del Medio granite, tables 3.2 and 3.3.

pv, primary ilmenite or hematite in vug.

pvi, primary hematite with ilmenite exsolution products, in vug.

m2 to m5, ilmenite "exsolved" from magnetite, types (2) to (5).

m, hematite derived by oxidation of magnetite (martite).

s, secondary ilmenite after sphene (ilmenite aggregates).

Table A.1.1: Magnetite, Virgin Canyon pluton.

	PERALKALINE								EARLIER METALUMINOUS			
	83QC29		Q83J62	Q83J67	82QC38		Q83J63		82QC39	82QC33	Q83J65	
(*)	(4a)	(4b)	(8)	(7)	(5)	(1)	(1)	(8)	(4)	(5)	(5)	(6)
Al2O3	0.05	0.05	0.03	0.07	0.04	0.03	0.06	0.04	0.36	0.14	0.14	0.18
FeOt	86.9	87.2	85.8	85.4	86.6	86.7	85.5	87.9	90.3	91.9	92.0	91.9
Fe2O3	62.34	62.51	63.04	61.44	62.10	61.55	61.11	63.35	65.67	68.41	67.93	67.65
FeO	30.80	30.95	29.08	30.12	30.72	31.32	30.51	30.89	31.21	30.34	30.88	31.03
TiO2	3.29	3.15	2.99	3.75	3.03	3.56	3.91	2.77	1.03	0.21	0.33	0.44
MnO	2.70	2.37	3.94	3.20	2.03	2.41	3.38	2.10	0.18	0.16	0.22	0.13
ZnO	0.52	0.54	0.75	1.17	0.71	0.43	0.71	0.56	0.30	0.79	0.16	0.18
Total	99.70	99.57	99.83	99.75	98.63	99.30	99.68	99.71	98.75	100.05	99.66	99.61
Al	0.002	0.002	0.001	0.003	0.002	0.001	0.003	0.002	0.016	0.006	0.006	0.008
Fe3+	1.807	1.814	1.825	1.779	1.820	1.790	1.770	1.837	1.921	1.981	1.973	1.965
Fe2+	0.992	0.998	0.936	0.969	1.001	1.012	0.982	0.995	1.015	0.976	0.997	1.002
Ti	0.095	0.091	0.087	0.109	0.089	0.103	0.113	0.080	0.030	0.006	0.010	0.013
Mn	0.088	0.077	0.128	0.104	0.067	0.079	0.110	0.069	0.006	0.005	0.007	0.004
Zn	0.015	0.015	0.021	0.033	0.020	0.012	0.020	0.016	0.009	0.022	0.005	0.005

	EARLY METALUMINOUS				RH.DIKE	LATER METALUMINOUS						
	Q83J65	83QC25	Q83J66	82QC41	83QC31	Q83J78A1		83QC33	82QC35		Q83J79	
(*)	(8)	(1)	(5)	(9)	(3)	(8)	(9)	(5)	(2)	(3)	(3)	(4)
Al2O3	0.14	0.12	0.52	0.06	0.06	0.67	0.14	0.32	0.46	0.10	0.44	0.39
FeOt	92.0	92.5	89.5	91.6	92.7	91.0	92.1	91.9	91.3	92.3	90.5	91.3
Fe2O3	67.87	68.16	65.36	67.96	68.55	66.60	68.08	67.82	67.10	68.28	66.56	67.25
FeO	30.93	31.17	30.69	30.45	31.02	31.07	30.84	30.88	30.92	30.86	30.61	30.79
TiO2	0.34	0.39	1.41	0.18	0.21	0.57	0.31	0.27	0.68	0.21	1.00	0.45
MnO	0.15	0.17	1.26	0.35	0.07	0.18	0.27	0.12	0.46	0.14	0.98	0.17
ZnO	0.14	0.09	0.31	0.12	0.10	0.24	0.14	0.24	0.37	0.12	0.44	0.39
Total	99.57	100.10	99.55	99.12	100.06	99.33	99.78	99.65	99.99	99.62	100.03	99.44
Al	0.006	0.005	0.024	0.003	0.003	0.030	0.006	0.015	0.021	0.000	0.020	0.018
Fe3+	1.972	1.972	1.894	1.987	1.985	1.935	1.975	1.969	1.940	1.987	1.922	1.956
Fe2+	0.999	1.002	0.988	0.989	0.998	1.003	0.994	0.996	0.993	0.998	0.983	0.995
Ti	0.010	0.011	0.041	0.005	0.006	0.017	0.009	0.008	0.020	0.006	0.029	0.013
Mn	0.005	0.006	0.041	0.012	0.002	0.006	0.009	0.004	0.015	0.005	0.032	0.006
Zn	0.004	0.003	0.009	0.003	0.003	0.007	0.004	0.007	0.010	0.003	0.012	0.011

Table A.1.2: Ilmenite, Virgin Canyon pluton.

	PERALKALINE											
	82QC34	83QC29							Q83J62		Q83J67	
(*)	(5)m5	(2a)p	(2b)p	(1)p	(4a)p	(4b)p	(18)s	(4a)m5	(8)p	(10)p	(8)p	(9)p
FeOt	20.3	28.0	25.5	34.4	22.0	23.8	25.8	19.8	27.4	26.8	26.7	29.1
Fe2O3	3.79	4.90	4.33	4.78	4.37	3.89	2.22	3.30	3.11	3.09	4.3	3.02
FeO	16.89	23.59	21.61	30.10	18.07	20.30	23.8	16.83	24.61	24.02	22.83	26.38
TiO2	50.1	49.1	49.5	49.3	49.7	49.7	50.6	50.2	50.00	49.7	49.8	50.2
MnO	23.8	19.6	22.3	12.4	25.9	23.6	20.8	27.0	20.2	20.5	20.7	18.0
Nb2O5	0.94	0.99	0.79	0.10	0.73	0.73	1.11	1.00	0.79	0.98	0.40	1.04
ZnO	5.07	1.37	0.83	1.90	0.80	0.91	1.27	1.61	0.52	0.42	1.26	1.10
Total	100.59	99.55	99.36	98.58	99.57	99.13	99.8	99.94	99.23	98.71	99.29	99.74
Fe3+	0.072	0.094	0.083	0.092	0.084	0.075	0.042	0.063	0.060	0.060	0.082	0.058
Fe2+	0.357	0.503	0.461	0.647	0.384	0.433	0.505	0.357	0.526	0.515	0.487	0.560
Ti	0.953	0.942	0.949	0.952	0.950	0.954	0.966	0.957	0.961	0.959	0.954	0.959
Mn	0.510	0.423	0.482	0.270	0.558	0.510	0.447	0.580	0.433	0.445	0.447	0.387
Nb	0.011	0.011	0.009	0.001	0.008	0.008	0.013	0.011	0.009	0.011	0.005	0.012
Zn	0.095	0.026	0.016	0.036	0.015	0.017	0.024	0.030	0.010	0.008	0.024	0.021

Table A.1.2, continued.

	PERALKALINE											
	Q83J67		82QC38							Q83J63		
(*)	(10)p	(7)m5	(16)p	(17)p	(5)p	(15)p	(15')p	(14)m4	(14)m5	(7)p	(9)p	(10)p
FeOt	27.5	17.5	15.5	27.8	24.4	24.5	26.8	14.6	14.0	33.0	33.1	29.7
Fe203	3.40	4.26	3.49	2.86	3.21	1.09	3.63	3.33	3.84	5.86	5.23	5.53
FeO	24.44	13.67	12.36	25.22	21.51	23.52	23.54	11.61	10.55	27.63	28.39	24.73
TiO2	50.0	49.4	49.4	49.6	49.9	50.9	49.8	50.1	49.8	48.7	48.6	49.2
MnO	19.8	28.2	31.9	19.3	22.4	21.2	21.0	32.8	33.7	16.1	15.6	18.8
Nb2O5	0.97	0.95	1.42	1.26	0.54	0.99	0.92	1.04	1.17	0.95	1.31	0.35
ZnO	1.03	2.99	0.47	0.33	0.80	0.62	0.36	0.77	0.73	0.21	0.17	0.50
Total	99.64	99.47	99.04	98.57	98.36	98.32	99.25	99.65	99.79	99.45	99.30	99.11
Fe3+	0.065	0.082	0.067	0.055	0.062	0.021	0.070	0.064	0.073	0.112	0.101	0.106
Fe2+	0.520	0.292	0.264	0.540	0.461	0.502	0.502	0.246	0.224	0.591	0.607	0.526
Ti	0.956	0.948	0.949	0.955	0.962	0.976	0.955	0.956	0.950	0.933	0.934	0.941
Mn	0.427	0.610	0.690	0.419	0.486	0.458	0.453	0.705	0.723	0.347	0.338	0.405
Nb	0.011	0.011	0.016	0.015	0.006	0.011	0.011	0.012	0.013	0.011	0.015	0.004
Zn	0.019	0.056	0.009	0.006	0.015	0.012	0.007	0.014	0.014	0.004	0.003	0.009

	EARLY METALUMINOUS											
	82QC40				82QC39					82QC33	Q83J65	83QC25
(*)	(8)ph	(1')m3	(1)m5	(7)m5	(6)core	(6)rim	(6')p	(3)p	(4)p	(5)m5	(9)p	(2)core
FeOt	32.1	30.0	24.3	28.0	30.5	28.1	26.4	26.4	27.9	30.2	28.3	33.6
Fe203	8.94	7.98	6.74	7.71	8.77	7.73	6.68	6.17	6.34	6.87	1.86	9.04
FeO	24.06	22.82	18.23	21.06	22.61	21.14	20.39	20.84	22.19	24.02	27.63	25.47
TiO2	48.2	48.2	48.4	48.7	47.2	48.1	48.4	48.1	47.8	48.6	50.5	47.1
MnO	18.8	19.4	24.1	22.2	19.8	21.9	22.3	22.1	19.9	19.3	17.9	16.9
Nb2O5	0.13	0.07	0.71	0.21	1.07	0.85	0.35	1.04	0.98	0.50	0.17	0.77
ZnO	0.21	0.88	1.35	0.23	0.31	0.31	0.69	0.52	1.09	0.31	0.46	0.13
Total	100.34	99.35	99.53	100.11	99.76	100.03	98.81	98.77	98.30	99.60	98.52	99.41
Fe3+	0.169	0.153	0.129	0.146	0.168	0.147	0.129	0.119	0.123	0.131	0.036	0.174
Fe2+	0.507	0.485	0.388	0.444	0.481	0.448	0.436	0.447	0.479	0.510	0.599	0.544
Ti	0.913	0.921	0.927	0.924	0.904	0.917	0.932	0.928	0.927	0.929	0.979	0.904
Mn	0.401	0.417	0.520	0.474	0.427	0.470	0.483	0.480	0.435	0.415	0.371	0.365
Nb	0.001	0.001	0.008	0.002	0.012	0.010	0.004	0.012	0.011	0.006	0.003	0.009
Zn	0.004	0.017	0.025	0.004	0.006	0.006	0.013	0.010	0.021	0.006	0.009	0.002

	EARLY METALUMINOUS			RH.DIKE	LATER METALUMINOUS							
	83QC25	82QC41		83QC31	Q83J78		83QC33				82QC35	
(*)	(2)rim	(7)p	(8)p	(3)	(7)ph	(8)ph	(9)ph	(11)p	(11')ph	(10)m5	(3)p	(3')p
FeOt	30.9	39.5	38.5	38.1	34.8	27.9	35.4	33.2	34.3	25.1	30.7	26.7
Fe203	6.25	14.71	9.78	8.64	9.24	9.98	8.81	5.14	8.73	7.54	9.09	6.7
FeO	25.27	26.27	29.70	30.33	26.49	18.92	27.47	28.58	26.45	18.32	22.52	20.68
TiO2	48.7	44.1	46.7	47.4	45.9	45.6	46.9	48.8	46.9	48.1	47.2	48.5
MnO	18.5	13.0	11.7	11.2	15.4	22.1	14.5	15.2	15.3	24.7	19.6	22.5
Nb2O5	0.84	0.25	0.21	0.27	1.92	1.07	0.44	0.68	0.24	0.65	0.25	0.29
ZnO	0.20	0.25	0.53	1.13	0.18	0.25	0.19	0.22	0.31	0.21	0.17	0.25
Total	99.76	98.58	98.62	99.04	97.92	98.31	98.62	97.93	99.52	98.83	98.92	
Fe3+	0.120	0.285	0.189	0.167	0.179	0.195	0.171	0.099	0.170	0.144	0.175	0.129
Fe2+	0.537	0.566	0.638	0.650	0.570	0.410	0.592	0.614	0.572	0.389	0.482	0.442
Ti	0.930	0.854	0.903	0.913	0.888	0.888	0.909	0.942	0.912	0.919	0.909	0.932
Mn	0.398	0.284	0.255	0.243	0.336	0.485	0.317	0.331	0.335	0.531	0.425	0.487
Nb	0.010	0.003	0.002	0.003	0.022	0.013	0.005	0.008	0.003	0.007	0.003	0.003
Zn	0.004	0.005	0.010	0.021	0.003	0.005	0.004	0.004	0.006	0.004	0.003	0.005

Table A.1.2, continued.

	LATER METALUMINOUS					
	82QC35		Q83J79			
(*)	(2)m5	(2)m4	(1)p	(2)p	(6)s	(3)m5
FeOt	26.4	21.0	31.8	35.3	31.8	16.9
Fe2O3	8.57	4.72	7.65	7.65	7.58	2.80
FeO	18.69	16.75	24.92	28.42	24.98	14.38
TiO2	47.6	50.2	46.4	47.8	48.1	50.4
MnO	23.8	27.0	17.3	14.7	18.1	30.2
Nb2O5	0.79	0.13	1.60	1.03	0.71	0.19
ZnO	0.33	0.82	0.16	0.15	0.16	0.26
Total	99.78	99.62	98.03	99.75	99.63	98.23
Fe3+	0.164	0.090	0.149	0.146	0.145	0.054
Fe2+	0.397	0.354	0.541	0.605	0.531	0.308
Ti	0.909	0.953	0.906	0.915	0.919	0.970
Mn	0.512	0.577	0.380	0.317	0.390	0.655
Nb	0.009	0.001	0.019	0.012	0.008	0.002
Zn	0.006	0.015	0.003	0.003	0.003	0.005

Table A.2.1: Magnetite, Canada Pinabete pluton.

	PERALKALINE							METALUMINOUS				
	84QC7		Q83J94					82QC46.1		82QC45		Q83J81
(*)	(1)	(5)	(2)	(3)	(1')	(2')	(3')	(2)	(3)	(4)	1(4)	(7)
Al2O3	0.04	0.05	0.96	0.02	0.06	0.05	0.04	0.12	0.17	0.64	0.46	0.16
FeOt	85.2	85.8	83.1	84.8	83.7	87.0	86.5	92.2	92.6	91.2	89.5	91.8
Fe2O3	58.37	58.36	57.45	59.10	58.43	60.48	60.63	68.23	68.46	66.74	65.17	67.25
FeO	32.68	33.29	31.41	31.62	31.12	32.58	31.94	30.81	31.00	31.15	30.86	31.29
TiO2	5.27	5.30	5.37	4.97	5.42	4.38	4.39	0.13	0.16	0.62	1.25	0.68
MnO	2.52	2.30	4.18	3.23	4.21	1.78	2.64	0.14	0.12	0.26	0.72	0.25
ZnO	0.67	0.26	0.66	0.77	0.79	0.86	0.72	0.03	0.06	0.13	0.29	0.05
Total	99.55	99.56	100.03	99.71	100.03	100.13	100.36	99.46	99.97	99.54	98.75	99.68
Al	0.002	0.002	0.043	0.001	0.003	0.002	0.002	0.005	0.008	0.029	0.021	0.007
Fe3+	1.691	1.689	1.647	1.710	1.683	1.744	1.744	1.987	1.983	1.935	1.905	1.953
Fe2+	1.052	1.071	1.001	1.017	0.997	1.044	1.021	0.997	0.998	1.004	1.003	1.009
Ti	0.153	0.153	0.154	0.144	0.156	0.126	0.126	0.004	0.005	0.018	0.037	0.020
Mn	0.082	0.075	0.135	0.105	0.137	0.058	0.085	0.005	0.004	0.008	0.024	0.008
Zn	0.019	0.007	0.019	0.022	0.022	0.024	0.020	0.001	0.002	0.004	0.008	0.001

	METALUMINOUS	
	82QC47	Q83J82
(*)	(4)	(6)
Al2O3	0.13	0.13
FeOt	91.5	92.6
Fe2O3	67.63	68.18
FeO	30.65	31.25
TiO2	0.23	0.38
MnO	0.15	0.15
ZnO	0.12	0.05
Total	98.91	100.14
Al	0.006	0.006
Fe3+	1.980	1.971
Fe2+	0.997	1.004
Ti	0.007	0.011
Mn	0.005	0.005
Zn	0.003	0.001

Table A.2.2: Ilmenite, Canada Pinabete pluton.

	PERALKALINE										METALUMINOUS	
	82QC49		84QC7						Q83J94		82QC46.1	
(*)	(3)p	(4)p	(4)p	(6)p	(1)p	(5)p	(1')m5	(5')m5	(1)p	(4)p	(10)p	(3)ph
FeOt	23.9	23.2	35.3	36.2	35.6	34.1	33.3	32.4	31.7	30.7	21.4	28.3
Fe203	1.32	2.26	2.65	2.06	3.49	5.15	1.85	2.47	0.50	2.07	1.65	3.11
FeO	22.71	21.16	32.91	34.34	32.46	29.46	31.54	30.18	31.25	28.84	19.92	25.50
TiO2	50.5	49.5	49.9	50.0	49.4	48.2	50.7	49.6	50.6	50.1	50.7	50.2
MnO	22.0	23.5	12.0	10.8	12.1	14.3	12.9	14.6	14.1	16.0	25.6	19.6
Nb2O5	0.93	1.42	1.16	1.18	1.27	1.65	0.45	1.66	1.06	1.28	0.95	0.96
ZnO	0.94	0.30	0.46	0.33	0.39	0.27	1.21	0.53	0.63	0.71	0.17	0.19
Total	98.40	98.14	99.08	98.71	99.11	99.03	98.65	99.04	98.14	99.00	98.99	99.56
Fe3+	0.026	0.044	0.051	0.040	0.067	0.100	0.036	0.048	0.010	0.040	0.032	0.060
Fe2+	0.488	0.457	0.704	0.738	0.695	0.633	0.678	0.647	0.674	0.618	0.425	0.542
Ti	0.976	0.961	0.960	0.966	0.952	0.931	0.977	0.956	0.981	0.965	0.972	0.959
Mn	0.479	0.514	0.260	0.235	0.263	0.311	0.280	0.317	0.308	0.347	0.553	0.422
Nb	0.011	0.017	0.013	0.014	0.015	0.019	0.005	0.019	0.012	0.015	0.011	0.011
Zn	0.018	0.006	0.009	0.006	0.007	0.005	0.023	0.010	0.012	0.013	0.003	0.004

	METALUMINOUS											
	82QC46.1		Q83J88		Q83J81		82QC47	Q83J82				
(*)	(11)m4	(6)p	(7)p	(8)p	(7)ph	(8)ph	(3)p	(7)ph	(4b)p	(4b)p	(6)ph	(4a)ph
FeOt	20.3	40.7	37.0	34.2	37.1	32.6	34.5	39.0	36.0	38.4	32.1	31.5
Fe203	2.38	5.00	4.38	0.65	9.22	4.72	6.72	4.94	10.98	7.49	3.40	2.18
FeO	18.16	36.2	33.06	33.62	28.80	28.35	29.36	34.52	26.12	31.66	29.04	29.54
TiO2	50.8	47.9	48.3	50.0	46.7	48.8	47.1	48.9	46.0	47.9	49.8	49.8
MnO	27.1	7.71	11.3	12.1	13.2	15.2	13.1	9.33	15.3	11.3	15.8	15.2
Nb2O5	0.53	2.05	2.31	2.18	0.81	0.66	1.31	0.71	0.70	0.44	0.90	1.00
ZnO	0.33	0.16	0.17	0.28	0.26	0.52	0.40	0.10	0.07	0.12	0.18	0.29
Total	99.30	99.02	99.52	98.83	98.99	98.25	97.99	98.50	99.17	98.91	99.12	98.01
Fe3+	0.045	0.097	0.085	0.013	0.178	0.092	0.131	0.095	0.212	0.144	0.065	0.042
Fe2+	0.386	0.780	0.709	0.724	0.618	0.611	0.637	0.741	0.560	0.678	0.621	0.638
Ti	0.971	0.928	0.931	0.968	0.902	0.946	0.919	0.944	0.886	0.922	0.957	0.967
Mn	0.584	0.168	0.245	0.264	0.287	0.332	0.288	0.203	0.332	0.245	0.342	0.332
Nb	0.006	0.024	0.027	0.025	0.009	0.008	0.015	0.008	0.008	0.005	0.010	0.012
Zn	0.006	0.003	0.003	0.005	0.005	0.010	0.008	0.002	0.001	0.002	0.003	0.006

	METALUMINOUS	
	Q83J82	
(*)	(6)m4	(6)m3
FeOt	29.7	34.8
Fe203	4.25	6.92
FeO	25.88	28.57
TiO2	50.05	48.6
MnO	18.6	14.6
Nb2O5	0.03	0.09
ZnO	0.27	0.32
Total	99.08	99.10
Fe3+	0.081	0.133
Fe2+	0.551	0.610
Ti	0.958	0.933
Mn	0.401	0.316
Nb	0.000	0.001
Zn	0.005	0.006

Table A.2.3: Hematite and ilmenorutile, Canada Pinabete pluton.

	HEMATITE						ILMENORUTILE					
	82QC45				82QC45.1		82QC45				82QC45.1	
(*)	(1)	(1')	(3)	(6)	(1)	(2)	(1)	(1')	(3)	(6)	(1)	(2)
Al2O3	0.03	0.29	0.01	0.30	0.00	0.02	0.08	0.05	0.07	0.06	0.05	0.07
FeOt	85.7	88.4	87.5	83.2	87.1	85.0	11.2	7.83	9.15	7.68	10.9	10.3
Fe2O3	91.49	97.81	94.79	86.70	94.60	89.61						
FeO	3.37	0.39	2.21	5.19	1.98	4.36						
TiO2	3.86	0.52	2.55	5.82	2.28	4.95	61.2	73.7	70.2	76.7	64.4	65.4
MnO	0.03	0.02	0.03	0.13	0.02	0.04	0.02	0.00	0.01	0.00	0.02	0.00
Nb2O5	0.03	0.00	0.02	0.33	0.04	0.02	25.4	16.2	17.4	14.0	22.7	21.4
Total	98.90	99.08	99.68	98.64	99.00	99.07	99.03	99.12	98.40	98.93	98.15	97.22
Al	0.001	0.009	0.000	0.009	0.000	0.001	0.004	0.003	0.004	0.003	0.003	0.004
Fe3+	1.843	1.970	1.897	1.746	1.907	1.800						
Fe2+	0.076	0.009	0.049	0.116	0.044	0.097	0.429	0.287	0.342	0.279	0.415	0.394
Ti	0.078	0.010	0.051	0.117	0.046	0.099	2.106	2.431	2.361	2.506	2.205	2.247
Mn	0.001	0.000	0.001	0.003	0.000	0.001	0.001	0.000	0.000	0.000	0.001	0.000
Nb	0.000	0.000	0.000	0.004	0.000	0.000	0.526	0.321	0.352	0.275	0.467	0.442

Table A.2.4: Davidite, columbite, Canada Pinabete pluton.

	DAVIDITE, 82QC46						
	Oxide weight percent			Cations, based on 38 O			
(*)	(2)	(4)	(5)		(2)	(4)	(5)
Na2O	0.03	0.03	0.03	Na	0.021	0.020	0.020
MgO	0.11	0.11	0.11	Mg	0.056	0.054	0.055
Al2O3	0.37	0.40	0.40	Al	0.149	0.156	0.159
CaO	0.07	0.08	0.08	Ca	0.025	0.028	0.029
TiO2	47.1	50.6	48.9	Ti	12.232	12.674	12.466
MnO	2.37	1.89	2.03	Mn	0.693	0.532	0.583
FeOt	27.5	26.8	27.3	Fe	7.941	7.465	7.740
ZnO	0.46	0.51	0.49	Zn	0.118	0.126	0.122
Nb2O5	2.74	2.28	2.58	Nb	0.427	0.344	0.395
Ta2O5	0.73	0.95	0.79	Ta	0.071	0.084	0.073
Y2O5	1.49	2.87	2.01	Y	0.274	0.508	0.363
La2O3	4.75	4.40	4.16	La	0.606	0.540	0.521
Ce2O3	4.14	4.67	4.80	Ce	0.523	0.568	0.595
Pr2O3	0.00	0.00	0.07	Pr	0.000	0.000	0.008
Nd2O3	0.17	0.24	0.28	Nd	0.021	0.028	0.033
Sm2O3	0.05	0.11	0.06	Sm	0.004	0.012	0.008
Dy2O3	0.42	0.34	0.26	Dy	0.046	0.036	0.029
Yb2O3	0.73	0.71	0.79	Yb	0.079	0.072	0.082
ThO2	0.88	0.90	0.99	Th	0.069	0.068	0.075
UO2	4.95	2.35	3.40	U	0.380	0.174	0.257
Total	99.06	100.24	99.53				

COLUMBITE, 82QC45 (3)			
Oxide wt%		Cations, (6 O)	
Al2O3	0.04	Al	0.003
FeOt	11.2	Fe	0.523
MgO	0.15	Mg	0.012
TiO2	7.31	TI	0.307
MnO	7.35	Mn	0.348
Nb2O5	69.3	Nb	1.750
ZnO	0.08	Zn	0.003
Ta2O5	3.08	Ta	0.047
Total	98.51		

Table A.3.1: Magnetite, Rito del Medio pluton.

	81S31		82QC18A			82QC19		82QC16		82QC17	82QC22	
(*)	(1)	(2)	(1)	(2)	(3)	(5)	(3)	(2)	(5)	(5)	(9)	(10)
Al2O3	0.29	0.27	0.26	0.25	0.20	0.75	0.31	0.27	0.38	0.18	0.15	0.21
FeOt	92.3	93.0	90.9	91.8	91.9	89.2	90.3	91.7	91.8	91.7	90.7	90.5
Fe2O3	68.94	68.93	67.74	68.39	68.36	66.72	68.00	68.63	68.77	67.92	67.11	67.15
FeO	30.27	30.98	29.94	30.26	30.39	29.17	29.11	29.94	29.92	30.58	30.31	30.08
TiO2	0.16	0.15	0.20	0.19	0.13	0.59	0.27	0.09	0.14	0.14	0.34	0.36
MnO	0.96	0.31	1.01	1.00	0.69	2.03	1.99	1.14	1.55	0.35	0.36	0.75
ZnO	0.28	0.21	0.03	0.01	0.00	0.46	0.19	0.14	0.00	0.04	0.21	0.15
Total	100.90	100.85	99.18	100.10	99.77	99.72	99.87	100.21	100.76	99.21	98.48	98.70
Al	0.013	0.012	0.012	0.011	0.009	0.034	0.014	0.012	0.017	0.008	0.007	0.010
Fe3+	1.977	1.979	1.976	1.977	1.983	1.931	1.970	1.982	1.974	1.983	1.972	1.968
Fe2+	0.965	0.988	0.971	0.972	0.980	0.938	0.938	0.961	0.954	0.992	0.990	0.980
Ti	0.005	0.004	0.006	0.005	0.004	0.017	0.008	0.003	0.004	0.004	0.010	0.011
Mn	0.031	0.010	0.033	0.033	0.023	0.066	0.065	0.037	0.050	0.011	0.012	0.025
Zn	0.008	0.006	0.001	0.000	0.000	0.013	0.005	0.004	0.000	0.001	0.006	0.004

Table A.3.2: Ilmenite, Rito del Medio pluton.

	81S28				82QC18B			82QC18A			
(*)	1(4)ph	(1)s	(1')m3	1(1)pv	(1)p	(2)p	(3)p	(2b)s	(2a)m5	(5)m3	(1)him
FeOt	34.4	24.2	20.3	18.1	24.1	15.6	17.4	13.8	15.0	5.65	11.0
Fe2O3	6.08	4.98	8.58	9.65	4.43	4.14	5.04	4.58	4.53	5.62	3.69
FeO	28.83	19.72	12.58	9.42	20.11	11.87	12.86	9.68	10.92	0.59	7.68
TiO2	47.0	49.1	47.3	45.8	47.8	47.9	47.4	48.5	48.7	49.6	49.9
MnO	13.9	23.7	28.8	32.4	24.0	32.1	30.8	34.3	33.5	43.2	37.2
Nb2O5	1.82	1.05	0.04	2.45	3.34	3.12	3.45	2.29	2.45	0.09	1.09
ZnO	0.22	0.85	0.72	0.22	0.32	0.33	0.37	0.40	0.26	0.31	0.04
Total	97.85	99.40	98.02	99.94	100.00	99.46	99.92	99.75	100.36	99.41	99.60
Fe3+	0.119	0.095	0.163	0.185	0.085	0.080	0.097	0.088	0.086	0.107	0.070
Fe2+	0.627	0.420	0.266	0.201	0.430	0.255	0.275	0.206	0.222	0.013	0.163
Ti	0.919	0.940	0.899	0.879	0.919	0.924	0.912	0.930	0.929	0.945	0.952
Mn	0.306	0.511	0.616	0.700	0.520	0.697	0.667	0.741	0.720	0.927	0.800
Nb	0.021	0.012	0.000	0.028	0.039	0.036	0.040	0.026	0.028	0.001	0.013
Zn	0.004	0.016	0.013	0.004	0.006	0.006	0.007	0.008	0.005	0.006	0.001

	82QC19				81S24			82QC16				
(*)	(1)s	(2)m5	(5)m5	(5')m4	(7)p	(8)ph	(6)ph	(11)p	(12)ph	(2)m5	(5)m5	(5')m3
FeOt	18.1	17.5	17.6	8.79	41.8	40.5	35.2	11.7	10.2	13.5	13.6	15.8
Fe2O3	4.93	5.58	9.83	2.94	8.91	12.28	12.09	4.16	4.01	4.65	4.51	3.04
FeO	13.67	12.47	8.76	6.15	33.78	29.45	24.32	7.96	6.59	9.32	9.54	13.06
TiO2	48.6	48.6	47.0	50.5	46.2	44.7	45.6	49.7	50.0	48.8	49.9	51.2
MnO	30.0	31.1	33.3	39.0	7.75	10.7	16.4	36.2	37.8	34.2	34.4	32.5
Nb2O5	0.90	0.83	0.57	0.60	0.86	0.74	0.36	0.69	0.47	1.21	0.09	0.14
ZnO	0.17	0.16	0.08	0.08	0.24	0.12	0.17	0.39	0.25	0.64	0.48	0.12
Total	98.27	98.74	99.54	99.27	97.74	97.99	98.94	99.10	99.12	98.82	98.92	100.06
Fe3+	0.095	0.108	0.188	0.056	0.174	0.240	0.233	0.080	0.077	0.090	0.086	0.058
Fe2+	0.294	0.267	0.186	0.131	0.734	0.638	0.521	0.169	0.140	0.200	0.203	0.275
Ti	0.941	0.937	0.899	0.965	0.903	0.872	0.879	0.951	0.956	0.940	0.955	0.968
Mn	0.654	0.675	0.718	0.839	0.171	0.235	0.356	0.780	0.814	0.742	0.742	0.692
Nb	0.010	0.010	0.007	0.007	0.010	0.009	0.004	0.008	0.005	0.014	0.001	0.002
Zn	0.003	0.003	0.002	0.002	0.005	0.002	0.003	0.007	0.005	0.012	0.009	0.002

Table A.3.2, continued.

	82QC17			
(*)	(4)m5	(8)pvi	(8')pvi	(5)him
FeOt	12.0	20.6	18.4	25.4
Fe2O3	2.60	4.54	2.86	6.11
FeO	9.66	16.51	15.82	19.90
TiO2	50.6	50.3	50.8	48.8
MnO	35.6	28.4	29.7	23.9
Nb2O5	0.84	0.52	0.96	0.73
ZnO	0.18	0.15	0.19	0.08
Total	98.27	100.42	100.33	99.52
Fe3+	0.050	0.086	0.054	0.117
Fe2+	0.205	0.347	0.333	0.423
Ti	0.966	0.951	0.961	0.933
Mn	0.765	0.605	0.633	0.515
Nb	0.010	0.006	0.011	0.008
Zn	0.003	0.003	0.004	0.002

Table A.3.3: Hematite, Rito del Medio pluton.

	81S31	82QC18A		82QC16		82QC17					
(*)	(2)him	(1)him	(3)m	(10)pvi	(10')pvi	(8)pvi	(8')pvi	(3)pih	(5)him	(12)p	(13)p
Al2O3	0.18	0.12	0.10	0.09	0.02	0.08	0.05	0.03	0.05	0.14	0.08
FeOt	78.8	74.6	89.0	82.3	87.4	83.8	88.3	86.5	73.0	81.3	73.8
Fe2O3	78.82	76.32	98.71	85.42	95.49	86.38	95.83	91.80	70.19	82.50	74.24
FeO	7.88	5.93	0.18	5.44	1.48	6.07	2.07	3.90	9.84	7.07	7.00
TiO2	11.7	12.2	0.31	7.47	1.98	7.30	2.33	4.66	15.6	8.49	12.9
MnO	2.44	4.95	0.07	1.19	0.14	0.44	0.08	0.26	4.06	0.32	4.44
Nb2O5	0.11	0.08	0.03	0.37	0.07	0.03	0.10	0.00	0.05	0.00	0.14
ZnO	0.22	0.03	0.02	0.23	0.17	0.00	0.00	0.01	0.04	0.20	0.15
Total	101.35	99.63	99.42	100.21	99.35	100.30	100.46	100.66	99.83	98.72	98.95
Al	0.005	0.004	0.003	0.003	0.001	0.002	0.002	0.001	0.002	0.004	0.002
Fe3+	1.536	1.511	1.984	1.693	1.918	1.708	1.904	1.814	1.383	1.655	1.480
Fe2+	0.171	0.130	0.004	0.120	0.033	0.133	0.046	0.086	0.215	0.158	0.155
Ti	0.228	0.241	0.006	0.148	0.040	0.144	0.046	0.092	0.307	0.170	0.257
Mn	0.054	0.110	0.002	0.027	0.003	0.010	0.002	0.006	0.090	0.007	0.100
Nb	0.001	0.001	0.000	0.004	0.001	0.000	0.001	0.000	0.001	0.000	0.002
Zn	0.004	0.001	0.000	0.004	0.003	0.000	0.000	0.000	0.001	0.004	0.003

Table A.3.4: Ilmenorutile and columbite, Rito del Medio pluton, 81S31 (1)

ILMENORUTILE				COLUMBITE			
Oxide wt%		Cations, (6 O)		Oxide wt%		Cations, (6 O)	
Al2O3	0.13	Al	0.007	Al2O3	0.11	Al	0.007
FeOt	10.2	Fe	0.380	FeOt	2.33	Fe	0.106
MgO	0.04	Mg	0.003	MgO	0.10	Mg	0.008
TiO2	68.9	Ti	2.305	TiO2	6.75	Ti	0.278
MnO	0.08	Mn	0.003	MnO	18.1	Mn	0.838
Nb2O5	19.7	Nb	0.396	Nb2O5	72.4	Nb	1.789
ZnO	0.09	Zn	0.003	ZnO	0.16	Zn	0.007
Total	99.24			Total	99.95		

Table A.4.1: Magnetite, Cabresto Lake pluton.

	GRANITE								MIXED		
	78L172	CL	82QC51	82QC51b	83QC10	83QC16	83QC18	83QC20	83QC14	85QC11	85QC12
*	1	2	2	2	1	3	3	3	2	1	1
Al2O3	0.25	0.20	0.14	0.20	0.14	0.11	0.20	0.14	0.28	0.26	0.46
FeOt	92.3	91.7	91.3	92.2	91.9	91.6	92.3	92.4	92.3	92.1	92.4
Fe2O3	67.92	66.96	67.35	68.14	67.90	67.58	67.88	68.26	68.04	67.79	68.09
FeO	31.18	31.45	30.60	30.89	30.81	30.79	31.12	30.98	31.08	31.10	31.13
TiO2	0.42	1.04	0.31	0.17	0.17	0.27	0.31	0.22	0.30	0.55	0.49
MnO	0.23	0.49	0.26	0.14	0.11	0.09	0.11	0.18	0.18	0.28	0.38
ZnO	0.11	0.20	0.09	0.10	0.00	0.09	0.06	0.07	0.08	0.26	0.24
Total	100.11	100.34	98.75	99.64	99.13	98.93	99.68	99.85	99.96	100.24	100.79
Al	0.011	0.009	0.006	0.009	0.006	0.005	0.009	0.006	0.013	0.012	0.021
Fe3+	1.963	1.930	1.974	1.979	1.983	1.977	1.971	1.979	1.969	1.956	1.951
Fe2+	1.002	1.008	0.996	0.997	1.000	1.001	1.004	0.998	0.999	0.997	0.991
Ti	0.012	0.030	0.009	0.005	0.005	0.008	0.009	0.006	0.009	0.016	0.014
Mn	0.007	0.016	0.009	0.005	0.004	0.003	0.004	0.006	0.006	0.009	0.012
Zn	0.003	0.006	0.003	0.003	0.000	0.003	0.002	0.002	0.002	0.007	0.007

	BIOTITE-BEARING ENCLAVES				AMPHIBOLE-BEARING ENCLAVES	
	82QC51b	83QC16	83QC14	83QC17.3	83QC12	85QC9
*	1	1	1	3	2	2
Al2O3	0.06	0.10	0.07	0.22	0.22	0.75
FeOt	92.0	91.6	92.5	92.3	91.5	91.1
Fe2O3	68.13	67.65	68.33	67.97	67.27	66.34
FeO	30.70	30.73	31.02	31.14	30.87	31.41
TiO2	0.11	0.22	0.26	0.49	0.37	0.91
MnO	0.12	0.11	0.17	0.28	0.10	0.24
ZnO	0.11	0.11	0.10	0.16	0.08	0.20
Total	99.23	98.92	99.95	100.26	98.91	99.85
Al	0.003	0.005	0.003	0.010	0.010	0.034
Fe3+	1.988	1.980	1.979	1.961	1.968	1.913
Fe2+	0.996	1.000	0.999	0.998	1.003	1.006
Ti	0.003	0.006	0.008	0.014	0.011	0.026
Mn	0.004	0.004	0.006	0.009	0.003	0.008
Zn	0.003	0.003	0.003	0.005	0.002	0.006

Table A.4.2: Ilmenite, Cabresto Lake pluton.

	GRANITE											
	78L172	82QC51	82QC51b								83QC10	
(*)	(1)m5	(7)ph	(2)p	(5)p	(7)ph	(1)ps	(6)ps	(4)m3	1(1)ph	1(2)m5	(8)ph	(7)m4
FeOt	33.0	39.9	37.2	39.7	53.0	38.9	40.9	27.6	44.3	25.7	39.7	32.5
Fe2O3	8.63	9.54	7.56	9.18	21.62	13.08	10.82	5.05	11.16	5.36	11.15	3.77
FeO	25.34	31.31	30.40	31.44	33.54	27.13	31.17	23.06	34.26	20.88	29.66	29.21
MgO	0.03	0.05	0.05	0.03	0.07	0.09	0.05	0.05	0.05	0.02	0.05	0.05
CaO	0.01	0.13	0.11	0.19	0.16	0.38	0.33	0.01	0.07	0.16	0.01	0.02
TiO2	48.1	46.7	47.9	46.8	40.7	45.5	46.3	50.0	46.0	49.3	45.9	50.1
MnO	17.6	10.4	12.3	10.2	2.63	12.9	9.75	21.4	6.94	22.8	11.6	15.6
Nb2O5	0.11	0.36	0.27	0.31	0.26	0.24	0.21	0.04	0.27	0.04	0.77	0.30
ZnO	0.10	0.11	0.15	0.21	0.23	0.23	0.22	0.17	0.14	0.20	0.20	0.10
Total	99.92	98.6	98.74	98.36	99.21	99.55	98.85	99.78	98.89	98.76	99.34	99.15
Fe3+	0.164	0.185	0.146	0.178	0.419	0.251	0.209	0.096	0.215	0.103	0.215	0.072
Fe2+	0.537	0.674	0.652	0.678	0.722	0.578	0.669	0.488	0.735	0.446	0.635	0.623
Mg	0.001	0.002	0.002	0.001	0.003	0.003	0.002	0.002	0.002	0.001	0.002	0.002
Ca	0.000	0.004	0.003	0.005	0.004	0.010	0.009	0.000	0.002	0.004	0.000	0.001
Ti	0.916	0.903	0.924	0.907	0.787	0.872	0.893	0.951	0.887	0.947	0.884	0.960
Mn	0.378	0.227	0.267	0.223	0.057	0.278	0.212	0.459	0.151	0.493	0.252	0.337
Nb	0.001	0.004	0.003	0.004	0.003	0.003	0.002	0.000	0.003	0.000	0.009	0.003
Zn	0.002	0.002	0.003	0.004	0.004	0.004	0.004	0.003	0.003	0.004	0.004	0.002

Table A.4.2, continued.

	GRANITE									MIXED		
	83QC10		83QC16		83QC18		83QC20			83QC14		
(*)	(4)m4	(9')m3	(1)ph	(2)ph	(2)ph	(1)m5	(1)m5	(2)m5	(3)m5	(1)ph	(3)p	(4)m3
FeOt	33.7	30.1	47.2	39.9	36.8	26.9	24.4	17.6	27.5	38.6	35.2	32.4
Fe2O3	3.83	4.88	13.88	8.19	6.11	3.90	5.07	2.17	7.05	11.53	7.06	4.43
FeO	30.25	25.71	34.71	32.53	31.31	23.39	19.84	15.64	21.16	28.22	28.85	28.41
MgO	0.06	0.05	0.04	0.03	0.02	0.04	0.01	0.02	0.02	0.06	0.05	0.03
CaO	0.03	0.09	0.09	0.10	0.12	0.08	0.02	0.02	0.02	0.00	0.02	0.03
TiO2	49.7	49.9	44.3	47.2	48.2	49.7	48.9	51.0	48.7	46.7	48.6	50.0
MnO	13.9	18.5	5.03	9.88	12.2	20.7	23.8	29.7	22.3	13.6	14.6	16.3
Nb2O5	0.14	0.02	0.31	0.70	0.96	0.32	0.23	0.03	0.20	0.37	0.32	0.06
ZnO	0.33	0.26	0.04	0.13	0.01	0.42	0.05	0.13	0.12	0.09	0.14	0.14
Total	98.24	99.41	98.40	98.76	98.93	98.55	97.92	98.71	99.57	100.57	99.64	99.40
Fe3+	0.074	0.093	0.270	0.158	0.118	0.075	0.098	0.042	0.135	0.219	0.135	0.085
Fe2+	0.649	0.546	0.750	0.699	0.672	0.501	0.427	0.334	0.449	0.596	0.613	0.602
Mg	0.002	0.002	0.002	0.001	0.001	0.002	0.000	0.001	0.001	0.002	0.002	0.001
Ca	0.001	0.002	0.002	0.003	0.003	0.002	0.001	0.001	0.001	0.000	0.001	0.001
Ti	0.959	0.953	0.861	0.912	0.930	0.958	0.947	0.978	0.930	0.886	0.929	0.953
Mn	0.302	0.398	0.110	0.215	0.265	0.449	0.522	0.642	0.480	0.291	0.314	0.350
Nb	0.002	0.000	0.004	0.008	0.011	0.004	0.003	0.000	0.002	0.004	0.004	0.001
Zn	0.006	0.005	0.001	0.002	0.000	0.008	0.001	0.002	0.002	0.002	0.003	0.003

	MIXED										
	85QC11						85QC12				
(*)	(2)ps	(3)ps	(3')ps	(1)m4	(1)ph	(3)p	(2)p	(2')p	(4)ps	(4')ps	(5)m5
FeOt	40.5	40.6	51.2	26.8	27.0	43.1	39.8	36.7	48.9	42.6	32.3
Fe2O3	13.99	10.58	22.39	2.84	3.67	11.58	11.40	7.52	20.24	11.76	6.43
FeO	27.92	31.08	31.06	24.25	23.70	32.68	29.54	29.94	30.69	32.02	26.51
MgO	0.07	0.04	0.04	0.05	0.04	0.06	0.05	0.05	0.07	0.12	0.05
CaO	0.99	0.05	0.15	0.01	0.55	0.04	0.25	0.49	0.64	0.79	0.07
TiO2	44.7	46.4	39.6	50.6	50.9	46.2	46.3	48.1	41.8	46.4	49.2
MnO	10.9	10.3	4.28	20.5	21.1	8.66	11.5	12.4	5.86	8.30	17.2
Nb2O5	0.28	0.37	0.43	0.05	0.35	0.43	0.23	0.14	0.31	0.19	0.04
ZnO	0.20	0.31	0.21	0.47	0.13	0.19	0.18	0.13	0.21	0.20	0.17
Total	99.05	99.13	98.16	98.77	100.44	99.84	99.45	98.77	99.82	99.78	99.67
Fe3+	0.269	0.204	0.439	0.055	0.069	0.222	0.219	0.145	0.389	0.225	0.123
Fe2+	0.596	0.665	0.676	0.518	0.498	0.695	0.630	0.641	0.655	0.680	0.562
Mg	0.003	0.002	0.002	0.002	0.001	0.002	0.002	0.002	0.003	0.005	0.002
Ca	0.027	0.001	0.004	0.000	0.015	0.001	0.007	0.013	0.017	0.021	0.002
Ti	0.859	0.893	0.775	0.972	0.961	0.884	0.888	0.926	0.802	0.886	0.938
Mn	0.236	0.223	0.094	0.444	0.449	0.187	0.248	0.269	0.127	0.178	0.369
Nb	0.003	0.004	0.005	0.001	0.004	0.005	0.003	0.002	0.004	0.002	0.000
Zn	0.004	0.006	0.004	0.009	0.002	0.004	0.003	0.002	0.004	0.004	0.003

	BIOTITE-BEARING ENCLAVES								AMPHIBOLE-BEARING ENCLAVES			
	82QC51b		83QC17.3					83QC14	83QC12			
(*)	1(7)ph	1(7')ph	(15)ph	(15')phi	(14)m5	(12)m3	(13)m3	(2)p	(2)ph	(19)ph	(17)ph	(11)ps
FeOt	46.7	41.3	39.6	30.7	22.2	21.6	20.9	33.8	43.7	40.1	54.1	49.1
Fe2O3	13.99	13.65	20.69	8.80	6.12	5.44	4.06	9.38	9.07	4.32	22.26	16.59
FeO	34.12	29.02	20.99	22.79	16.69	16.70	17.24	25.36	35.54	36.21	34.07	34.17
MgO	0.08	0.02	0.06	0.05	0.05	0.05	0.04	0.05	0.05	0.05	0.26	0.10
CaO	0.23	0.12	0.15	0.26	0.04	0.04	0.01	0.02	0.09	0.32	0.00	0.26
TiO2	44.3	44.7	41.4	47.2	49.2	49.5	50.2	47.8	46.6	49.1	40.9	43.6
MnO	5.14	10.8	15.8	19.1	27.1	27.3	27.4	17.4	6.13	7.34	2.15	4.41
Nb2O5	0.25	0.29	0.34	0.35	0.22	0.21	0.08	0.35	0.30	0.31	0.22	0.25
ZnO	0.24	0.23	0.14	0.09	0.09	0.15	0.12	0.10	0.13	0.20	0.21	0.22
Total	98.35	98.83	99.57	98.64	99.51	99.39	99.15	100.46	97.91	97.85	100.07	99.60
Fe3+	0.272	0.264	0.398	0.170	0.117	0.104	0.078	0.178	0.177	0.084	0.427	0.319
Fe2+	0.736	0.624	0.449	0.489	0.354	0.355	0.367	0.535	0.770	0.782	0.726	0.730
Mg	0.003	0.001	0.002	0.002	0.002	0.002	0.002	0.002	0.002	0.002	0.010	0.004
Ca	0.006	0.003	0.004	0.007	0.001	0.001	0.000	0.001	0.002	0.009	0.000	0.007
Ti	0.860	0.865	0.797	0.911	0.939	0.946	0.960	0.907	0.908	0.954	0.784	0.837
Mn	0.112	0.235	0.342	0.415	0.582	0.587	0.590	0.372	0.135	0.161	0.046	0.095
Nb	0.003	0.003	0.004	0.004	0.003	0.002	0.001	0.004	0.004	0.004	0.003	0.003
Zn	0.005	0.004	0.003	0.002	0.002	0.003	0.002	0.002	0.002	0.004	0.004	0.004

Table A.4.2, continued.

	AMPHIBOLE-BEARING ENCLAVES				
	83QC12			85QC9.2	
(*)	(1)m3	(2')m3	(3)m3	(1)m3	(2)m3
FeOt	40.3	39.1	39.6	31.3	32.7
Fe2O3	5.23	3.33	4.10	6.79	5.07
FeO	35.59	36.11	35.91	25.19	28.14
MgO	0.06	0.05	0.08	0.06	0.06
CaO	0.05	0.08	0.05	0.14	0.06
TiO2	48.8	49.7	49.2	48.9	49.5
MnO	8.08	8.36	8.03	18.2	16.0
Nb2O5	0.23	0.22	0.24	0.04	0.11
ZnO	0.12	0.16	0.16	0.09	0.05
Total	98.16	98.01	97.77	99.41	98.99
Fe3+	0.101	0.064	0.080	0.130	0.097
Fe2+	0.767	0.776	0.776	0.536	0.600
Mg	0.002	0.002	0.003	0.002	0.002
Ca	0.001	0.002	0.001	0.004	0.002
Ti	0.945	0.960	0.957	0.935	0.949
Mn	0.176	0.182	0.176	0.392	0.346
Nb	0.003	0.003	0.003	0.000	0.001
Zn	0.002	0.003	0.003	0.002	0.001

Table A.5.1: Magnetite, Rio Hondo pluton.

	GRANITE							GRANODIORITE				
	82QC5	Q83SL25	Q83SL27	84QC9	84QC11	84QC14	82QC30.1	82QC2	82QC12	82QC26	82QC28	Q83J55
*	2	2	2	2	2	2	2	2	4	3	2	2
Al2O3	0.04	0.10	0.05	0.07	0.08	0.06	0.06	0.11	0.15	0.08	0.05	0.08
FeOt	92.6	92.8	92.7	92.2	92.1	92.8	91.6	92.4	92.2	92.5	92.1	92.4
Fe2O3	68.67	68.77	68.76	68.53	68.32	69.06	67.92	68.35	68.32	68.35	68.15	68.24
FeO	30.81	30.92	30.82	30.54	30.62	30.66	30.49	30.90	30.72	31.00	30.78	31.00
TiO2	0.13	0.11	0.08	0.08	0.12	0.08	0.14	0.15	0.11	0.22	0.15	0.22
MnO	0.25	0.21	0.19	0.40	0.35	0.43	0.27	0.14	0.18	0.10	0.08	0.12
ZnO	0.08	0.09	0.10	0.13	0.11	0.19	0.08	0.04	0.12	0.09	0.01	0.00
Total	99.98	100.20	100.00	99.75	99.60	100.48	98.96	99.69	99.60	99.84	99.22	99.66
Al	0.002	0.005	0.002	0.003	0.004	0.003	0.003	0.005	0.007	0.004	0.002	0.004
Fe3+	1.990	1.988	1.992	1.990	1.986	1.992	1.988	1.986	1.986	1.983	1.989	1.983
Fe2+	0.992	0.993	0.992	0.985	0.989	0.983	0.992	0.998	0.992	0.999	0.998	1.001
Ti	0.004	0.003	0.002	0.002	0.003	0.002	0.004	0.004	0.003	0.006	0.004	0.006
Mn	0.008	0.007	0.006	0.013	0.011	0.014	0.009	0.005	0.006	0.003	0.003	0.004
Zn	0.002	0.003	0.003	0.004	0.003	0.005	0.002	0.001	0.003	0.003	0.000	0.000

	GRANODIORITE				ENCLAVES			DIKES	
	Q83J59	Q83J61	84QC31	84QC32.2	Loc 12.1	84QC31	Loc 12.3	Q83J100	82QC27
*	2	2	2	2	2	2	2	2	2
Al2O3	0.04	0.07	0.13	0.13	0.28	0.22	0.16	0.08	0.60
FeOt	92.0	92.1	92.3	92.5	91.5	92.2	91.5	91.9	88.4
Fe2O3	67.86	67.86	68.27	68.41	67.76	68.21	67.85	67.98	62.74
FeO	30.94	31.04	30.87	30.94	30.53	30.82	30.45	30.73	31.94
TiO2	0.27	0.33	0.15	0.14	0.15	0.10	0.11	0.18	2.67
MnO	0.04	0.08	0.10	0.12	0.25	0.08	0.24	0.11	0.83
ZnO	0.04	0.03	0.06	0.09	0.17	0.09	0.14	0.14	0.21
Total	99.19	99.41	99.58	99.83	99.14	99.52	98.95	99.22	98.99
Al	0.002	0.003	0.006	0.006	0.013	0.010	0.007	0.004	0.027
Fe3+	1.982	1.977	1.985	1.985	1.977	1.983	1.984	1.984	1.817
Fe2+	1.004	1.005	0.998	0.997	0.990	0.996	0.989	0.997	1.028
Ti	0.008	0.010	0.004	0.004	0.004	0.003	0.003	0.005	0.077
Mn	0.001	0.003	0.003	0.004	0.008	0.003	0.008	0.004	0.027
Zn	0.001	0.001	0.002	0.003	0.005	0.003	0.004	0.004	0.006

Table A.5.2: Ilmenite, Rio Hondo pluton.

	GRANITE									GRANODIORITE	
	82QC5		Q83SL25	Q83SL27	84QC11	84QC12		84QC14		84QC31	
(*)	(1)m5	(3)m4	(1)ps	(2)ps	(1)p	(5)ps	(5')m3	(4)p	(9)m5	(14)ps	(15)psi
FeOt	21.5	19.8	34.6	34.3	17.5	16.0	14.9	15.3	9.93	50.6	39.4
Fe2O3	3.32	2.48	3.83	2.59	2.76	4.21	3.47	0.45	1.21	22.76	7.69
FeO	18.52	17.57	31.16	31.97	15.01	12.21	11.78	14.90	8.84	30.12	32.48
MgO	0.04	0.05	0.02	0.05	0.03	0.04	0.07	0.05	0.03	0.13	0.10
CaO	0.09	0.68	0.08	0.79	0.10	0.61	0.01	0.08	0.02	0.23	0.75
TiO2	51.2	50.6	50.3	50.9	50.3	50.0	50.9	50.6	51.0	40.1	48.3
MnO	27.0	27.0	14.0	12.5	30.0	31.2	33.3	30.5	36.4	5.24	9.46
Nb2O5	0.05	0.03	0.60	0.32	0.81	0.30	0.04	1.51	0.49	0.05	0.06
ZnO	0.02	0.08	0.09	0.24	0.10	0.52	0.17	0.38	0.38	0.15	0.30
Total	100.24	98.49	100.08	99.36	99.11	99.09	99.74	98.47	98.37	98.78	99.14
Fe3+	0.063	0.047	0.073	0.049	0.053	0.081	0.066	0.009	0.023	0.442	0.147
Fe2+	0.389	0.373	0.659	0.678	0.320	0.260	0.249	0.320	0.190	0.650	0.692
Mg	0.001	0.002	0.001	0.002	0.001	0.002	0.003	0.002	0.001	0.005	0.004
Ca	0.002	0.018	0.002	0.021	0.003	0.017	0.000	0.002	0.001	0.006	0.020
Ti	0.968	0.966	0.957	0.971	0.964	0.956	0.966	0.978	0.983	0.778	0.926
Mn	0.575	0.580	0.300	0.269	0.647	0.672	0.712	0.664	0.790	0.115	0.204
Nb	0.001	0.000	0.007	0.004	0.009	0.003	0.000	0.018	0.006	0.001	0.001
Zn	0.000	0.001	0.002	0.004	0.002	0.010	0.003	0.007	0.007	0.003	0.006

	GRANODIORITE			ENCLAVES			
	84QC32.3			Loc 12.1		85QC27	
(*)	(1)psh	(1')psi	(2)ps	(13)psi	(14)psi	(1)p	(2)ps
FeOt	74.3	49.9	47.9	45.1	43.6	38.5	46.2
Fe2O3	65.52	13.85	18.91	8.61	7.01	7.93	7.27
FeO	15.34	37.44	30.89	37.35	37.29	31.36	34.36
MgO	0.07	0.23	0.24	0.53	0.40	0.07	0.31
CaO	0.20	0.24	0.29	0.78	0.43	0.02	2.64
TiO2	18.2	45.3	42.3	48.0	48.9	48.4	47.5
MnO	0.63	2.48	6.21	3.70	5.25	11.8	6.34
Nb2O5	0.01	0.11	0.07	0.04	0.09	0.07	0.06
ZnO	0.01	0.14	0.11	0.16	0.17	0.11	0.14
Total	99.98	99.79	99.02	99.17	99.54	99.76	98.62
Fe3+	1.285	0.265	0.365	0.165	0.134	0.151	0.216
Fe2+	0.335	0.796	0.663	0.793	0.790	0.665	0.765
Mg	0.003	0.009	0.009	0.020	0.015	0.003	0.014
Ca	0.006	0.007	0.008	0.021	0.012	0.001	0.006
Ti	0.357	0.866	0.817	0.917	0.932	0.923	0.892
Mn	0.014	0.053	0.135	0.080	0.113	0.254	0.105
Nb	0.000	0.001	0.001	0.000	0.001	0.001	0.000
Zn	0.000	0.003	0.002	0.003	0.003	0.002	0.003

Table A.6: Opaque oxides, Bear Canyon pluton.

	MAGNETITE				
	82QC8			82QC10	
(*)	(4)	(6)	(7)	(4)	(5)
Al2O3	0.44	0.32	0.39	0.28	0.24
FeOt	90.7	90.6	90.1	92.1	91.9
Fe2O3	65.83	66.01	64.89	67.83	67.72
FeO	31.46	31.21	31.71	31.06	30.97
TiO2	1.33	0.92	1.50	0.29	0.29
MnO	0.58	0.27	0.28	0.08	0.06
ZnO	0.27	0.11	0.18	0.08	0.11
Total	99.91	98.84	98.95	99.62	99.39
Al	0.020	0.015	0.018	0.013	0.011
Fe3+	1.902	1.931	1.894	1.970	1.971
Fe2+	1.010	1.014	1.029	1.002	1.002
Ti	0.038	0.027	0.044	0.008	0.008
Mn	0.019	0.009	0.009	0.003	0.002
Zn	0.008	0.003	0.005	0.002	0.003

	ILMENITE			
	82QC8		82QC10	
	(5)p	(7)m5	(4)m5	(5)m5
FeOt	37.5	38.5	39.3	38.3
Fe2O3	7.80	9.10	5.06	4.67
FeO	30.49	30.32	34.75	34.10
TiO2	46.7	45.9	48.8	49.3
MnO	11.9	11.3	9.27	10.3
Nb2O5	1.37	1.35	0.82	0.70
ZnO	0.18	0.22	0.08	0.07
Total	98.44	98.19	98.78	99.14
Fe3+	0.152	0.177	0.098	0.090
Fe2+	0.659	0.657	0.745	0.728
Ti	0.908	0.895	0.941	0.947
Mn	0.261	0.248	0.201	0.223
Nb	0.016	0.016	0.010	0.008
Zn	0.003	0.004	0.002	0.001

Table A.7.1: Magnetite, Sulphur Gulch pluton.

	CARAPACE								SOURCE APLITE	
	3417			3439			3440		3438	
(*)	(1)	(2)	(4)	(1)	(2)	(3)	(2)	(5)	(1)	(2)
Al2O3	0.28	0.23	0.22	0.17	0.19	0.24	0.22	0.30	0.18	0.23
FeOt	91.3	89.8	91.9	90.7	92.2	90.7	92.0	92.3	92.6	92.5
Fe2O3	66.68	64.54	67.95	65.46	67.89	65.88	67.60	68.05	68.28	68.19
FeO	31.10	31.72	30.75	31.80	31.11	31.42	31.18	31.07	31.16	31.15
TiO2	1.00	2.11	0.31	1.68	0.40	1.26	0.56	0.28	0.32	0.33
MnO	0.53	1.06	0.34	0.67	0.17	0.43	0.25	0.12	0.13	0.14
ZnO	0.15	0.12	0.14	0.07	0.08	0.10	0.07	0.09	0.06	0.11
Total	99.74	99.78	99.71	99.85	99.84	99.33	99.88	99.91	100.13	100.15
Al	0.013	0.010	0.010	0.008	0.009	0.011	0.010	0.014	0.008	0.010
Fe3+	1.928	1.867	1.971	1.894	1.968	1.914	1.956	1.970	1.973	1.970
Fe2+	1.006	1.020	0.991	1.022	1.002	1.015	1.003	0.999	1.001	1.000
Ti	0.029	0.061	0.009	0.049	0.012	0.037	0.016	0.008	0.009	0.010
Mn	0.017	0.035	0.011	0.022	0.006	0.014	0.008	0.004	0.004	0.005
Zn	0.004	0.003	0.004	0.002	0.002	0.003	0.002	0.003	0.002	0.003

Table A.7.2: Ilmenite, hematite, and ilmenorutile, Sulphur Gulch pluton.

	CARAPACE							SOURCE APLITE		
	3417		3439		3440			82QC55		
(*)	(3)m4	(4)m5	(3)psi	(3)psh	(1)p	(3)phi	(3)phh	(2)p	(3)	(3')
FeOt	25.6	24.4	33.8	74.2	35.0	40.7	69.5	88.8	10.8	9.85
Fe2O3	5.07	6.63	12.01	69.94	7.96	15.38	65.11	98.36		
FeO	21.04	18.43	22.99	11.27	27.84	26.86	10.92	0.29		
TiO2	50.6	49.3	46.2	15.6	48.3	44.4	18.5	0.39	61.6	65.6
MnO	23.4	24.8	16.3	1.60	15.4	12.9	5.62	0.05	0.00	0.00
Nb2O5	0.03	0.05	0.18	0.07	0.33	0.25	0.08	0.10	24.5	22.2
ZnO	0.00	0.09	0.05	0.00	0.05	0.03	0.00	0.00	0.00	0.00
Total	100.14	99.30&	97.73#	98.48@	99.88	99.82	100.23	99.19	96.90	97.65
Fe3+	0.095	0.126	0.230	1.366	0.152	0.294	1.273	1.978		
Fe2+	0.440	0.389	0.488	0.245	0.590	0.572	0.237	0.007	0.418	0.374
Ti	0.952	0.936	0.882	0.304	0.920	0.850	0.362	0.008	2.144	2.238
Mn	0.496	0.531	0.351	0.035	0.331	0.278	0.124	0.001	0.000	0.000
Nb	0.000	0.001	0.002	0.001	0.004	0.003	0.001	0.001	0.513	0.455
Zn	0.000	0.002	0.001	0.000	0.001	0.001	0.000	0.000	0.000	0.000

Notes. &, + 0.54 wt% CaO. #, + 1.62 wt% CaO. @, + 1.29 wt% CaO.
82QC55 (3) and (3'), analyses of ilmenorutile.

Table A.8.1: Magnetite, Red River intrusive complex.

	QUARTZ MONZONITE			ALK. GRANITE		GRANITE	ENCLAVE		QUARTZ DIORITE		
	82QC44			82QC32		85QC36.1			85QC37b		
(*) *	(9)	(10)	(12)	(7)	(8)	4	(6)	(7)	(4)	(5)	(6)
Al2O3	0.06	0.1	0.1	0.07	0.33	0.44	0.31	0.30	1.02	0.41	1.16
FeOt	91.8	91.7	91.9	92.2	91.1	89.7	90.7	91.2	90.8	92.3	90.3
Fe2O3	68.01	67.91	68.07	68.34	67.24	64.69	66.15	66.61	66.25	68.10	64.95
FeO	30.60	30.60	30.65	30.71	30.60	31.46	31.18	31.27	31.18	31.03	31.86
TiO2	0.08	0.07	0.08	0.08	0.37	1.81	1.12	1.01	0.62	0.20	1.19
MnO	0.08	0.06	0.07	0.15	0.43	0.99	0.63	0.57	0.25	0.08	0.08
ZnO	0.07	0.05	0.09	0.09	0.17	0.15	0.17	0.10	0.09	0.09	0.20
Total	98.90	98.79	99.06	99.44	99.14	99.54	99.56	99.86	99.41	99.91	99.44
Al	0.003	0.005	0.005	0.003	0.015	0.020	0.014	0.014	0.046	0.190	0.053
Fe3+	1.991	1.990	1.990	1.991	1.962	1.874	1.920	1.927	1.917	1.968	1.878
Fe2+	0.996	0.997	0.996	0.994	0.992	1.013	1.006	1.005	1.003	0.997	1.024
Ti	0.002	0.002	0.002	0.002	0.011	0.052	0.032	0.029	0.018	0.006	0.034
Mn	0.003	0.002	0.002	0.005	0.014	0.032	0.021	0.019	0.008	0.003	0.003
Zn	0.002	0.001	0.003	0.003	0.005	0.004	0.005	0.003	0.003	0.003	0.006

Table A.8.2: Ilmenite and hematite, Red River intrusive complex.

	GRANODIORITE 82QC44								ALK.GR 82QC32	GRANITE 85QC36.1		
(*)	(14)phi	(11)ps	(13)ph	(13)phi	(13)phh	(15)ph	(15)phi	(15)phh	(10)p	(1)p	(4)p	(5)p
FeOt	48.5	45.9	54.2	49.6	72.3	50.9	46.6	74.7	78.3	39.7	28.1	29.0
Fe2O3	10.47	10.28	21.82	11.86	60.94	19.28	10.44	66.77	75.88	6.45	5.56	6.39
FeO	39.08	36.65	34.57	38.93	17.46	33.55	37.20	14.62	10.03	33.90	23.09	23.25
TiO2	46.7	46.7	40.4	45.5	20.0	41.4	46.5	17.4	11.6	47.9	49.5	48.1
MnO	2.70	4.34	1.49	1.72	0.45	3.50	4.36	0.85	0.33	9.42	21.1	20.1
Nb2O5	0.12	0.08	0.12	0.13	0.09	0.12	0.12	0.03	0.16	0.95	0.25	0.96
ZnO	0.11	0.05	0.08	0.12	0.00	0.11	0.12	0.07	0.08	0.06	0.11	0.08
Total	99.18	98.10&	98.48	98.26	98.94	97.96#	98.74	99.74	98.08	98.68	99.61	98.88
Fe3+	0.201	0.197	0.424	0.230	1.207	0.374	0.202	1.316	1.528	0.125	0.106	0.123
Fe2+	0.835	0.779	0.747	0.840	0.384	0.724	0.799	0.320	0.224	0.729	0.490	0.498
Ti	0.898	0.892	0.785	0.883	0.396	0.803	0.898	0.342	0.233	0.927	0.944	0.927
Mn	0.058	0.093	0.033	0.038	0.010	0.076	0.095	0.019	0.007	0.205	0.453	0.436
Nb	0.001	0.001	0.001	0.002	0.001	0.001	0.001	0.000	0.002	0.011	0.003	0.011
Zn	0.002	0.001	0.002	0.002	0.000	0.002	0.002	0.001	0.002	0.001	0.002	0.002

	GRANITE 85QC36.1					ENCLAVE		QUARTZ DIORITE 85QC37b			
(*)	(8)ps	(2)s	(3)m5	(10)m5	(9)m3	(6)p	(7)p	(1)p	(2)p	(3)p	(4)m5
FeOt	35.8	30.9	29.5	25.2	30.7	32.3	33.5	41.0	48.7	43.4	37.3
Fe2O3	6.18	4.89	5.43	5.99	7.73	6.82	7.74	12.08	17.20	13.15	9.50
FeO	30.24	26.50	24.62	19.81	23.75	26.17	26.54	30.13	33.22	31.57	28.76
TiO2	48.2	48.9	49.0	49.1	48.1	48.3	47.9	45.3	42.8	45.2	46.5
MnO	12.4	17.2	19.2	23.9	18.9	17.2	16.6	10.3	5.07	8.92	12.5
Nb2O5	0.99	0.63	0.54	0.17	0.13	0.72	0.77	0.15	0.26	0.23	0.14
ZnO	0.10	0.19	0.16	0.07	0.38	0.10	0.01	0.13	0.10	0.06	0.15
Total	98.11@	98.31	98.95	99.04	98.99	99.31	99.56	98.09	98.65	99.13	97.55
Fe3+	0.119	0.095	0.104	0.115	0.149	0.131	0.148	0.235	0.334	0.253	0.185
Fe2+	0.648	0.570	0.526	0.422	0.507	0.558	0.565	0.652	0.716	0.676	0.623
Ti	0.929	0.945	0.942	0.941	0.924	0.926	0.917	0.881	0.830	0.871	0.906
Mn	0.269	0.374	0.416	0.516	0.409	0.372	0.358	0.226	0.111	0.194	0.274
Nb	0.011	0.007	0.006	0.002	0.002	0.008	0.009	0.002	0.003	0.003	0.002
Zn	0.002	0.004	0.003	0.001	0.007	0.002	0.000	0.002	0.002	0.001	0.003

Notes. &, + 0.85 CaO + 0.27 SiO2. #, + 0.27 CaO + 0.28 SiO2. @, + 0.72 CaO.

Table A.9: Opaque oxides, Lucero Peak pluton.

	MAGNETITE 82QC15			82QC25	
(*)	(4)	(5)	(6)	(7)	(8)
Al2O3	0.09	0.13	0.14	0.15	0.07
FeOt	92.0	91.9	91.7	92.2	92.1
Fe2O3	67.99	67.91	67.84	68.17	68.31
FeO	30.82	30.79	30.66	30.86	30.63
TiO2	0.19	0.26	0.20	0.12	0.06
MnO	0.10	0.25	0.29	0.09	0.12
ZnO	0.09	0.08	0.02	0.02	0.10
Total	99.28	99.42	99.15	99.41	99.29
Al	0.004	0.006	0.006	0.007	0.003
Fe3+	1.983	1.977	1.981	1.985	1.992
Fe2+	0.999	0.996	0.995	0.999	0.993
Ti	0.006	0.008	0.006	0.003	0.002
Mn	0.003	0.008	0.010	0.003	0.004
Zn	0.003	0.002	0.001	0.001	0.003

	ILMENITE 82QC15		82QC25			
(*)	(8)ph	(9)ph	(5)p	(6)p	(7)p	(8)m5
FeOt	37.2	35.7	30.8	32.9	30.0	22.1
Fe2O3	9.30	9.41	1.99	2.39	2.90	1.36
FeO	28.83	27.24	29.01	30.75	27.39	20.88
TiO2	46.6	46.6	49.7	49.3	49.1	51.1
MnO	13.2	14.9	16.2	14.2	17.4	24.7
Nb2O5	1.17	1.21	1.67	1.80	1.85	0.57
ZnO	0.24	0.16	0.1	0.12	0.08	0.30
Total	99.34	99.52	98.67	98.56	98.72	98.91
Fe3+	0.179	0.181	0.038	0.046	0.056	0.026
Fe2+	0.617	0.582	0.624	0.663	0.590	0.445
Ti	0.897	0.896	0.961	0.955	0.950	0.980
Mn	0.286	0.323	0.353	0.310	0.379	0.534
Nb	0.014	0.014	0.019	0.021	0.022	0.007
Zn	0.005	0.003	0.002	0.002	0.002	0.006

APPENDIX B: WHOLE-ROCK CHEMICAL ANALYSES FOR A SUPPLEMENTARY SUITE OF QUESTA GRANITIC ROCKS (IN WT%).

	81S31	81S43	81S44	82QC5	82QC9	82QC13	82QC18B	82QC19
SiO_2	77.4	74.6	77.2	74.1	67.2	76.8	77.4	76.9
Al_2O_3	12.3	13.3	12.3	13.6	16.5	12.5	12.5	12.7
Fe_2O_3	0.64*	1.08*	0.60*	0.83	1.59	0.35	0.45	0.47
FeO	-	-	-	0.49	0.82	0.29	0.15	0.18
MgO	<0.10	0.22	0.12	0.41	0.58	<0.10	0.12	0.14
CaO	0.24	0.54	0.31	0.97	1.26	0.40	0.14	0.19
Na_2O	3.91	3.64	3.66	3.90	5.12	4.02	4.10	3.91
K_2O	4.52	5.17	4.70	4.53	4.84	3.85	4.52	4.68
TiO_2	0.07	0.20	0.09	0.21	0.47	0.06	0.07	0.08
P_2O_5	<0.05	<0.05	<0.05	0.06	0.12	<0.05	<0.05	<0.05
MnO	0.06	0.04	<0.02	<0.02	0.07	0.02	0.04	0.04
CO_2	-	-	-	-	-	<0.01	-	-
LOI	0.18	0.50	0.30	0.60	0.58	0.26	0.04	0.18
Total**	99.47	99.34	99.35	99.72	99.15	98.70	99.58	99.52

	82QC27	82QC28	82QC30	82QC32F	82QC34	82QC40	82QC45	82QC46
SiO_2	74.0	69.0	78.5	77.4	75.6	72.8	76.8	79.0
Al_2O_3	12.5	14.9	10.8	12.3	11.9	13.4	12.5	11.2
Fe_2O_3	0.94	1.38	0.58	0.49	1.27	1.06	0.49	0.74
FeO	0.66	1.50	0.31	0.25	0.24	0.54	0.18	0.13
MgO	0.36	1.28	0.18	<0.10	<0.10	0.25	0.17	<0.10
CaO	1.23	2.60	0.46	0.18	0.13	0.79	0.32	0.15
Na_2O	2.54	3.89	2.84	3.80	4.01	3.76	3.99	3.46
K_2O	4.64	3.81	4.41	4.76	4.68	4.77	4.63	4.40
TiO_2	0.20	0.49	0.15	0.10	0.19	0.28	0.10	0.09
P_2O_5	0.09	0.18	<0.05	<0.05	<0.05	0.05	<0.05	<0.05
MnO	0.02	0.04	0.02	<0.02	0.11	0.09	<0.02	<0.02
CO_2	-	<0.01	<0.01	-	<0.01	<0.01	-	-
LOI	1.82	0.50	0.25	0.43	0.46	0.55	0.63	0.41
Total	99.00	99.57	98.55	99.88	98.74	98.34	99.88	99.75

* Total iron as Fe_2O_3. FeO analyses by G. Mason and N. Elsheimer, U.S. Geological Survey.

** Does not include CO_2 if value for LOI is listed.
Analyses by XRF by J. Taggart, U.S. Geological Survey.

	82QC47	82QC49	82QC50	82QC51A	82QC52	82QC54	82QC55	82QC56
SiO_2	74.1	75.9	76.6	76.9	74.2	76.6	77.0	76.1
Al_2O_3	13.6	11.7	12.6	12.3	12.7	12.3	11.8	12.4
Fe_2O_3	0.93	1.17	0.53	0.48	0.94	0.36	0.33	0.59
FeO	0.23	0.28	0.33	0.27	0.18	0.20	0.17	0.26
MgO	0.26	<0.10	0.15	<0.10	0.21	0.12	<0.10	0.14
CaO	0.64	0.05	0.33	0.47	0.58	0.34	0.35	0.62
Na_2O	3.74	4.17	3.77	3.26	3.49	3.18	3.04	3.58
K_2O	5.27	4.42	4.71	5.10	4.83	5.31	5.16	4.66
TiO_2	0.23	0.15	0.17	0.15	0.19	0.10	0.12	0.11
P_2O_5	<0.05	<0.05	<0.05	<0.05	<0.05	<0.05	<0.05	<0.05
MnO	0.04	0.13	0.03	<0.02	0.04	0.03	0.03	0.04
CO_2	-	<0.01	-	<0.01	0.24	-	0.14	-
LOI	0.66	0.37	0.44	0.26	0.94	0.77	0.69	0.65
Total	99.75	98.49	99.71	99.36	98.35	99.36	98.84	99.20

	83QC1	83QC2	83QC8	83QC9	83QC10	83QC20	83QC21	83QC22
SiO_2	76.1	78.3	78.4	77.1	72.2	70.6	76.0	76.7
Al_2O_3	12.5	11.6	11.4	12.5	14.4	15.0	12.1	12.1
Fe_2O_3	0.67	0.55	0.53	0.56	1.03	1.23	1.34	1.26
FeO	0.36	0.15	0.20	0.19	0.65	0.69	0.06	0.08
MgO	0.31	0.12	0.21	0.13	0.46	0.50	0.11	<0.10
CaO	0.64	0.47	0.38	0.43	1.07	0.90	0.10	0.08
Na_2O	3.68	3.32	3.09	4.00	4.28	4.51	3.36	3.43
K_2O	4.53	4.45	4.60	4.31	4.73	4.68	4.89	4.89
TiO_2	0.15	0.08	0.11	0.11	0.33	0.38	0.14	0.14
P_2O_5	<0.05	<0.05	<0.05	<0.05	0.10	0.10	<0.05	<0.05
MnO	<0.02	<0.02	<0.02	<0.02	0.05	0.07	<0.02	<0.02
CO_2	-	-	-	-	-	-	-	-
LOI	0.08	0.55	0.34	0.34	0.25	0.39	1.27	1.30
Total	99.09	99.66	99.33	99.74	99.55	99.05	99.44	100.15

	83QC23	83QC25	83QC26	83QC32	83QC33	83QC34	Q83SL27	Q83SL28
SiO_2	75.8	72.9	76.1	76.9	76.0	73.4	75.9	75.7
Al_2O_3	12.2	13.7	12.8	11.7	12.7	13.4	12.6	13.0
Fe_2O_3	1.83	1.26	0.66	1.62	0.98	1.18	0.80	0.44
FeO	0.07	0.55	0.30	0.43	0.31	0.49	0.47	0.27
MgO	<0.10	0.33	0.11	<0.10	0.17	0.38	0.36	0.19
CaO	0.21	0.82	0.47	0.12	0.37	0.81	0.79	0.59
Na_2O	3.49	3.97	3.92	3.55	3.79	3.87	3.63	3.69
K_2O	4.80	4.82	4.83	4.82	4.98	4.69	4.22	4.80
TiO_2	0.14	0.29	0.11	0.12	0.20	0.28	0.20	0.11
P_2O_5	<0.05	0.06	<0.05	<0.05	<0.05	0.06	0.05	<0.05
MnO	<0.02	0.08	0.04	0.04	0.07	0.07	<0.02	<0.02
CO_2	-	-	-	-	-	-	-	-
LOI	1.42	0.60	0.51	0.47	0.41	0.34	0.52	0.38
Total	100.13	99.38	99.90	99.92	100.03	98.97	99.56	99.24

	84QC5	84QC14	84QC32	85QC11	85QC12	85QC23	85QC32	85QC36
SiO_2	74.6	77.4	66.8	70.2	68.2	73.0	55.4	71.7
Al_2O_3	13.2	12.4	14.7	14.4	14.5	13.4	16.5	13.8
Fe_2O_3	0.74	0.38	1.99	1.27	1.79	0.91	3.62	1.03
FeO	0.27	0.20	1.82	0.80	1.06	0.58	4.30	0.59
MgO	0.24	0.10	1.72	0.66	1.34	0.45	3.81	0.49
CaO	0.53	0.49	3.27	1.34	2.25	1.39	5.23	0.89
Na_2O	3.84	3.49	4.22	4.17	4.27	3.64	4.75	3.79
K_2O	5.20	5.12	3.13	4.52	4.05	4.18	2.29	5.06
TiO_2	0.22	0.07	0.63	0.39	0.47	0.21	1.32	0.32
P_2O_5	<0.05	<0.05	0.24	0.13	0.18	0.08	0.59	0.10
MnO	0.04	0.02	0.05	0.06	0.11	0.05	0.13	0.07
CO_2	-	-	-	0.04	0.05	0.05	0.08	0.13
LOI	0.70	0.32	1.31	0.38	0.39	0.55	1.03	0.50
Total	99.63	100.04	99.88	98.36	98.66	98.49	99.05	98.47

APPENDIX C: TRACE ELEMENT DATA FOR QUESTA GRANITIC ROCKS (IN PPM).

	81S28	81S31	81S43	81S44	82QC8	82QC10	82QC13	82QC15	82QC26	82QC27	82QC28	82QC30	82QC33	82QC34	82QC35
As	0	9	7	15	8	0	16	0	3	0	4	3	11	0	7
Ba*	-	-	-	-	116	724	26	220	3200	465	1140	278	1360	120	715
Cr*	-	-	-	-	1	2	2	2	41	5	23	4	1	1	1
Cu	55	0	65	27	27	23	36	31	58	38	27	27	15	17	11
Ga	18	20	29	27	34	9	24	9	14	6	5	22	10	12	25
Mo	4	3	5	9	16	3	4	2	0	5	0	4	0	3	0
Mn	98	160	100	31	2.9	104	14	133	272	156	147	76	209	292	200
Nb	-	-	-	-	-	-	-	-	-	-	-	-	-	-	-
Ni*	-	-	-	-	<2	<2	<2	<2	32	3	19	3	<2	<2	<2
Pb	15	3	0	0	1	12	1	18	3	12	0	5	4	5	3
Rb	147	185	134	148	226	144	207	190	56	126	47	182	108	118	117
Sc*	-	-	-	-	3	3	6	3	7	2	4	<2	4	3	4
Se	2	27	44	83	67	2	52	2	6	10	0	13	10	11	10
Sr	5	7	51	3	36	151	6	100	1121	109	616	72	178	8	86
Th	11	11	4	8	11	8	8	1	0	5	0	11	3	1	0
U	13	14	12	11	23	19	26	11	7	14	8	16	14	16	14
Y*	-	-	-	-	8	13	5	7	14	5	8	5	44	46	34
Zn	45	67	124	196	135	43	87	46	66	82	41	46	92	106	72
Zr	71	91	150	87	82	116	70	67	133	100	97	63	311	377	206

	82QC38	82QC39	82QC40	82QC41	82QC44	82QC49	82QC51	82QC51A	82QC52	82QC55	85QC11**	85QC12**	85QC23**	85QC32**	85QC36**
As	8	4	10	0	11	7	11	3	7	0	-	-	-	-	-
Ba*	137	1260	1040	1750	1230	7	809	130	304	94	860	820	700	480	640
Cr*	1	1	<1	2	73	<1	5	1	2	2	<20	<20	<20	<20	<20
Cu	22	2	22	40	39	28	34	30	78	17	<10	<10	<10	14	<10
Ga	20	26	7	3	10	12	11	0	0	0	-	-	-	-	-
Mo	4	1	4	0	0	5	2	4	9	167	-	-	-	-	-
Mn	306	231	236	409	262	317	226	8.8	139	11.8	-	-	-	-	-
Nb	-	-	-	-	-	-	-	-	-	-	32	34	20	34	38
Ni*	<2	<2	<2	<2	46	<2	4	<2	<2	<2	<10	15	<10	44	<10
Pb	6	0	7	23	6	3	7	3	0	0	-	-	-	-	-
Rb	119	103	117	118	70	143	116	210	196	221	110	100	110	105	115
Sc*	3	5	5	7	7	3	2	<2	<2	<2	-	-	-	-	-
Se	8	9	2	1	4	10	0	10	10	17	-	-	-	-	-
Sr	17	154	146	227	865	5	302	52	108	43	295	350	285	630	145
Th	11	4	3	1	2	0	7	18	9	23	-	-	-	-	-
U	12	9	16	16	20	13	9	11	11	15	-	-	-	-	-
Y*	46	42	32	68	14	40	18	6	9	7	20	22	10	24	24
Zn	83	66	76	215	74	134	63	24	44	72	100	75	105	140	115
Zr	276	268	233	490	127	219	162	46	96	68	190	200	100	190	190

	82QC2	82QC9	82QC18A	82QC18B	82QC19	82QC22	82QC31	82QC32C	82QC32F	82QC43	82QC47	82QC48
Ba*	876	95	9	7	10	13	1270	122	50	622	520	623
Cr*	14	1	1	<1	<1	<1	1	<1	1	2	1	1
Ni*	13	<2	<2	<2	<2	<2	<2	<2	<2	<2	<2	<2
Sc*	3	3	<2	2	2	3	4	<2	<2	2	3	3
Y*	8	9	12	14	15	29	20	11	8	18	29	28

	82QC54	82QC56	83QC1	83QC8	83QC9	83QC10	83QC12I	83QC14	83QC18	83QC20	83QC21	83QC23
Ba*	132	60	270	272	1390	740	880	860	574	1010	21	14
Cr*	2	1	4	3	2	3	11	37	<1	3	<1	<1
Ni*	3	2	3	3	3	3	12	26	<2	3	<2	<2
Sc*	3	2	<2	<2	3	3	7	5	2	3	<2	<2
Y*	8	8	5	4	30	19	19	19	20	22	22	65

	83QC26	83QC31	83QC32	Q83SL27	Q83J59	Q83J63	Q83J82	Q83J88	Q83J93	Q83J100	Q84J6
Ba*	418	1800	140	330	1180	136	512	176	1190	1350	875
Cr*	2	2	<1	5	23	<1	1	<1	2	30	18
Ni*	<2	<2	<2	5	24	<2	<2	<2	<2	31	18
Sc*	5	4	2	<2	-	3	3	3	5	5	-
Y*	15	49	50	6	11	51	21	13	42	11	9

* Analyses by ICP, acid digestion by P.H. Briggs, U.S. Geological Survey; remaining values determined by energy dispersive Kevex technique by W. Jones, U.S. Geological Survey.

** All values based on Kevex technique, by B. King, U.S. Geological Survey.

APPENDIX D: KEVEX AND EMISSION SPECTROSCOPIC (*) ANALYSES OF QUESTA GRANITIC ROCKS (IN PPM).

	81S28	81S31	81S43	82QC8	82QC15	82QC18A	82QC18B	82QC22	82QC30
Ba	12*	18*	370	130	230	9.5*	10*	16*	290
Nb	30	40	28	32	24	52	50	44	24
Ni	<10	<10	<10	<10	<10	<10	<10	<10	<10
Rb	140	170	125	220	180	200	170	75	170
Sr	3.1*	2.7*	55	40	95	2*	1.2*	4.6*	70
Y	12	17	22	10	<10	16	15	25	<10
Zn	30	20	40	25	30	20	22	37	30
Zr	70	90	145	75	85	95	100	90	75

	82QC32C	82QC32F	82QC35	82QC41	82QC43	82QC44	82QC48	82QC51	82QC51A
Ba	140	40	720	1800	610	1250	670	840	140
Nb	40	34	30	40	38	14	25	30	22
Ni	<10	<10	<10	<10	<10	30	<10	<10	<10
Rb	175	165	115	120	125	75	110	115	190
Sr	20	10	85	230	190	790	115	290	50
Y	14	<10	34	82	22	14	30	20	<10
Zn	25	25	70	270	30	65	40	40	20
Zr	110	95	200	500	195	140	190	155	50

	83QC25	83QC29	83QC30	83QC31	83QC33	84QC1	84QC7	84QC13	85QC36
Ba	1400	146*	72*	1500	630	9.5*	64*	220	630
Nb	30	44	50	32	30	44	40	27	40
Ni	<10	<10	<10	<10	<10	<10	<10	<10	<10
Rb	100	110	160	140	130	160	130	185	120
Sr	160	21*	9*	160	70	5.9*	10*	90	145
Y	46	38	42	42	30	14	50	<10	24
Zn	65	125	180	40	50	25	120	30	100
Zr	280	390	420	280	195	110	385	85	200

	Q83J59	Q83J63	Q83J82	Q83J88	Q83J93	Q83J101	Q84J6
Ba	1200	150	560	190	1250	1300	890
Nb	18	38	30	32	35	14	18
Ni	20	<10	<10	<10	<10	14	12
Rb	70	110	125	145	105	68	80
Sr	680	20	70	25	130	740	560
Y	12	60	25	14	48	12	10
Zn	40	100	34	50	100	50	50
Zr	135	330	180	130	280	150	130

Analysts: B. King and R. Mays, U.S. Geological Survey, Menlo Park, CA

APPENDIX E: INAA ANALYSES OF QUESTA GRANITIC ROCKS (IN PPM, EXCEPT * INDICATES WEIGHT PERCENT).

	81S28	81S31	81S43	82QC8	82QC15	82QC18A	82QC18B	82QC22	82QC30
Ba	<10	<10	354	107	207	20	<10	<10	271
Co	0.17	0.14	0.50	24.2	26.6	57.7	41.4	38.2	30.8
Cr	1.4	0.8	0.8	1.2	1.0	1.3	1.7	<2	2.7
Cs	0.96	3.27	0.93	1.67	2.49	2.96	0.98	0.35	1.14
Fe*	0.56	0.51	0.80	0.46	0.74	0.51	0.45	1.21	0.68
Hf	4.18	5.79	6.05	3.95	3.63	5.79	6.42	4.75	3.43
K*	3.73	3.80	3.98	4.13	3.50	3.86	3.66	5.02	3.47
Mn	379	504	290	207	395	517	352	365	244
Na*	3.04	3.08	2.77	2.74	2.91	3.12	3.12	2.68	2.30
Ni	3.1	2.1	2.3	1.9	5.0	12	2.5	6.4	4.2
Rb	147	184	131	222	191	209	178	87	178
Sb	0.089	0.204	0.088	0.025	0.086	0.101	0.127	0.088	0.078
Sc	1.78	1.80	2.95	3.62	3.32	2.14	2.15	3.13	2.04
Ta	2.84	3.62	2.55	4.48	3.87	5.91	6.11	5.29	3.50
Th	21.1	30.2	19.7	29.1	23.0	33.2	36.1	24.4	24.2
U	4.79	5.53	4.89	13.1	10.8	5.90	8.64	3.11	4.48
Zn	38.7	23.7	56.0	29.7	33.6	25.8	18	43.5	28.4
Zr	<120	93.1	156	51	<99	90	97	99	<110
La	33.1	33.7	46.8	26.7	25.4	34.7	34.0	80.3	27.5
Ce	51.2	54.7	95.2	43.0	39.5	51.2	46.3	138	36.3
Nd	8.93	9.29	30.8	10.1	10.1	7.46	5.47	24.7	9.34
Sm	1.08	1.31	5.87	1.33	1.57	1.07	0.72	3.17	1.33
Eu	0.045	0.062	0.777	0.167	0.258	0.045	0.022	0.149	0.226
Gd	1.67	-	4.24	-	-	-	-	2.99	-
Tb	0.198	0.214	0.725	0.134	0.147	0.192	0.141	0.508	0.120
Dy	1.42	1.55	4.93	0.96	1.04	1.71	1.35	3.74	0.86
Tm	-	-	0.503	-	0.142	0.343	0.355	0.580	-
Yb	2.52	3.10	3.25	1.49	1.03	2.81	3.14	4.00	0.84
Lu	0.410	0.497	0.499	0.294	0.184	0.484	0.526	0.595	0.130

	82QC32C	82QC32F	82QC35	82QC41	82QC43	82QC44	82QC48	82QC51	82QC51A
Ba	120	35	719	1680	660	1220	686	789	127
Co	67.8	75.8	53.3	41.2	58.7	26.7	54.7	22.3	29.2
Cr	0.8	<0.9	1.1	1.3	1.6	61	<1.4	2.8	1.7
Cs	2.12	2.30	1.39	1.59	1.26	1.26	2.36	1.60	3.08
Fe*	0.64	0.56	0.97	2.31	1.09	3.12	1.05	1.51	0.56
Hf	5.42	5.82	7.16	14.2	6.77	4.26	6.16	6.11	2.87
K*	4.39	3.92	3.97	4.10	4.08	2.86	4.22	3.60	4.09
Mn	184	106	626	748	406	464	454	469	159
Na*	3.00	2.82	2.90	2.86	3.48	3.13	2.94	3.33	2.65
Ni	3.1	1.9	7.3	20	9.0	36	8.9	10	1.8
Rb	190	170	120	116	125	74	122	114	200
Sb	0.274	0.182	0.148	0.288	0.038	0.118	0.055	0.067	0.136
Sc	1.74	1.59	4.25	8.90	2.68	8.36	3.55	2.91	1.17
Ta	5.24	5.04	4.02	4.26	4.97	1.43	4.22	3.52	3.42
Th	19.1	24.7	15.6	13.8	19.0	10.2	17.7	14	41.8
U	3.55	3.73	2.64	3.66	5.35	2.67	2.42	2.78	4.62
Zn	17	12	76.5	254	28.5	61	44.1	43.0	11.5
Zr	99	88	213	553	178	144	192	192	52
La	36.4	28.6	50.7	109	48.4	38.6	56.8	46.5	33.7
Ce	65.2	45.5	111	235	93.0	75.7	115	86.3	40.3
Nd	13.8	7.60	44	128	28.3	33	42.9	27.2	7.85
Sm	1.98	0.93	8.07	26.7	4.82	5.83	7.19	4.46	1.17
Eu	0.188	0.111	1.25	4.07	0.748	1.43	1.12	0.829	0.191
Gd	-	-	6.18	19.6	3.22	3.97	5.95	3.39	-
Tb	0.219	0.141	1.04	3.02	0.554	0.552	0.935	0.509	0.145
Dy	1.55	0.95	6.79	18.6	3.65	3.22	6.17	3.38	1.06
Tm	-	-	0.633	1.38	-	-	0.565	-	-
Yb	2.08	1.72	4.02	7.33	2.73	1.30	3.61	2.33	1.02
Lu	0.343	0.312	0.607	0.861	0.430	0.184	0.524	0.348	0.191

	83QC25	83QC29	83QC30	83QC31	83QC33	84QC1	84QC7	84QC13	85QC36
Ba	1410	114	57	1580	618	<10	68	208	628
Co	76.5	59.7	40.2	24.3	40.4	56.4	70.3	71.1	62.7
Cr	0.1	1.8	1.1	1.0	<3.4	1.6	0.9	3.8	3.1
Cs	1.19	0.62	0.91	1.45	1.36	2.85	1.18	1.18	1.10
Fe*	1.36	1.12	1.05	1.21	0.88	0.54	1.10	0.76	1.20
Hf	9.10	13.2	14.5	9.15	6.97	5.79	12.2	3.79	6.56
K*	3.83	3.63	3.77	4.30	4.08	3.60	3.85	3.45	3.99
Mn	632	918	422	249	566	192	1030	232	554
Na*	3.02	3.29	3.33	3.18	2.87	2.99	3.36	2.74	2.95
Ni	13	9.5	7.8	14	3.2	1.9	5.6	6.5	4.2
Rb	112	119	161	146	138	167	137	186	118
Sb	0.079	0.091	0.165	0.126	0.083	0.136	0.130	0.034	0.137
Sc	6.04	3.21	3.07	4.63	4.14	2.21	3.23	2.12	2.70
Ta	4.15	5.35	5.08	3.55	3.73	4.95	5.21	4.97	4.56
Th	13.8	16.1	18.2	21.3	18.3	28.2	15.8	27.0	19.7
U	2.37	3.51	4.02	3.41	3.15	6.85	4.61	4.70	4.35
Zn	73.8	149	185	41.6	49.6	20.6	129	23.9	103
Zr	312	413	421	297	197	112	380	<120	176
La	68.6	32.9	27.7	79.6	52.5	33.8	32.2	31.8	50.2
Ce	148	83.9	68.8	173	107	50.5	78.6	41.9	92.6
Nd	62.1	30.6	22.6	64.4	39.6	7.97	33.3	8.05	28.4
Sm	11.9	7.25	5.14	12.6	7.15	1.01	8.45	1.25	4.76
Eu	2.29	0.529	0.314	2.39	1.17	0.068	0.526	0.219	0.748
Gd	8.73	6.96	5.37	9.77	5.79	-	8.03	-	-
Tb	1.45	1.20	0.907	1.48	0.925	0.159	1.38	0.086	0.552
Dy	9.30	8.18	6.31	9.59	6.01	1.38	9.72	0.652	3.92
Tm	0.802	0.878	0.760	0.846	0.571	0.324	1.03	-	-
Yb	4.97	5.97	5.65	5.17	3.61	2.61	6.59	0.734	2.92
Lu	0.750	0.954	0.908	0.769	0.563	0.505	0.997	0.137	0.443

	Q83J59	Q83J63	Q83J82	Q83J88	Q83J93	Q83J101	Q84J6
Ba	1240	129	577	191	1270	1040	925
Co	62.0	70.9	65.2	63.3	69.3	50.1	37.2
Cr	28	1.7	0.9	1.9	0.6	20	20
Cs	0.92	0.79	0.92	1.66	1.26	0.36	1.05
Fe*	2.67	1.19	0.89	0.59	1.33	1.97	2.38
Hf	4.42	11.2	6.69	5.57	9.00	3.16	3.88
K*	2.86	3.85	4.09	3.78	4.01	2.13	2.74
Mn	357	944	289	395	447	286	450
Na*	3.18	3.33	2.95	2.91	2.96	2.48	3.16
Ni	26	3.4	10	3.8	17	12	27
Rb	78	120	141	155	118	53	82
Sb	0.054	0.125	0.073	0.075	0.574	-	0.053
Sc	6.51	3.57	3.10	3.70	5.38	4.63	5.66
Ta	2.76	5.07	4.72	4.52	4.37	2.18	2.35
Th	8.85	16.5	17.9	23.0	16.4	5.48	12.7
U	2.42	4.55	3.39	4.34	2.95	1.26	3.36
Zn	41.0	101	30.8	45.8	92.1	37.3	48.8
Zr	133	373	191	123	297	104	107
La	40.1	43.9	41.3	47.5	75.3	31.4	35.4
Ce	77.4	98.3	94.2	70.6	156	62.5	58.5
Nd	28.4	43.7	31.3	19.4	62.6	22.8	22.4
Sm	4.60	10.2	5.70	3.30	11.8	3.56	3.54
Eu	1.21	0.805	0.861	0.507	2.18	0.909	0.946
Gd	3.72	10.1	5.22	2.70	10.0	2.51	2.58
Tb	0.473	1.66	0.731	0.359	1.51	0.304	0.365
Dy	2.90	11.0	4.92	2.48	9.59	1.82	2.15
Tm	0.202	1.06	0.501	0.310	0.799	0.130	0.151
Yb	1.13	6.59	3.27	2.34	4.90	0.758	0.871
Lu	0.160	0.994	0.492	0.412	0.722	0.106	0.117

Cr values ± 0.6 ppm; Ni values ± 1.0 ppm

Analyses by J. Budahn, R. Knight, and D. McKown, Branch of Geochemistry, U.S. Geological Survey, Lakewood, CO.

APPENDIX F: ELECTRON MICROPROBE ANALYSES OF SPHENE(S) IN THE QUESTA GRANITIC ROCKS (IN WT%)
(Analyses of cores and edges for most grains.)

SAMPLE NUMBER	Na2O	MgO	Al2O3	SiO2	CaO	TiO2	MnO	FeOt	La2O3	Ce2O3	Pr2O3	Nd2O3	Sm2O3	Dy2O3	Y2O3	Yb2O3	ThO2	UO2	TOTAL
820C38 S C CORE	0.47	0.16	0.47	29.64	23.73	31.26	0.94	5.12	0.34	1.26	0.23	0.80	0.12	0.19	1.03	0.22	0.10	0.12	96.20
820C38 S C EDGE	0.52	0.14	0.38	29.76	23.68	32.33	0.95	4.37	0.34	1.19	0.16	0.77	0.17	0.30	1.13	0.10	0.10	0.31	96.71
820C38 S B CORE	1.11	0.14	0.31	29.29	20.99	31.64	0.93	4.71	0.15	0.97	0.21	1.11	0.41	0.81	3.00	0.40	0.20	0.40	96.78
820C38 S B EDGE	0.55	0.13	0.46	29.62	23.19	31.37	0.90	5.17	0.33	1.15	0.19	0.90	0.28	0.34	1.24	0.24	0.12	0.19	96.37
820C38 S H CORE	0.24	0.16	0.67	29.31	23.09	33.02	0.72	3.51	0.34	1.65	0.30	1.65	0.52	0.52	1.60	0.22	0.17	0.38	98.07
820C38 S H EDGE	0.09	0.16	1.45	29.35	23.44	32.37	0.36	3.10	0.38	1.48	0.18	1.69	0.53	0.50	1.80	0.22	0.07	0.24	97.41
083363 S E CORE	0.25	0.15	0.58	29.19	23.48	32.82	0.73	3.95	0.35	1.76	0.28	1.30	0.42	0.40	1.95	0.20	0.24	0.11	98.16
083363 S E EDGE	0.24	0.14	0.52	29.19	24.03	33.61	0.72	3.82	0.28	1.48	0.14	1.19	0.40	0.37	1.61	0.20	0.09	0.26	98.31
083363 S F CORE	0.69	0.12	0.30	29.38	23.70	32.51	0.81	4.29	0.34	1.28	0.12	0.76	0.20	0.20	1.32	0.17	0.24	0.08	96.52
083363 S F EDGE	0.47	0.13	0.38	29.42	24.03	31.73	0.90	5.20	0.35	1.22	0.09	0.60	0.19	0.21	1.34	0.23	0.11	0.12	96.70
083363 S G CORE	0.46	0.13	0.35	29.11	24.51	31.96	0.94	5.11	0.40	1.35	0.16	0.68	0.15	0.26	1.23	0.19	0.21	0.26	97.46
083363 S G EDGE	0.50	0.13	0.39	29.18	24.30	31.87	0.93	5.02	0.37	1.19	0.16	0.63	0.21	0.23	1.13	0.19	0.16	0.03	96.62
820C39 S B	0.11	0.24	2.91	29.93	24.68	29.23	0.83	3.52	0.27	1.29	0.18	1.03	0.17	0.12	1.04	0.18	0.19	0.29	96.32
820C39 S D CORE	0.05	0.15	1.79	29.98	25.27	32.51	0.41	3.00	0.38	1.33	0.16	0.82	0.11	0.23	1.02	0.11	0.17	0.20	97.69
820C39 S D EDGE	0.15	0.42	2.92	29.69	23.65	28.72	0.92	3.77	0.21	0.97	0.19	1.07	0.32	0.42	2.10	0.30	0.30	0.32	96.54
820C41 S B CORE	0.07	0.14	1.63	29.54	24.40	33.05	0.44	2.75	0.56	1.91	0.15	1.12	0.22	0.22	1.05	0.14	0.00	0.31	97.70
820C41 S B EDGE	0.07	0.12	1.51	29.89	24.94	33.75	0.42	2.39	0.46	1.61	0.21	0.91	0.16	0.08	0.73	0.16	0.06	0.00	97.46
820C41 S C CORE	0.27	0.14	0.64	29.45	23.62	34.09	0.78	3.48	0.33	1.47	0.20	1.30	0.49	0.34	1.47	0.14	0.01	0.26	98.39
820C41 S C EDGE	0.07	0.14	1.61	29.66	24.54	33.67	0.41	2.66	0.41	1.59	0.20	1.28	0.39	0.18	1.25	0.14	0.12	0.21	98.44
820C41 S E CORE	0.07	0.17	1.65	29.12	23.77	32.29	0.35	2.93	0.36	1.61	0.19	1.66	0.39	0.39	1.71	0.14	0.28	0.40	97.49
820C41 S E EDGE	0.05	0.13	1.69	29.73	24.97	33.17	0.44	2.95	0.42	1.52	0.16	1.03	0.16	0.03	0.86	0.08	0.12	0.18	97.59
820C41 S F CORE	0.05	0.14	1.85	29.75	24.93	32.61	0.41	2.95	0.40	1.56	0.22	1.13	0.18	0.24	0.95	0.15	0.42	0.27	98.21
820C41 S F EDGE	0.04	0.12	1.87	30.23	26.10	32.54	0.42	2.95	0.41	1.25	0.17	0.50	0.03	0.00	0.39	0.08	0.16	0.32	97.97
820C35 S E CORE	0.06	0.17	1.85	29.56	24.23	31.83	0.39	3.11	0.28	1.33	0.26	1.34	0.39	0.46	1.57	0.10	0.13	0.35	97.42
820C35 S E EDGE	0.05	0.14	1.80	29.75	24.89	32.86	0.44	2.79	0.34	1.51	0.28	1.06	0.17	0.17	0.87	0.11	0.22	0.22	97.48
820C35 S A CORE	0.08	0.16	1.80	29.39	23.63	32.41	0.41	2.74	0.46	1.80	0.27	1.84	0.52	0.32	1.57	0.22	0.22	0.33	98.16
820C35 S A EDGE	0.07	0.14	1.69	29.55	24.15	33.13	0.41	2.65	0.35	1.57	0.29	1.40	0.37	0.20	1.09	0.17	0.05	0.22	97.59
820C35 S C CORE	0.06	0.16	1.89	29.79	24.60	32.97	0.40	3.07	0.41	1.53	0.15	1.22	0.30	0.25	1.13	0.17	0.10	0.22	98.33
820C35 S C EDGE	0.15	0.15	2.00	30.16	25.53	32.23	0.51	3.30	0.44	1.33	0.23	0.47	0.04	0.03	0.57	0.18	0.22	0.22	97.67
820C33 S D CORE	0.00	0.04	5.49	30.86	28.18	30.41	0.05	0.95	0.01	0.00	0.01	0.03	0.00	0.00	0.06	0.00	0.00	0.00	98.09
820C33 S D EDGE	0.00	0.05	5.26	30.92	27.92	30.79	0.07	1.13	0.00	0.02	0.01	0.03	0.00	0.00	0.11	0.07	0.02	0.17	96.58
083079 S A CORE	0.01	0.08	5.67	30.67	27.75	29.83	0.09	0.79	0.02	0.21	0.04	0.32	0.05	0.01	0.44	0.00	0.09	0.16	96.24
083079 S A EDGE	0.00	0.06	6.79	30.42	27.65	28.40	0.04	0.98	0.04	0.26	0.05	0.23	0.09	0.05	0.46	0.04	0.00	0.00	95.56
083079 S B CORE	0.29	0.15	0.61	29.09	23.09	33.10	0.77	3.49	0.34	1.65	0.25	1.65	0.57	0.52	1.67	0.20	0.14	0.36	97.94
083079 S B EDGE	0.06	0.12	1.71	29.86	25.07	32.54	0.42	2.90	0.42	1.49	0.15	1.00	0.17	0.13	0.89	0.20	0.09	0.08	97.69
083079 S C	0.06	0.13	1.72	29.68	24.77	32.89	0.39	2.79	0.43	1.54	0.16	1.15	0.19	0.20	0.95	0.18	0.02	0.39	97.63
083079 S C CORE	0.31	0.14	0.54	29.55	23.60	33.46	0.82	3.64	0.45	1.53	0.09	1.23	0.41	0.41	1.68	0.25	0.16	0.31	98.58
083079 S C EDGE	0.06	0.12	1.60	29.73	25.19	33.42	0.40	2.70	0.35	1.44	0.23	0.90	0.16	0.15	0.92	0.20	0.29	0.12	97.97
083079 S D CORE	0.06	0.17	2.06	29.72	23.97	31.48	0.32	3.19	0.32	1.49	0.18	1.47	0.41	0.43	1.72	0.25	0.41	0.36	97.61
083079 S D EDGE	0.05	0.14	1.83	29.75	25.12	32.57	0.44	2.72	0.47	1.48	0.16	0.77	0.15	0.08	0.84	0.16	0.28	0.23	97.24
81E43 S B	0.05	0.11	1.75	29.80	25.03	34.01	0.27	2.46	0.46	1.42	0.17	0.75	0.13	0.08	0.65	0.01	0.06	0.12	97.32
81E43 S D	0.04	0.10	1.45	29.74	24.94	33.08	0.26	2.66	0.33	1.39	0.17	0.86	0.24	0.19	0.94	0.13	0.06	0.16	96.73
820C47 S C1 CORE	0.03	0.09	1.55	30.01	25.93	34.08	0.31	2.82	0.42	1.35	0.13	0.73	0.09	0.06	0.55	0.09	0.07	0.23	98.54
820C47 S C1 EDGE	0.13	0.32	3.07	29.97	24.93	30.19	0.58	3.56	0.17	0.75	0.10	0.98	0.30	0.28	1.99	0.19	0.10	0.16	97.69
820C47 S C2 CORE	0.17	0.33	2.85	29.58	24.25	29.79	0.78	3.48	0.20	0.91	0.14	0.89	0.25	0.31	1.88	0.19	0.10	0.06	96.17
820C47 S C2 EDGE	0.16	0.31	3.14	29.93	24.50	29.94	0.89	3.41	0.15	0.95	0.21	0.97	0.21	0.30	1.62	0.18	0.08	0.11	96.56
820C47 S F CORE	0.04	0.15	1.55	29.75	24.94	32.40	0.35	3.23	0.31	1.11	0.15	0.94	0.31	0.39	1.23	0.19	0.17	0.17	97.25
820C47 S F EDGE	0.06	0.12	1.49	29.77	25.02	33.22	0.36	2.92	0.30	1.38	0.20	0.99	0.21	0.14	1.05	0.10	0.07	0.14	97.64
820C49 S C CORE	0.12	0.22	3.44	30.31	25.54	30.20	0.27	1.87	0.08	0.22	0.04	0.46	0.23	0.37	1.95	0.27	0.00	0.31	95.90
820C48 S C EDGE	0.09	0.18	3.37	30.49	25.92	30.46	0.26	1.89	0.05	0.15	0.06	0.44	0.16	0.27	1.79	0.18	0.31	0.28	96.26
820C49 S D	0.09	0.19	3.20	30.65	26.17	31.21	0.25	1.87	0.07	0.24	0.07	0.48	0.20	0.30	1.61	0.22	0.13	0.21	97.16

SAMPLE NUMBER	Na2O	MgO	Al2O3	SiO2	CaO	TiO2	MnO	FeOt	La2O3	Ce2O3	Pr2O3	Nd2O3	Sm2O3	Dy2O3	Y2O3	Yb2O3	ThO2	UO2	TOTAL
083J82 S A	0.12	0.20	2.24	30.04	25.41	31.78	0.59	3.09	0.32	1.18	0.22	0.68	0.14	0.11	0.87	0.16	0.18	0.00	97.34
083J82 S D CORE	0.08	0.20	2.59	29.90	25.60	30.96	0.52	3.33	0.33	1.13	0.23	0.69	0.14	0.04	0.59	0.09	0.07	0.34	96.83
083J82 S D EDGE	0.05	0.08	1.65	29.53	25.31	33.76	0.31	2.38	0.45	1.70	0.21	0.95	0.16	0.14	0.81	0.08	0.17	0.18	97.92
083J82 S E CORE	0.05	0.10	1.60	29.72	25.31	33.48	0.29	2.68	0.30	1.26	0.12	0.83	0.10	0.18	0.90	0.08	0.43	0.14	97.56
083J82 S E EDGE	0.05	0.10	1.47	29.90	25.78	33.28	0.40	2.66	0.51	1.28	0.03	0.50	0.03	0.02	0.50	0.09	0.03	0.18	96.81
083J82 S G CORE	0.06	0.09	1.39	29.71	24.87	34.46	0.25	2.18	0.57	2.01	0.25	1.17	0.30	0.12	0.86	0.15	0.08	0.16	98.69
083J82 S G EDGE	0.03	0.09	1.60	29.85	25.22	33.99	0.25	2.45	0.49	1.63	0.16	0.94	0.19	0.16	0.82	0.12	0.06	0.19	98.24
083J92 AV3	0.22	0.13	0.54	29.44	23.82	33.42	0.81	4.03	0.39	1.40	0.11	0.93	0.28	0.10	1.59	0.03	0.07	0.00	97.31
820C22 S A CORE	0.07	0.12	1.43	29.89	25.29	31.61	0.55	3.45	0.34	1.21	0.15	0.54	0.07	0.12	1.17	0.13	0.00	0.10	96.23
820C22 S A EDGE	0.09	0.12	1.74	30.02	25.25	31.22	0.59	3.40	0.37	1.34	0.13	0.40	0.06	0.07	1.09	0.20	0.00	0.00	96.10
820C22 S B	0.07	0.11	1.37	29.93	25.21	32.01	0.49	3.13	0.42	1.51	0.14	0.58	0.12	0.17	1.10	0.16	0.00	0.00	96.52
820C51b S C CORE	0.02	0.07	1.11	30.38	26.94	34.22	0.25	2.13	0.53	1.26	0.07	0.45	0.07	0.01	0.33	0.12	0.21	0.24	98.41
820C51b S C EDGE	0.03	0.05	0.99	30.56	27.01	34.89	0.22	1.76	0.44	1.02	0.16	0.42	0.01	0.00	0.26	0.00	0.18	0.24	98.23
820C51b S D CORE	0.06	0.08	1.12	30.12	25.93	32.76	0.20	2.24	0.56	1.58	0.19	0.52	0.09	0.02	0.49	0.12	0.21	0.25	96.54
820C51b S D EDGE	0.04	0.07	1.03	30.08	26.47	33.86	0.21	1.85	0.69	1.63	0.09	0.45	0.08	0.01	0.34	0.10	0.25	0.19	97.45
820C51b S F CORE	0.05	0.08	1.03	29.54	25.68	32.55	0.20	2.23	0.58	1.93	0.22	0.82	0.19	0.10	0.67	0.14	0.40	0.30	96.71
820C51b S F EDGE	0.03	0.07	1.14	30.05	26.56	33.40	0.22	2.29	0.56	1.49	0.12	0.45	0.06	0.00	0.37	0.09	0.17	0.22	97.29
820C51b S I CORE	0.03	0.07	0.91	30.47	27.64	34.39	0.30	2.10	0.22	0.37	0.06	0.19	0.02	0.00	0.11	0.06	0.25	0.34	97.54
820C51b S I EDGE	0.04	0.05	0.86	30.69	27.39	34.96	0.32	1.72	0.23	0.44	0.04	0.20	0.01	0.00	0.14	0.00	0.29	0.19	97.58
830C17.3 11	0.05	0.10	1.40	30.00	24.90	34.70	0.28	2.69	0.47	1.57	0.18	0.72	0.15	0.08	0.66	0.16	0.36	0.11	98.58
830C17.3 9&10	0.04	0.11	1.47	30.30	26.10	35.40	0.36	2.51	0.58	1.00	0.08	0.29	0.03	0.01	0.13	0.07	0.21	0.11	98.80
830C17.3 AV3EC	0.03	0.06	1.37	30.30	26.20	35.10	0.34	2.28	0.44	0.83	0.10	0.29	0.04	0.02	0.18	0.04	0.18	0.09	98.91
830C17.3 6EE	0.01	0.04	4.23	31.00	28.00	34.90	0.08	0.56	0.00	0.02	0.10	0.09	0.02	0.01	0.06	0.00	0.07	0.23	99.41
830C14A 5&5	0.05	0.11	1.22	30.10	25.70	34.00	0.22	2.61	0.46	1.45	0.11	0.74	0.15	0.09	0.59	0.15	0.14	0.20	98.09
830C14A 5	0.03	0.12	1.39	30.20	26.50	34.20	0.29	2.62	0.58	1.06	0.07	0.24	0.02	0.00	0.04	0.03	0.10	0.30	97.60
830C14A AV2EC	0.04	0.09	1.15	30.00	25.80	34.20	0.34	2.15	0.58	1.24	0.09	0.45	0.06	0.03	0.27	0.08	0.16	0.30	97.02
830C14A AV2EE	0.04	0.07	1.08	30.30	26.50	35.40	0.25	1.72	0.39	0.82	0.07	0.34	0.06	0.00	0.21	0.09	0.13	0.14	97.60
830C16 11	0.05	0.10	1.25	30.30	26.30	34.20	0.40	2.20	0.33	0.77	0.03	0.32	0.04	0.03	0.16	0.04	0.24	0.33	97.09
830C16 12	0.06	0.11	1.48	30.00	25.80	33.60	0.35	2.61	0.45	1.32	0.16	0.57	0.08	0.08	0.40	0.11	0.11	0.23	97.52
830C16 AV3EC	0.05	0.10	1.31	30.30	26.50	34.70	0.39	2.22	0.37	0.72	0.06	0.26	0.01	0.01	0.16	0.00	0.11	0.22	97.49
830C16 AV3EE	0.09	0.10	1.34	29.90	25.00	33.50	0.30	2.39	0.22	1.06	0.17	0.88	0.23	0.22	1.43	0.17	0.16	0.22	97.39
830C12 14&16	0.06	0.09	1.28	30.00	25.60	34.10	0.25	2.21	0.62	1.60	0.18	0.64	0.11	0.05	0.24	0.11	0.11	0.19	97.44
830C12 AV2EC	0.06	0.10	1.23	29.50	24.80	33.60	0.25	2.36	0.57	1.86	0.20	1.09	0.22	0.11	0.63	0.10	0.20	0.29	97.18
830C12 11EE	0.04	0.09	1.15	30.10	26.30	34.60	0.27	2.28	0.44	1.11	0.04	0.40	0.00	0.03	0.12	0.02	0.12	0.23	97.33
820C30.2 S A1 CORE	0.02	0.06	1.35	30.13	26.05	34.94	0.19	2.32	0.48	1.35	0.20	0.76	0.08	0.07	0.29	0.13	0.15	0.04	98.60
820C30.2 S A1 EDGE	0.06	0.12	1.91	30.35	26.67	32.06	0.44	3.29	0.34	0.79	0.10	0.09	0.00	0.00	0.14	0.05	0.16	0.35	96.91
820C30.2 S A2 CORE	0.04	0.07	1.29	30.30	26.41	34.45	0.32	2.55	0.46	1.08	0.07	0.34	0.07	0.00	0.21	0.01	0.23	0.21	98.11
820C30.2 S A2 EDGE	0.05	0.11	1.92	30.57	26.42	31.81	0.47	3.35	0.35	0.70	0.06	0.17	0.02	0.02	0.12	0.05	0.19	0.19	96.57
820C30.2 S E CORE	0.03	0.06	1.25	29.96	26.27	35.13	0.19	2.08	0.47	1.36	0.09	0.43	0.07	0.00	0.23	0.07	0.20	0.27	98.16
840C13 S B CORE	0.03	0.07	1.23	30.35	26.28	35.61	0.16	1.81	0.49	1.43	0.12	0.64	0.03	0.06	0.26	0.10	0.16	0.07	98.89
840C13 S B EDGE	0.04	0.08	1.33	30.07	26.74	33.66	0.34	2.63	0.47	1.14	0.06	0.29	0.05	0.00	0.18	0.06	0.05	0.00	97.19
840C13 S B2 CORE	0.02	0.06	1.28	30.20	26.43	35.13	0.18	1.89	0.45	1.25	0.17	0.49	0.03	0.01	0.18	0.07	0.03	0.04	97.91
840C13 S B2 EDGE	0.06	0.11	1.76	30.31	26.50	32.36	0.36	2.62	0.37	0.91	0.13	0.21	0.00	0.00	0.15	0.06	0.00	0.22	96.33
840C13 S D	0.03	0.21	1.53	30.19	25.88	34.44	0.22	2.11	0.46	1.35	0.11	0.57	0.09	0.09	0.32	0.08	0.08	0.07	97.93
E40C11 S F CORE	0.03	0.07	1.10	30.16	26.32	34.66	0.20	2.02	0.44	1.11	0.10	0.46	0.02	0.01	0.21	0.03	0.11	0.24	97.28
E40C11 S F EDGE	0.04	0.09	1.44	30.12	26.58	33.05	0.29	2.65	0.47	0.81	0.04	0.15	0.00	0.05	0.10	0.01	0.00	0.06	95.54
E40C11 S B CORE	0.03	0.07	1.19	29.54	25.32	35.21	0.12	1.58	0.66	2.16	0.14	1.05	0.12	0.08	0.45	0.09	0.10	0.20	98.50
E40C11 S B EDGE	0.03	0.09	1.71	30.68	27.09	33.47	0.27	2.71	0.49	0.43	0.00	0.14	0.05	0.00	0.22	0.00	0.00	0.05	97.43

SAMPLE NUMBER	Na2O	MgO	Al2O3	SiO2	CaO	TiO2	MnO	FeOt	La2O3	Ce2O3	Pr2O3	Nd2O3	Sm2O3	Dy2O3	Y2O3	Yb2O3	ThO2	UO2	TOTAL
883059 S A1 CORE	0.03	0.05	1.17	30.64	26.81	35.49	0.13	1.72	0.42	1.08	0.09	0.40	0.03	0.01	0.19	0.10	0.26	0.00	98.62
883059 S A1 EDGE	0.02	0.12	1.14	30.79	26.35	35.32	0.11	1.60	0.36	1.01	0.10	0.48	0.06	0.00	0.27	0.06	0.00	0.17	97.56
883059 S A2 CORE	0.02	0.05	1.02	30.47	26.93	35.56	0.13	1.47	0.38	0.86	0.11	0.33	0.04	0.00	0.13	0.06	0.16	0.00	97.72
883059 S A2 EDGE	0.02	0.06	1.06	30.55	26.63	35.18	0.12	1.65	0.31	0.94	0.09	0.44	0.06	0.02	0.15	0.00	0.27	0.12	97.66
883059 S B CORE	0.02	0.05	1.16	30.53	26.58	34.89	0.10	1.96	0.41	1.40	0.13	0.72	0.11	0.01	0.27	0.10	0.16	0.09	98.69
883059 S B EDGE	0.02	0.06	0.53	30.52	26.94	35.84	0.11	1.56	0.42	0.93	0.09	0.31	0.05	0.03	0.09	0.00	0.19	0.00	98.08
883059 S C CORE	0.01	0.07	1.26	30.57	27.13	35.24	0.10	1.74	0.33	0.79	0.13	0.33	0.09	0.05	0.17	0.10	0.11	0.09	98.31
883059 S C EDGE	0.02	0.06	1.03	30.50	27.06	35.66	0.12	1.80	0.38	0.77	0.05	0.23	0.04	0.00	0.10	0.06	0.16	0.00	98.04
883C12 S A CORE	0.02	0.07	1.17	30.08	26.15	35.53	0.12	1.78	0.40	1.28	0.23	0.92	0.18	0.05	0.29	0.08	0.22	0.11	98.69
883C12 S A EDGE	0.02	0.05	1.07	30.54	27.14	35.95	0.12	1.50	0.34	0.76	0.03	0.35	0.00	0.02	0.12	0.00	0.08	0.29	98.39
883C12 S B	0.02	0.07	0.99	30.64	26.96	36.53	0.13	1.38	0.32	0.88	0.08	0.43	0.02	0.04	0.19	0.04	0.16	0.26	99.13
883C12 S C	0.02	0.07	1.17	29.90	25.55	34.88	0.12	1.82	0.48	1.67	0.25	1.02	0.18	0.08	0.44	0.08	0.11	0.27	98.11
883C15 S D CORE	0.03	0.05	1.18	30.31	26.39	34.56	0.21	1.89	0.42	1.39	0.12	0.60	0.11	0.10	0.45	0.08	0.07	0.10	98.06
883C15 S D EDGE	0.11	0.15	2.30	30.53	26.08	31.34	0.70	2.79	0.26	0.97	0.11	0.46	0.11	0.07	0.52	0.12	0.14	0.02	96.79
883C15 S E CORE	0.04	0.06	1.38	30.38	26.89	33.78	0.33	2.21	0.27	0.80	0.04	0.47	0.04	0.04	0.29	0.06	0.00	0.04	97.13
883C15 S E EDGE	0.04	0.05	1.50	30.49	26.80	33.51	0.37	2.38	0.25	0.93	0.12	0.37	0.09	0.08	0.41	0.10	0.08	0.00	97.57
883C15 S F CORE	0.12	0.16	2.40	30.46	26.10	30.55	0.76	2.90	0.23	0.96	0.00	0.66	0.09	0.04	0.98	0.19	0.07	0.12	96.79
883C15 S F EDGE	0.04	0.06	1.38	30.48	26.74	33.47	0.42	2.56	0.19	0.96	0.14	0.43	0.00	0.06	0.54	0.12	0.10	0.06	97.75
889L20 S C CORE	0.04	0.07	1.41	29.96	26.44	34.30	0.34	2.45	0.37	1.25	0.18	0.45	0.09	0.06	0.43	0.16	0.25	0.01	98.26
889L20 S C EDGE	0.06	0.08	1.53	30.13	26.38	34.21	0.53	2.44	0.31	0.92	0.07	0.39	0.05	0.07	0.45	0.08	0.18	0.12	98.00
889L20 S F CORE	0.05	0.09	1.61	30.17	26.55	34.29	0.53	2.60	0.28	0.88	0.10	0.32	0.03	0.03	0.46	0.05	0.23	0.01	98.68
889L20 S F EDGE	0.08	0.13	2.18	30.13	26.84	32.42	0.71	3.05	0.24	0.76	0.08	0.23	0.01	0.00	0.41	0.10	0.05	0.00	97.41
889L20 S G CORE	0.05	0.06	1.31	29.98	26.75	34.83	0.30	2.09	0.31	1.16	0.18	0.41	0.08	0.05	0.30	0.08	0.21	0.07	98.23
889L20 S G EDGE	0.09	0.12	1.99	30.00	26.58	32.70	0.70	2.80	0.17	0.72	0.09	0.21	0.03	0.05	0.33	0.04	0.20	0.17	96.60
889C10 S A	0.05	0.06	1.27	30.28	25.84	34.03	0.33	2.33	0.37	1.44	0.15	0.77	0.18	0.06	0.72	0.13	0.00	0.00	98.02
3417 S B CORE	0.01	0.05	1.44	29.90	25.64	34.59	0.16	2.04	0.48	1.55	0.16	0.84	0.05	0.14	0.41	0.07	0.04	0.08	97.65
3417 S B EDGE	0.01	0.06	1.29	30.10	25.95	35.14	0.16	1.74	0.42	1.19	0.14	0.53	0.02	0.09	0.23	0.12	0.06	0.08	97.33
3417 S C CORE	0.01	0.06	1.39	29.90	25.58	34.51	0.15	2.16	0.48	1.57	0.26	0.84	0.11	0.08	0.44	0.14	0.00	0.00	97.65
3417 S C EDGE	0.00	0.05	1.25	30.20	26.00	35.27	0.16	1.83	0.36	1.29	0.14	0.55	0.09	0.09	0.29	0.11	0.05	0.10	97.83
3439 S B CORE	0.03	0.04	1.28	30.24	26.62	35.14	0.18	1.79	0.52	1.66	0.21	0.67	0.09	0.02	0.46	0.09	0.00	0.03	99.08
3439 S B EDGE	0.03	0.04	1.16	30.36	26.74	34.66	0.24	1.94	0.56	1.37	0.13	0.49	0.09	0.05	0.40	0.09	0.00	0.06	98.42
3439 S C CORE	0.03	0.05	1.44	30.06	26.35	34.30	0.18	1.94	0.54	1.53	0.18	0.73	0.04	0.07	0.54	0.12	0.07	0.02	98.20
3439 S C EDGE	0.03	0.03	1.25	30.28	26.40	34.55	0.21	1.79	0.45	1.52	0.20	0.58	0.12	0.00	0.46	0.09	0.00	0.00	97.96
3439 S E CORE	0.04	0.05	1.22	30.12	26.08	34.14	0.19	2.06	0.47	1.70	0.14	0.84	0.14	0.07	0.71	0.12	0.03	0.00	98.12
3439 S E EDGE	0.03	0.04	1.36	30.38	26.62	34.58	0.19	1.80	0.45	1.36	0.17	0.50	0.09	0.06	0.36	0.02	0.00	0.00	98.01
3440 S B	0.03	0.06	1.09	30.35	26.19	35.30	0.20	1.72	0.48	1.52	0.12	0.55	0.12	0.03	0.38	0.17	0.00	0.13	98.44
3440 S C CORE	0.02	0.06	1.38	30.38	26.15	34.99	0.17	1.96	0.49	1.53	0.13	0.69	0.11	0.08	0.53	0.10	0.15	0.00	98.92
3440 S C EDGE	0.03	0.05	1.32	30.44	26.52	35.19	0.18	1.93	0.45	1.27	0.13	0.59	0.06	0.05	0.39	0.07	0.00	0.10	98.77
889C10.2 S E EDGE	0.04	0.10	1.88	30.17	26.50	32.31	0.45	3.25	0.32	0.77	0.04	0.16	0.03	0.00	0.20	0.08	0.37	0.21	96.87
889C36.2 S A CORE	0.09	0.18	1.45	29.86	24.81	30.39	0.62	3.60	0.67	2.12	0.24	0.80	0.11	0.15	1.02	0.17	0.33	0.20	96.82
889C36.2 S A EDGE	0.06	0.08	1.10	30.17	26.00	33.96	0.37	2.22	0.50	1.73	0.25	0.71	0.12	0.09	0.55	0.11	0.17	0.19	98.38
889C36.2 S B CORE	0.06	0.11	1.21	30.01	25.76	33.24	0.45	2.53	0.48	1.57	0.18	0.72	0.14	0.11	0.77	0.10	0.19	0.26	97.89
889C36.2 S B EDGE	0.06	0.09	1.07	30.10	25.83	33.83	0.37	2.24	0.54	1.66	0.15	0.64	0.13	0.00	0.61	0.12	0.36	0.26	99.06
889C36.2 S C CORE	0.05	0.10	1.20	30.07	24.99	33.31	0.22	2.42	0.45	2.00	0.32	1.35	0.27	0.19	1.17	0.15	0.33	0.17	98.76
889C36.2 S C EDGE	0.05	0.10	1.19	30.30	25.89	33.58	0.36	2.33	0.57	1.62	0.16	0.66	0.13	0.10	0.60	0.08	0.41	0.16	98.29
889C36.2 S D CORE	0.07	0.12	1.38	30.26	25.90	33.14	0.49	2.57	0.48	1.46	0.09	0.55	0.03	0.10	0.54	0.10	0.30	0.21	97.79
889C36.2 S D EDGE	0.05	0.10	1.39	30.33	25.60	33.97	0.37	2.34	0.61	1.66	0.04	0.72	0.07	0.09	0.42	0.12	0.06	0.15	98.00
889C44 S A CORE	0.02	0.06	1.12	30.11	26.24	35.39	0.11	1.82	0.32	1.33	0.21	0.72	0.08	0.04	0.23	0.09	0.11	0.06	97.98
889C44 S A EDGE	0.02	0.07	0.97	29.99	26.15	35.46	0.10	1.85	0.49	1.46	0.19	0.59	0.08	0.01	0.25	0.00	0.16	0.00	97.83
889C44 S B	0.02	0.07	1.18	30.20	26.25	35.97	0.11	1.54	0.39	1.25	0.14	0.73	0.11	0.05	0.26	0.00	0.05	0.13	98.44
889C44 S C	0.02	0.06	1.26	30.17	26.75	35.87	0.11	1.36	0.20	0.66	0.10	0.47	0.08	0.03	0.20	0.09	0.07	0.12	97.52

APPENDIX G: ELECTRON MICROPROBE ANALYSES OF ALLANITE(AL) AND EPIDOTE(E) IN THE QUESTA GRANITIC ROCKS (IN WT%).

SAMPLE NUMBER	Na2O	MgO	Al2O3	SiO2	CaO	TiO2	MnO	FeOt	La2O3	Ce2O3	Pr2O3	Nd2O3	Sm2O3	Dy2O3	Y2O3	Yb2O3	ThO2	UO2	TOTAL
820C33 AL B CORE	0.06	0.46	13.92	31.45	9.67	0.56	2.10	13.84	6.00	11.32	1.18	3.93	0.63	0.17	0.74	0.24	0.77	0.22	97.17
820C33 AL B EDGE	0.03	0.18	18.15	32.65	12.05	0.14	1.54	11.93	5.20	9.79	0.80	2.98	0.42	0.23	0.69	0.18	0.33	0.13	97.42
820C33 AL D CORE	0.03	0.23	19.37	33.22	12.58	0.15	1.57	11.14	5.88	9.96	0.70	2.47	0.31	0.11	0.24	0.19	0.24	0.00	98.39
820C33 AL D EDGE	0.04	0.18	18.81	32.63	12.26	0.16	1.33	11.25	5.61	10.56	0.71	2.87	0.45	0.16	0.33	0.14	0.29	0.00	97.78
820C35 AL B	0.08	0.40	16.90	31.84	8.96	0.31	2.91	12.56	5.99	11.89	1.06	4.26	0.73	0.27	0.73	0.28	0.52	0.32	100.02
820C49 AL A	0.04	0.56	11.97	31.01	9.38	2.66	0.86	15.80	6.29	13.05	1.15	4.41	0.65	0.12	0.33	0.17	1.39	0.24	100.08
820C48 AL B	0.04	0.44	11.03	30.79	9.24	2.79	0.65	17.04	6.10	13.16	0.95	4.31	0.69	0.20	0.50	0.10	1.25	0.50	99.78
820C48 AL E	0.02	0.42	9.78	30.58	9.32	3.10	0.69	18.39	5.92	13.96	1.04	3.99	0.50	0.15	0.69	0.23	0.95	0.35	100.09
820C48 AL G	0.03	0.37	9.25	30.61	9.39	3.28	0.52	17.73	6.56	13.27	1.14	3.70	0.55	0.07	0.55	0.19	1.03	0.52	98.86
820C48 AL F CORE	0.03	0.23	11.51	31.25	9.52	1.69	0.98	17.17	4.87	11.83	1.19	5.68	1.04	0.17	0.36	0.20	1.27	0.64	100.04
820C48 AL F EDGE	0.04	0.50	10.65	30.89	9.50	2.65	0.88	16.00	5.40	13.26	1.22	5.13	0.68	0.18	0.37	0.19	1.70	0.63	99.86
820C48 AL F OTHER	0.03	0.20	11.76	31.44	9.55	1.57	0.87	16.90	4.94	11.87	1.10	5.73	1.00	0.18	0.42	0.22	1.05	0.64	99.87
820C48 AL H CORE	0.05	0.33	9.13	30.65	9.03	3.21	0.52	18.48	5.87	13.12	1.21	4.34	0.67	0.22	0.69	0.25	1.77	0.61	100.15
820C48 AL H EDGE	0.04	0.35	9.98	30.56	9.47	2.91	0.49	18.12	5.56	13.40	1.33	4.26	0.68	0.15	0.63	0.24	1.39	0.54	100.10
883J92 AL E	0.00	0.36	13.52	31.68	12.34	0.27	0.46	16.74	5.30	10.46	0.60	3.50	0.59	0.00	0.19	0.05	0.76	0.00	96.82
883J92 AL A	0.04	0.27	18.87	31.65	10.59	0.45	1.68	12.94	6.07	11.91	0.80	4.14	0.70	0.00	0.40	0.12	0.00	0.00	100.63
883J92 AL B steps	0.00	0.30	14.66	32.22	13.39	0.25	0.45	16.71	5.38	9.57	0.60	3.16	0.52	0.00	0.14	0.09	0.09	0.00	97.53
883J92 AL B rim	0.02	0.45	15.73	31.28	9.96	0.62	1.88	14.62	6.20	12.20	0.70	4.14	0.61	0.00	0.59	0.13	0.00	0.00	99.13
883J93 AL avg	0.02	0.92	12.86	30.60	9.19	0.87	1.81	16.04	8.27	14.70	0.59	3.27	0.31	0.00	0.01	0.09	0.00	0.00	99.55
820C51b AL G	0.03	1.04	11.88	31.59	10.39	0.87	0.84	15.71	11.14	12.45	0.44	1.42	0.12	0.04	0.09	0.11	0.45	0.54	99.15
820C51b AL B	0.03	0.95	11.67	31.78	10.51	1.22	0.99	15.86	10.19	12.75	0.48	1.52	0.14	0.09	0.11	0.11	0.74	0.34	99.08
820C10 AL A1 CORE	0.06	0.34	14.20	31.64	8.89	0.40	3.32	13.57	6.48	12.38	0.90	3.58	0.46	0.19	0.28	0.10	0.05	0.04	96.88
820C10 AL A1 EDGE	0.06	0.38	15.70	31.98	9.09	0.26	3.01	13.13	6.65	12.61	0.83	3.57	0.54	0.10	0.22	0.15	0.17	0.00	98.44
820C10 AL A2	0.06	1.70	11.10	31.51	9.82	1.47	1.08	14.92	8.43	13.75	0.55	2.80	0.31	0.09	0.07	0.12	0.65	0.11	98.54
3417 AL B CORE	0.02	0.76	15.98	32.07	10.43	0.43	1.60	12.50	6.52	13.40	0.11	3.26	0.37	0.00	0.13	0.15	0.48	0.11	98.42
3417 AL B EDGE	0.02	0.56	16.06	32.47	10.72	0.54	1.82	13.28	4.86	13.07	0.46	4.06	0.41	0.00	0.00	0.11	0.81	0.23	99.47
3439 AL A1	0.06	1.80	10.50	31.08	9.58	1.82	1.21	15.94	13.78	11.37	0.11	0.66	0.00	0.08	0.00	0.08	0.66	0.14	98.87
3439 AL A2	0.03	0.57	14.40	32.19	10.71	0.31	2.05	13.17	11.00	10.78	0.25	1.08	0.10	0.12	0.17	0.05	0.12	0.12	97.23
3439 AL D	0.05	1.83	10.30	31.21	9.48	2.07	1.17	15.97	15.33	10.14	0.27	0.46	0.00	0.12	0.04	0.22	0.91	0.15	99.73
3440 AL A1	0.05	0.53	17.39	32.11	10.35	0.40	1.52	13.66	5.15	13.05	1.02	4.12	0.58	0.12	0.39	0.03	0.52	0.17	101.07
3440 AL A2	0.05	0.50	17.10	32.30	10.98	0.45	1.41	13.61	3.23	11.06	1.15	5.36	0.67	0.27	0.61	0.13	0.45	0.00	99.83
3440 AL A3 CORE	0.06	0.47	17.60	32.62	10.93	0.41	1.65	13.53	3.16	10.92	0.97	5.22	0.65	0.22	0.93	0.17	0.55	0.11	100.48
3440 AL A3 EDGE	0.04	0.62	16.30	32.29	10.51	0.54	1.37	13.55	4.01	12.67	1.11	5.25	0.91	0.25	0.60	0.15	0.46	0.05	100.71
3440 AL D	0.05	0.46	16.40	32.07	10.89	0.34	1.24	13.51	4.21	12.02	1.16	4.43	0.81	0.25	0.54	0.15	0.74	0.09	99.67
849C11 AL A CORE	0.04	1.73	11.38	31.47	9.96	1.67	0.76	15.62	12.75	10.63	0.40	0.67	0.00	0.10	0.04	0.24	1.34	0.18	98.98
849C11 AL A EDGE	0.05	1.74	11.64	31.28	9.66	1.61	0.55	15.79	14.36	10.37	0.29	0.40	0.00	0.03	0.06	0.22	0.87	0.20	99.52
849C13 AL A	0.05	1.44	10.59	31.06	9.64	1.70	1.72	16.74	12.72	10.77	0.43	0.42	0.00	0.02	0.10	0.26	1.49	0.22	99.78
849C13 AL C	0.05	1.70	11.16	31.15	9.72	1.67	1.06	15.80	12.66	11.01	0.48	0.69	0.00	0.06	0.06	0.26	1.22	0.32	99.08
820C30.2 AL A	0.05	1.49	10.89	31.11	9.58	1.58	1.37	16.49	13.26	10.85	0.16	0.51	0.03	0.05	0.02	0.04	1.37	0.58	99.22
820C30.2 AL B	0.04	0.65	12.76	31.03	9.51	1.04	2.03	15.70	5.78	14.63	1.09	3.87	0.41	0.06	0.14	0.19	0.52	0.55	100.00
820C15 AL C CORE	0.07	1.46	10.49	31.16	9.60	1.36	1.75	15.46	10.60	12.72	0.46	1.05	0.05	0.07	0.04	0.17	0.99	0.16	97.58
820C15 AL C EDGE	0.08	1.08	10.20	30.87	9.80	1.22	2.41	15.70	10.56	13.51	0.30	1.38	0.12	0.12	0.04	0.08	0.59	0.29	97.39
820C15 AL A CORE	0.08	1.47	11.50	31.41	10.22	1.47	1.23	15.24	10.17	12.12	0.25	1.22	0.15	0.14	0.00	0.09	1.67	0.26	98.69
820C15 AL A EDGE	0.09	1.13	10.40	30.97	8.83	1.32	2.18	15.79	9.11	14.23	0.52	2.02	0.30	0.12	0.08	0.17	0.61	0.24	99.11
820C15 AL B CORE	0.09	1.09	11.40	31.25	8.79	1.16	2.32	15.71	6.30	14.98	0.91	3.64	0.41	0.20	0.23	0.16	0.59	0.19	99.42
820C15 AL B EDGE	0.08	1.06	10.30	31.18	8.60	1.06	2.21	16.02	8.51	14.82	0.59	2.65	0.29	0.14	0.12	0.13	0.58	0.21	98.54
820C15 AL B1 CORE	0.08	1.53	10.80	31.19	9.45	1.66	1.86	15.42	10.47	12.62	0.40	1.05	0.10	0.17	0.02	0.08	1.38	0.13	98.41
820C15 AL B1 EDGE	0.08	1.03	11.40	31.31	8.96	1.34	2.50	15.95	9.08	14.20	0.64	2.96	0.21	0.03	0.10	0.07	0.63	0.21	100.00
820C15 AL B2 CORE	0.06	1.27	11.60	31.46	10.16	1.28	1.55	15.00	10.45	11.90	0.25	1.14	0.07	0.08	0.00	0.16	1.69	0.18	98.29
820C15 AL B2 EDGE	0.08	1.45	10.20	31.27	9.15	1.56	2.13	15.43	10.86	12.98	0.70	0.67	0.06	0.10	0.03	0.13	1.04	0.18	96.23
80L20 AL A	0.06	0.54	13.18	31.06	9.34	0.98	2.44	15.47	4.58	13.54	1.17	4.48	0.52	0.10	0.28	0.15	1.27	0.38	99.55
80L20 AL B CORE	0.05	1.75	12.91	31.43	10.42	1.55	0.53	14.63	8.25	12.88	0.56	2.47	0.31	0.05	0.11	0.04	0.79	0.29	98.94
80L20 AL B EDGE	0.05	1.59	11.42	31.07	9.45	1.54	1.66	15.42	11.48	12.47	0.25	0.55	0.02	0.12	0.07	0.05	0.96	0.33	99.00
80L20 AL D CORE	0.05	1.61	11.63	30.75	9.41	1.60	1.77	15.59	11.21	12.54	0.16	1.03	0.14	0.07	0.05	0.05	1.18	0.21	99.20
80L20 AL D EDGE	0.05	1.53	11.75	30.96	9.63	1.57	1.65	15.48	11.18	12.47	0.24	0.92	0.09	0.07	0.08	0.12	1.32	0.43	99.54
80L20 AL E CORE	0.06	1.43	11.81	31.07	9.61	1.57	1.74	15.60	10.71	12.60	0.40	0.95	0.10	0.06	0.10	0.15	1.52	0.30	99.48
80L20 AL E EDGE	0.05	1.41	11.74	31.10	9.74	1.49	1.79	15.61	10.98	12.66	0.13	0.85	0.09	0.04	0.08	0.16	1.27	0.46	99.65
80L20 AL E TIP	0.03	1.09	11.47	30.77	8.45	1.32	3.42	16.05	8.15	14.98	0.72	2.10	0.17	0.11	0.10	0.14	0.69	0.63	100.53
883C92 E E steps	0.00	0.05	20.22	36.41	22.21	0.12	0.74	16.52	0.12	0.38	0.07	0.15	0.02	0.00	0.22	0.00	0.00	0.00	94.65
883C92 E E	0.00	0.06	21.42	36.97	22.65	0.08	0.32	14.76	0.02	0.00	0.00	0.06	0.01	0.00	0.10	0.00	0.00	0.00	96.45
883C92 E A	0.00	0.05	21.83	37.02	22.04	0.04	0.58	14.28	0.02	0.12	0.08	0.07	0.00	0.00	0.21	0.00	0.00	0.00	96.74
883C92 E B	0.00	0.04	20.59	36.57	21.84	0.06	0.9	15.78	0.07	0.06	0.00	0.08	0.01	0.00	0.06	0.00	0.00	0.00	94.37
820C51b E B	0.01	0.06	21.40	37.64	23.14	0.03	0.32	12.15	0.33	0.28	0.04	0.04	0.00	0.00	0.00	0.20	0.00	0.00	96.04

APPENDIX H: ELECTRON MICROPROBE ANALYSES OF CHEVKINITE-PERRIERITE(P) IN THE QUESTA GRANITIC ROCKS (IN WT%).

SAMPLE NUMBER	Na2O	MgO	Al2O3	SiO2	CaO	TiO2	MnO	FeOt	La2O3	Ce2O3	Pr2O3	Nd2O3	Sm2O3	Gy2O3	Y2O3	Yb2O3	ThO2	UO2	TOTAL
B20C38 P C	0.08	0.24	0.14	20.33	3.45	17.26	1.48	10.33	14.14	23.11	1.18	4.75	0.48	0.41	0.43	0.65	1.72	0.66	100.83
B20C38 P E	0.06	0.19	0.33	20.08	2.41	16.37	1.85	11.05	13.38	22.76	1.38	5.86	0.67	0.36	0.61	0.78	2.33	0.72	101.19
883063 P A	0.08	0.19	0.15	19.94	2.70	16.86	1.84	10.48	14.38	24.14	1.23	4.98	0.81	0.36	0.61	0.60	1.82	0.65	101.81
883063 P B	0.14	0.19	0.12	20.61	2.95	17.67	1.61	10.36	12.04	23.52	1.54	6.97	0.87	0.32	0.43	0.53	0.91	0.55	101.34
883063 P J	0.07	0.17	0.06	19.52	1.55	15.45	2.08	11.05	9.94	23.70	1.67	8.20	1.77	0.69	1.30	0.78	2.90	0.59	101.49
883063 P I	0.11	0.17	0.14	20.09	2.49	17.02	1.79	10.43	12.62	24.00	1.50	7.14	0.93	0.37	0.48	0.54	0.94	0.69	101.44
B20C39 P A	0.04	0.45	2.47	21.06	4.42	17.38	0.92	8.36	11.02	21.79	1.50	6.82	0.82	0.46	0.79	0.64	1.55	0.64	101.13
B20C39 P C	0.04	0.39	2.23	20.77	4.28	16.90	1.05	8.38	11.22	21.83	1.74	6.56	0.71	0.51	0.82	0.70	2.02	0.68	100.83
B20C39 P E	0.04	0.38	2.47	20.87	4.54	16.75	1.04	8.10	9.65	21.19	1.66	7.43	0.92	0.48	0.82	0.81	2.97	0.76	100.87
B20C41 P A	0.03	0.59	2.86	21.30	5.10	18.28	0.47	7.79	14.01	21.68	1.07	4.52	0.33	0.15	0.29	0.61	1.22	0.43	100.64
B30C33 P A	0.03	0.61	2.26	20.97	5.29	18.34	0.57	8.13	13.24	21.09	0.90	4.54	0.49	0.26	0.52	0.55	1.55	0.67	100.00
B30C33 P C	0.03	0.57	2.28	21.33	5.72	18.52	0.51	8.19	14.76	20.63	0.77	3.07	0.32	0.13	0.33	0.50	2.03	0.56	100.25
B20C35 P D	0.05	0.34	2.85	20.85	4.36	16.89	0.97	7.98	9.51	20.60	1.69	7.18	1.19	0.56	1.38	0.66	1.85	0.70	99.61
B20C35 P E	0.02	0.78	2.92	21.31	5.51	18.53	0.34	7.50	12.24	20.82	1.41	5.58	0.62	0.30	0.43	0.62	1.26	0.59	100.77
B20C47 P G	0.03	0.37	2.60	20.77	3.94	17.05	0.91	8.84	12.92	22.24	1.55	6.10	0.66	0.36	0.44	0.63	1.59	0.52	101.52
B20C47 P B	0.03	0.37	2.48	21.02	4.58	16.83	0.90	8.78	14.87	21.66	1.05	4.01	0.33	0.16	0.32	0.64	1.90	0.54	100.47
B20C47 P A	0.02	0.35	2.65	20.93	3.87	17.11	0.98	8.32	11.74	23.10	1.66	6.59	0.69	0.44	0.49	0.59	1.32	0.48	101.33
B20C47 P H	0.03	0.39	2.60	20.79	4.16	17.02	0.87	8.65	10.56	22.65	1.71	6.91	0.75	0.41	0.66	0.76	1.71	0.63	101.25
B20C47 P B1	0.03	0.35	2.50	20.96	4.56	16.71	0.91	8.81	15.00	21.53	0.86	3.91	0.39	0.19	0.32	0.70	2.05	0.65	100.42
B20C47 P E2	0.02	0.37	2.65	20.86	4.25	17.21	0.96	8.69	11.52	23.09	1.79	6.21	0.60	0.21	0.58	0.68	1.51	0.48	101.69
B20C47 P B3	0.02	0.41	2.43	21.24	4.67	16.97	0.81	8.74	18.20	20.79	0.51	2.18	0.06	0.11	0.15	0.51	1.89	0.53	100.22
B20C47 P B4	0.03	0.35	2.36	21.00	4.85	16.41	0.91	8.88	14.73	21.19	1.09	3.73	0.26	0.13	0.21	0.67	2.15	0.59	99.44
883082 P B	0.03	0.78	2.98	21.22	5.19	18.39	0.42	7.79	11.97	21.68	1.31	6.37	0.69	0.30	0.38	0.52	1.67	0.48	102.16
883082 P F	0.03	0.53	2.44	20.96	4.70	17.55	0.69	8.43	15.22	21.65	0.67	4.28	0.36	0.23	0.27	0.52	2.09	0.55	101.19
B20C19 P A	0.04	0.67	2.11	21.17	4.87	18.03	0.70	8.59	15.71	21.98	0.79	2.65	0.27	0.27	0.44	0.70	2.48	0.44	101.91
B20C19 P B	0.08	0.39	2.42	20.31	4.66	18.43	1.01	8.58	14.27	19.00	0.58	1.52	0.06	0.23	0.37	0.70	4.96	0.85	98.42
B20C19 P THIN B	0.05	0.41	1.95	21.34	6.21	18.70	0.93	8.03	14.27	20.13	0.76	2.03	0.21	0.27	0.47	0.61	2.81	0.79	99.96
B20C19 P D	0.03	0.32	1.84	20.95	4.27	16.23	1.50	8.59	18.03	22.29	0.13	1.86	0.13	0.25	0.51	0.73	2.12	0.84	100.63
B20C22 P A1	0.04	0.61	2.17	21.40	5.03	17.57	0.68	8.55	15.92	21.76	0.48	2.49	0.25	0.28	0.40	0.55	1.96	0.12	100.27
B20C22 P A2	0.04	0.60	2.20	21.48	5.11	17.50	0.64	8.46	15.76	20.69	0.71	2.30	0.29	0.27	0.36	0.58	2.03	0.04	99.06
81528.1 P A	0.03	0.52	1.89	21.63	5.88	17.99	0.67	8.26	14.78	20.76	0.81	2.10	0.26	0.34	0.40	0.58	3.40	0.75	101.25
B30C12 P A	0.03	0.85	2.35	21.21	4.93	18.13	0.42	8.12	16.72	21.05	1.02	2.56	0.17	0.22	0.17	0.62	1.92	0.72	101.21
B20C10 P A	0.06	0.40	2.40	21.40	4.24	17.20	0.80	8.51	9.56	21.67	1.21	7.90	1.20	0.45	1.20	0.62	0.70	0.21	99.73

APPENDIX I: ELECTRON MICROPROBE ANALYSES OF APATITE (IN WT%).

	Grains/ Host*	CaO	P_2O_5	SiO_2	FeO	La_2O_3	Ce_2O_3	Y_2O_3	Cl	F
VIRGIN CANYON										
82QC35	3/B,O	54.0	40.2	0.30	0.32	0.20	0.46	0.19	0.02	2.6-3.5
(74.8)**	1/O	54.1	40.2	0.42	0.46	0.24	0.59	0.27	0.01	3.5
	2/B	53.3	40.1	0.87	0.24	0.42	1.02	0.34	0.04	2.7-3.3
83QC33	1/O	53.4	40.4	0.32	0.42	0.22	0.52	0.45	0.02	3.8
(76.0)	5/B,O	53.7	40.2	0.62	0.38	0.32	0.75	0.29	0.01	3.7-4.8
	1/F	53.3	40.1	0.70	0.11	0.34	0.82	0.53	0.01	4.2
	1/O	53.9	39.7	0.81	0.68	0.43	0.99	0.38	0.02	3.2
82QC33	1/O	54.3	41.4	0.31	0.42	0.22	0.51	0.21	0.02	3.2
(72.9)	1/O,F	53.5	39.9	0.55	0.08	0.24	0.74	0.32	0.02	3.5
	2/O,F	53.6	40.6	0.67	0.27	0.35	0.86	0.32	0.02	2.8-3.5
82QC39	1/B	53.6	40.2	0.54	0.20	0.18	0.69	0.36	0.02	3.1
(72.7)	3/B,O,F	53.2	40.1	0.84	0.15	0.26	0.83	0.69	0.02	3.1-3.7
82QC41	3/B,Q	54.3	40.2	0.52	0.15	0.29	0.59	0.16	0.03	3.1-3.5
(69.6)	1/B	53.2	37.7	1.50	0.32	0.70	1.51	0.42	0.02	3.4
82QC38	2/A	51.6	37.9	1.29	0.36	0.46	1.40	0.90	0.01	3.6
(75.2)	1/A	50.5	37.8	1.36	0.24	0.61	1.67	1.22	0.02	3.6
	1/B,O,F	49.9	38.2	1.36	0.13	1.01	2.45	1.26	0.01	3.4
Q83J63	1/A	52.7	40.1	0.48	0.26	0.29	0.86	0.31	0.00	3.7
(75.3)	1/A	51.8	38.9	1.12	0.27	0.45	1.37	0.45	0.01	3.6
	2/A,O	50.4	37.5	1.21	0.34	0.81	1.91	1.08	0.00	3.3-3.5
CANADA-PINABETE										
81S43	2/B	53.3	40.6	0.49	0.25	0.21	0.54	0.44	0.01	3.1-3.9
(74.6)	1/B	53.2	39.9	0.64	0.25	0.33	0.63	0.17	0.03	3.2
	1/F,Q	52.4	40.6	0.80	0.03	0.19	0.67	1.18	0.02	3.1
Q83J82	2/B	54.0	40.4	0.38	0.18	0.22	0.48	0.20	0.02	3.5-3.7
(73.8)	3/B,F	54.2	40.6	0.49	0.18	0.28	0.71	0.29	0.02	3.1-3.7
	1/B	52.9	40.1	0.67	0.26	0.40	0.92	0.37	0.02	4.0
82QC47	2/B,O	53.2	40.0	0.35	0.15	0.21	0.51	0.25	0.03	3.3-3.6
(74.1)	1/B	52.7	39.7	0.58	0.20	0.26	0.78	0.40	0.02	3.9
	2/B,O	53.3	39.4	0.80	0.35	0.41	0.98	0.32	0.02	3.3-3.5
	1/F,O	52.3	39.8	0.92	0.10	0.38	1.02	0.48	0.03	3.2
82QC48	2/B	54.3	40.5	0.40	0.39	0.20	0.48	0.17	0.05	3.6
(73.9)	1/B,F	54.9	40.6	0.47	0.25	0.36	0.65	0.19	0.02	3.0
Q83J92	2/B,O,F	53.2	40.5	0.29	0.32	0.20	0.52	0.22	0.06	4.2-4.4
	1/B	52.9	40.5	0.60	0.20	0.32	0.89	0.29	0.06	4.1
	2/B,F	53.1	39.8	0.74	0.25	0.31	0.87	0.43	0.04	4.0-4.4
	1/O	52.2	39.5	0.88	0.35	0.3	0.83	0.96	0.04	3.6
Q83J93	3/B	53.6	40.5	0.43	0.17	0.24	0.66	0.30	0.06	3.6-4.2
	2/B,O,F	53.3	39.9	0.64	0.40	0.37	0.95	0.36	0.07	4.1-4.3
RITO DEL MEDIO										
82QC22 (75.3)	4/B,O	53.3	40.0	0.72	0.19	0.46	0.88	0.31	0.04	2.6-3.6
CABRESTO LAKE										
82QC51b	3/B,O	54.3	40.9	0.25	0.41	0.20	0.27	0.07	0.14	3.8
	3/B,O	53.4	40.2	0.53	0.41	0.31	0.58	0.16	0.18	3.8
	1/O	52.3	40.1	0.76	0.80	0.50	0.85	0.20	0.36	2.8
	3/En	54.1	40.1	0.58	0.16	0.20	0.31	0.05	0.14	3.0-4.3

	Grains/ Host*	CaO	P_2O_5	SiO_2	FeO	La_2O_3	Ce_2O_3	Y_2O_3	Cl	F
BEAR CANYON										
82QC10	3/B	54.7	40.2	0.42	0.45	0.29	0.58	0.16	0.01	3.6-4.2
(75.0)	1/B	54.9	40.6	0.58	0.19	0.34	0.70	0.36	0.01	3.4
	2/B,O	54.7	39.9	0.54	0.51	0.23	0.59	0.54	0.01	3.2-3.8
SULPHUR GULCH										
3417	3/B	54.8	40.8	0.27	0.25	0.24	0.31	-	0.04	3.3-3.5
(72.0)	4/B	54.5	40.6	0.47	0.34	0.44	0.56	-	0.05	3.0-3.3
3439	2/B	54.8	40.3	0.39	0.33	0.33	0.51	-	0.04	3.3-3.4
(70.0)										
3440	4/B,F,O	53.5	40.5	0.47	0.29	0.40	0.67	-	0.02	3.1-3.3
(72.4)										
RED RIVER										
82QC44	5/B	55.6	40.7	0.18	0.18	0.19	0.34	0.08	0.59	1.8-2.8
(64.3)										
85QC36	2/B	55.8	40.6	0.31	0.18	0.26	0.37	0.09	0.14	3.6-3.7
(71.7)	4/B,O	55.0	40.3	0.64	0.32	0.48	0.75	0.17	0.15	3.1-3.3
82QC32C	3/B	53.1	39.7	0.10	0.22	0.27	0.69	0.72	0.02	2.8-3.7
(75.8)	1/B	52.6	39.0	0.69	0.35	0.47	1.15	1.16	0.02	3.6
	1/B,F	51.6	38.7	1.09	0.11	0.45	1.24	1.67	0.02	3.7
RIO HONDO										
Q83J59	2/B,F	54.8	40.5	0.16	0.18	0.17	0.32	0.08	0.56	2.8-3.0
(66.3)										
82QC12	2/B	55.3	40.2	0.21	0.16	0.20	0.25	0.08	0.07	3.1-3.2
-										
Q84J6	4/B,H	53.9	40.4	0.23	0.16	0.17	0.18	0.06	0.12	3.0-3.4
(68.8)										
84QC11	1/B,F	54.9	40.8	0.27	0.09	0.21	0.27	0.05	0.01	3.0
-	3/B	54.5	40.6	0.28	0.27	0.24	0.39	0.09	0.01	3.2-3.7
84QC13	2/B,O	54.5	40.4	0.35	0.58	0.27	0.48	0.14	0.01	3.3-3.5
(76.9)										
82QC30	3/B	54.2	39.6	0.36	0.23	0.32	0.47	0.10	0.01	2.9-3.6
(78.5)										
LUCERO PEAK										
82QC15	2/B	53.9	40.4	0.23	0.13	0.20	0.38	0.13	0.01	3.2-3.9
(75.9)	2/B	53.8	40.5	0.38	0.17	0.24	0.54	0.19	0.01	2.5-3.7
80L20	1/B	53.7	40.0	0.30	0.11	0.08	0.39	0.30	0.01	3.8
(76.8)	4/B,O	53.3	39.5	0.36	0.15	0.26	0.55	0.17	0.01	2.9-3.8

* Hosts: A, arfvedsonite; B, biotite; En, enclave; F, alkali feldspar; H, hornblende; O, opaque oxide; Q, quartz.

** Value in parentheses is SiO_2 content of host rock.

*** SiO_2 content of comparable specimen 82QC51.

APPENDIX J: SUPPLEMENTAL ELECTRON MICROPROBE ANALYSES OF APATITE FOR THE HEAVIER RARE-EARTH ELEMENTS (IN WT%).

ID	SiO2	La2O3	Ce2O3	Nd2O3	Sm2O3	Dy2O3	Y2O3	Yb2O3
83QC29(1)	0.65	0.387	1.008	0.625	0.103	0.115	0.205	0.024
(1)	1.03	0.322	1.018	0.7	0.143	0.264	0.409	0.065
(1)	1.01	0.505	1.398	0.819	0.166	0.095	0.283	0.045
(1)	0.16	0.949	2.71	1.414	0.331	0.205	0.479	0.08
(1)	0.15	1.012	2.925	1.596	0.334	0.219	0.537	0.111
Q83J63(1)	1.51	0.384	1.351	1.07	0.375	0.456	1.144	0.052
(1)	1.19	0.536	1.494	0.896	0.196	0.247	0.425	0.039
(1)	1.17	0.507	1.518	0.938	0.235	0.274	0.717	0.021
(1)	1.18	0.744	1.972	0.876	0.24	0.385	0.946	0.035
(1)	1.18	0.981	2.167	0.902	0.23	0.338	1.107	0.061
82QC38(1)	0.58	0.275	0.809	0.486	0.112	0.231	0.318	0.032
(1)	0.96	0.356	1.041	0.698	0.123	0.199	0.346	0.03
(1)	1.08	0.51	1.373	0.835	0.225	0.315	0.928	0.063
(2)	1.54	0.679	2.039	1.142	0.322	0.405	1.346	0.064
(1)	1.39	1.126	2.498	1.112	0.224	0.348	1.195	0.07
82QC38.1(1)	0.58	0.265	0.848	0.5	0.088	0.068	0.169	0.02
(1)	0.71	0.348	1.067	0.658	0.123	0.083	0.219	0.02
(1)	1.12	0.428	1.335	0.812	0.156	0.131	0.345	0.026
82QC41(4)	0.5	0.252	0.579	0.219	0.038	0.102	0.141	0.024
(1)	1.5	0.635	1.548	0.699	0.12	0.118	0.38	0.022
82QC35(3)	0.34	0.217	0.414	0.155	0.031	0.118	0.148	0.007
(2)	0.38	0.2	0.503	0.215	0.035	0.134	0.262	0.038
(2)	0.93	0.449	1.026	0.451	0.091	0.14	0.332	0.048
83QC33(1)	0.33	0.22	0.5	0.21	0.025	0.25	0.337	0.044
(1)	0.59	0.277	0.816	0.39	0.083	0.268	0.402	0.024
(1)	0.69	0.346	0.867	0.33	0.09	0.157	0.249	0.001
(1)	0.83	0.344	0.981	0.637	0.127	0.21	0.31	0.001
Q83J92(3)	0.48	0.228	0.729	0.468	0.104	0.129	0.272	0.016
81S43(2)	0.49	0.171	0.535	0.315	0.092	0.155	0.411	0.022
(1)	0.8	0.189	0.668	0.507	0.183	0.218	1.083	0.043
(1)	0.83	0.279	0.88	0.544	0.141	0.189	0.437	0.023
82QC22(3)	0.71	0.43	0.925	0.155	0.021	0.094	0.275	0.029
82QC51b(2)	0.34	0.252	0.351	0.077	0.001	0.052	0.061	0.018
(1)	0.31	0.177	0.407	0.155	0.023	0.07	0.105	0.02
(1)	0.46	0.333	0.473	0.157	0.018	0.055	0.122	0.001
(E)	0.52	0.427	0.555	0.15	0.019	0.05	0.084	0.001
(L)	0.57	0.316	0.708	0.267	0.052	0.086	0.162	0.033

ID	SiO2	La2O3	Ce2O3	Nd2O3	Sm2O3	Dy2O3	Y2O3	Yb2O3
82QC10(1)	0.25	0.193	0.298	0.092	0.039	0.132	0.143	0.016
(1)	0.29	0.136	0.357	0.066	0.019	0.106	0.1	0.025
(1)	0.48	0.177	0.581	0.341	0.068	0.141	0.5	0.059
(2)	0.47	0.245	0.658	0.182	0.023	0.094	0.141	0.011
(1)	0.54	0.312	0.706	0.209	0.027	0.114	0.238	0.026
82QC32C(1)	0.09	0.285	0.643	0.235	0.063	0.509	0.601	0.079
(1)	0.38	0.245	0.764	0.217	0.086	0.594	0.838	0.092
(1)	0.31	0.327	0.862	0.29	0.073	0.531	0.796	0.048
(1)	0.59	0.346	0.987	0.344	0.067	0.588	0.97	0.089
(1)	0.72	0.444	1.283	0.387	0.057	0.62	0.978	0.061
(1)	1.45	0.528	1.463	0.655	0.163	0.698	1.9	0.161
(1)	1.2	0.502	1.48	0.618	0.161	0.685	1.466	0.123
82QC36(3)	0.32	0.247	0.417	0.089	0.006	0.075	0.103	0.004
(3)	0.55	0.428	0.749	0.153	0.003	0.083	0.114	0.008
82QC43(1)	0.01	0.075	0.245	0.072	0.048	0.31	0.578	0.1
(1)	0.01	0.114	0.303	0.11	0.03	0.361	0.507	0.083
(1)	0.2	0.082	0.368	0.148	0.061	0.446	0.78	0.065
(1)	0.42	0.169	0.484	0.222	0.032	0.315	0.427	0.093
(1)	0.29	0.279	0.513	0.124	0.037	0.21	0.11	0.001
82QC44(1)	0.21	0.222	0.254	0.059	0.002	0.015	0.024	0.017
(2)	0.19	0.183	0.321	0.103	0.01	0.028	0.061	0.029
(1)	0.28	0.246	0.385	0.122	0.01	0.028	0.071	0.01
84QC13(3)	0.31	0.21	0.474	0.062	0.001	0.091	0.077	0.002
82QC27(2)	0.19	0.105	0.213	0.086	0.025	0.04	0.058	0.001
Q84J6(1)	0.13	0.074	0.094	0.001	0.001	0.01	0.029	0.018
(1)	0.19	0.134	0.183	0.031	0.001	0.028	0.04	0.008
82QC15(1)	0.32	0.189	0.423	0.076	0.006	0.122	0.097	0.032
(2)	0.42	0.266	0.616	0.14	0.007	0.122	0.142	0.006

APPENDIX K: ELECTRON MICROPROBE ANALYSES OF FELDSPARS IN THE QUESTA GRANITOIDS AND RELATED ROCKS (IN WT%).

		SiO_2	Al_2O_3	FeO	CaO	Na_2O	K_2O	SrO	BaO
VIRGIN CANYON									
Peralkaline Porphyry									
82QC38	(rc)	64.8	20.3	0.26	1.06	5.76	7.41	0.05	0.77
	(rr)	63.1	23.3	0.10	3.99	9.32	0.33	0.05	0.08
	(a)	66.9	18.8	0.55	0.01	6.22	7.75	0.02	0.02
83QC29	(a)	65.2	18.8	0.13	0.75	5.72	8.37	0.03	0.50
	(a)	67.0	18.3	0.49	0.03	6.17	8.04	0.00	0.01
	(a)	66.6	17.6	0.61	0.01	6.88	7.15	0.01	0.02
83QC30	(a)	65.9	18.5	0.45	0.05	5.24	9.29	0.02	0.05
Early Metaluminous Granite									
82QC40	(p)	65.9	21.2	0.18	2.09	9.94	0.93	0.02	0.02
	(a)	64.5	19.8	0.18	0.30	5.54	7.87	0.07	2.38
	(a)	63.9	19.8	0.18	0.34	4.98	8.22	0.08	3.02
	(a)	65.7	18.9	0.13	0.13	4.56	10.2	0.01	0.18
82QC41	(c)	62.3	22.5	0.23	4.36	8.53	1.06	0.12	0.23
	(r)	64.2	21.5	0.23	3.07	9.11	1.27	0.07	0.14
Early Metaluminous Dike									
83QC31	(p,2)	68.8	19.8	0.11	0.11	11.7	0.33	0.01	0.03
	(a)	64.7	19.6	0.15	0.33	4.44	9.77	0.04	1.78
	(a)	64.2	19.5	0.14	0.40	4.51	9.49	0.08	2.19
Later Metaluminous Granite									
82QC35	(c)	65.2	21.6	0.23	2.57	9.90	0.73	0.05	0.07
	(r)	66.8	20.7	0.16	1.51	10.2	0.91	0.00	0.03
	(a)	66.3	19.0	0.13	0.21	4.88	9.59	0.02	0.17
83QC33	(c)	63.4	21.6	0.24	3.67	9.09	1.01	0.11	0.18
	(r)	64.9	21.4	0.27	2.96	9.08	1.18	0.04	0.13
	(c)	65.1	21.6	0.18	2.57	9.74	0.91	0.01	0.01
	(r)	66.3	21.3	0.20	1.63	10.2	1.03	0.00	0.02
	(a)	66.0	19.0	0.16	0.22	5.66	8.54	0.03	0.24
	(a,3)	65.7	18.8	0.15	0.28	5.14	8.88	0.03	0.64
CANADA PINABETE									
Peralkaline Porphyry									
84QC7	(ac)	66.6	19.3	0.11	0.11	6.31	8.09	0.01	0.19
	(ar)	66.3	19.3	0.03	0.04	5.31	9.33	0.02	0.28
	(a)	67.4	18.2	0.53	0.04	6.57	7.80	0.00	0.01
	(a)	67.3	18.0	0.54	0.02	6.92	7.03	0.01	0.00

		SiO_2	Al_2O_3	FeO	CaO	Na_2O	K_2O	SrO	BaO
Early Metaluminous Granite									
Q83J92	(a)	64.1	19.3	0.19	0.39	4.22	9.57	0.09	2.08
	(a)	65.6	19.0	0.16	0.20	4.35	10.3	0.06	0.38
	(a)	66.0	18.1	0.51	0.03	4.64	10.2	0.05	0.04
Later Metaluminous Granite									
82QC47	(p)	62.5	22.8	0.29	4.53	8.73	0.43	0.15	0.12
	(c,a)	64.6	21.9	0.23	2.86	9.66	0.59	0.07	0.09
	(c)	64.6	21.5	0.23	2.83	9.69	0.67	0.03	0.02
	(r)	65.8	21.0	0.24	2.05	10.1	0.76	0.00	0.03
	(a)	65.5	18.7	0.13	0.16	4.46	10.2	0.03	0.09
	(a)	64.9	18.6	0.19	0.13	3.19	11.5	0.03	0.04
Q83J82	(c)	62.3	23.2	0.29	4.38	8.95	0.55	0.13	0.10
	(c)	62.4	22.9	0.26	4.11	8.97	0.61	0.10	0.13
	(r)	65.0	21.4	0.22	2.54	9.93	0.61	0.07	0.06
	(a)	65.4	19.2	0.17	0.25	5.64	8.43	0.04	0.43
	(a)	64.9	19.3	0.17	0.31	4.86	9.42	0.06	0.80
	(a)	65.5	18.9	0.15	0.17	4.73	9.83	0.03	0.22
Q83J88	(c)	65.5	21.1	0.20	2.32	9.93	0.81	0.02	0.03
	(r)	66.3	20.5	0.21	1.48	10.4	0.73	0.01	0.01
	(v)	68.4	19.4	0.03	0.13	11.6	0.08	0.01	0.03
	(a)	65.0	19.0	0.18	0.26	5.05	9.23	0.06	0.49
84QC1	(c)	66.7	20.8	0.18	1.82	10.3	0.53	0.01	0.01
	(r)	68.2	20.7	0.08	0.69	11.6	0.39	0.00	0.00
	(c)	67.2	20.6	0.22	1.69	10.1	0.90	0.00	0.02
	(r)	67.3	20.5	0.20	1.09	10.8	0.47	0.01	0.02
	(a,2)	66.4	19.2	0.13	0.07	4.59	10.1	0.01	0.00
Magnetite-free Granite									
82QC48	(c)	61.5	24.9	0.24	5.92	8.06	0.36	0.15	0.17
	(r)	67.6	21.0	0.27	1.71	10.6	0.37	0.00	0.00
	(c)	63.0	24.0	0.25	4.86	8.47	0.31	0.13	0.05
	(r)	65.0	22.7	0.22	3.43	9.04	0.89	0.04	0.04
	(a)	65.2	19.3	0.16	0.28	4.61	9.19	0.11	1.78
	(a,2)	66.4	18.6	0.13	0.15	4.85	9.70	0.00	0.17
RITO del MEDIO									
Granite									
82QC18	(p,2)	66.2	20.7	0.18	1.67	10.7	0.33	0.00	0.02
	(p)	67.9	19.6	0.05	0.37	11.3	0.26	0.01	0.03
	(a)	66.2	18.7	0.15	0.24	5.83	8.27	0.02	0.03
Contact facies									
82QC22	(a)	66.0	19.0	0.16	0.22	5.86	8.18	0.00	0.01
	(a,3)	65.8	18.9	0.16	0.18	5.52	8.67	0.00	0.02
	(a)	65.8	18.7	0.17	0.16	5.26	8.93	0.01	0.02

	SiO_2	Al_2O_3	FeO	CaO	Na_2O	K_2O	SrO	BaO
CABRESTO LAKE								
Monzogranite								
82QC51 (c)	63.0	23.7	0.23	4.46	8.85	0.64	0.15	0.07
(r)	65.4	22.1	0.21	2.69	9.91	0.61	0.02	0.00
(c)	63.3	23.2	0.24	4.21	8.99	0.83	0.14	0.10
(r)	65.9	21.8	0.21	2.42	10.0	0.86	0.00	0.00
(c)	64.0	23.2	0.23	4.10	9.17	0.56	0.10	0.07
(r)	65.7	21.9	0.24	2.60	9.90	0.60	0.02	0.02
(a)	65.7	19.2	0.16	0.27	4.63	9.86	0.10	0.54
(a)	66.3	19.2	0.14	0.22	4.90	9.72	0.00	0.03
82QC51b (c)	64.0	22.9	0.23	3.85	9.13	0.59	0.06	0.02
(r)	65.8	21.7	0.17	2.44	9.77	0.65	0.00	0.02
(p)	63.8	22.5	0.18	3.80	9.08	0.55	0.06	0.05
(a)	65.9	18.8	0.11	0.26	4.34	10.1	0.04	0.63
(a)	65.3	19.6	0.11	0.16	3.45	11.1	0.07	1.20
(a)	66.1	19.1	0.11	0.15	3.74	11.3	0.05	0.19
83QC10 (rc)	65.9	19.2	0.19	0.31	5.07	9.31	0.16	0.21
(rr)	65.3	21.9	0.16	2.47	10.4	0.22	0.00	0.01
Mixed unit								
83QC14 (c)	63.8	22.9	0.26	3.92	8.90	0.92	0.15	0.13
(r)	65.6	22.1	0.26	2.87	9.67	0.60	0.05	0.02
(c)	64.7	22.4	0.27	3.26	9.49	0.52	0.05	0.03
(r)	64.2	22.5	0.25	3.08	9.82	0.53	0.10	0.05
(a)	65.5	19.2	0.17	0.17	3.54	11.5	0.04	0.05
BEAR CANYON								
82QC8 (p)	65.7	20.4	0.13	2.02	10.7	0.58	0.02	0.02
(a)	65.6	18.3	0.09	0.04	3.30	12.2	0.00	0.03
82QC10 (c)	65.4	21.0	0.18	2.39	10.5	0.37	0.00	0.02
(d)	64.2	21.5	0.09	2.59	10.2	0.24	0.08	0.04
(r)	65.9	21.3	0.12	2.02	10.6	0.32	0.04	0.01
(a)	64.4	18.4	0.08	0.03	1.42	14.4	0.05	0.61
(a)	64.6	19.0	0.11	0.04	1.68	14.0	0.06	1.21
SULPHUR GULCH								
Source Aplite								
82QC52 (a)	64.4	18.8	0.02	0.00	0.54	16.0	0.00	0.12
RED RIVER								
Alkali-feldspar Granite								
82QC32 (a)	66.9	19.2	0.14	0.22	6.35	7.99	0.00	0.01

	SiO_2	Al_2O_3	FeO	CaO	Na_2O	K_2O	SrO	BaO
Granite								
82QC43 (c)	61.8	23.8	0.16	5.02	8.72	0.44	0.13	0.10
(r)	64.9	22.0	0.24	2.90	9.68	0.84	0.04	0.03
(a)	66.4	18.6	0.17	0.20	5.99	8.13	0.02	0.02
85QC36 (c)	63.5	22.3	0.24	3.99	9.08	0.73	0.14	0.16
(r)	64.6	22.3	0.24	2.80	9.92	0.58	0.05	0.04
(a)	66.0	18.2	0.18	0.25	5.38	9.04	0.04	0.14
Granodiorite								
82QC44 (c)	59.8	23.5	0.17	6.46	7.83	0.56	0.23	0.07
(r)	62.3	23.0	0.17	4.84	8.66	0.66	0.24	0.12
(c)	61.2	23.3	0.17	5.55	8.26	0.56	0.24	0.08
(r)	61.5	22.9	0.20	5.08	8.43	0.61	0.29	0.06
(p)	62.2	22.7	0.18	4.72	8.93	0.43	0.17	0.06
(a)	64.0	18.6	0.11	0.19	3.83	10.4	0.18	1.99
(a)	63.4	18.8	0.10	0.19	3.68	10.8	0.14	1.65
RIO HONDO								
Granite								
82QC30 (p,3)	66.1	21.1	0.15	1.62	10.5	0.39	0.00	0.01
(a)	64.3	19.1	0.11	0.11	2.97	12.1	0.04	0.81
(a)	64.0	18.7	0.11	0.06	1.69	14.0	0.03	0.33
Q83SL28 (O)	65.2	19.0	0.11	0.09	3.17	12.2	0.04	0.07
84QC11 (c)	63.2	21.7	0.17	3.45	9.96	0.41	0.04	0.02
(r)	65.3	21.1	0.16	1.96	10.7	0.39	0.00	0.02
(rc)	65.0	18.7	0.09	0.16	3.91	11.0	0.01	0.59
(rr)	65.4	21.4	0.14	2.33	10.5	0.13	0.02	0.00
84QC13 (c)	63.8	22.7	0.16	3.50	9.27	0.59	0.05	0.03
(r)	65.1	21.7	0.17	2.29	10.2	0.39	0.03	0.00
(p)	65.9	20.8	0.16	1.80	10.6	0.42	0.00	0.01
(a)	64.2	18.4	0.12	0.04	1.49	14.6	0.00	0.00
Rhyolite Dike								
82QC27 (a,2)	64.5	18.9	0.00	0.00	0.31	16.2	0.00	0.31
Granodiorite								
81S38 (c)	61.9	23.5	0.22	4.76	8.56	0.37	0.25	0.10
(r)	63.2	22.9	0.11	4.38	8.98	0.18	0.13	0.04
82QC12 (c)	64.1	21.8	0.19	4.86	8.36	0.21	0.18	0.08
(r)	64.1	21.8	0.17	3.57	9.35	0.25	0.07	0.02
(a,2)	64.3	18.5	0.11	0.07	2.30	13.0	0.16	1.07
Loc 12.2 (rc)	64.9	18.8	0.11	0.07	2.31	13.4	0.05	0.06
(p,i)	62.6	23.4	0.19	4.63	8.93	0.26	0.18	0.01
(rr,e)	62.6	23.5	0.22	4.58	8.93	0.34	0.14	0.04
(rr,g)	62.8	23.5	0.19	4.58	8.95	0.32	0.08	0.03

	SiO_2	Al_2O_3	FeO	CaO	Na_2O	K_2O	SrO	BaO
Loc 12.5 (p,3)	62.7	23.1	0.22	4.43	9.01	0.33	0.17	0.08
82QC26 (p)	62.6	23.3	0.20	4.86	8.54	0.40	0.28	0.06
(p)	62.9	23.0	0.22	4.59	8.65	0.54	0.21	0.06
(a)	62.6	19.2	0.11	0.14	2.94	10.8	0.20	3.98
(a)	63.9	18.7	0.12	0.11	2.77	11.8	0.18	2.15
Q83J59 (c)	62.0	23.5	0.19	4.73	8.24	0.85	0.27	0.10
(r)	64.5	22.1	0.15	3.43	9.25	0.48	0.08	0.01
(a)	64.9	19.2	0.10	0.14	3.81	10.8	0.14	0.80
Quartz Latite Dikes								
Q83J100 (c)	60.0	25.3	0.12	6.32	7.76	0.34	0.19	0.01
(r)	62.4	23.9	0.14	4.84	8.62	0.48	0.21	0.05
(c)	61.0	24.1	0.13	5.44	8.25	0.53	0.27	0.04
(r)	62.2	23.9	0.18	4.82	8.53	0.51	0.11	0.07
(p,2)	61.7	23.9	0.16	5.10	8.39	0.47	0.20	0.10
Q83J131 (ac)	65.4	19.7	0.12	0.21	3.24	11.4	0.14	1.75
(ar)	64.8	18.8	0.02	0.05	1.07	14.9	0.05	0.97
LUCERO PEAK								
82QC15 (c)	63.8	21.4	0.12	3.33	9.77	0.56	0.07	0.01
(r)	66.9	19.9	0.09	1.30	11.2	0.16	0.01	0.00
(c)	64.5	21.4	0.17	2.96	10.0	0.57	0.07	0.02
(r)	65.7	20.4	0.15	1.87	10.6	0.51	0.04	0.03
(c)	65.7	20.6	0.16	2.05	10.3	0.78	0.03	0.00
(r)	66.8	20.9	0.14	1.69	10.5	0.57	0.03	0.01
(a)	65.4	18.9	0.10	0.12	3.66	11.4	0.03	0.11
(a)	65.3	18.8	0.10	0.06	2.90	12.5	0.02	0.08
Basal Vitrophyre to Amalia Tuff								
Q82J27 (a)	66.4	19.4	0.14	0.22	5.62	8.68	0.00	0.01
(a)	66.2	19.6	0.13	0.24	5.60	8.88	0.02	0.00
Lower Amalia Tuff								
Q84J205 (a)	66.9	19.4	0.16	0.22	5.58	8.71	0.03	0.00
(a)	66.7	19.7	0.14	0.24	5.67	8.71	0.02	0.02
(a)	67.3	19.5	0.15	0.23	5.61	8.86	0.00	0.00
Upper Amalia Tuff								
Q82J39 (a)	66.6	18.6	0.28	0.19	6.69	7.27	0.01	0.00
(a)	66.6	18.7	0.50	0.04	6.25	7.89	0.00	0.03
Peralkaline Rhyolite								
Q83J124 (a)	66.3	19.4	0.48	0.06	7.20	6.98	0.02	0.01
(a)	66.5	19.4	0.48	0.06	6.94	7.27	0.00	0.00
(a)	66.5	19.4	0.49	0.07	6.88	7.30	0.00	0.02

		SiO_2	Al_2O_3	FeO	CaO	Na_2O	K_2O	SrO	BaO
Peralkaline Intrusion									
Q3QC23	(a)	66.7	18.9	0.75	0.02	7.59	6.03	0.00	0.02
	(a)	67.1	19.0	0.17	0.11	6.69	7.21	0.02	0.02
	(ac)	66.9	19.7	0.16	0.12	6.90	7.22	0.00	0.00
	(ar)	66.5	19.3	0.16	0.66	7.03	6.98	0.00	0.01
Comendite									
Q83J140B	(ac)	64.7	20.5	0.18	0.91	5.78	7.79	0.04	0.81
	(ar)	63.5	22.1	0.23	2.52	7.42	4.24	0.00	0.35
	(l)	64.6	20.5	0.20	1.07	5.88	7.24	0.06	1.18
	(s)	64.8	20.9	0.22	1.43	6.58	6.26	0.03	0.60
	(a)	65.2	20.8	0.16	1.30	6.36	6.95	0.01	0.15

(a) alkali feldspar; (ac) alkali feldspar core; (ar) alkali feldspar rim; (c) plagioclase core; (c,a) plagioclase core to alkali feldspar; (d) "dusty" band; (l) large; (o) overgrowth on alkali feldspar megacryst; (p) unzoned plagioclase; (p,i) plagioclase included in alkali feldspar megacryst; (r) plagioclase rim; (rc) rapakivi core; (rr) rapakivi rim; (rr,e) rapakivi rim in enclave; (rr,g) rapakivi rim in granodiorite; (s) small; (v) vug crystal; ,2) or ,3) average of 2 or 3 grains of similar composition.

APPENDIX L: LATITUDE AND LONGITUDE OF SAMPLE LOCATIONS, SAMPLE WEIGHTS IN KILOGRAMS, AND HOST PLUTON.

81S24	36°46.59'	105°31.50'	-	RDM
81S28	36°47.16'	105°31.82'	1.80	RDM
81S31	36°47.54'	105°32.50'	1.03	RDM
81S43	36°46.16'	105°33.76'	0.34	CP-M
81S44	36°46.12'	105°33.83'	1.12	CP-M
82QC2	36°38.89'	105°31.26'	4.38	RH
82QC5	36°38.90'	105°31.77'	3.48	RH
82QC8	36°41.75'	105°33.03'	1.94	BC
82QC9	36°40.97'	105°33.26'	1.56	BC
82QC10	36°41.04'	105°33.15'	3.96	BC
82QC12	36°33.74'	105°31.67'		RH
82QC13	36°32.92'	105°30.36'	2.66	LP
82QC15	36°33.15'	105°30.52'	6.35	LP
82QC16	36°47.69'	105°32.22'	-	RDM
82QC17	36°47.68'	105°32.09'	-	RDM
82QC18A	36°47.72'	105°32.05'	2.73	RDM
82QC18B	36°47.72'	105°32.05'	0.95	RDM
82QC19	36°47.75'	105°32.02'	3.55	RDM
82QC22	36°47.75'	105°32.02'	3.56	RDM
82QC25	36°32.16'	105°31.33'	-	LP
82QC26	36°37.70'	105°31.35'	2.16	RH
82QC27	36°37.69'	105°31.37'	1.21	RH dike
82QC28	36°37.68'	105°31.38'	5.58	RH
82QC30	36°39.42'	105°31.59'	5.16	RH
82QC31	36°43.64'	105°24.01'	1.18	RR
82QC32C	36°42.73'	105°24.48'	5.55	RR
82QC32F	36°42.73'	105°24.48'	1.25	RR
82QC33	36°47.06'	105°30.27'	3.56	VC-M
82QC34	36°47.10'	105°30.26'	3.41	VC-P
82QC35	36°47.08'	105°29.84'	3.08	VC-M
82QC38	36°47.25'	105°29.75'	2.67	VC-P
82QC39	36°47.25'	105°29.75'	3.23	VC-M
82QC40	36°47.24'	105°29.75'	4.35	VC-M
82QC41	36°47.04'	105°30.23'	3.26	VC-M
82QC43	36°43.99'	105°24.13'	4.17	RR
82QC44	36°42.22'	105°23.76'	4.91	RR
82QC45	36°45.83'	105°33.85'	5.85	CP-M
82QC46	36°45.95'	105°33.99'	1.13	CP-M
82QC47	36°46.17'	105°34.03'	2.50	CP-M
82QC48	36°46.36'	105°33.96'	1.33	CP-M
82QC49	36°46.47'	105°33.93'	2.98	CP-P
82QC50	36°46.58'	105°33.77'	2.53	CP-M
82QC51	36°44.77'	105°30.38'	8.72	CL
82QC51A	36°44.77'	105°30.38'	6.64	CL
82QC51b	36°44.05'	105°29.56'	6.40	CL
82QC52	7180 Grizzly level; E 51,680; N 21,530.		5.70	SG
82QC54	7120 Haulage level; E 55,400; N 23,750.		3.75	SG
82QC55	7120 Haulage level; E 52,660; N 23,890.		5.94	SG
82QC56	7120 Haulage level; E 52,440; N 21,620.		-	SG

83QC1	36°39.53'	105°31.50'	3.91	RH
83QC2	36°39.53'	105°31.56'	1.88	RH dike
83QC8	36°39.42'	105°31.62'	1.26	RH
83QC9	36°44.24'	105°28.62'	0.91	CL
83QC10	36°44.35'	105°28.53'	5.31	CL
83QC12	36°44.35'	105°28.53'	1.49	CL enclave
83QC14	36°44.34'	105°28.47'	2.07	CL
83QC16	36°44.21'	105°28.52'	-	CL
83QC17	36°44.09'	105°28.52'	-	CL
83QC18	36°43.85'	105°30.19'	1.62	CL
83QC20	36°43.85'	105°30.19'	2.10	CL
83QC21	36°49.20'	105°27.76'	2.46	LC-P
83QC22	36°49.34'	105°28.08'	3.78	LC-P
83QC23	36°49.22'	105°28.16'	1.37	LC-P
83QC25	36°47.24'	105°29.75'	2.36	VC-M
83QC26	36°47.25'	105°29.75'	1.77	VC-M
83QC29	36°47.25'	105°29.75'	3.50	VC-P
83QC30	36°47.27'	105°29.74'	-	VC-P
83QC31	36°47.26'	105°29.74'	2.71	VC dike
83QC32	Float		1.92	VC-P
83QC33	36°47.21'	105°29.87'	-	VC-M
83QC34	36°47.20'	105°29.83'	4.57	VC-M
84QC1	36°45.80	105°33.76'	-	CP-M
84QC5	36°46.17'	105°33.87'	-	CP-M
84QC7	36°46.56'	105°33.75'	-	CP-P
84QC9	36°39.15'	105°31.35'	-	RH
84QC11	36°39.16'	105°31.55'	-	RH
84QC12	36°39.21'	105°31.60'	-	RH
84QC13	36°39.23'	105°31.64'	-	RH
84QC14	36°39.24'	105°31.65'	-	RH
84QC31	36°36.79'	105°30.02'	-	RH enclave
84QC32	36°36.73'	105°30.00'	-	RH enclave
85QC9	36°44.17'	105°28.71'	-	CL
85QC11	36°44.34'	105°28.47'	-	CL
85QC12	36°44.34'	105°28.47'	-	CL
85QC23	36°35.31'	105°29.76'	-	RH dike
85QC27	36°35.19'	105°29.61'	-	RH enclave
85QC32	36°35.19'	105°29.61'	-	RH enclave
85QC36	36°43.64'	105°24.01'	-	RR
85QC37	36°43.64'	105°24.01'	-	RR

Loc. 12	36°33.74'	105°31.67'	-	RH
78L172	36°44.77'	105°30.38'	-	CL
80L20	36°31.65'	105°30.66'	-	LP
Q83SL25	36°39.11'	105°31.74'	-	RH
Q83SL27	36°39.08'	105°31.88'	4.42	RH
Q83SL28	36°39.06'	105°31.92'	1.26	RH
Q83J55	36°35.44'	105°34.96'	8.47	RH
Q83J59	36°35.90'	105°33.64'	5.17	RH
Q83J61	36°35.84'	105°33.90'	6.11	RH
Q83J62	36°47.10'	105°30.27'	3.50	VC-P
Q83J63	36°47.07'	105°30.31'	3.90	VC-P
Q83J65	36°47.06'	105°30.30'	2.77	VC-M
Q83J66	36°47.06'	105°30.23'	2.90	VC-M
Q83J67	36°47.08'	105°30.23'	2.69	VC-P
Q83J72	36°47.99'	105°30.08'	-	P dike
Q83J76	36°47.50'	105°29.92'	1.50	P dike
Q83J78	36°47.22'	105°29.82'	2.16	VC-M
Q83J79	36°47.13'	105°29.81'	1.70	VC-M
Q83J81	36°45.60'	105°33.47'	2.45	CP-M
Q83J82	36°45.68'	105°33.36'	3.76	CP-M
Q83J86	36°45.85'	105°33.51'	-	CP-M
Q83J88	36°46.17'	105°33.18'	3.23	CP-M
Q83J92	36°46.70'	105°33.57'	1.81	CP-M
Q83J93	36°46.64'	105°33.69'	3.03	CP-M
Q83J94	36°46.63'	105°33.89'	2.69	CP-P
Q83J100	36°36.69'	105°30.21'	2.68	RH dike
Q83J101	36°36.78'	105°30.55'	8.30	RH
Q84J6	36°33.78'	105°31.61'	-	RH
1685	7180 Grizzly level; E 51,478; N 22,322.		-	SG
3417	7180 Grizzly level; E 52,133; N 21,524.		-	SG
3438	7120 Haulage level; E 51,166; N 21,641.		-	SG
3439	7120 Haulage level; E 51,694; N 21,368.		-	SG
3440	7120 Haulage level; E 51,679; N 21,365.		-	SG

Key to plutons: BC, Bear Canyon; CL, Cabresto Lake; CP-M, Canada Pinabete-metaluminous; CP-P, Canada Pinabete-peralkaline; LC-P, Latir Creek peralkaline dome; LP, Lucero Peak; RDM, Rito del Medio; RH, Rio Hondo; RR, Red River; SG, Sulphur Gulch; VC-M, Virgin Canyon-metaluminous; VC-P, Virgin Canyon-peralkaline.